PROPERTIES OF AQUEOUS SOLUTIONS OF TRIBLOCK COPOLYMERS OF ETHYLENE OXIDE AND PROPYLENE OXIDE AND THEIR MIXTURES WITH SURFACTANTS STUDIED BY SURFACE TENSION AND NEUTRON REFLECTION

A thesis submitted in fulfilment of the requirement for the degree of Doctor of Philosophy at the University of Oxford

by

Josélio Vieira

University College

Hilary Term 2002



PROPERTIES OF AQUEOUS SOLUTIONS OF TRIBLOCK COPOLYMERS OF ETHYLENE OXIDE AND PROPYLENE OXIDE AND THEIR MIXTURES WITH SURFACTANTS STUDIED BY SURFACE TENSION AND NEUTRON REFLECTION

Josélio Vieira
University College, University of Oxford
D. Phil. Thesis
Hilary Term 2002

Abstract

The adsorption and the aggregation behaviour of poly(ethylene oxide-b-propylene oxide-b-ethylene oxide) copolymers (EPE) and their mixtures with surfactants of different ionic characters: sodium dodecyl sulphate (SDS), dodecyltrimethylammonium chloride (DTAC) and tetraethylene glycol monooctyl ether (C_8E_4), have been investigated using surface tension and neutron reflection measurements.

The first part of the thesis is concerned with the adsorption properties of EPE copolymers at the air-solution interface. The surface tension curves for the copolymers show two breaks similar to those published for Pluronic[a] surfactants (commercially available EPE copolymers). Earlier explanations of this behaviour are inconsistent with the neutron reflection results. The adsorption isotherms obtained by neutron reflection have two steps, one at low concentrations leading to a plateau followed by a substantial rise up to the CMC. The low-concentration breakpoint is attributed to two different effects, the depletion of copolymer molecules in the bulk of the solution and the composition polydispersity. In general, the structure of the adsorbed layer can be described in terms of four layers. The outermost layer is always water free and contains only PO units. The EO residues form tails, which extend into the solution over a distance shorter than the fully extended length. Depending on the conditions, some PO is also found in this tail region.

The second part of the thesis is concerned with the effect of mixing EPE copolymers with surfactants of different ionic characters. The formation of mixed micelles and monolayer between EPE 3000-14 and ionic surfactants show a surprisingly strong attractive interaction, which is attributed to a dehydration mechanism. In the mixed micelle formation, in particular, the loss of hydration water molecules found in the micelle core of the copolymer would lead to a substantial gain in entropy. The surface compositions from neutron reflection generally disagree with the predictions of Pseudophase Separation Model. It is believed that changes of hydration upon mixing may be responsible for the deviations as it is not taken into account by the Pseudophase Separation Model. From the neutron reflection studies, DTAC appears to accumulate preferably in the uppermost part of the mixed interfacial layer, while SDS would rather stay in the aqueous phase region.

In the C_8E_4/EPE 3000-14 system, the mixed micellization results in strong repulsive interaction, which is attributed to a further hydration of the copolymer micelle core by the incorporation of the solvated C_8E_4 headgroups. However at the air-solution interface, both C_8E_4 and EPE 3000-14 are found to mix ideally. The difference between mixed micelle and monolayer formation observed for such a system is believed to be associated with the structure of the two states. The orientation of the copolymer molecules in the interfacial layer is such that the contact of PO groups with water molecules is significantly reduced. C_8E_4 molecules appeared to adsorb preferentially within the uppermost part of the interfacial layer rich in PO groups.

---

[a] Trademark of BASF

PROPERTIES OF AQUEOUS SOLUTIONS OF TRIBLOCK COPOLYMERS OF ETHYLENE OXIDE AND PROPYLENE OXIDE AND THEIR MIXTURES WITH SURFACTANTS STUDIED BY SURFACE TENSION AND NEUTRON REFLECTION

Josélio Vieira

University College, University of Oxford

D. Phil. Thesis

Hilary Term 2002

Longer Abstract

In this study, the adsorption and the aggregation behaviour of poly(ethylene oxide-b-propylene oxide-b-ethylene oxide) triblock copolymers (EPE) and their mixtures with surfactants of different ionic characters: sodium dodecyl sulphate (SDS), dodecyltrimethylammonium chloride (DTAC) and tetraethylene glycol monooctyl ether (C_8E_4), have been investigated using surface tension and neutron reflection measurements. The study is described in two separate parts of the thesis.

The first part is concerned with the adsorption properties of EPE block copolymers at the air-solution interface. The surface-active properties of such copolymers were examined for a number of triblock compositions over a range of concentration, and at two temperatures. The surface tension curves for most of the monodisperse copolymers show two break points similar to those for Pluronic surfactants (commercially available EPE block copolymers) published in the literature. Earlier explanations of this surface tension behaviour are shown to be inconsistent with the neutron reflection results. The high-concentration breakpoint is attributed to the CMC as indicated by steady values of surface tension and surface excess obtained as the bulk concentration exceeds this breakpoint. Neutron reflection has been used to measure the surface excesses of two triblock copolymers with approximate formulae $E_{23}P_{52}E_{23}$ and $E_9P_{22}E_9$. The copolymers have similar adsorption isotherms in terms of their molar adsorption, though quite different in

terms of segment adsorption. The isotherms have two steps, one at low concentrations leading to a plateau over about two decades of concentrations followed by a substantial rise over the decade of concentration leading to the critical micelle concentration. In the plateau region the area per ethylene oxide segment was found to be about 9 and 22 $Å^2$ respectively for the two copolymers decreasing to 6.5 and 12 $Å^2$ at the CMC at 25°C. The thickness of the adsorbed layer shows little change between these coverages. An increase in temperature to 35°C shifts the adsorption isotherm pattern to a concentration about $1/30^{th}$ of those at 25°C, in line with the change in CMC. The neutron surface excesses were incorporated into the integrated Gibbs equation and fit the surface tension curves well over most of the range of adsorption. The sharp upturn in surface tension at low polymer concentrations is believed to be caused by a mix of three effects, i.e. the depletion of EPE copolymer molecules in the bulk of the solution, and polydispersity in both molecular weight and composition.

The structural evolution of the interfacial layer with concentration was investigated by neutron reflectometry. Measurements were made at the air/water interface at the critical micelle concentration and at two much lower concentrations, and at temperatures of 25°C and 35°C. In general, the adsorbed layer can be described in terms of four uniform sub-layers. The outermost layer is always a water free layer containing only propylene oxide units. The ethylene oxide residues form tails below this layer, which extend into the solution over a distance slightly shorter than the fully extended length. Depending on the conditions, some propylene oxide is also mixed in with this tail region. For example, at the lower surface concentrations the segment density of the propylene oxide decays rapidly and there is a relatively small proportion of PO immersed in the water but, at the highest concentrations, there is a much larger amount of PO in the aqueous/EO region and this extends some way into the solution. At the higher temperature there is little PO in the aqueous region of the layer but there is significant mixing of PO with EO in a sublayer just below the main PO layer out of the water. The smaller molecular weight copolymer gives a much more disordered structure with greater mixing of all three ingredients.

The second part of the thesis is concerned with the effect of mixing EPE block copolymers with conventional surfactants of different ionic characters. The mixed micelle and monolayer formation was analysed using Pseudophase Separation Models.

A surprisingly strong attractive interaction between SDS and EPE 3000-14 was observed in mixed micelle formation. The strong interaction is attributed to a substantial gain in entropy associated with the dehydration of the mixed micelle core. The variation of interaction parameter with the composition of the mixture is also believed to result from the changes in hydration of the micelles. The addition of salt increases the surface activity of the mixture but there is no significant variation in the net attractive interaction of the system. In comparison with the SDS/EPE 3000-14 system, a much reduced interaction parameter was obtained for the DTAC/EPE 3000-14 mixed systems. Mixed micelle formation in C_8E_4/EPE 3000-14 system results in strong repulsive interaction, which is attributed to hydration of the copolymer micelle core by the incorporation of the solvated C_8E_4 headgroups.

Surface tension in combination with specular neutron reflection was used to investigate the adsorption of EPE copolymers in binary mixtures with surfactants such as SDS, DTAC, and C_8E_4 at the air/liquid interface. The surface composition predictions obtained from the Pseudophase Separation Model were compared with results of surface composition directly measured by neutron reflection.

For the mixtures of EPE 3000-14 with ionic surfactants, the large difference in surface activity makes the determination of β^s impossible. However in the presence of electrolytes β^s values are large and negative. The surface compositions from neutron reflection generally disagree with the predictions of Pseudophase Separation Model, particularly for the DTAC/EPE 3000-14 systems. We argue that the nonideality observed in the co-micellization of both SDS and DTAC with EPE 3000-14 could be driven by a dehydration mechanism and it would therefore be reasonable to assume that dehydration should also be an important factor in the thermodynamics of monolayer formation. Pseudophase Separation Model does not take into account the hydration changes upon mixing, and we believe that hydration may be responsible for the deviations observed.

The variation of layer thickness with the surface coverage of the block copolymer suggests that DTAC accumulates preferably in the uppermost part of the interfacial layer, while SDS would rather stay in the aqueous phase region, which is more hydrophilic. For the binary mixtures of C_8E_4/EPE 3000-14, the pseudophase separation model analysis of the surface tension data shows that the two surfactant species mix ideally at the interfacial layer. The surface composition data from the neutron reflection are consistent with the pseudophase separation model predictions. The difference in interaction mechanism observed in mixed micelles and monolayer formation for such a binary mixtures is believed to be associated with the structure of the two states. The orientation of the copolymer molecules in the interfacial layer is such that the contact of PO groups with water molecules is significantly reduced. C_8E_4 molecules appeared to adsorb preferentially within the uppermost part of the interfacial layer rich in PO groups. The displacement mechanism of copolymer molecules from the interface was noticeably different in the nonionic mixed system compared to the mixtures with ionic surfactants. In the nonionic mixed system, it seems to be dictated by a changeover in surface activity with concentration rather than by the presence of micelles.

Contents

Chapter 1 – Introduction

Introduction 1

References 5

Chapter 2 – Experimental Techniques and Sample Preparation

1 Surface Tension of Solutions

1.1 Introduction 6

1.2 Surface tension measurement techniques 8

1.2.1 Du Noüy ring method 9

1.2.2 Wilhemy plate method 10

Appendix 1 – Harkins and Jordan correction factors 12

2 Neutron Reflectivity – Theory and Measurement

2.1 Introduction 13

2.2 Principles of neutron scattering 14

2.3 Neutron reflection on flat surfaces 16

2.4 Neutron reflectivity of stratified media 19

2.5 Neutron reflection experiments 22

2.5.1 The SURF reflectometer 23

2.5.2 Air –solution neutron reflection experimental details 26

2.5.3 Data processing of reflectivity profiles 27

2.5.4 Data analysis using the Optical Matrix Method 28

3 Purification and Characterization of Surfactants

3.1 Introduction 30

3.2 Purification of monodisperse EPE copolymers 32

3.2.1 Purification of block copolymers 33

3.2.2 Characterization of block copolymers 33

3.3 Purification of sodium n-dodecylsulfate (SDS) 36
3.3.1 Purification of SDS 36
3.3.2 Characterization of SDS 37
3.4 Purification of dodecyltrimethylammonium chloride (DTAC) 38
3.4.1 Purification of DTAC 38
3.4.2 Characterization of DTAC 39
3.5 Purification of tetraethylene glycol monooctyl ether (C_8E_4) 40
3.5.1 Purification of C_8E_4 40
3.5.2 Characterization of C_8E_4 41
Appendix 2 – GPC chromatogram peaks of EPE copolymers 43

References 45

Chapter 3 – Thermodynamics of Surfactant Solutions

1 General Description of Surfactant Solutions 47

2 Surfactant Adsorption at Air-Liquid Interface 48
2.1 The Gibbs surface excess 49

3 Surfactant Micellization 54
3.1 Micelle formation 54
3.1.1 Phase separation model 55
3.1.2 Mass action model 56

References 57

Chapter 4 – Surface Activity of EPE Copolymers Studied by Surface Tension

1 Introduction 58

2 Experimental Details 58
2.1 Materials 58
2.2 Surface tension measurements 58

3 Results and Discussion 60
3.1 Surface tension of EPE 3000-14 copolymer 60
3.2 Comparison between Wilhemy plate and du Noüy ring methods for measuring surface tension of EPE copolymers 62
3.3 Effect of EPE copolymer composition 64
3.4 Effect of temperature 69

4 Summary 72

References 74

Chapter 5 – Adsorption of EPE Copolymers at the Air-Solution Interface Studied by Neutron Reflection

1 Introduction 75

2 Experimental Details 76
2.1 Materials 76
2.2 Neutron reflectivity measurement and data analysis 76
2.3 Determination of adsorbed amounts 77
2.4 Determination of the surface tension–log C curve from the neutron reflectivity data 78

3 Results and Discussion 79
3.1 Amount of EPE 3000-14 adsorbed at the air-solution interface 79
3.2 Effect of temperature 83
3.3 Effect of EPE copolymer composition 85
3.4 Comparison with surface tension data 88
3.4.1 Surface excess and area per copolymer molecule at saturation 88
3.4.2 Bulk depletion effect 90
3.4.3 Copolymer polydispersity effect 95

4 Summary 96

Appendix 3-5 – Neutron reflectivity curves of EPE copolymers in NRW 100

References 108

Chapter 6 – Structure of Monolayers of EPE Copolymers at the Air-Solution Interface Studied by Neutron Reflection

1 Introduction 110

2 Experimental Details 111
2.1 Materials 111
2.2 Neutron reflectivity measurement and data analysis 111
2.3 Determination of surfactant configuration within the monolayer 111

3 Results and Discussion 114
3.1 Structure of EPE 3000-14 monolayer 114
3.2 Effect of temperature on the monolayer structure 125
3.3 Effect of EPE copolymer composition 130

4 Adsorption Modelling for Block Copolymers 137
4.1 Marques and Joanny (MJ) scaling theory of copolymer adsorption 138

5 Summary 145

References 148

Chapter 7 – EPE Copolymer-Surfactant Systems

1 Introduction 149

2 Surfactant Mixtures 152

3 The Modelling of Surfactant Mixing 155

4 Mixed Surfactant Micelles 155
4.1 Pseudophase separation approach 156
4.1.1 Ideal mixing 159
4.1.2 Nonideal mixing 159

5 Mixed Surfactant Monolayer Models 162
5.1 Pseudophase separation approach – Regular Solution Approximation 164
5.2 Changes in molar areas on mixing 165

References 170

Chapter 8 – Micellization of Binary Mixtures of EPE copolymers and Surfactants

1 Introduction 172

2 Experimental Details 174
2.1 Materials 174
2.2 Surface tension measurements 174
2.3 Determination of micellar interaction parameter (β^M) 175

3 Results and Discussion 176
3.1 Micellization in the SDS/EPE 3000-14 system 176
3.2 Micellization in the DTAC/EPE 3000-14 system 187
3.3 Micellization in the C_8E_4/EPE 3000-14 system 192
3.4 Comparison of mechanism of interaction in systems containing ionic surfactants/polyglycol ethers and ionic surfactants/EPE copolymers 199
3.5 Considerations on thermodynamic modelling for nonideal mixing of EPE copolymers in mixed solution 206
3.5.1 Mean field lattice theory of EPE copolymer micellization 209

4 Summary 217

References 219

Chapter 9 – Adsorbed Layers of Binary Mixtures of EPE copolymers and Surfactants

1 Introduction 224

2 Experimental Details 226

2.1 Materials 226

2.2 Surface tension measurements 226

2.3 Determination of the surface interaction parameter (β^s) 226

2.4 Neutron reflectivity measurement and data analysis 228

2.5 Determination of surface excess by neutron reflectivity 228

3 Results and Discussion 230

3.1 Mixed Monolayer Formation in the SDS/EPE 3000-14 system 230

3.2 Mixed Monolayer Formation in the DTAC/EPE 3000-14 system 248

3.3 Mixed Monolayer Formation in the C_8E_4/EPE 3000-14 system 264

4 Summary 272

References 276

Acknowledgements

Firstly I would like to thank my supervisors, Bob Thomas in Oxford and Vijay Bhuva at Dow AgroSciences, for all their help, encouragement and advice throughout these challenging years. Bob, in particular, I would like to thank for his remarkable support and guidance, without which I would never have progressed so far. I would like to thank all of members of Bob's group, who are numerous to mention by name, for their camaraderie which have made me feel welcome, despite my erratic visits to the lab. In particular I would to thank Z.X. Li for his help with the neutron reflection experiments and GPC analysis.

I also wish to thank Jeff Penfold and John Webster from the Rutherford Laboratory for their help with the neutron scattering experiments.

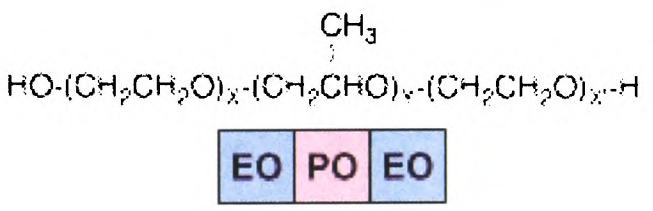
I must also thank Dow AgroSciences for allowing me to pursue this degree in the first place and for funding it, and especially Vijay Bhuva who gave me tremendous support. I am also grateful to all my other colleagues for their assistance and encouragement, in particular Andy Fowles, and John Dawson.

Finally, and most importantly, I would like to thank my wife, Alice, and my daughter, Isabella, for their ever present love, understanding and encouragement, throughout these years. I feel have a lot to catch up with them now, which will be certainly rectified. Thanks to my mom, dad and my mother-in-law (I must be the first one to acknowledge a mother-in-law, but she really deserves it) for their encouragement and prayers. I also thank all my friends, who, in their own way, were very supportive.

Chapter 1

Introduction

Triblock copolymers of poly(ethylene oxide)-poly(propylene oxide)-poly(ethylene oxide), abbreviated as EPE in this study, are nonionic surfactants commercially available as Pluronic or Synperonic[b]. Pluronic copolymers were first introduced by BASF in the early 1950s. Polyoxypropylene glycol with a molecular weight of 900 or more, is water insoluble and functions as a hydrophobic chain. The sequential addition of ethylene oxide to either end of the polyoxypropylene glycol chain yields a water-soluble polyol which exhibits surface-active properties and a tendency to self-assemble in solution. The structure of such block copolymers is presented below.



Most other common nonionic surfactants rely on a single hydrophobic chain and the selection of chains is restricted by the need to satisfy solubility requirements. This means that any changes in performance of the surfactant can effectively only be achieved by altering the hydrophilic group. EPE copolymers allow the incremental alteration of both hydrophobic and hydrophilic chains. Because block copolymer structures effectively provide unlimited freedom in molecular design, the PPO and PEO chain length and arrangement can be tailored to satisfy many specific needs and requirements. The grid shown in Figure 1 provides a graphic presentation of the various commercially available grades of Pluronic surfactants.

The Pluronic copolymer grid is a plot of molecular weight ranges of the hydrophobic chain, PPO, against the weight-percent of the hydrophilic chain, PEO, present in each molecule. The grade of each Pluronic copolymer is identified by a letter-number combination as shown in the grid. The alphabetical designation refers to the physical form

[b] Trademark of Uniqema

of the product: 'L' for liquids, 'P' for pastes, 'F' for solid forms. The first two digits in the designation, multiplied by 300, indicate the approximate molecular weight of the PPO chain. The last digit, when multiplied by 10, indicates the approximate weight percent of PEO in the molecule. For example, from the Grid, we can immediately deduce that Pluronic P105 is a paste, the molecular weight of the PPO is approximately 3000 (10 X 300), and the PEO chain comprises approximately 50% of the molecule by weight, (5 X 10).

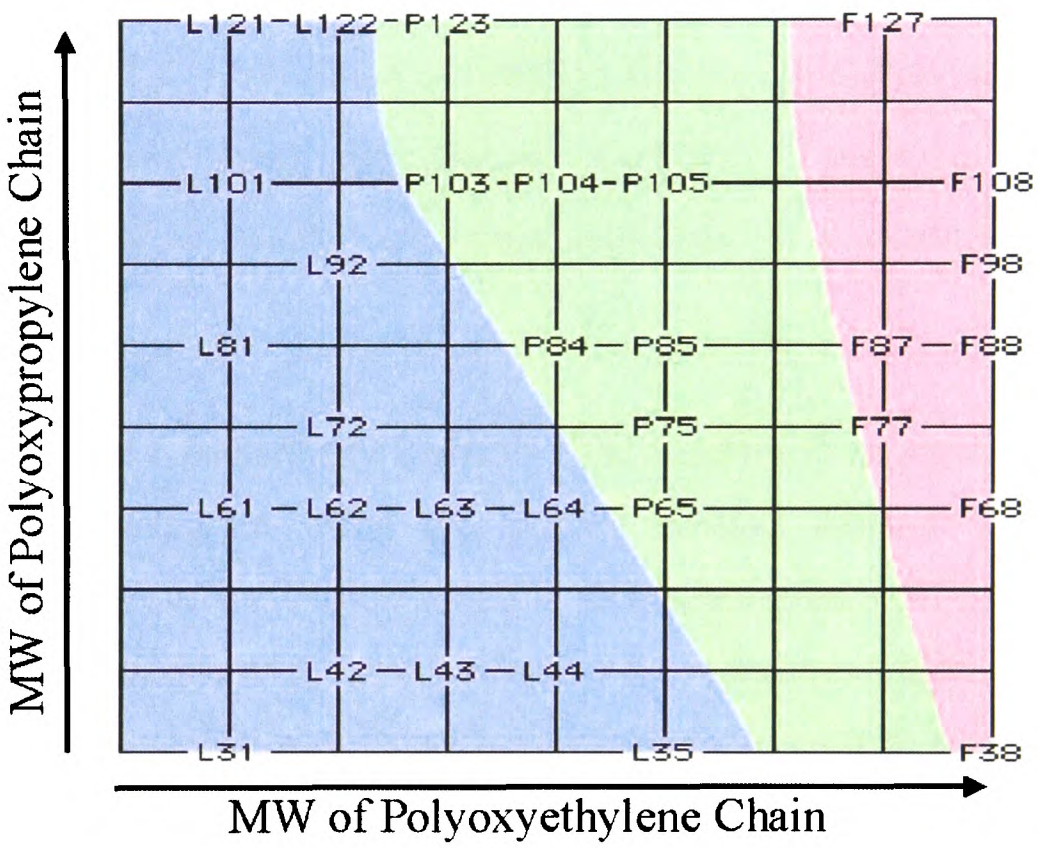


Figure 1. Grid showing a series of commercially available Pluronic copolymers

EPE block copolymers are extremely surface active and are able to provide an effective steric barrier that prevents flocculation and/or coalescence of emulsion droplets and foam bubbles. They are therefore an important class of surfactants with a widespread usage in various industrial applications, including detergency, dispersion, foaming, defoaming and emulsification[1,2].

This study focuses on two key aspects of the applications of EPE copolymers by industry: their adsorption behaviour from aqueous solution and their behaviour in mixed systems containing conventional surfactants of different ionic character. These two aspects are

described in separate parts in the thesis, following a description of experimental techniques and sample preparation in Chapter 2.

The study of the adsorption characteristics of EPE block copolymers at the air-water interface using surface tension and neutron reflection is the main subject of the first part of the thesis. Surface tension measurements have been extensively used to study the surface activity of surfactants at air/liquid and liquid/liquid interfaces. From the slope of a plot of the surface tension against log(concentration) it is possible to determine the concentration of surfactant molecules adsorbed at the surface, Γ_{sat}, by using the Gibbs adsorption isotherm, $\Gamma_{sat} = -(1/RT)(d\gamma/d\ln(C))$. The area per copolymer molecule, A, can then be calculated using the relation $A = 1/\Gamma N$. Therefore, surface tension measurements provide a simple and convenient way of constructing the surface adsorption isotherm.

The surface activity of commercially available EPE copolymers in aqueous solutions has been previously investigated using the surface tension method[3-6]. However, the unexpectedly complex surface tension variation with concentration found for the various Pluronic surfactants considered in these studies has led to some ambiguous conclusions. It is probable that the composition polydispersity of these commercial samples contributes to this ambiguity and has therefore restricted the understanding of the surface behaviour of the EPE copolymers. In the present study, we have used highly monodisperse EPE copolymers for our adsorption studies at the air-water interface and this has allowed us to explain the ambiguities inherent in earlier surface tension work. The surface tension measurements on our EPE copolymers are described in Chapter 4. The effects of copolymer composition and temperature are investigated and the results are compared with published data for commercial samples and with those for common nonionic surfactants. The methods developed to produce monodisperse EPE copolymers were then used to synthesise a series of monodisperse deuterated EPE copolymers for neutron reflectivity studies. Chapter 5 describes the application of the neutron reflectivity technique to a study of the adsorption properties of these deuterated EPE copolymers at air-water interface. The results are related to those obtained by surface tension and the combination reveals some important new features of the adsorption of EPE copolymers at

the air-water interface. The first part of the thesis ends with a discussion in Chapter 6 of the structure of EPE copolymer layers as determined using neutron reflection.

Part II is concerned with the effect of mixing EPE copolymers with conventional surfactants of different ionic character. Many studies have been undertaken to investigate the bulk solution behaviour of EPE copolymers in mixtures with various surfactants[6-8], electrolytes[9,10], homopolymers[11], additives[12,13], and in mixtures with other EPE copolymers[12]. Although the Pseudophase Separation Model has been extensively applied with some success to explain micellization in mixed surfactant systems[14,15], to the best of our knowledge it has never been employed to study binary systems containing EPE copolymers and surfactants. The Pseudophase Separation Approach together with other models of surfactant mixing are reviewed in Chapter 7. Chapter 8 describes the surface activity characteristics of binary mixtures of EPE copolymer with sodium dodecyl sulphate (SDS), dodecyltrimethylammonium chloride (DTAC) and tetraethylene glycol monooctyl ether (C_8E_4) using the surface tension technique. The experimental data was used to assess the interaction between the surfactant species in mixed micelles according to the Regular Solution Model.

Although there have been several previous studies of the bulk properties of solutions of EPE copolymer surfactant mixtures, mixed monolayer formation of such systems at interfaces has been neglected. It is possible that this results in part from the lack of well-characterized samples of EPE copolymers, in contrast to polydisperse Pluronic or related commercial equivalents. Our monodisperse EPE copolymers were used to study the formation of mixed monolayers at the air-water interface from binary systems containing SDS, DTAC and C_8E_4. In Chapter 9, the adsorption at the air-water interface of such systems is studied using the surface tension technique and neutron reflection. The Regular Solution Model is applied to describe the monolayer composition and the interaction between surfactant and polymer at the interface. Specular neutron reflection is used as a direct technique to probe the monolayer composition to verify the predictions of the Regular Solution Model for binary mixtures of EPE copolymer and conventional surfactants.

References

[1] Schmolka, I.R. *J.Am.Oil Chem. Soc.*, 54, 110 (1977)

[2] Alexandridis, P. *Colloid Interface Sci*, 1, 490 (1996)

[3] Prasad, K.N.; Luong, T.T.; Florence, A..T.; Paris, J.; Vaution, C.; Seiller, M.; and Puisieux, F. *J. Colloid Interface Sci.*, 69, 225 (1979)

[4] Wanka, G.; Hoffmann, H.; and Ulbricht, W. *Macromolecules*, 27, 4145 (1994)

[5] Alexandridis, P.; Athanassiou, V.; Fukuda, S.; and Hatton, T.A. *Langmuir*, 10, 2604 (1994)

[6] Hecht, E.; and Hoffmann, H. *Langmuir*, 10, 86 (1994)

[7] Almgren, M.; Stam, J.V.; Lindblad, C.; Li, P.; Stilbs, P.; and Bahadur, P. *J. Phys. Chem.*, 95, 5677 (1991)

[8] Hecht, E.; and Hoffmann, H. *Colloids Surfaces A: Physicochem. Eng. Aspects* , 96, 181 (1995)

[9] Alexandridis, P.; and Holzwarth, J.F. *Langmuir*, 13, 6074 (1997)

[10] Alexandridis, P.; Athanassiou, V.; and Hatton, T.A. *Langmuir*, 11, 2442 (1995)

[11] Malmsten, M.; and Lindman, B. *Macromolecules*, 25, 1282 (1993)

[12] Silva, R.C; and Loh, W. *J. Colloid Interface Sci.*, 202, 385 (1998)

[13] Loh, W.; Beezer, A.E.; and Mitchell, J. C. *Langmuir*, 10, 3431 (1994)

[14] Philips, J.N. *Trans. Faraday Soc.*, 51, 561 (1955)

[15] Rubingh, D.N. "*Solution Chemistry of Surfactants*", Mittal, K.L., (ED.), Vol. 1, pp 337-354, Plenum, New York (1979)

Chapter 2

Experimental Techniques and Sample Preparation

1 Surface Tension of Solutions

1.1 Introduction

Molecules in the liquid state are attracted to each other by forces such as van der Waals or hydrogen bonding. Molecules in bulk solution experience on average an equal attraction in all directions from the surrounding molecules. In contrast, molecules at the air-liquid interface must experience only a net inward attraction. To expand an air-liquid interface, bringing more molecules from the bulk phase to the surface therefore requires work, and the work required, *W*, to increase the area of a surface by unit area, A, is defined as the surface tension, γ[1].

$$dW = \gamma dA \tag{2.1}$$

If the surface is expanded whilst keeping the temperature and pressure constant, then the work done may be identified with the Gibbs surface free energy, *G*, per unit area

$$dG = \gamma dA \tag{2.2}$$

Liquids, in which the cohesive forces (intermolecular forces of attraction) are strong, such as hydrogen bonding, exhibit higher surface tensions than those in which molecules are only weakly attracted by van der Waals forces.

In the case of aqueous solutions, the solute can affect the surface tension in three different ways, as depicted in Figure 1. Curve 1 is the type of surface tension-concentration profile characteristic of inorganic electrolytes. Electrolytes prefer to stay in the bulk solution rather than migrate to the surface, i.e. there is a negative adsorption of ions at the air-

water interface. This can be viewed as a disruption of the long range electrostatic interactions between ions and there will also be a contribution associated with partial dehydration of the ions. Curve 2 is typical of uncharged organic compounds, which normally cause the surface tension to decrease with increasing concentration. Organic liquids have lower surface tensions than water and therefore adsorb preferentially at the air-water interface. The type of behaviour indicated by curve 3 is typical of surfactants. Surfactants give a drastic reduction of surface tension at low concentrations before reaching a concentration, above which the surface tension is practically constant. The concentration at which the surface tension flattens out is the critical micelle concentration (CMC). At concentrations higher than the CMC all additional surfactant molecules will self-assemble to form aggregates in the bulk solution, thus keeping the surfactant monomer activity more or less constant. The large reduction in surface tension results from strong adsorption of the surfactants at the air-water interface. The nature of this adsorption will be discussed further later in the thesis.

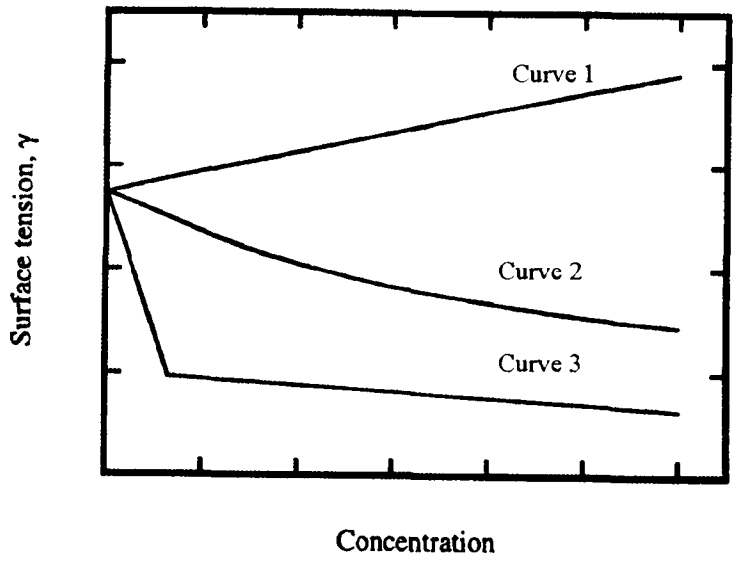


Figure 1. Three types of variation of surface tension with concentration for aqueous solutions.

The curve of the surface tension plotted against the logarithm of the bulk concentration of a surfactant solution provides important physical information such as the CMC and the maximum surface pressure, π_{max}. From the slope of this curve it is also possible to determine the concentration of surfactant molecules adsorbed at the surface, Γ_{sat}, by using the Gibbs adsorption isotherm.

$$\Gamma_{sat} = -\left(\frac{-1}{RT}\right)\left(\frac{d\gamma}{d\ln C}\right) \tag{2.3}$$

where R is the molar gas constant and T is the absolute temperature. The area per adsorbed molecule, A, can be then calculated using the relation

$$A = \frac{1}{\Gamma N} \tag{2.4}$$

where N is Avogadro's number. Surface tension measurements therefore provide a simple and convenient way of constructing the surface adsorption isotherm. In addition, the surface tension curve may also yield information about the presence of surface-active contaminants and this will be discussed later in this chapter.

1.2 Surface tension measurement techniques

A number of techniques are available for the measurement of surface tension[2]. The du Noüy ring and Wilhemy plate methods are relatively simple methods and because of their simplicity, are the most commonly used methods. All the surface tension measurements in this study were made using the Krüss K10T maximum pull digital tensiometer, depicted in Figure 2. This type of tensiometer is in effect simply a very fine balance, with which the surface tension of liquids can be measured either using a rectangular plate (Wilhemy plate) or using a small platinum-iridium ring (du Noüy ring).



Figure 2. Krüss K10 T tensiometer

1.2.1 Du Noüy Ring Method

The Du Nouy ring method is named after the French physicist who developed it in the late 1800s. A ring with defined geometry is suspended on the precision microbalance arm of the tensiometer. In this study all measurements were performed using a ring made of a platinum/iridium alloy with a radius, R, of 9.585mm and a cross sectional radius, r, of 0.185mm. The ring is immersed into the liquid, following which the sample container is lowered, leading to the pulling up of a meniscus above the surface of the liquid. The apparatus measures the maximum force required to pull the ring just before its detachment from the liquid. The maximum force applied to the ring, K_{max}, is related to the surface tension by

$$\gamma = \frac{K_{\max}}{4\pi R} F \qquad (2.5)$$

where R is the radius of the ring and F is a correction factor, which allows for the non-vertical direction of the tension forces and the asymmetric shape of the meniscus. For stability reasons, the requirement R/r$\rightarrow\infty$ (where R is the ring radius and r is the cross sectional radius of the ring) is not satisfied, which makes the meniscus of the lamella of liquid on the inside of the ring different from that on the outside. Figure 3 shows

schematically how a meniscus of liquid is pulled up above the liquid surface by the ring. Tables of correction factors have been compiled and tabulated by Harkins and Jordan[3]. In order to find the appropriate values of F (see Appendix 1), two parameters, R/r and R^3/V, must be calculated. Values for R and r are specific for the ring employed. In this study R/r was approximately 0.52. The value of V is calculated from the following equation:

$$V = \frac{2L\gamma}{g(D-d)} \tag{2.6}$$

where:

L = ring circumference

γ = uncorrected surface tension

d = density of air saturated with vapor of the liquid

g = gravity constant

D = density of the liquid

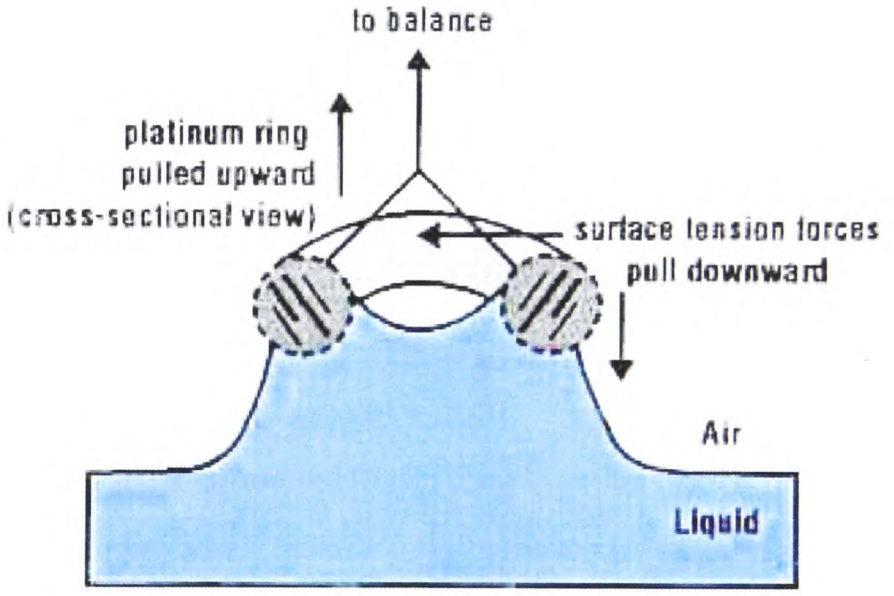


Figure 3. Liquid meniscus being pulled up above the surface by the du Noüy ring.

1.2.2 Wilhemy Plate Method

The Wilhemy plate method uses the same balance as the ring method. In the static plate method the plate is lowered to the surface until its lower edge nearly touches the surface. At this point, the liquid "jumps" onto the edge and sides of the plate (Figure 4). The liquid wets the plate perimeter and increases its effective mass to some maximum value. Assuming the apparatus is balanced before the liquid surface is raised to the contact position, the imbalance that occurs on contact is due to the weight of the entrained meniscus. Since the meniscus is held up by the surface tension on the liquid surface, the

meniscus weight, w, measured by the apparatus can be analyzed to yield a value for the surface tension.

$$w = 2(l + t)\gamma \cos\theta \tag{2.7}$$

where:

l = plate length

t = plate thickness

θ = contact angle formed by the meniscus

γ = surface tension

The method obviously requires a knowledge of the contact angle. This is usually avoided by using the method only for systems for which θ=0, in which case Equation 2.7 becomes

$$w = 2(l + t)\gamma \tag{2.8}$$

The Wilhemy plate method does not require any correction factors.

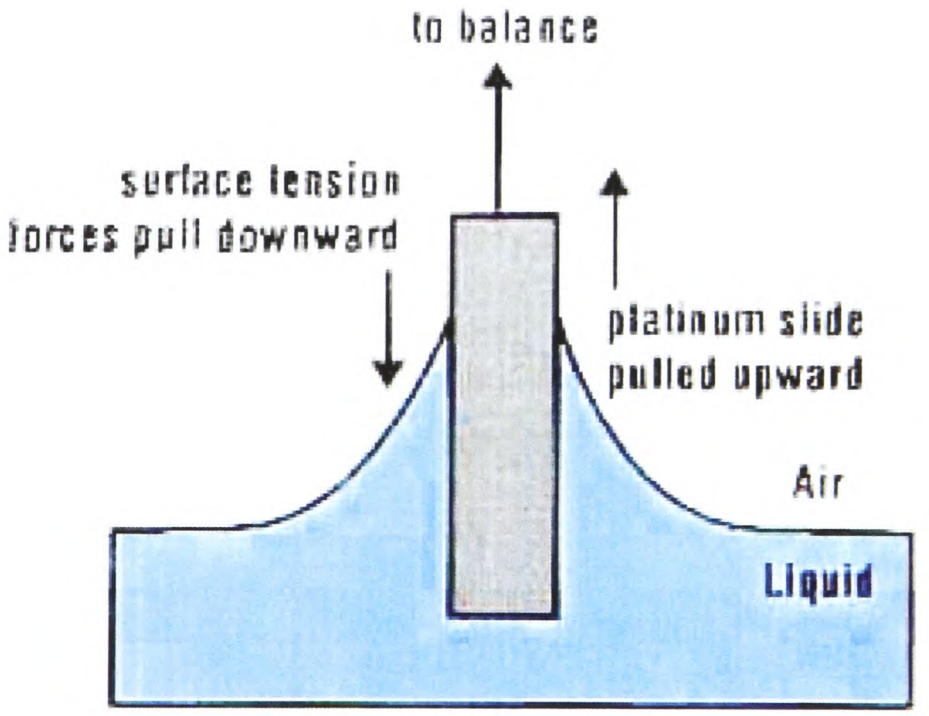


Figure 4. Liquid meniscus being pulled up above the surface by the Wilhemy plate.

APPENDIX 1

Harkins and Jordan correction factors[3]

R^3/V	R/r	R^3/V	R/r	R^3/V	R/r
	52		52		52
0.40	1.016	0.70	0.960	1.00	0.933
0.41	1.013	0.71	0.959	1.01	0.932
0.42	1.010	0.72	0.957	1.02	0.931
0.43	1.007	0.73	0.956	1.03	0.931
0.44	1.005	0.74	0.955	1.04	0.930
0.45	1.002	0.75	0.954	1.05	0.929
0.46	1.000	0.76	0.953	1.06	0.928
0.47	0.998	0.77	0.952	1.07	0.927
0.48	0.995	0.78	0.951	1.08	0.927
0.49	0.993	0.79	0.950	1.09	0.926
0.50	0.991	0.80	0.949	1.10	0.925
0.51	0.989	0.81	0.948	1.11	0.924
0.52	0.987	0.82	0.947	1.12	0.924
0.53	0.985	0.83	0.947	1.13	0.923
0.54	0.983	0.84	0.946	1.14	0.923
0.55	0.981	0.85	0.945	1.15	0.922
0.56	0.980	0.86	0.944	1.16	0.922
0.57	0.978	0.87	0.943	1.17	0.921
0.58	0.976	0.88	0.942	1.18	0.921
0.59	0.975	0.89	0.941	1.19	0.920
0.60	0.973	0.90	0.940	1.20	0.920
0.61	0.972	0.91	0.940	1.21	0.919
0.62	0.970	0.92	0.939	1.22	0.918
0.63	0.969	0.93	0.938	1.23	0.918
0.64	0.968	0.94	0.937	1.24	0.917
0.65	0.967	0.95	0.937	1.25	0.916
0.66	0.965	0.96	0.936	1.26	0.916
0.67	0.964	0.97	0.935	1.27	0.915
0.68	0.963	0.98	0.934	1.28	0.915
0.69	0.962	0.99	0.934	1.29	0.914

2 Neutron Reflectivity – Theory and Measurement

2.1 Introduction

When an electromagnetic wave propagates through a boundary between two dissimilar media having different refractive indices, it can experience refraction, reflection, interference and diffraction. These phenomena result from interaction of the electromagnetic wave with the structure and nature of the media boundaries and, under suitable conditions, they can be exploited to give information about the boundary region. Techniques based on optical phenomena, such as light scattering and interferometry, are extensively used to measure particle size of colloidal systems and the thicknesses of thin films respectively.

Using similar principles, other types of radiation, including X-rays and neutrons, have the potential to be used for material characterization. X-rays have the advantage over visible light that their wavelengths (ranging in wavelength from 10^{-3} to 10nm), are orders of magnitude smaller than that of visible light (400 - 700nm), making them comparable with molecular dimensions. Since interference phenomena are maximized when the wavelength and dimensions of the object being studied are comparable, x-rays are suitable for investigating molecular structure. The interaction of x-rays with matter depends on both the atomic density and atomic numbers, Z_i, of the constituent atoms of the material.

Neutron radiation can be produced to cover a range of wavelengths of 10^{-2} to 3nm, comparable with those obtainable with X-rays. There is a fundamental difference between neutron and electromagnetic radiation in the mechanism by which each interacts with matter. Light and X-rays are both scattered by the electrons surrounding atomic nuclei, but neutrons are scattered by the nucleus itself. This has several consequences, the most important of which is that the strength of the neutron-nucleus interaction not only varies irregularly with Z but may even be quite different for two isotopes of the same element, i.e. two isotopes may scatter neutrons to different extents. Thus, unlike X-rays, neutrons can often differentiate between isotopic species. This opens up the possibility of using selective isotopic substitution to enhance structural resolution and hence boost the

effective resolution of a neutron scattering experiment. The interaction of neutrons with matter is weak and the absorption of neutrons by most materials is correspondingly small. Neutron radiation is therefore very penetrating. The present work is mainly concerned with coherent elastic scattering of neutrons. In coherent scattering the neutrons scattered from different nuclei in the sample retain their coherence and can interfere with each other and hence yield information about the structural arrangement of the atoms. Incoherent elastic scattering can also occur. Here, the scattering from different chemically identical nuclei is not coherent and there are no interference effects. This is particularly marked for protons where neutron scattering has a high probability of being accompanied by a change of spin and hence proton containing samples give rise to strong incoherent scattering. Inelastic neutron scattering also occurs but will not be the concern of this thesis.

The appropriate wavelength range of neutrons for the investigation of the molecular structure of condensed matter has led to the development of a wide range of neutron scattering techniques for this purpose, such as neutron diffraction, small angle neutron scattering, and inelastic scattering, and these have been applied to study a wide range of systems in physics, biology, chemistry, materials science and engineering. However, although Fermi & Zinn[4] showed as early as 1944 that neutrons could exhibit optical properties such as refraction and reflection, the use of neutron reflection was limited until relatively recently. However, it is now a well-established technique for probing interfacial structure and, in this study, the reflection technique has been used to investigate the adsorption of surfactant systems at the air-liquid interface. This chapter describes the theory of neutron reflection, the experimental methods that were used to obtain the neutron reflectivity data presented in this thesis, and the methods for analysing the data.

2.2 Principles of neutron scattering[5,6]

Neutron optical phenomena arise from the coherent elastic scattering of neutrons from the individual nuclei in a sample of condensed matter. This type of scattering is not accompanied by any energy exchange between the neutrons and the medium through which they are travelling and it may be described by the one-body Schrödinger equation as given below

$$\frac{-h^2}{8\pi^2 m}\nabla^2\psi(r)+V(r)\psi(r)=E\psi(r) \qquad (2.9)$$

where $\psi(r)$ is the neutron wavefunction, h is Planck's constant, m and E are the mass and the energy of the neutron respectively, and $V(r)$ is the potential which a neutron at a position $\underline{R}$ experiences due to the presence of a nucleus positioned at $\underline{r_j}$. This potential is usually approximated by a potential with the form of a δ function, which is known as the Fermi pseudo-potential. In fact, the incoming neutron wave will interact with the whole assembly of nuclei, which make up the medium. To a good approximation, the Fermi pseudo-potential for a coherent wave travelling through a medium may be obtained by averaging the potential over all the atoms in the assembly:

$$V(r)=\frac{h^2}{2\pi m}\left\langle \Sigma_j b_j \delta(\underline{R}-\underline{r}_j)\right\rangle \qquad (2.10)$$

The δ function takes the value of unity when $\underline{r_j}$ is equal to $\underline{R}$ and is zero elsewhere, and this is an adequate representation of the very short range of the nuclear forces (10^{-4}-10^{-5}Å) when the wavelength of the neutrons is relatively long (typically 1 - 15Å). The quantity b_j determines the amplitude and phase of the scattering and is referred to as the coherent scattering length of the nucleus located at $\underline{r_j}$. Unlike the corresponding X-ray scattering length, which is always positive and which increases regularly with the number of electrons in an atom, the neutron scattering length varies irregularly across the periodic table and can be either positive and negative, the sign determining the phase change on scattering. Different isotopes of the same element may have quite different neutron scattering lengths, and this is particularly notable in the case of hydrogen and deuterium, which have scattering lengths of opposite signs. This feature, almost more than any other, has been central to the development of neutron scattering techniques as tools for investigating the structure of soft condensed matter, and will be discussed fully in a later section. Table 1 lists the neutron scattering lengths of some of the common elements and those that have been used in this work.

Isotope	Scattering length, *b*, $x10^5$(Å)
H	-3.74
D	6.67
C^{12}	6.65
O^{16}	5.80
N^{14}	9.40
S^{32}	2.85
$Cl^{(35.5)}$	9.58
Na^{23}	3.62

Table 1. Neutron scattering lengths of elements relevant to this thesis[7]

The mean potential, *V*, experienced by a neutron travelling through a medium may be described in terms of the average coherent scattering length density of the medium, ρ

$$V = \frac{h^2 \rho}{2\pi m} \tag{2.11}$$

where

$$\rho = \sum_i n_i b_i \tag{2.12}$$

and n_j is the number density of atom *j* in the medium.

2.3 Neutron Reflection on Flat Surfaces

A neutron incident on a smooth interface between two media may undergo various scattering processes at the interface. These are specular reflection (where the angle of reflection is equal to the angle of incidence), refraction (transmission), incoherent scattering and also multiple coherent scattering. Figure 5 shows the first two of these processes, reflection and refraction.

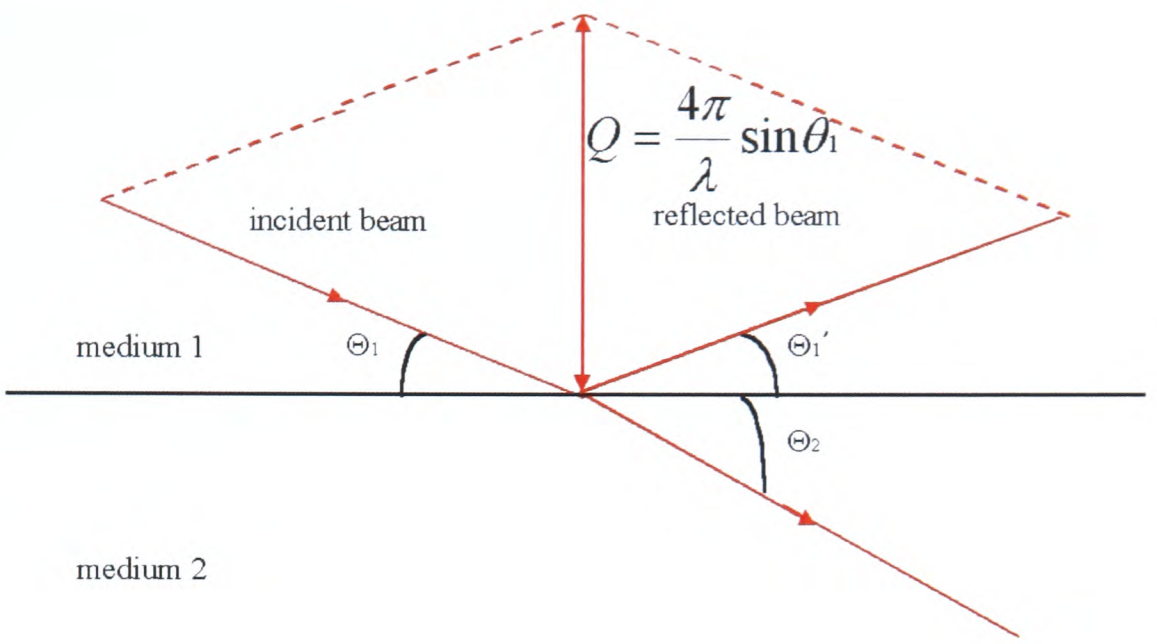


Figure 5. Reflection and refraction at a planar interface between two media.

In neutron experiments it is usually convenient to express the reflectivity in terms of the momentum transfer, which is normal to the interface, as depicted in Figure 5. The momentum transfer Q is given by

$$Q = 2k\sin\theta = \frac{4\pi\sin\theta}{\lambda} \tag{2.13}$$

Each medium can be characterized by a neutron refractive index, n, which is the ratio of the neutron velocity in vacuum to that in the medium

$$n^2 = \frac{2m\lambda^2}{h^2}\left(E - V_j\right) \tag{2.14}$$

where λ is the neutron wavelength. E is the energy of the neutron given by the de Broglie relation,

$$E = \frac{h^2}{2m\lambda^2} \tag{2.15}$$

The potential, V(j), experienced by a neutron in medium j is given by Equation 2.11. Equations 2.11 and 2.15 may be introduced into Equation 2.14 to yield an expression for n_j:

$$n_j^{\,2} = 1 - \frac{\rho_j \lambda^2}{\pi} \tag{2.16}$$

As ρ_j is small, the expression above can be expanded as a power series to give the result:

$$n = 1 - \frac{\rho_j \lambda^2}{2\pi} \tag{2.17}$$

The reflectivity of a simple interface depicted in Figure 5 may be obtained using the Fresnel formula. In this case, the reflectivity, r, is given by:

$$r = \frac{\sin\theta_1 - n\sin\theta_2}{\sin\theta_1 + n\sin\theta_2} \tag{2.18}$$

Since θ_2 can be expressed in terms of n and the angle of incidence, θ_1, and n can also be expressed in terms of the scattering length densities of the two media ρ_1 and ρ_2 and the neutron wavelength, Equation 2.18 can be used to calculate the reflectivity of an interface, given the scattering length densities of the two media. Alternatively, if the reflectivity is measured, Equation 2.18 can be used to determine the scattering length density of one of the media, if the other is known.

A neutron passing from a medium of higher refractive index to a medium of lower refractive index will be totally reflected when the grazing angle is less than the critical angle, θ_c, which may be calculated using Snell's Law

$$\cos\theta_c = \frac{n_1}{n_2} \tag{2.19}$$

Since the value of the refractive index is typically extremely close to unity, the critical angle is always low. From Equation 2.17 the critical angle at the air-water interface is related simply to the scattering length density of the aqueous solution via the relation

$$\theta_c = \lambda\sqrt{\frac{\rho_j}{\pi}} \tag{2.20}$$

2.4 Neutron Reflectivity of Stratified Media

The previous sections showed how the reflectivity of a planar interface between two media is related to the neutron scattering length densities of the media, assuming that the interface itself is of zero thickness and that the compositions of each of the media are invariant with distance between the interface and the bulk. This section is concerned with the determination of the composition of interfacial layers, such as that which would be formed when surfactant molecules adsorb at an air-liquid interface.

The reflectivity in multi-reflecting boundary systems can be calculated by two distinct methods, the Optical Matrix Method[8] and the Kinematic Approximation[9]. The Optical Matrix Method provides a convenient form to calculate exactly the neutron reflectivity profile from a structural model of the interface. This has been extensively used in the analysis of data from a wide range of different thin films and multilayers. An alternative approach is the Kinematic or Born Approximation which originates from classical scattering theory. This is particularly effective for thin layers such as adsorbed monolayers, and at glancing angles significantly larger than that for total reflection. The Kinematic Approximation used with partial isotopic labelling has proved to be a powerful method of studying adsorbed monolayers of surfactants. All the reflectivity data presented in this thesis have been treated using the first of these two methods, the Optical Matrix Method, which will now be described. The Kinematic Approximation method has been described in detail elsewhere[9,10].

In optics a number of matrix methods exist for calculating reflectivity profiles for arbitrary interfacial profiles divided into a series of steps. In the case of a single interface,

as depicted in Figure 6, the reflected signal is a summation of the wave which has been reflected at the upper interface, and those which have been refracted at the upper interface, then reflected at least once within the layer and refracted out into the upper medium again. These waves will naturally have traveled a longer path length than the wave which has been reflected from the upper interface, and this results in the refracted waves being phase shifted relative to the primary reflected wave, the magnitude of the phase shift being dependent on the thickness of the layer and the angle of refraction, θ_2. This phase shift will therefore result in an interference pattern which will give information about the structure of the adsorbed layer.

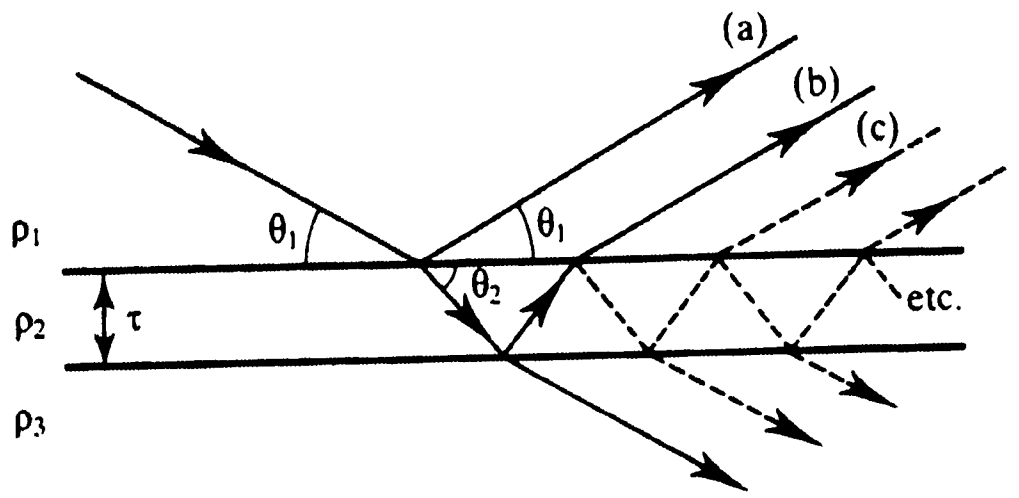


Figure 6. Reflection and refraction at a single layer adsorbed at the interface between two media

Using this approach, the overall reflectivity of the interfacial region, R, is given by

$$R = \left| \frac{r_{12} + r_{23} e^{2i\beta}}{1 + r_{12} r_{23} e^{2i\beta}} \right|^2 \qquad (2.21)$$

where r_{ij} is the Fresnel coefficient of reflection at the ij interface, and β is the phase difference between any two successive reflected rays, β being given by

$$\beta = \frac{2\pi k_2 d \sin\theta_2}{\lambda} \qquad (2.22)$$

where k_2 is the magnitude of the wavevector of the refracted beam, θ_2 is the angle of refraction, d is the layer thickness, and λ is the neutron wavelength. Combining with Equation 2.21 gives

$$R = \frac{r_{12}^2 + r_{23}^2 + 2r_{12}r_{23}\cos 2\beta}{1 + r_{12}^2 r_{23}^2 + 2r_{12}r_{23}\cos 2\beta} \tag{2.23}$$

In a multi-layer system, the reflection and refraction behaviour of a given layer, j, may be represented by a characteristic matrix $[M_j]$, which results from the application of Maxwell's equations and the appropriate boundary conditions to the system. $[M_j]$ is given by

$$\left[M_j\right] = \begin{bmatrix} \cos\beta_j & \frac{-i}{q_j}\sin\beta_j \\ iq_j \sin\beta_j & \cos\beta_j \end{bmatrix} \tag{2.24}$$

where q_j and β are as defined previously. For a series of n layers, the product of these characteristic matrices, $[M]$, is given by

$$[M] = [M_1]x[M_2]x....[M_n] \tag{2.25}$$

The reflectivity may then be expressed in terms of the elements of $[M]$

$$R = \left| \frac{(m_{11} + m_{12}q_{n+1})q_0 - (m_{21} + m_{22}q_{n+1})}{(m_{11} + m_{12}q_{n+1})q_0 + (m_{21} + m_{22}q_{n+1})} \right|^2 \tag{2.26}$$

where q_0 and q_{n+1} are the values of q for the upper and lower media respectively.

Two major difficulties arise in interpreting real profiles using the Optical Matrix Method. First, a real interface may require many layers to describe it accurately and secondly, in a complex layer scheme it becomes increasingly difficult to relate the component scattering length densities of isotopically different but chemically identical species. The former of

these problems may be solved either by the introduction of roughness[11] or by using a matrix with linear gradations in scattering length density between successive layers[12].

2.5 Neutron Reflection Experiments

The essence of a neutron reflectivity experiment is to measure the neutron specular reflectivity, R, as a function of the momentum transfer perpendicular to the reflecting surface, Q. R and Q are given by

$$R = \frac{I}{I_0} \tag{2.27}$$

where I is the intensity of the reflected neutron beam and I_0 is that of the incident beam, and

$$Q = \frac{4\pi \sin\theta}{\lambda} \tag{2.28}$$

where θ and λ are respectively the incident angle of grazing incidence and the wavelength of the incoming neutrons. Reflectivity data are generally displayed as a plot of log R versus Q. There are two ways of varying Q in the experiment. Using a constant wavelength reflectometer, the reflectivity of a well collimated, monochromatic beam of neutrons is measured as a function of the angle of incidence, θ. Alternatively, a fixed-angle reflectometer may be used, in which case, Q is varied by varying the wavelength at the fixed incident angle. The neutron reflectivity data presented in this thesis were obtained on the SURF fixed-angle reflectometer at the ISIS neutron source at Didcot, Oxfordshire (Figure 7). The purpose of this section is to provide a background to the instrument, to describe how it functions and to give some of the details of the execution of the experiment. In addition, the main features of the method of neutron generation will be examined.

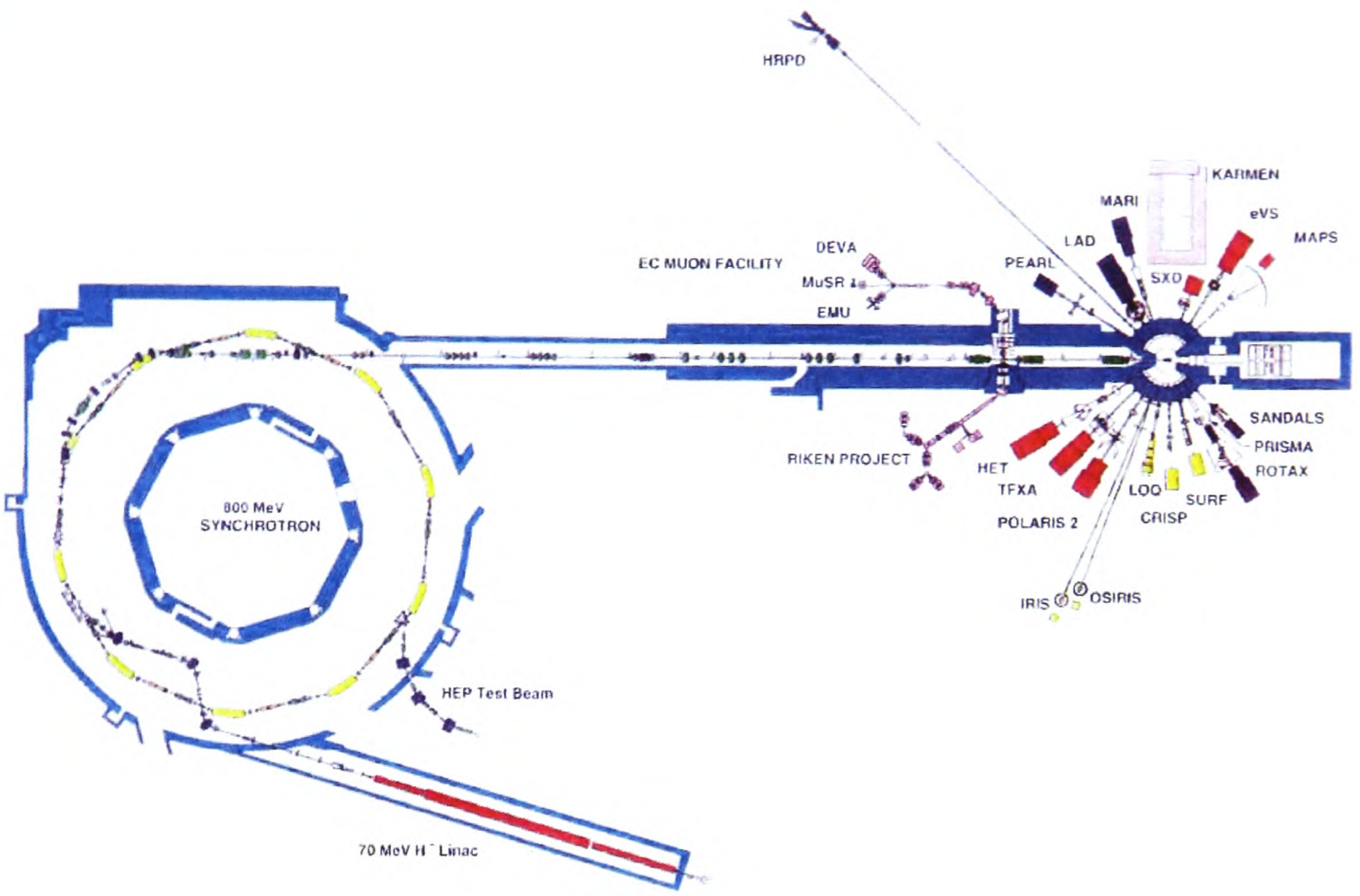


Figure 7. ISIS facilities at Rutherford Appleton Laboratories

2.5.1 *The SURF Reflectometer*[13]

The neutron production process at the spallation source, ISIS at the Rutherford Appleton Laboratory, Didcot, is depicted in Figure 8.

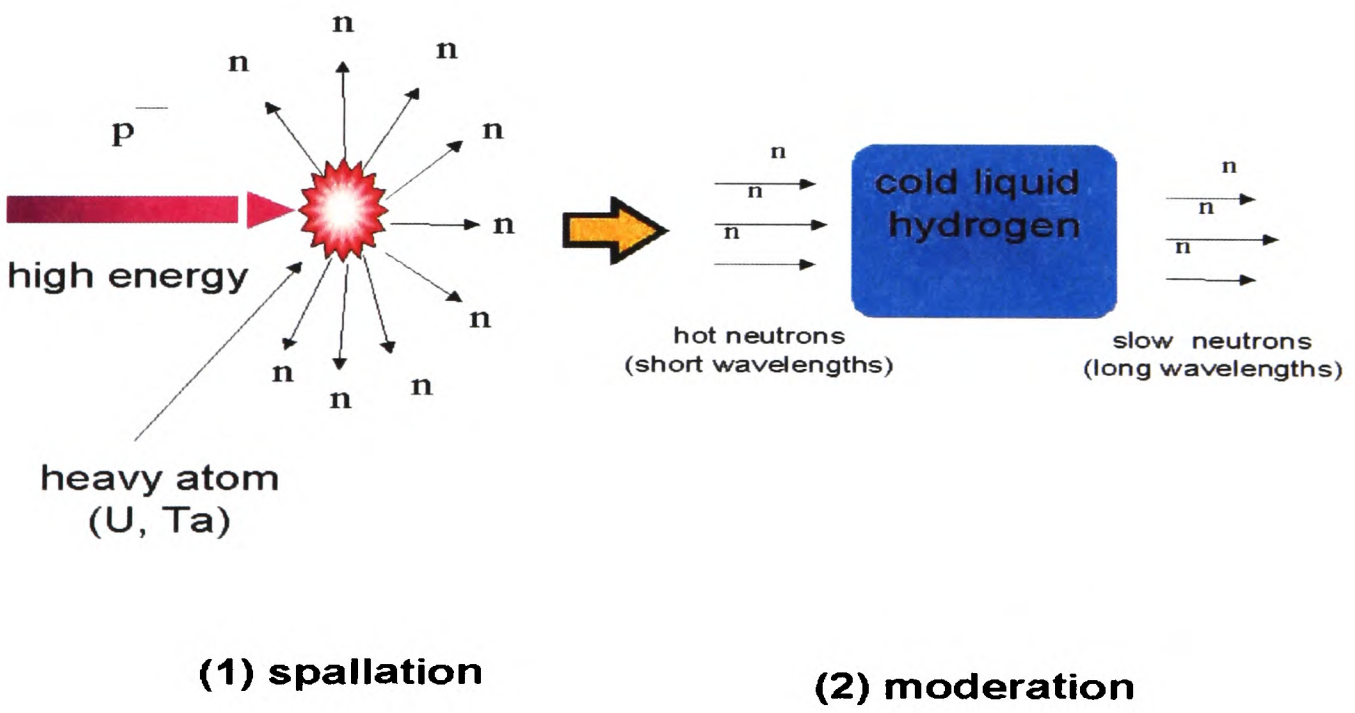


Figure 8. Generation of neutrons in a spallation source

First, H^- ions are produced by an ion-source and accelerated in a linear accelerator. Before being injected as protons and then accelerated in a synchrotron, the ions are stripped of electrons by the action of a very thin aluminum foil and this produces a circulating beam of protons. A pulse of high-energy protons from the synchrotron is then fired at the uranium or tantalum target causing disintegration of the nuclei into neutrons. The synchrotron at ISIS is 25m in diameter and accelerates $25x10^{13}$ protons per pulse up to 800MeV at a pulse rate of 50Hz. The neutrons generated by this spallation process are of very high energy and are slowed to suitable energies for use in condensed matter experiments by passing them through hydrogenous moderators (water, liquid methane or liquid hydrogen). The resultant pulsed white beam of neutrons, which contains a range of wavelengths, is fed to the various instruments at the facility.

Following moderation, the beam passes through a "chopper", which is a large rotating metal disc. The speed of the chopper is synchronized with the initial proton pulse so that only neutrons with a given velocity range, which corresponds to the desired wavelength range, are transmitted. For the neutron reflectometer SURF, a wavelength range that will give the desired momentum transfer range (typically $0.05 \leq Q \leq 0.65$ Å^{-1}) is selected. The SURF experiments make use of "time of flight" (TOF) analysis of the neutron beam, for which it is necessary to know with accuracy the velocity of neutrons in the beam. This is achieved essentially by "time stamping" each pulse of neutrons as it leaves the chopper and then measuring its time of arrival at the detector. Very slow neutrons from a given pulse may arrive at the detector at the same time as fast neutrons from the next pulse and to prevent this frame overlap contamination frame overlap mirrors, which are nickel coated mirrors designed to reflect long wavelength neutrons out of the beam, are inserted in the beam to remove the longer wavelength neutrons.

A schematic diagram of the SURF reflectometer is shown in Figure 9. The beam arriving at SURF passes through a set of collimating slits, which are adjusted to a suitable width and height depending upon the nature of the sample. These slits control the illumination of the sample and have to be set carefully to prevent over-illumination, which would result in contamination of the reflectivity profile, by scattering from the sample holders. Under-illumination, on the other hand, would waste flux by generating only a low signal.

The collimated beam passes through a low efficiency lithium gas scintillation detector, which characterizes the grazing neutron beam before it impinges on the sample. The incoming neutron beam is aligned at a fixed glazing angle to the horizontal. The experimental arrangement is extremely flexible and liquid surfaces, solid thin films, multilayers, liquid-solid and liquid-liquid interfaces can all be measured in the angular range 0.2 to 3.0°. Once reflected from the sample, the beam then passes through two further collimating slits to ensure that no off-specular reflection is detected before it reaches the single well-shielded He^3 gas detector. Since neutrons are uncharged particles they cannot be detected directly but their reaction with He^3 gives rise to an energetic ion pair which can be detected using a conventional electrode-type set-up. The time of arrival of each reflected neutron at the detector is determined and hence its velocity is characterized. The wavelength of the neutrons arriving at the detector cannot be determined directly. It is however essential to be able to calculate λ in order to calculate Q. On SURF, λ is calculated from the neutron velocity which is determined by the amount of time from the initial pulse that it takes a neutron to arrive at the detector. This is the reason the method is called "time-of-flight".

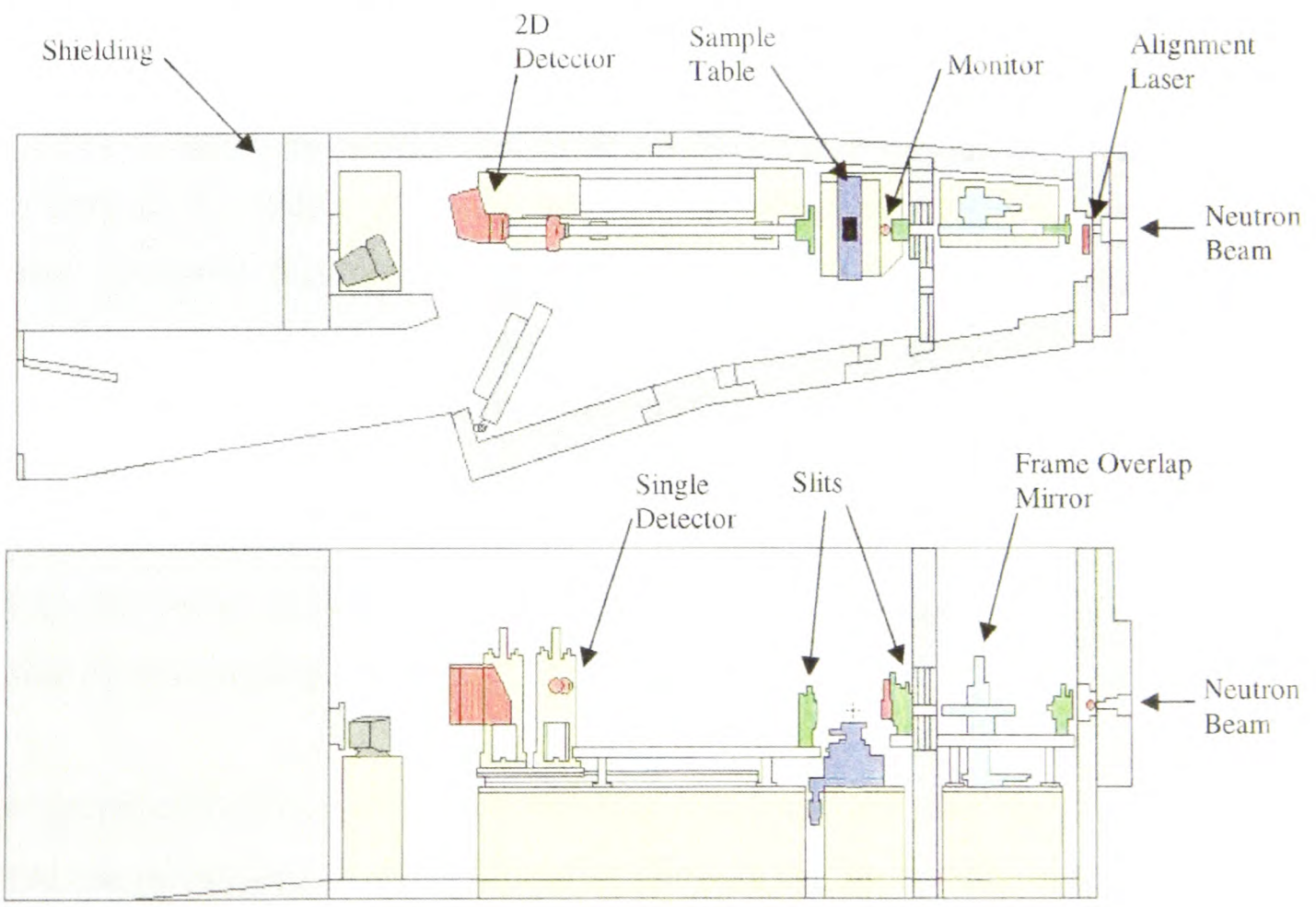


Figure 9. Schematic diagram of the SURF reflectometer

2.5.2 *Air-solution neutron reflection experimental details*

All of the air-liquid reflectivity measurements were carried out with the solutions contained in a series of 25mL troughs. A schematic diagram of one of these troughs is shown in Figure 10. The trough is made from a solid block of Teflon, which is machined out to form a shallow trough (about 5 mm deep) in which the sample is contained during the experiment. Teflon is a suitable material for holding aqueous samples since it does not readily wet, and a meniscus proud of the trough edges can therefore be formed relatively easily. This reduces the possibility of neutron scattering from the sample holder. In addition Teflon is readily cleaned of impurities. For these experiments the troughs were cleaned by soaking in an alkaline detergent solution (Decon). They were then gently scrubbed with a soft brush and rinsed thoroughly with UHQ water and dried. The Teflon central portion of each trough is placed on an aluminum base and secured with bolts. Each trough fits into an outer box in its own numbered compartment. Once in the housing, each trough was filled with the sample solution. Any air bubbles present in the solution were removed by suction. The sample solutions were then aligned with respect to the neutron beam using a laser guide, which had been previously aligned to follow the same path as the beam. The vertical and horizontal movement of the outer container is computer controlled. The outer box was positioned horizontally so that the beam would fall in the middle of the sample. The sample height was then adjusted so that the reflected laser beam hit the middle of slits S3 and S4, which signified that the sample was correctly aligned. Following final alignment, the lids of each trough were locked in place and the lid of the outer box replaced. Each trough compartment had an O-ring sealed lid to prevent loss of solution by evaporation or contamination of D_2O containing samples with H_2O from the atmosphere, and quartz windows at either end to allow the passage of neutrons in and out of the housing. The temperature of each trough could be controlled individually by a combination of heating each sample compartment directly, as well as heating the surrounding housing.

After preparation of samples, the low efficiency detector and the supermirror, which were moved out of position to allow the alignment with the laser guide, were placed back in position. The measurements are controlled by a computer, which can follow a set of preset sequences in a command file.

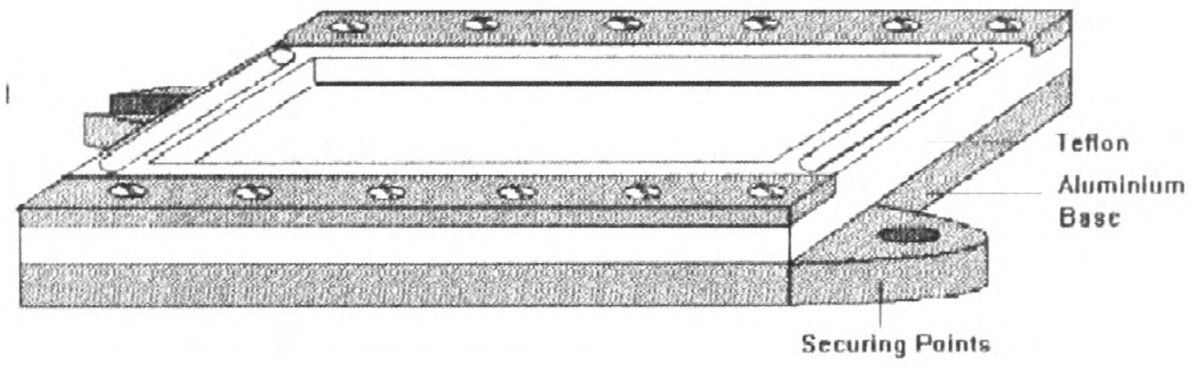


Figure 10. Schematic diagram of trough used in air-liquid experiments.

2.5.3 Data processing of reflectivity profiles

Before analysis of the reflectivity measured as a function of Q, the data need some corrections. Two main factors contribute to a difference between the raw data and the true neutron reflectivity and these are the scale factor and the background subtraction.

The scale factor is used to correct the effects of the different monitor and detector efficiencies and the effect of the slit sizes on the detected signal. The most convenient method for determining the experimental scale factor is to normalize the apparent reflectivity to the neutron reflectivity of a standard surface such as D_2O. For each set of experiments performed on SURF, the measured profile of D_2O was compared with the calculated theoretical reflectivity profile of the air/D_2O interface. A correction factor was applied to the measured profile such that the two profiles matched each other in the low Q range, and this factor was taken to be the scale factor. Since the reflectivity profiles measured on SURF were collected at constant instrument geometry (i.e. at a fixed angle with constant slit sizes) this scale factor should be constant across the Q range. Sample reflectivity profiles were then divided by the same scale factor.

The available Q range is important when considering the range of dimensions that can be probed, and is determined not only by instrumental but also by sample effects. The theoretical minimum and maximum values of Q are ~3×10^{-3}Å^{-1} and ~0.65Å^{-1} respectively. Q_{max} is often, however, sample limited because the reflectivity falls off typically as Q^{-4} (according to Fresnel's law) and even faster for a imperfect surface. Unfortunately, the background scattering, which is generally approximately constant with Q, is quite large. The combination of these two effects limits the range of Q over which

the reflectivity can be accurately measured. The level of the background is often dominated by sample rather than instrumental contributions. The contribution from the sample, in general, arises from incoherent scattering, which is approximately isotropic and independent of Q. In general the level of incoherent scattering adds between 10^{-6} and 10^{-5} to the scaled reflectivity across the Q range. Therefore at low Q, the contribution of the incoherent scattering to the measured profile is negligible, but its contribution increases as Q increases until at around a Q of 0.25Å^{-1} the measured signal arises mainly from incoherent scattering. The absolute intensity arising from neutrons incoherently scattered from the sample cannot be measured directly during a reflectivity experiment. The level of incoherent scattering must instead be estimated for each individual sample, since different samples may contain different chemical or isotopic species and give rise to different levels of incoherent scattering.

For the reflectivity profiles measured on SURF the amount of scattering at high Q was used to estimate the background scattering and this value was subtracted from the whole data set. Obviously this method of background subtraction is subject to error. Whilst at low Q, the data is likely to be subject to negligible error as result of the estimated background subtraction, the relative error increases as Q increases, and this factor must be taken into consideration in the data analysis stage.

2.5.4 Data analysis using the Optical Matrix Method

In this study, all the neutron reflectivity data were analysed using the Optical Matrix Method, which assumes that the interface can be described in terms of a number of discrete layers of different scattering length density and thickness. The reflectivity of this model interface can then be calculated exactly from these parameters, compared with the measured profile and the various parameters adjusted in order to achieve a good fit between the measured data and calculated profiles. Essentially this is a trial and error approach, with the only constraint on the choice of model being that it must be physically reasonable, given the volumes and scattering lengths of the possible components which could be present in the interfacial region. The data presented in this thesis were fitted with the aid of AFIT[14], a computer program which uses the basic Optical Matrix Method to

calculate the reflectivity for a given model and then superimposes the calculated and measured reflectivities for comparison.

The determination of the amount of surfactant adsorbed at the air-solution interface using neutron reflection is best done using "null reflecting water" (NRW) and partially or fully deuterated surfactant. Since protons and deuterons scatter neutrons with opposite phase, it is possible to generate an isotopic composition of water such that its scattering length density is the same as that of air and hence its surface will not reflect neutrons. Any neutrons reflected from the surface of such a solution can then only be due to adsorbed surfactant. The parameters usually obtained from fitting the data from a null reflecting solution are the scattering length density of the layer ρ, and its thickness, τ. With these data the area per molecule, A, can be calculated from

$$A = \frac{b}{\rho\tau} \tag{2.29}$$

where b is the scattering length of the surfactant. The adsorbed amount, or surface excess, Γ, is given by

$$\Gamma = \frac{1}{AN} \tag{2.30}$$

where N is Avogadro's number.

3 Purification and Characterization of Surfactants

3.1 Introduction

Any precise study on the physical properties of surfactant solution requires special attention to the presence of contaminants. Minor impurities may have a very large effect on the surface tension of the solution of interest. This is particularly true for highly surface-active impurities, which even at very low concentrations may adsorb preferentially at the interface, lowering the surface tension. Impurities with surface activity equal to that of the surfactant, on a weight basis, do not introduce significant error, and those less surface active or having a negative surface activity would have to be present in large amounts to produce a significant effect. Impurities may have several origins, such as from the synthesis, from chemical degradation of the surfactant or from contamination. The most difficult ones to eliminate are the by-products resulting from degradation of the surfactant molecule. For example, sodium dodecylsulfate (SDS) can undergo hydrolysis producing free dodecyl alcohol, which is much more surface active than SDS. Hydrolysis is more rapid at higher temperatures and it is always advisable to store the dry surfactant samples in a fridge, keeping them in sealed containers to prevent take-up of moisture. For similar reasons, surfactant solutions, especially of ionic surfactants, should not be stored, but prepared and used in the same day. Impurities resulting from accidental contamination during handling are avoided by using rigorously cleaned equipment and ensuring that the quality of the water used for solution preparation is of the highest quality.

The selection of a suitable analytical method to test the purity of a surfactant sample is very important. There are many analytical methods capable of identifying other than standard impurities at very low concentrations, whereas the problem may be the presence of surface-active contaminants at concentrations high enough to disturb surface properties. The surface tension measurement is usually a very effective method to check for the purity of a surfactant sample. A minimum in the surface tension log(concentration) curve close to the CMC is a well known marker of the presence of a surface active impurity. Thus, whenever a minimum, or dip, in surface tension versus concentration is found, the surfactant sample contains an impurity of higher surface

activity than the surfactant itself. As shown in Figure 11, at low concentrations the air-water interface is dominated by highly surface-active impurity, generating a false lower value of the surface tension. However when the solution concentration reaches the CMC, the impurities are solubilised into the micelles, restoring the surface tension to its correct higher value. The absence of a dip in the surface tension curve, however, cannot be taken as proof of purity.

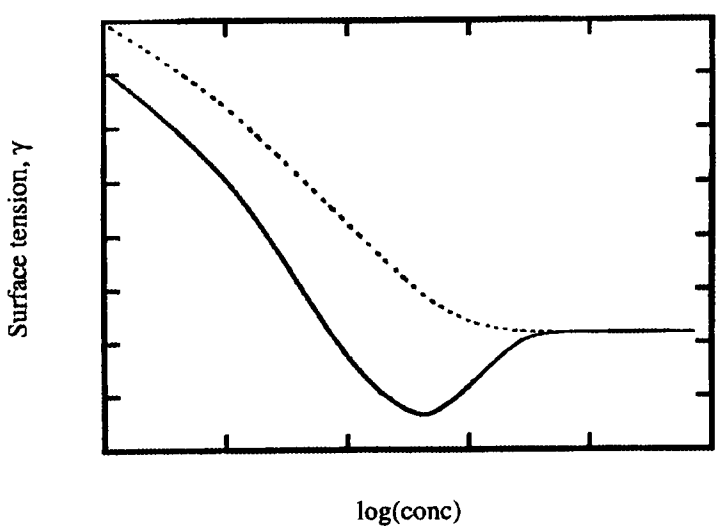


Figure 11. Surface-active impurities in a surfactant sample cause a minimum in the curve of surface tension against the log of concentration.

The dynamic surface tension[15] of the solution has also been found to be an effective method for identifying impurities. The surfactant is present at a much higher concentration than the impurity and is therefore adsorbed much faster than the latter so that the time to return to an equilibrium surface tension after rapid expansion of the surface should be much shorter for a "pure" surfactant solution than for one containing impurity. Lunkenheimer *et al.*[16] have proposed a technique for removing highly surface active impurities by repeatedly sucking off the surface after compression. This removes the surface, which is enriched in impurities along with a thin layer of the solution and seems to be effective with very dilute systems. The relative purity of a surfactant may be assessed by comparison with previously published results, although care is always needed in the selection of appropriate data.

Purification methods for surfactants described in the literature vary greatly and are mostly based on recrystallization, solvent extraction, fractional distillation, adsorption

chromatography, foam purification and filtration. The most suitable one will depend on the type and amount of both surfactant and impurity. In some cases, the combination of different methods may be the only effective way of ensuring surface purity.

In this study, considerable effort has been made to ensure as far as possible that all surfactants are of the highest standard. The methods used to purify and to characterize the various EPE copolymers and surfactants for the surface tension and neutron experiments, are described in this section. For the latter experiment, the surface activity of both protonated and deuterated analogues in aqueous solutions are also compared to ensure that it is valid to compare reflection data from different isotopes.

3.2 Purification of monodisperse EPE copolymers

The EPE copolymers were prepared by Dr R.K.Thomas using anionic polymerisation of polypropylene glycol with ethylene oxide in the presence of a potassium-based catalyst following, with some modifications, a procedure outlined by Altinok *et al.*[17]. Fully protonated EPE copolymers were prepared by polymerising protonated ethylene oxide on to a protonated polypropylene glycol sample, while the deuterated PEO chain analogues were obtained by polymerising fully deuterated ethylene oxide on the same starting protonated polypropylene glycol. The impurity profile of EPE copolymers is complex. There may be free PEO and PPO, as well as EPE molecules of various molecular weights and diblocks of EO and PO. PEO homopolymer is not surface active and has been found not to affect the surface tension of EPE copolymers[18]. Unlike PEO, free PPO homopolymers are highly surface active and residues of PPO homopolymer would be expected to produce a minimum in the surface tension curve of EPE copolymer solutions. Hexane is a good solvent for PPO but a poor one for PEO and has been used successfully to remove PPO from EPE copolymer samples[19]. The separation of undesired triblocks and diblocks from the main EPE copolymers is not a simple operation, although the surface behaviour of some commercial samples can be refined by fractionating them by gel permeation chromatography[20]. Avoiding their formation in the first place with an optimised synthesis procedure would, however, seem to be a better method.

3.2.1 *Purification of block copolymers*

Both protonated and deuterated analogues of EPE copolymers were washed with hexane to remove residual amounts of free PPO homopolymer and other hydrophobic impurities. The EPE copolymer samples were dissolved in warm hexane, and the solution allowed cooling down. The precipitated polymer was isolated and again dissolved in warm hexane for a further purification step. The collected precipitate was thoroughly dried under vacuum.

3.2.2 *Characterization of block copolymers*

The samples of EPE copolymers were characterised by gel permeation chromatography (GPC). The GPC system consisted of a 1x30cm Mixed-E column (Polymer Laboratories) eluted by THF at 37°C and a flow rate of 1ml/min. The sample was dissolved in THF at a concentration of 1mg/mL, with emerging polymer detected by a differential refractometer. Calibration was carried out with a series of poly(oxyethylene) samples of known molar mass, so that the derived molar mass are relative to poly(oxyethylene). The GPC results are listed in Table 2.

EPE Copolymer	Composition	MW g mol^{-1}	PPO Chain MW g mol^{-1}	PEO Chain MW g mol^{-1}	X_{EO} %	PPO/PEO	M_w/M_n	M_n g mol^{-1}	M_p g mol^{-1}
h-EPE 3000-14	$E_{23}P_{52}E_{23}$	5100	3000	2100	41	1.1	1.03	4892	5048
d-EPE 3000-14	$E_{23}P_{52}E_{23}$	5200	3000	2200	42	1.1	1.03	4971	5048
h-EPE 3000-21	$E_{44}P_{52}E_{44}$	6900	3000	3900	57	0.6	1.03	6518	6939
h-EPE 2000-14	$E_{23}P_{35}E_{23}$	4100	2000	2100	51	0.8	1.07	3595	3964
h-EPE 1250-14	$E_9P_{22}E_9$	2100	1250	850	40	1.2	1.04	2022	2075
d-EPE 1250-14	$E_9P_{22}E_9$	2150	1250	900	42	1.2	1.03	2042	2115
Pluronic P105	$E_{37}P_{56}E_{37}$	6500	3250	3250	50	0.8	1.18	4605	6053

Table 2. Molecular characteristics of the studied EPE copolymers. M_w/M_n, M_n and M_p determined by GPC.

Apart from EPE 2000-14, all the samples had a much smaller polydispersity than the commercial Pluronic P105. The GPC chromatogram peaks are shown in Appendix 2. The sample of Pluronic P105 was supplied by BASF and used as received.

The surface tension of the solutions of the various EPE copolymers was measured at 25°C using the Du Noüy ring method and the curves are presented in Figure 12. No minimum was observed in the vicinity of the CMC for any of the curves for the monodisperse EPE copolymers, but it was present in the curve of Pluronic P105, as shown in Figure 13.

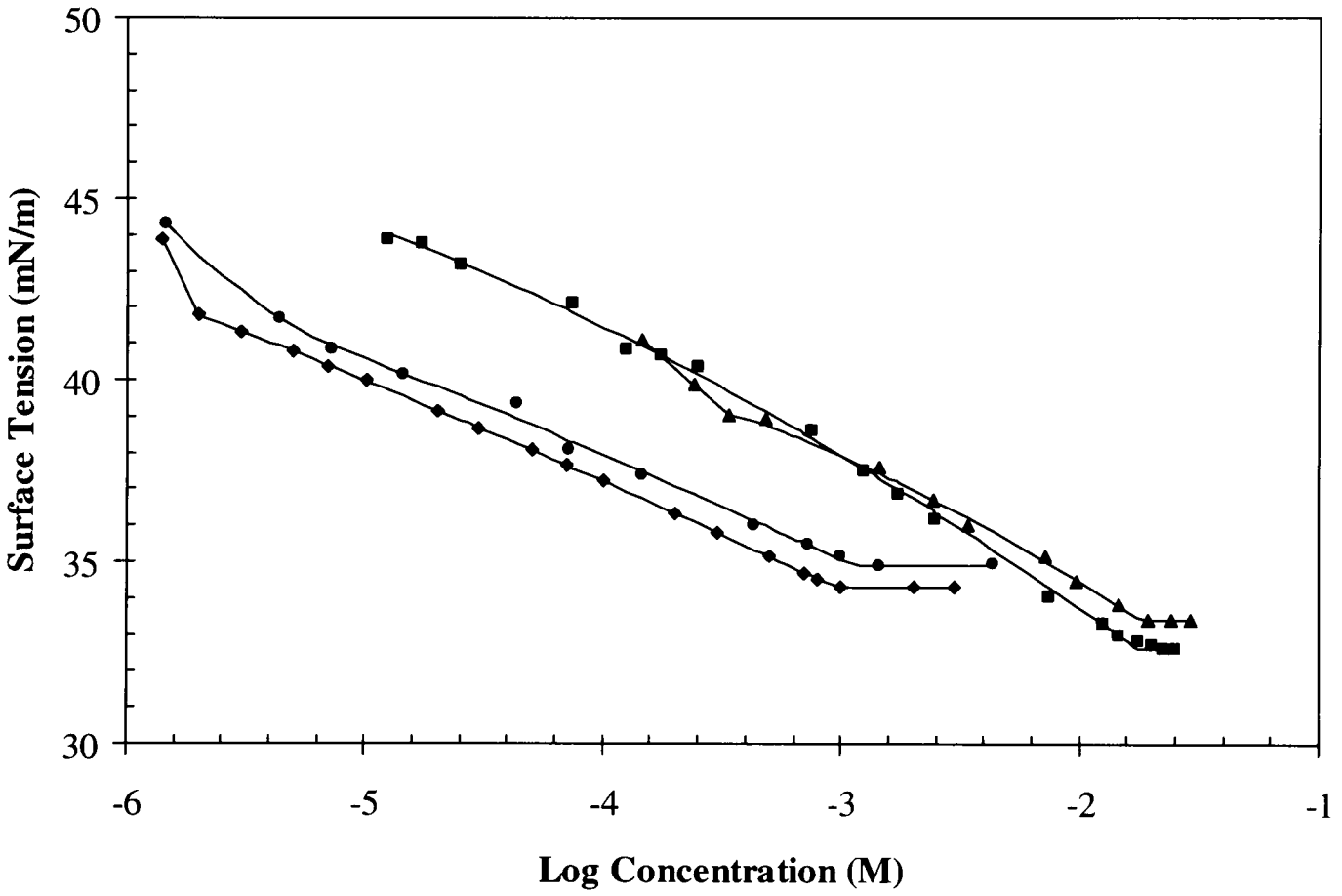


Figure 12. Surface tension against the log of the concentration for solutions of EPE copolymers at 25°C: h-EPE 1250-14 copolymer (▲); h-EPE 2000-14 copolymer (■); h-EPE 3000-21 copolymer (●); h-EPE 3000-14 copolymer (♦).

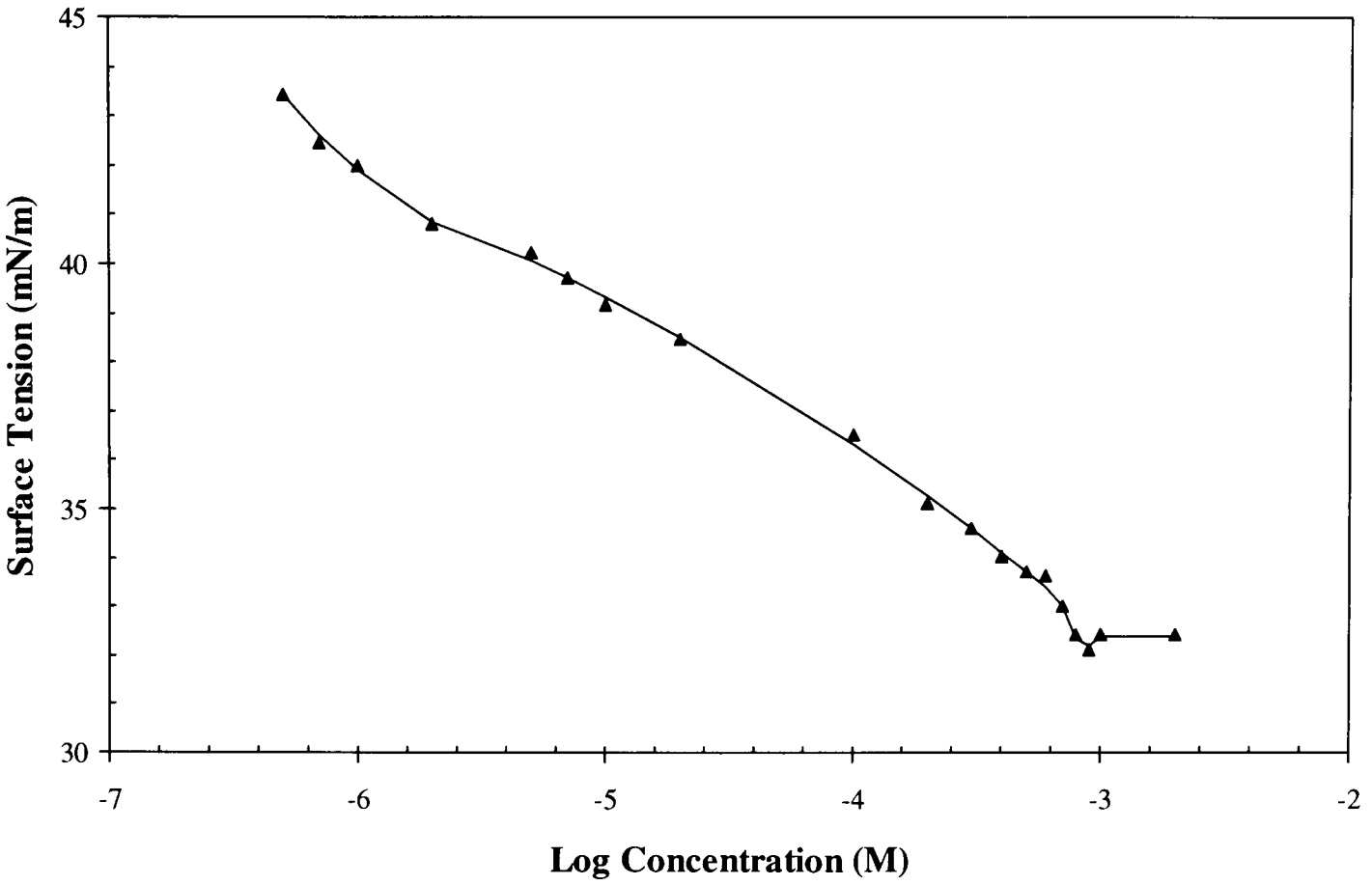


Figure 13. Surface tension against the log of the concentration for aqueous Pluronic P105 measured at 25°C using the Du Noüy ring method.

The surface tensions of aqueous solutions of both fully protonated and deuterated PEO chain analogues for EPE 3000-14, h-EPE 3000-14 and d-EPE 3000-14, were measured at 25°C. Both copolymers showed very similar surface activity properties (Figure 14). All the physical parameters, CMC, surface excess at saturation (Γ_{sat}) and area per copolymer molecule (A), for both analogues were found to be comparable, as shown in Table 3.

Copolymer	CMC (M)	γ_{min} (mN/m)	Γ_{sat} (mol/cm^2)	A (Å^2)
h-EPE 3000-14	9.5×10^{-4}	34.3	5.4×10^{-11}	308
d-EPE 3000-14	1.0×10^{-3}	34.9	5.2×10^{-11}	321

Table 3. Properties of aqueous solutions of EPE 3000-14 copolymers obtained from surface tension measurements at 25°C.

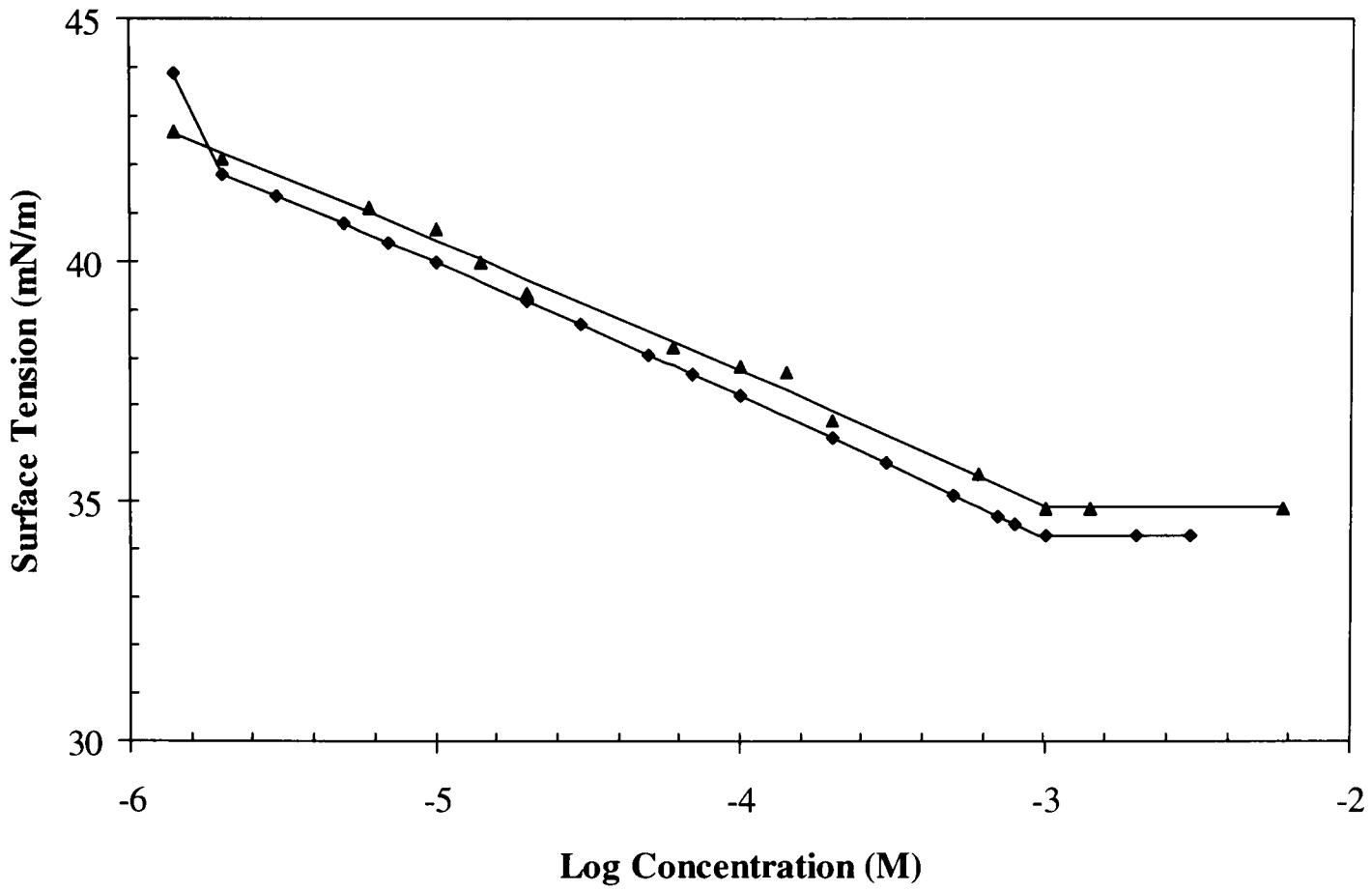


Figure 14. Surface tension against the log of the concentration for solutions of both analogues of monodisperse EPE 3000-14 copolymer, fully protonated (♦), and PEO chain deuterated (▲), measured at 25°C using the Du Noüy ring method.

3.3 Purification of Sodium n-Dodecylsulfate (SDS)

The protonated SDS was purchased from Polysciences Inc, as 99% pure, and is abbreviated as h-SDS. The basic sample of the deuterated analogue, abbreviated as d-SDS, was prepared by Dr R.K.Thomas in Oxford. Before use, both protonated and deuterated SDS samples were purified according to the procedure described below. Traces of dodecanol are the major concern when working with SDS and the purity of the samples was assessed by surface tension measurements.

3.3.1 Purification of SDS

SDS crystals were dissolved in boiling ethanol. The solution was then left standing to crystallise initially at ambient temperature and then in an ice bath. Following cooling the crystals were filtered off and washed with cold distilled ethanol. The collected crystals

were again dissolved in ethanol and the whole recrystallization process was repeated twice. At the end of the process, the crystals were dried under vacuum. The solutions of SDS were prepared immediately before any experiments. Samples of recrystallized SDS when not in use were kept under constant refrigeration in sealed vials.

3.3.2 Characterization of SDS

After recrystallization both samples of SDS were tested for purity by surface tension. The curves of surface tension plotted against the log of the concentration are shown in Figure 15.

Surfactant	CMC (M)	γ_{1mM} (mN/m)	Γ_{sat} (mol/cm^2)	A (Å^2)
h-SDS	$7.9x10^{-3}$	67.7	$3.4x10^{-10}$	48
d-SDS	$7.9x10^{-3}$	67.9	$3.8x10^{-10}$	44

Table 4. Properties of aqueous solutions of h-SDS and d-SDS obtained from surface tension measurements at 25°C.

Neither of the curves for d-SDS and h-SDS exhibited a minimum in the vicinity of the CMC and the two species had similar surface activities. The CMC value found here, $7.9x10^{-3}$M, is within the range of the literature values, $8.1x10^{-3}$M reported by Lu *et al.*[21] and $7.9x10^{-3}$M reported by Hines[22]. The surface tension value at a bulk concentration of 1mM has also been used to check the presence of impurities. The values found for h-SDS and d-SDS, 67.7 and 67.9mN/m respectively, are again close to what are generally considered to be the best published values, 68.0[23] and 68.2[24]mN/m. A summary of the key surface properties, i.e. CMC, surface tension at 1mM, surface excess and area per molecule are given in Table 4. The lack of minima and the satisfactory comparison with other published data in the sub-micellar region indicated that both isotopic species of SDS are pure materials from the point of view of their surface chemistry and that the surface properties are not significantly affected by isotopic substitution.

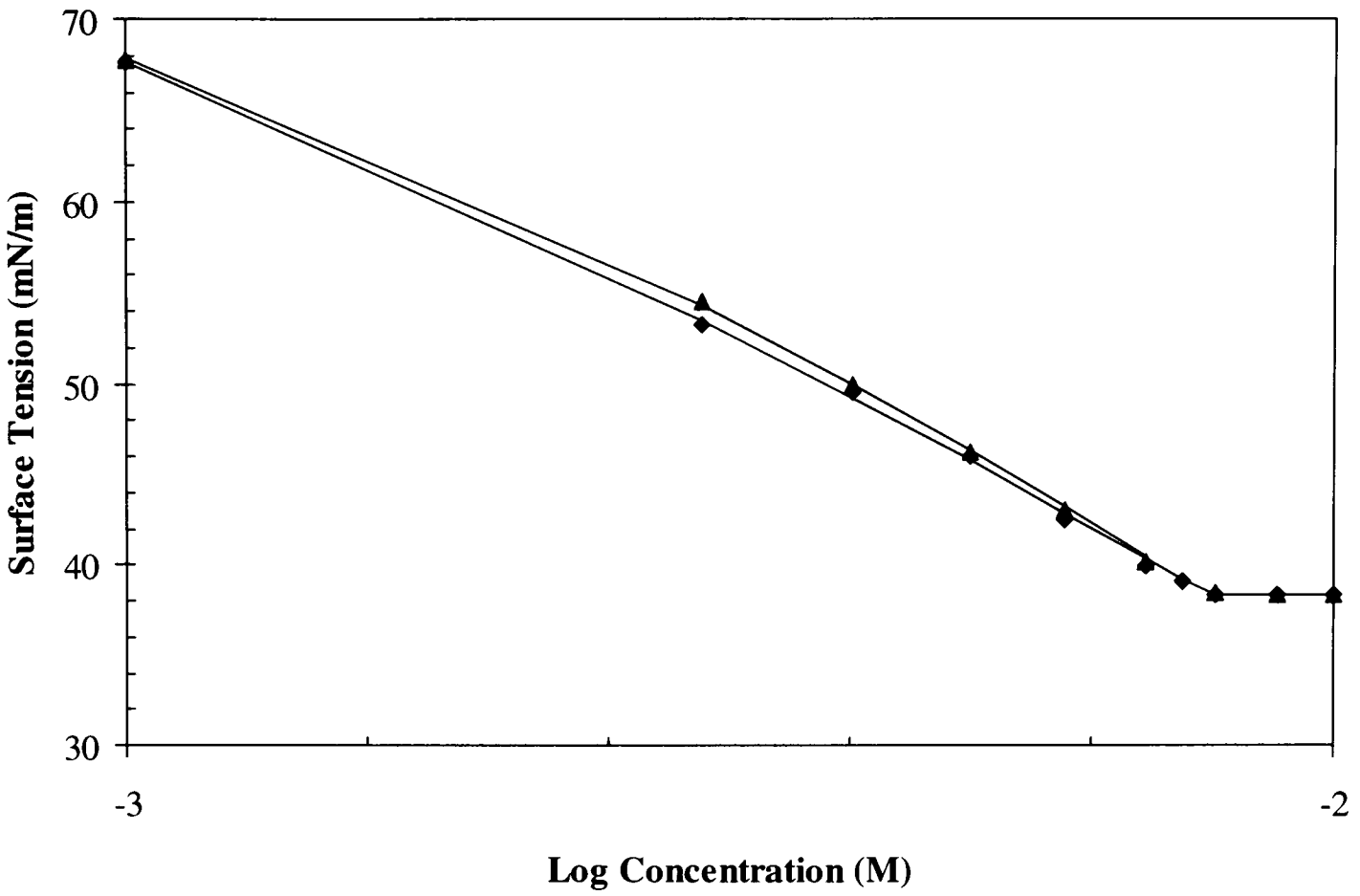


Figure 15. Surface tension against the log of the concentration for solutions of the two isotopic species of SDS, fully protonated (♦), and deuterated (▲), measured at 25°C and using the Du Noüy ring method.

3.4 Purification of Dodecyltrimethylammonium chloride (DTAC)

The protonated DTAC (designated h-DTAC) was purchased from Fluka as 99% pure. The crude deuterated C_{12} chain analogue (d-DTAC), was prepared by Dr R.K.Thomas using a procedure based on that described elsewhere[25]. Before use, both isotopic DTAC samples were purified as described below and the purity of the final material was tested by surface tension measurements.

3.4.1 Purification of DTAC

DTAC crystals were dissolved in hot acetone and the solution allowed to cool slowly. The crystals were filtered off and washed with cold distilled acetone. The product of the recrystallization was again dissolved in acetone and the process repeated twice. All residual solvent and water were removed under vacuum. DTAC is highly hygroscopic and

was therefore kept tightly sealed in a flask. The solutions of DTAC were prepared immediately before the experimental work.

3.4.2 Characterization of DTAC

After recrystallization both samples of DTAC were tested for purity by surface tension. The curves of surface tension plotted against the log of the concentration of the two isotopic species of DTAC are shown in Figure 16.

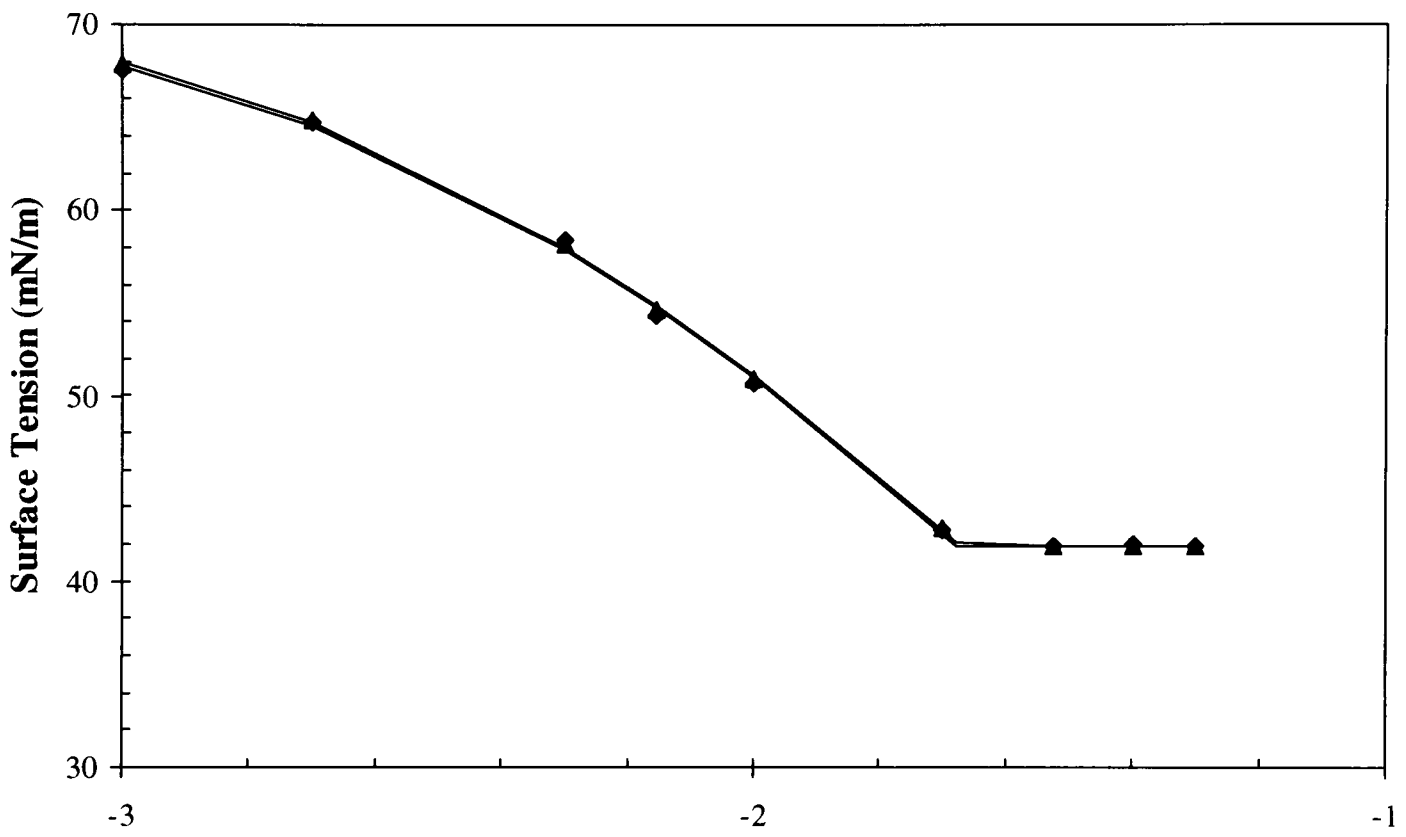


Figure 16. Surface tension against the log of the concentration for solutions of both isotopic species of DTAC, fully protonated (♦), and deuterated C_{12} chain (▲), measured at 25°C and using the Du Noüy ring method.

The values for CMC, surface tension at the CMC, surface excess and area per molecule are summarised in Table 5. h-DTAC and d-DTAC were found to have similar surface activity. The CMC obtained by surface tension was 2.1×10^{-2}M, which agreed with 2.03×10^{-2}M determined by specific conductivity[26]. Studies on the surface activity of DTAC are scarce, especially those using surface tension. Neither surface tension curve exhibited a minimum in the vicinity of the CMC, as can be seen from Figure 16 and the

two species of DTAC analogues can be taken to be pure enough for the purposes of the present work.

Surfactant	CMC (M)	γ_{1CMC} (mN/m)	Γ_{sat} (mol/cm^2)	A (Å^2)
h-DTAC	$2.1x10^{-2}$	41.9	$2.7x10^{-10}$	61
d-DTAC	$2.1x10^{-2}$	41.9	$2.7x10^{-10}$	62

Table 5. Properties of aqueous solutions of isotopic species of DTAC obtained from surface tension measurements at 25°C.

3.5 Purification of Tetraethylene glycol monooctyl ether (C_8E_4)

The protonated tetraethylene glycol monooctyl ether (abbreviated to C_8E_4) was purchased from Fluka. The crude form of the chain-deuterated version, abbreviated here as d-C_8E_4, was synthesised from perdeuterated bromooctane and tetraethylene glycol by Dr R.K.Thomas using the Williamson reaction[27]. Before use, both isotopic C_8E_4 samples were purified as now described to remove residual traces of n-octyl alcohol and species with smaller numbers of ethylene oxide groups. The chemical purity of the final material was again assessed by surface tension measurements.

3.5.1 Purification of C_8E_4

Both isotopic samples were purified by medium pressure silica column chromatography. Firstly the samples were tested on a TLC (Thin Layer Chromatography) plate to check level of contamination and the most suitable mobile phase to be used for the chromatography. Once the silica column was prepared, the sample was injected on the top portion of the column. The separation started with ether as the mobile phase. After the elution of the more hydrophobic impurities, the mobile phase was changed to a more polar mixture 75:25v/v ether:acetone. The fractions containing pure C_8E_4 were combined and the solvent was then removed by evaporation. The product was again tested on a TLC plate to ensure complete fractionation.

3.5.2 *Characterization of C_8E_4*

The surface tension curves of aqueous solutions of the columned samples of C_8E_4 as a function of log of the concentration are shown in Figure 17.

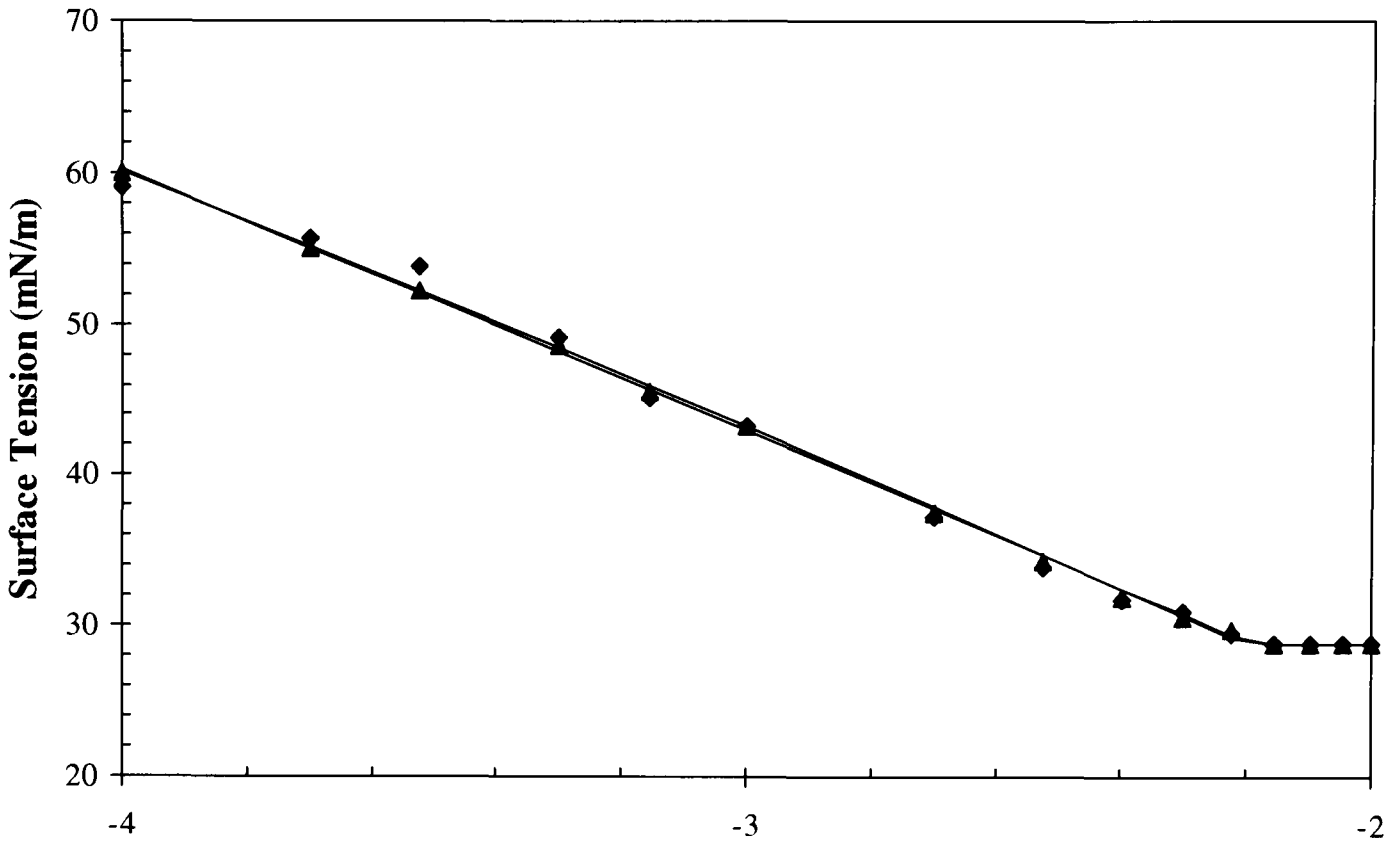


Figure 17. Surface tension against the log of the concentration for solutions of the two isotopic species of C_8E_4, fully protonated (♦), and deuterated EO chain (▲), measured at 25°C and using the Du Noüy ring method.

Surfactant	CMC (M)	γ_{1CMC} (mN/m)	Γ_{sat} (mol/cm^2)	A (Å^2)
h-C_8E_4	$6.3x10^{-3}$	28.8	$3.3x10^{-10}$	51
d-C_8E_4	$6.5x10^{-3}$	28.8	$3.1x10^{-10}$	54

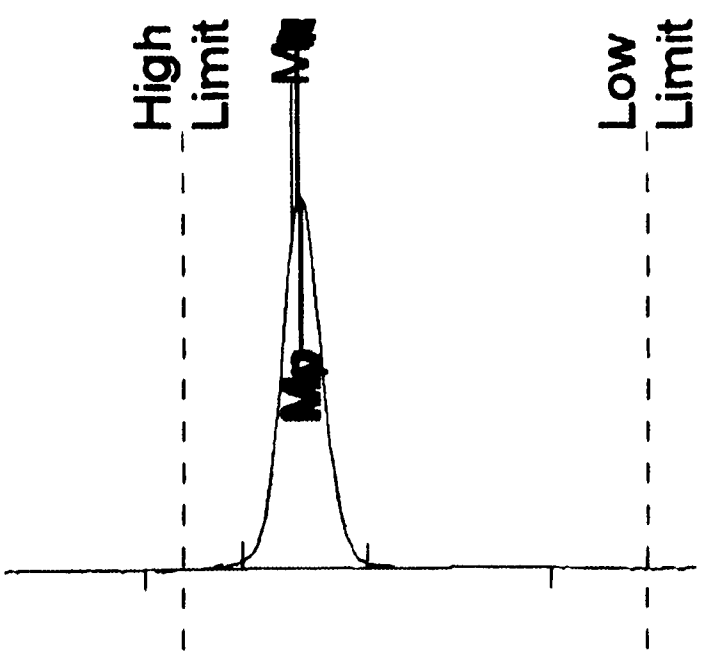
Table 6. Properties of aqueous solutions of isotopic species of C_8E_4 obtained from surface tension measurements at 25°C.

Figure 17 shows that the isotopic species have the same surface activity. The physical properties, CMC, surface tension at the CMC, surface excess and area per molecule,

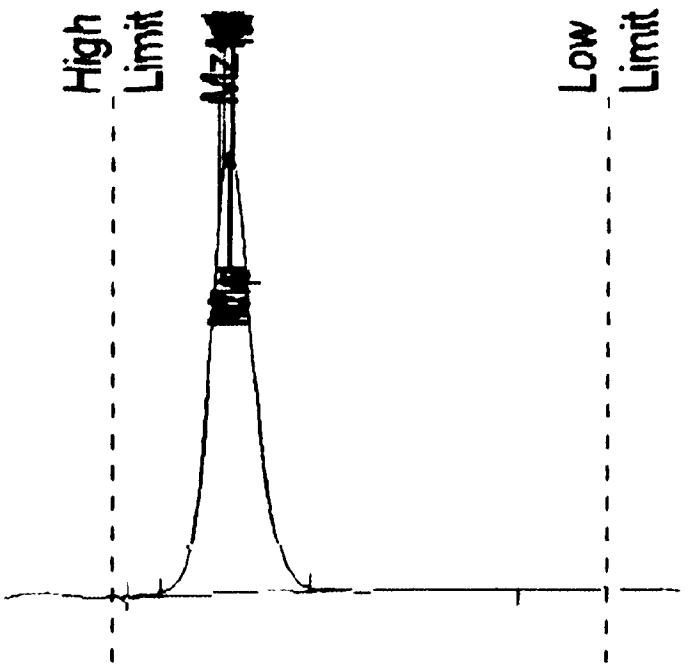
extracted from the surface tension curve, are summarised in Table 6. No minimum was found on the surface tension curve of Figure 17 and both C_8E_4 isotopes can be taken to be of adequate purity.

APPENDIX 2

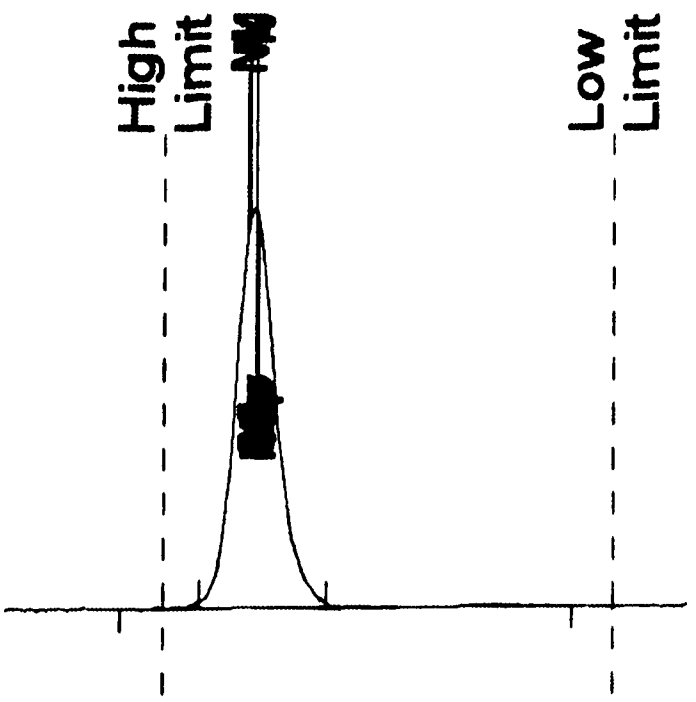
GPC Chromatogram Peaks of the EPE Copolymers



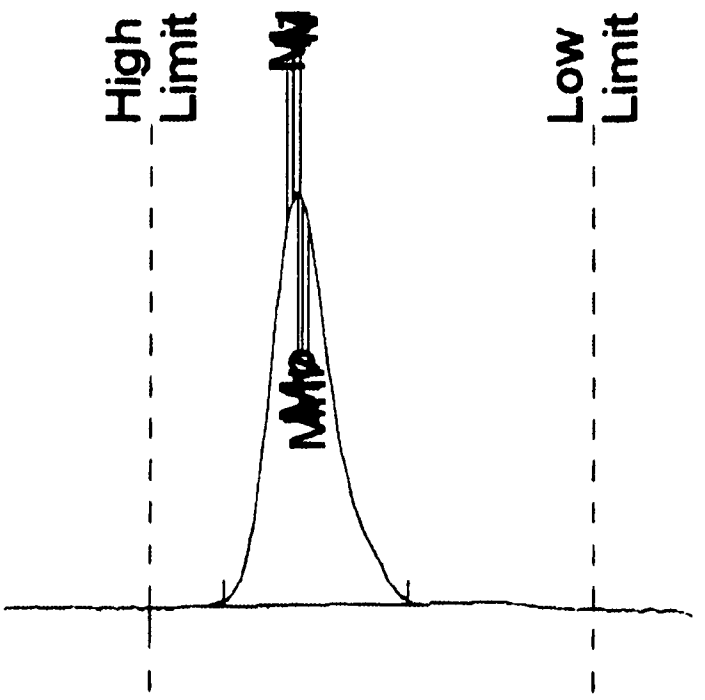
protonated EPE 3000-14, h-EPE 3000-14



PEO chain deuterated EPE 3000-14, d-EPE 3000-14



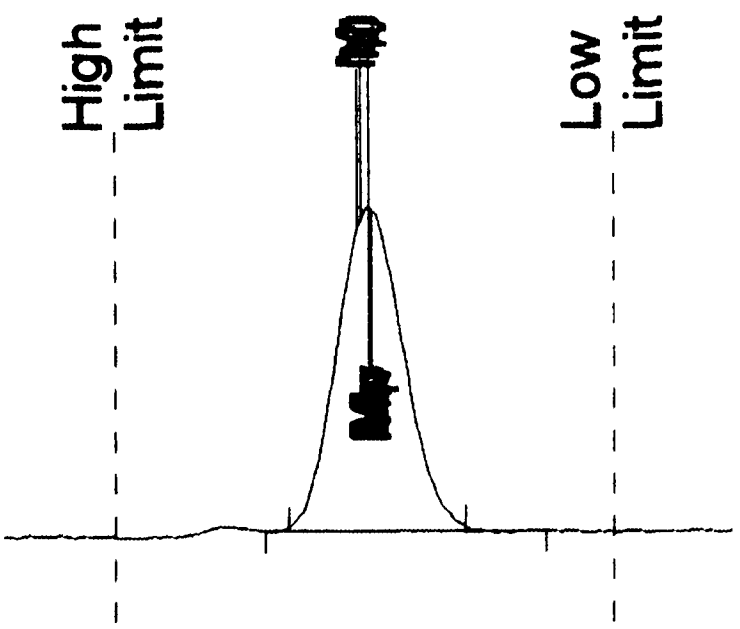
protonated EPE 3000-21, h-EPE 3000-21



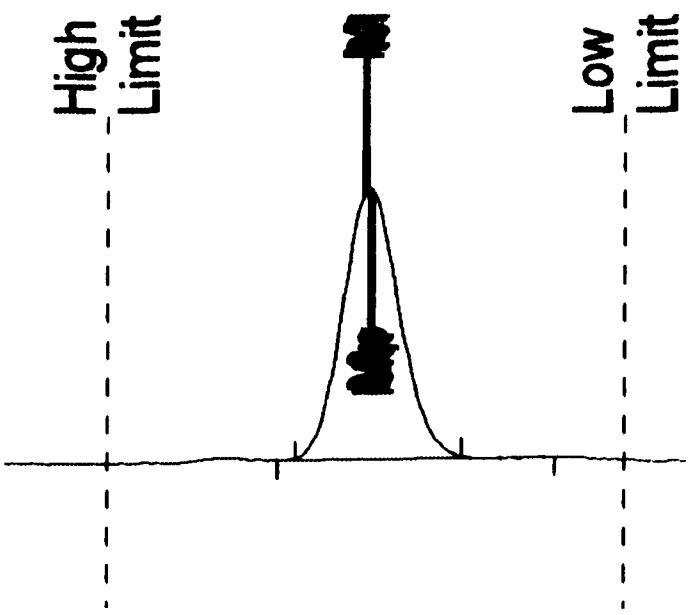
protonated EPE 2000-14, h-EPE 2000-14

APPENDIX 2 (Cont.)

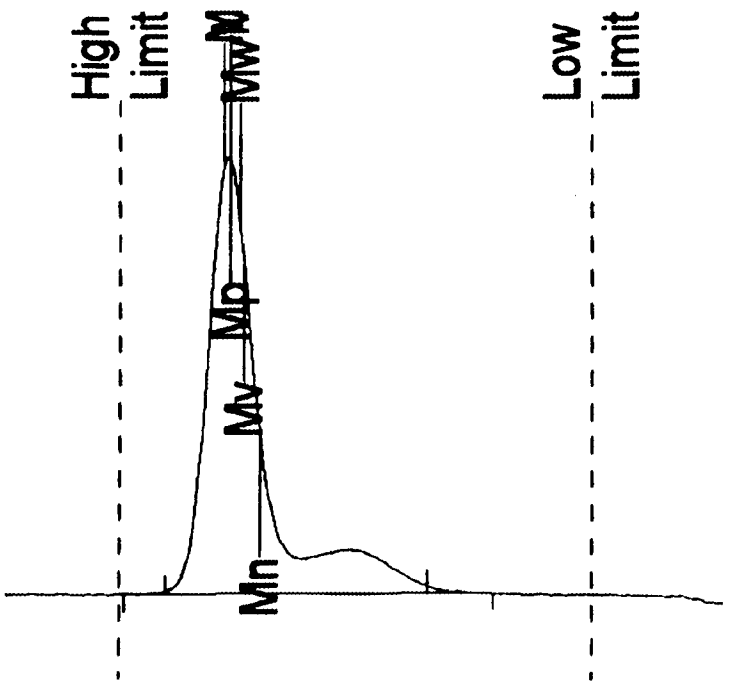
GPC Chromatogram Peaks of the EPE Copolymers



protonated EPE 1250-14, h-EPE 1250-14



PEO chain deuterated EPE 1250-14, d-EPE 1250-14



Pluronic P105

References

[1]Shaw, D.J. *Introduction to Colloid and Surface Chemistry*, Butterworth-Heinemann, 4th Ed., Oxford (1992)

[2] Rusanov, A.I.; and Prokorov, V.A. *J. Am. Chem. Soc.*, 52, 1751 (1930)

[3] Harkins, W.D.; and Jordan, H.F. *J. Am. Chem. Soc.*, 52, 1751 (1930)

[4] Fermi E.; and Zinn, W.H. *Phys. Re.*, 70, 103 (1946)

[5] Sears, V.F. *Neutron Optics*, Oxford University Press, Oxford (1989)

[6] Bacon, G.E. *Neutron Diffraction*, Oxford University Press, Oxford (1962)

[7] *Neutron News.*, 3, 29 (1992)

[8] Born, M.; and Wolf, E. *Principles of Optics*, Pergamon (1975)

[9] Crowley, T.L. *D.Phil. Thesis*, University of Oxford (1986)

[10] Crowley, T.L.; Lee, E.M.; Simister, E.A.; and Thomas, R.K. *Physica B*, 173, 143 (1991)

[11] Cowley, R.A.; and Ryan, T.W. *J. Phys. D.*, 20, 61 (1987)

[12] Lekner, J. *Theory of Reflection,* Nijhof, Dordrecht (1987)

[13] Bucknall, D.G.; Penfold, J.; and Webster, J.R.P. *ICANS 13 Proceedings* (1996)

[14] Thirtle, P.N. *D.Phil. Thesis*, University of Oxford (1999)

[15] Mysels, K.J. *Langmuir*, 2, 423 (1986)

[16] Lunkenheimer, K.; Miller, R.; and Fruhner, H. *Colloid Polym. Sci.* 260, 599 (1982)

[17] Atinok, H.; Yu, G.E.; Nixon, S.K.; Gorry, P.A.; Attwood, D.; and Booth, C. *Langmuir*, 13, 5837 (1997)

[18] Linse, P. *Macromolecules*, 27, 2685 (1994)

[19] Reddy, N.K.; Fordham, P.J.; Attwood, D.; and Booth, C. *J. Chem. Soc. Faraday Trans.*, 86, 1569 (1990)

[20] Yu, G.E.; Deng, Y.L.; Dalton, S.; Wang, Q.G.; Attwood, D.; Booth, C.; and Price, C. *J. Chem. Soc. Faraday Trans.*, 88, 2537 (1992)

[21] Lu, J.R.; Marrocco, A.; Su, T. J. S.; Thomas, R.K.; and Penfold, J. *J. Colloid Interface Sci.*, 158, 303 (1993)

[22] Hines, J.D. *PhD thesis*, University College, Oxford University, UK (1996)

[23] Mysels, K.J.; and Elworthy, PH. *J. Colloid Interface Sci.*, 21, 331 (1966)

[24] Lunkenheimer, K.; Fruhner, H.; and Theil, F. *Coll. Surf. A*, 76, 289 (1993)

[25] Simister, E.A.; Thomas, R.K.; Penfold, J.; Aveyard, R.; Binks, B.P.; Cooper, P.; Fletcher, D.I.; Lu, J.R; and Sokolowski, A. *J. Phys. Chem.*, 96, 1383 (1992)

[26] Osugi, J.; Sato, M.; and Ifuku, N. *Rev. Phys. Chem. Japan*, 35, 32 (1965)

[27] Lu, J.R.; Hromadova, M.; Thomas, R.K.; and Penfold, J. *Langmuir*, 9, 2417 (1993)

Chapter 3

Thermodynamics of Surfactant Solutions

1 General Description of Surfactant Solutions

Surfactants in solution exhibit a variety of striking properties which have been exploited and investigated for many years. This chapter outlines the thermodynamic treatments that describe the two main fundamental properties of surfactants in solution, adsorption at interfaces and micellization. Because of their amphiphilic nature surfactants adsorb at surfaces and interfaces. The driving force for a surfactant to adsorb at an interface is that it lowers the free energy of the phase boundary and the denser the surfactant packing at the interface, the larger the reduction in surface tension. The degree of surfactant concentration at a boundary depends on surfactant structure and also on the nature of the two phases that meet at the interface. Therefore, the choice of the most appropriate surfactant will depend on the application. There is, of course, a limit to the surface or interfacial tension lowering effect by the surfactant. That limit is generally reached when the surfactant molecules start to aggregate in the bulk of the solution to form micelles. Micellization can be viewed as an alternative mechanism to adsorption at the interface for removing hydrophobic groups from contact with water, thereby reducing the free energy of the system. The concentration where micelles start to form is the critical micelle concentration (CMC). In the micelles, the hydrophobic chains of the surfactant molecules reside in the interior while the hydrophilic head groups lie at the surface of the micelle facing and mixing with the water.

A key contribution to the behaviour of surfactants in solution is the hydrophobic effect. The hydrophobic effect arises from the fact that water does not interact favorably with the hydrophobic groups of surfactants and there is consequently a driving force for expelling them from the aqueous environment. The generally accepted explanation of the hydrophobic effect is that it results from a greater ordering of the hydrogen bonds in the vicinity of the hydrophobic group and is therefore an entropic effect.

2 Surfactant Adsorption at Air-Liquid Interface

The adsorption of surfactants has been studied to determine

(1) the concentration of surfactant at the interface, since this is a measure of how much of the interface has been covered (and thus changed) by the surfactant; the performance of the surfactant in many interfacial processes (e.g., foaming, detergency, emulsification) depends on its concentration at the interface;

(2) the orientation of the surfactant at the interface, since this determines how the interface will be affected by the adsorption, that is, whether it will become more hydrophilic or more hydrophobic;

(3) the energy changes, ΔG, ΔH, and ΔS, associated with the adsorption, since these quantities provide information on the type and mechanism of any interactions involving the surfactant at the interface and on the efficiency and effectiveness of its operation as a surface-active material

Changes in the standard thermodynamic parameters, $\Delta G°$, $\Delta H°$, and $\Delta S°$, provide important features on the adsorption process. $\Delta G°_{ad}$ for the adsorption of any surfactant at the air-water interface is always negative[2], reflecting the spontaneous adsorption of surfactant molecules at the air-water interface. Experimentally, this is found to be mainly due to the positive entropy change upon adsorption, $\Delta S°_{ad}$. The adsorption process is therefore dominated by the entropy gain associated with it, which indicates that the driving force for the process is the hydrophobic effect, i.e. the tendency of the hydrophobic group of the surfactant to transfer from bulk water to surface.

The direct determination of the amount of surfactant adsorbed per unit area of liquid-air interface, although feasible, has not generally been undertaken because of the difficulty of isolating the interfacial region from the bulk phase. Instead, the amount of material adsorbed per unit area of interface is calculated indirectly from surface tension measurements. As a result, a plot of surface tension as a function of (equilibrium) concentration of surfactant in the liquid phase, rather than an adsorption isotherm, is generally used to describe adsorption at the interface. From such a plot the amount of

surfactant adsorbed per unit area of interface can readily be calculated by use of the Gibbs adsorption equation.

2.1 The Gibbs Surface Excess[1,3,4]

Consider two phases α and β in equilibrium with a surface *s* dividing them. For this system, the Gibbs free energy can be defined as

$$G = G^{\alpha} + G^{\beta} + G^{s} \tag{3.1}$$

where G^{α} and G^{β} indicate the contribution from each bulk phase, which are given by

$$G = TS - pV + \sum_i \mu_i n_i \tag{3.2}$$

where the chemical potential terms are summed for all components *i*. An area term in the corresponding expression replaces the volume term for G^s

$$G^s = TS^S + \gamma A + \sum_i \mu_i n_i \tag{3.3}$$

The change in the free energy, *dG*, when the two phases are brought together gives

$$dG = \sum_{\alpha,\beta,s} (TdS + SdT - pdV - Vdp + \sum_i \mu_i dn_i + \sum_i n_i d\mu_i) + Ad\gamma + \gamma dA \tag{3.4}$$

For a system where *G*, *S*, *V*, *A*, and n_i are the extensive variables and *T*, *p*, γ, and μ_i, are the intensive variables, Equation 3.4 simplifies to

$$dG = TdS - pdV + \gamma dA + \sum_i \mu_i dn_i \tag{3.5}$$

Integrating Equation 3.5 gives

$$G = TS - pV + \gamma A + \sum_i \mu_i n_i \tag{3.6}$$

Taking the total differential of Equation 3.6 and comparing with Equation 3.5 gives a Gibbs-Duhem equation,

$$SdT - Vdp + Ad\gamma + \sum_i n_i d\mu_i = 0 \tag{3.7}$$

Equation 3.7 can be written for each of the bulk phases separately:

$$S^\alpha dT - V^\alpha dp + \sum_i n_i^\alpha d\mu_i^\alpha = 0 \tag{3.8}$$

$$S^\beta dT - V^\beta dp + \sum_i n_i^\beta d\mu_i^\beta = 0 \tag{3.9}$$

Subtracting Equations 3.8 and 3.9 from 3.7, and using the condition for equilibrium that $d\mu_i = d\mu_i^\alpha = d\mu_i^\beta$ gives

$$\left(S - S^\alpha - S^\beta\right)dT - \left(V - V^\alpha - V^\beta\right)dp + Ad\gamma + \sum \left(n - n_i^\alpha - n_i^\beta\right)d\mu_i = 0 \tag{3.10}$$

The surface excess quantities are defined as

$$S^S = S - S^\alpha - S^\beta \tag{3.11}$$

$$V^S = V - V^\alpha - V^\beta \tag{3.12}$$

$$n_i^S = n_i - n_i^\alpha - n_i^\beta \tag{3.13}$$

Hence

$$Ad\gamma + S^S dT - V^S dp + \sum_i n_i^S d\mu_i^S = 0 \tag{3.14}$$

At constant temperature and pressure,

$$A d\gamma + \sum_i n_i^s d\mu_i^S = 0 \tag{3.15}$$

Dividing Equation 3.15 by A gives

$$d\gamma = -\sum_i \Gamma_i d\mu_i \tag{3.16}$$

where

$$\Gamma_i = \frac{n_i^s}{A} \tag{3.17}$$

Equation 3.16 is known as the Gibbs adsorption equation; it relates changes in surface tension, γ, to changes in the chemical potentials of the components in the bulk solution. The quantity n_i^s/A is called the surface excess of component i.

The chemical potential depends on the activity according to the equation

$$\mu_2 = \mu_2^0 + RT \ln a_2 \tag{3.18}$$

Using the differential form of Equation 3.18 at constant temperature, and also replacing the surfactant activity, a_2, by fc, where f is the activity coefficient and c is the concentration of the surfactant, gives

$$d\mu_2 = RTd \ln(fc) \tag{3.19}$$

For dilute solutions, the activity coefficient approaches unity, in which case combining Equation 3.19 with Equation 3.16 gives

$$\Gamma_2^1 = -\frac{c}{RT}\left(\frac{d\gamma}{dc}\right)_T = -\frac{1}{RT}\left(\frac{d\gamma}{d\ln c}\right)_T = -\frac{1}{2.303RT}\left(\frac{d\gamma}{d\log c}\right)_T \qquad (3.20)$$

Γ_2^1 is the relative adsorption of component 2 with respect to component 1. This form of Gibbs equation shows that the slope of a plot of γ versus logarithm of concentration (or activity if the solution is nonideal) measures the surface excess of the solute.

Equation 3.20 is the form in which the Gibbs equation is commonly used for solutions of nonionic surfactants containing no other materials. When γ is in dyn/cm (=ergs/cm^2) and R=8.31x10^{-7}ergs mol^{-1} K^{-1}, then Γ_1 is in mol/cm^2; when γ is in mN/m (=mJ/m^2) and R=8.31J mol^{-1} K^{-1}, then Γ_1 is in mol/1000m^2.

For solutions of completely dissociated surfactant of the 1:1 electrolyte type, A^+B^-, as the only solute,

$$d\gamma = RT\left(\Gamma_{A^+} d\ln a_{A^+} + \Gamma_{B^-} d\ln a_{B^-}\right) \qquad (3.21)$$

Since $\Gamma_{A+} = \Gamma_{B-} = \Gamma_1$ to maintain electroneutrality and $a_{A+} = a_{B-} = C_1 \times f_\pm$ without significant error, then

$$d\gamma = -2RT\Gamma_1 d(\ln C_1 + \ln f_\pm) \qquad (3.22)$$

where $f_\pm$ is the mean activity coefficient of the surfactant. For dilute solutions (10^{-2}M or less),

$$d\gamma = -4.606RT\Gamma_1 d\log C_1 \qquad (3.23)$$

without significant error.

Where activity coefficients are expected to deviate significantly from unity, for example, when divalent or multivalent ions are present in the solution or concentrations of the

surfactant exceed 10^{-2}M, *dlog* C_1 in the appropriate equation may be replaced by $d(\log C_1 + \log f_\pm)$, and $\log f_\pm$ calculated in water at 25°C, from the Debye-Hückel equation,

$$\log f_\pm = \frac{-0.509[Z_+Z_-]\sqrt{I}}{1+0.33\alpha\sqrt{I}} \tag{3.24}$$

where I is the total ionic strength of the solution

$$I = \tfrac{1}{2}\sum_i C_i Z_i^2 \tag{3.25}$$

and α is the mean distance of approach of the ions, in Å. Log $f_\pm$ can be assumed to equal $(\log f_+ + \log f_-)/2$, α is taken as 0.3 for small counterions (Na^+, K^+, Br^-, Cl^-) and 0.6 for the surfactant ion.

For dilute solutions of a completely dissociated surfactant 1:1 electrolyte in the presence of a swamping, constant amount of electrolyte containing a common nonsurfactant counterion,

$$d\gamma = -2.303RT\Gamma_1 d\log C_1 \tag{3.26}$$

since under these conditions the change in the activity of the nonsurfactant common ion with concentration of surfactant is approximately zero. This is the same form as for a nonionic surfactant in dilute solution.

The area per molecule at the interface provides information on the degree of packing and the orientation of the adsorbed surfactant molecule, when compared with the dimensions of the molecule as obtained by use of molecular models. From the surface excess concentration, the area per molecule at the interface, *A*, in square angstroms is calculated from the relation

$$A = \frac{10^{16}}{\Gamma_2^1 N} \tag{3.27}$$

where N is Avogrado's number and Γ_1 is in mol/cm^2.

3 Surfactant Micellization

3.1 Micelle Formation

Micelle formation is another property of surfactants as fundamental as their tendency to be adsorbed at interfaces. When surfactants are dissolved in water, the hydrophobic groups distort the structure of the water and increase the free energy of the system. Distortion of the solvent structure can also be reduced by aggregation of the surfactant molecules into clusters with their hydrophobic groups directed toward the interior of the cluster and their hydrophilic groups directed toward the solvent. This aggregation is called micellization and is an alternative mechanism for removing hydrophobic groups from contact with the water. However, the transfer of surfactant molecules from the bulk to the micelle may generate some opposing forces, such as electrostatic repulsion in the case of ionic surfactants. Whether micellization occurs in a particular case and, if so, at what concentration of monomeric surfactant, therefore depends on the balance between the factors promoting micellization and those opposing it. The CMC value depends on surfactant architecture, solvent, presence of added components (such as co-surfactants or salts) and temperature. The determination of the concentration at which micellization occurs, i.e. the value of the CMC, can be made using several physical properties, such as electrical conductivity, surface tension, light scattering, or refractive index. In the present study, the CMCs of the surfactant solutions are determined by surface tension. Micellization is important not only because a number of important phenomena, such as detergency and solubilisation, depend on the existence of micelles in solution, but because it affects other interfacial phenomena, such as the reduction of surface or interfacial tension, phenomena that do not directly involve micelles. A clear understanding of the process of micellization is necessary for the rational explanation and prediction of the effects of structural and environmental factors on the value of the CMC. The determination of the thermodynamic parameters of micellization ΔG_{mic}, ΔH_{mic}, and ΔS_{mic}, has played an important role in developing such an understanding. As for adsorption at the air/water interface, the negative value of $\Delta G°_{mic}$ is due mainly to the

large positive value of ΔS°_{mic}. Therefore, the micellization process is governed primarily by the tendency of the hydrophobic group of the surfactant to transfer from the solvent to the interior of the micelle. The tendency of the hydrophobic group of the surfactant to aggregate as micelles promotes the entropy increase by lowering the structuring of water molecules surrounding the hydrocarbon chains in the aqueous medium, and by increasing the freedom of the hydrophobic chains in the nonpolar core of the micelles compared with the aqueous medium. There is therefore significant interest in developing theoretical models for determining critical micelle concentrations and aggregation behaviour in micellar solutions. In several respects, micellization resembles both phase separation and complex formation, and each of these has been used as the basis to develop thermodynamic models for micellization.

3.1.1 Phase Separation Model

In this model, micelle formation is considered as equivalent to a phase separation, with micelles being the separated phase and the CMC corresponding with the saturation concentration of surfactant in the monomeric state. Surfactant addition above the CMC consequently only affects the number of micelles, but not the unimer concentration. The model assumes that the chemical potential of the surfactant in the micellar state is a constant at a given temperature and may be adopted as the standard chemical potential, μ^{0}_{mic}, analogous to the standard chemical potential of a pure liquid or solid. Equilibrium with the surfactant in solution is then represented by

$$\mu^{0}{}_{mic} = \mu_1^{\,0} + RT \ln a_1 \tag{3.28}$$

where μ^{0}_{1} is the standard chemical potential in solution and a_1 is the activity of surfactant monomer in solution. Substitution of a_1 by $x_1 f_1$, where x_1 is the mole fraction of monomers, and taking the activity coefficient, f_1, to be unity, gives the standard free energy of micellization per mole of monomer, ΔG^{0}_{mic}, as

$$\Delta G^{0}{}_{mic} = \mu^{0}{}_{mic} - \mu^{0}{}_{1} = RT \ln x_1 \tag{3.29}$$

and the CMC may be identified with x_1. Equation 3.29 can therefore be written as

$$\Delta G^{0}_{mic} = RT \ln cmc \tag{3.30}$$

The phase separation model makes no provision for possible variation in the activity of surfactant as the total concentration of surfactant in the solution is increased, and an equation of state analogous to those used to describe adsorbed films is required to refine the model.

3.1.2 Mass Action Model

In its simplest form this postulates equilibrium between monomers, S, and a single micellar species of aggregation number, N:

$$\mathrm{N\,S_1} \rightleftarrows \mathrm{M_N}, \qquad K_m = x_N / x_1^{N} \tag{3.31}$$

where K_m is the equilibrium constant. The standard free energy of micellization per mole of monomer is then given by

$$\Delta G^{0}_{mic} = -(RT/N)\ln K_m \tag{3.32}$$

$$\Delta G^{0}_{mic} = -(RT/N)\ln x_N + RT \ln x_1 \tag{3.33}$$

For large values of N (>50) and at total concentrations not greatly exceeding the CMC, the first term is negligible and Equation 3.33 reduces to Equation 3.29 of the phase separation model.

References

[1] Hiemenz, P.C. *Principles of Colloid and Surface Chemistry*, Marcel Dekker, Inc., New York, 209-251 (1977)

[2] Rosen, M.J. *Surfactants and Interfacial Phenomena*, John Wiley & Sons, New York, 33-107 (1989)

[3]Atkins, P.W. *Physical Chemistry*, Oxford University Press, Oxford, 711-713 (1992)

[4]Morrison, I.D. and Ross, S. *Colloidal Dispersions – Suspensions, Emulsions and Foams*, Wiley-Interscience, New York, 292-296 (2002)

Chapter 4

Surface Activity of EPE Copolymers Studied by Surface Tension

1 Introduction

This chapter describes the study of the surface activity of monodisperse EPE copolymers by surface tension. As previously mentioned, the surface-active properties of such a surfactant are greatly affected by its composition. Although the copolymer architecture, i.e. the PEO and PPO block distribution in the molecule, is also known to affect the resulting surface activity, in this study we will only be working with the PEO-PPO-PEO triblock type of arrangement. To examine the effects of composition, four monodisperse EPE copolymers were prepared, for which the details of the preparation have been given in Chapter 2. Temperature has also been reported to change significantly the surface activities of these materials and the surface tensions were therefore measured at two temperatures, 25°C and 35°C, and over a wide range of concentration. The results found here are compared with previously reported ones for commercial Pluronic surfactants and with small conventional nonionic surfactants.

2 Experimental Details

2.1 Materials

The preparation and purification of monodisperse EPE copolymers have been described in Chapter 2. The solutions for surface tension measurements were prepared using ultrapure water.

2.2 Surface tension measurements

Surface tension measurements were carried out using a Krüss K10 maximum pull tensiometer using both the du Noüy ring and the Wilhemy plate. Further details of the technique can be found in Chapter 2. Before measurements, care was taken to ensure that all the glassware used was properly clean. The sample container consisted of a 30mL glass dish, placed in a metal jacket that was connected to a Haake water bath to allow

temperature control. Stock solutions of the EPE copolymers were prepared using UHQ water and diluted down to produce the desired concentration. The test solution flasks were placed in the Haake water bath and left to equilibrate at the desired temperature. Approximately 20mL test solution was required for the surface tension measurement. The ring or plate was washed with a copious amount of UHQ water and flamed until red-hot before each measurement. The calibration of the instrument and the cleanliness of the dish and ring were checked by measuring the surface tension of UHQ water, which has a value of 72.0mN/m at 25°C. With the Du Noüy ring, the measurements were repeated until a consistent reading was attained, i.e. to within 0.1mN/m. The surface tension readings were subsequently corrected using the Harkins and Jordan correction factors (See Appendix 1 of Chapter 2). Using the plate, the measurement was performed until the result was invariant within 0.1mN/m. No correction factors were applied to the values obtained with the Wilhemy plate method. The surface tension values below the CMC and above the low concentration break at about 10^{-3}w/v% (when clearly defined) were plotted against the logarithm of the surfactant bulk concentration and fitted to a quadratic equation. To determine the surface excess, Γ, the slope of the curve at a given concentration was first obtained by differentiating the fitted quadratic function and then substituted in the Gibbs' equation for nonionic surfactants.

$$\Gamma = -\frac{1}{2.30RT}\left(\frac{d\gamma}{d\log c}\right) \tag{4.1}$$

The area per adsorbed molecule, A, is readily obtained from Γ using

$$A = \frac{1}{\Gamma N} \tag{4.2}$$

where N is Avogadro's number.

The CMCs of the surfactants were calculated using the point of inflection on the γ-log c curve.

3 Results and Discussion

3.1 Surface tension of EPE 3000-14 copolymer

The surface tension of aqueous solutions of EPE 3000-14, whose composition is given in Table 2 of Chapter 2, was measured at 25°C using a Du Noüy Ring Tensiometer, and its variation with log(concentration) is presented in Figure 1.

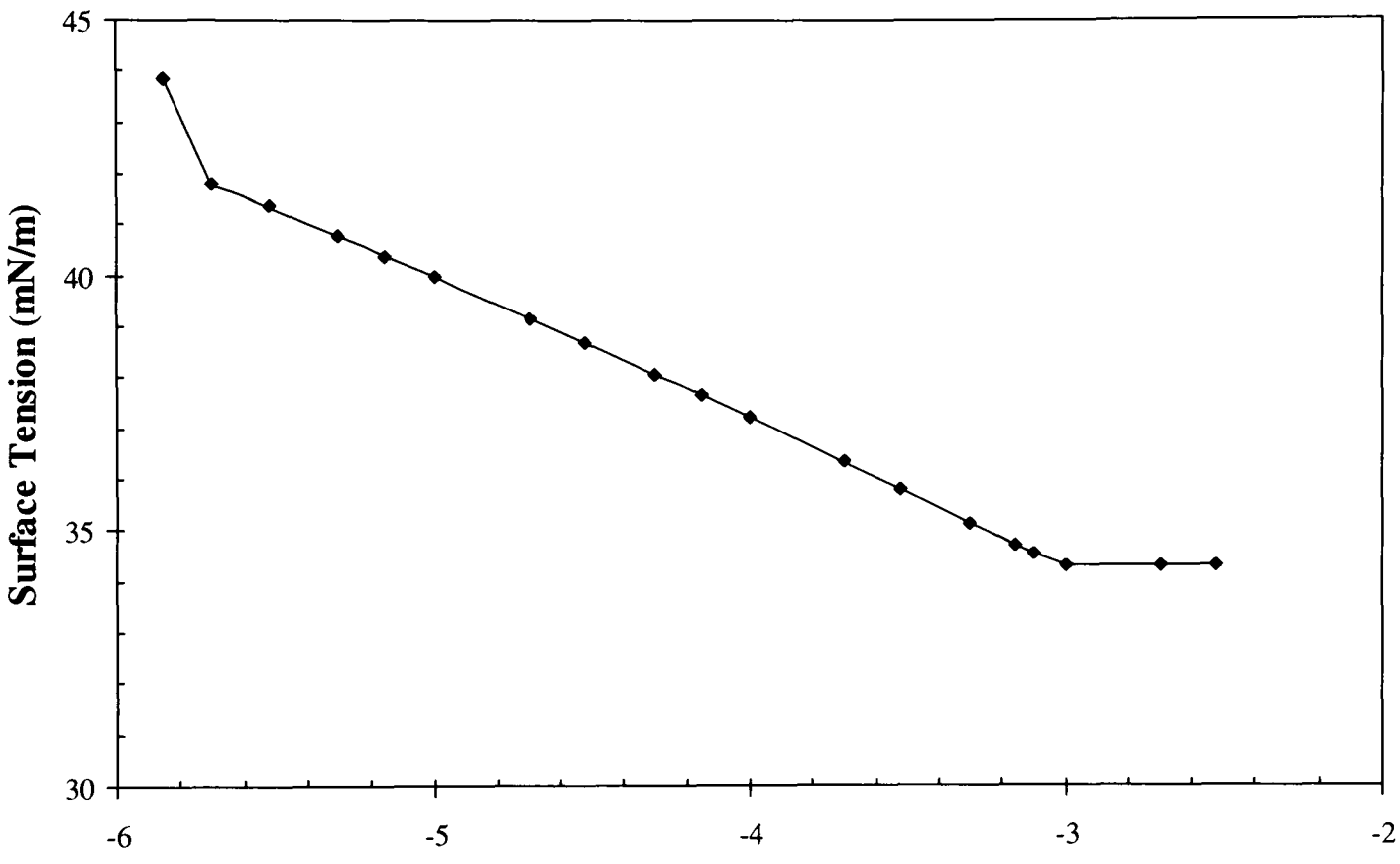


Figure 1. Surface tension against the log of concentration curves for solutions of monodisperse EPE 3000-14 copolymer measured at 25°C using the Du Noüy ring method.

Two breakpoints, referred to as low-concentration and high-concentration in this thesis, can be observed in the surface tension curve. The high-concentration breakpoint occurs at a concentration of 9.5×10^{-4}M. Above this concentration, the surface tension remained unchanged with increasing polymer concentration and it was therefore assumed to be the CMC. Between the CMC and the low-concentration breakpoint, a second-order polynomial was found to describe very well the increase of surface tension with decreasing bulk concentration. This convex curvature agrees with the predictions of Linse's Mean Field Model of the adsorption[1]. The curvature is due to an increased

copolymer adsorption at the air-water interface with increasing bulk concentration. The low-concentration breakpoint occurs at a concentration of approximately $2x10^{-6}$M. Below this breakpoint, a region was achieved where the surface tension readings were very inconsistent and could not be reliably assessed. This region will be referred to as "the experimentally inaccessible region" in this thesis for reasons that will be discussed below.

When compared with Pluronic P105, which is the nearest commercially available equivalent, the surface tension curve profile for EPE 3000-14 can be seen to show similar features in that both curves show the two breakpoints. The surface tension curves for aqueous solutions of EPE 3000-14 and Pluronic P105 are compared in Figure 2.

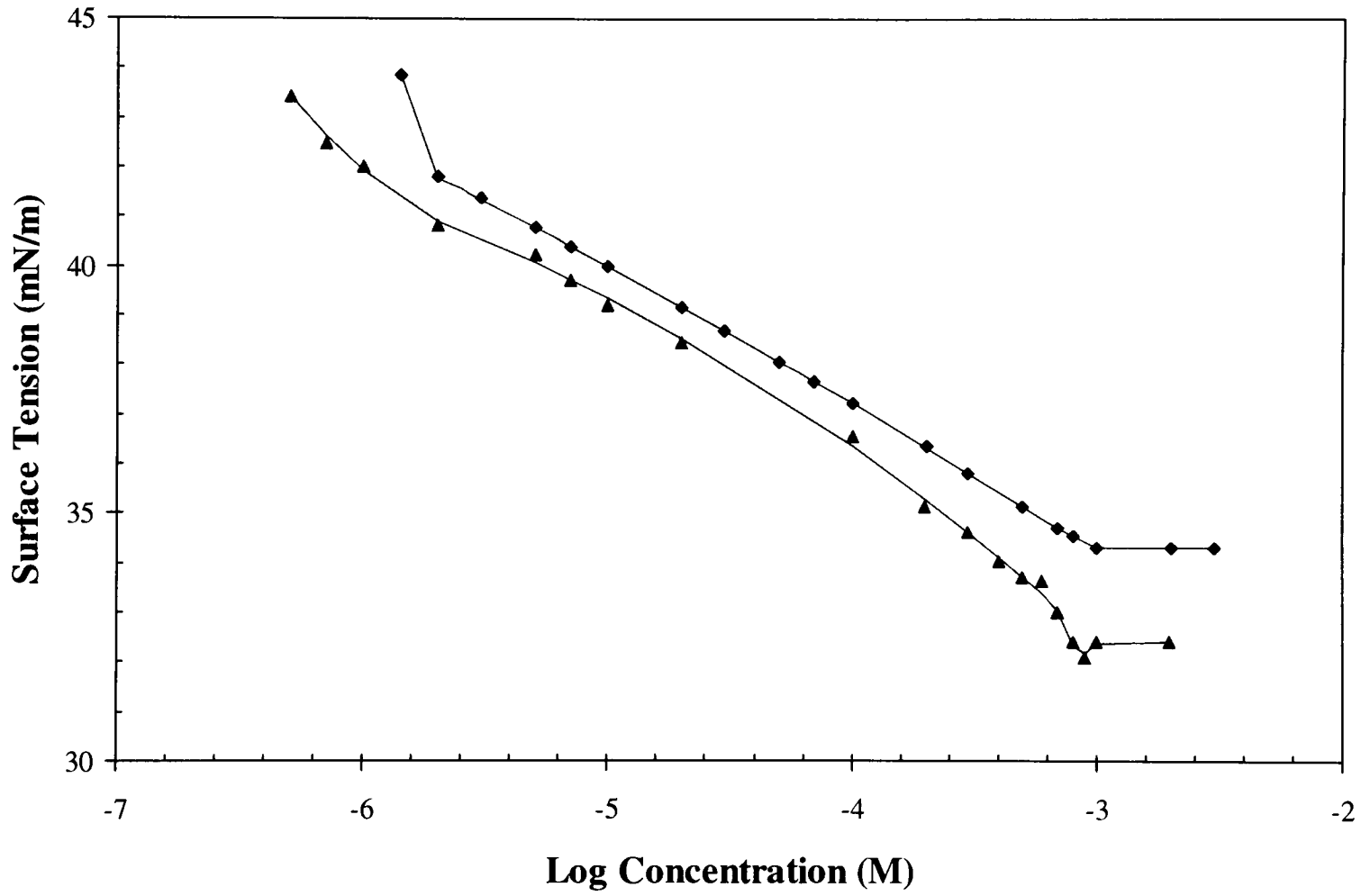


Figure 2. Surface tension against the log of concentration curves for solutions of Pluronic P105 (▲) and monodisperse EPE 3000-14 copolymer, (♦) measured at 25°C using the Du Noüy ring method.

The high-concentration breakpoint, after which the surface tension remains unchanged with increasing polymer concentration, is reached at $8.0x10^{-4}$M and is attributed to micelle formation. The value of the CMC also agrees within error with the value obtained

previously by the dye solubilisation method[2], which was $3.5x10^{-4}$M (or 0.23%w/v). In another study[3] also using the dye solubilisation technique, the CMC for Pluronic P105 was found to be $8.0x10^{-4}$M. Pluronic P105 is a polydisperse material, as demonstrated in the GPC analysis reported in Chapter 2, and some variation in CMC is to be expected. In our case a minimum in the vicinity of the CMC also occurred in the surface tension curve. Such a minimum would typically be attributed to the replacement of highly surface-active molecules at the interface by the major and less surface-active component as the highly surface-active molecules are solubilised in the micelles formed by the major component. The curvature of the region between the CMC and the low-concentration breakpoint was more pronounced in P105 than for EPE 3000-14. The shape of this region of the curve is therefore likely to be caused by a combination of the effects of polydispersity and the presence of highly surface-active impurities. The low-concentration breakpoint was attained at a copolymer concentration of 10^{-6}M. It was in this region that the largest difference was found between the surface tension curve obtained here and the one published in the literature[4,5], in which the Wilhemy Plate method was used. Using the Wilhemy plate, the surface tension of Pluronic P105 copolymer solutions was measured down to $1.5x10^{-8}$M (or 10^{-5}%w/v), but with the ring the surface tension could not be measured at concentrations lower than $5.0x10^{-7}$M (or $3.3x10^{-4}$%w/v). Below this concentration, just as found for EPE 3000-14, the results obtained were always inconsistent and unreliable.

3.2 Comparison between Wilhemy Plate and Du Noüy ring methods for measuring surface tension of EPE copolymers

The Wilhemy plate method has been extensively employed to measure the surface tension of aqueous solutions of Pluronic surfactants in previous studies[4,5]. To validate the use of the ring method in this study, the surface tension of aqueous solutions of EPE 3000-14 copolymer was also measured using the Wilhemy plate. The surface tension vs. log concentration curves obtained using both Du Noüy ring and Wilhemy plate are compared in Figure 3.

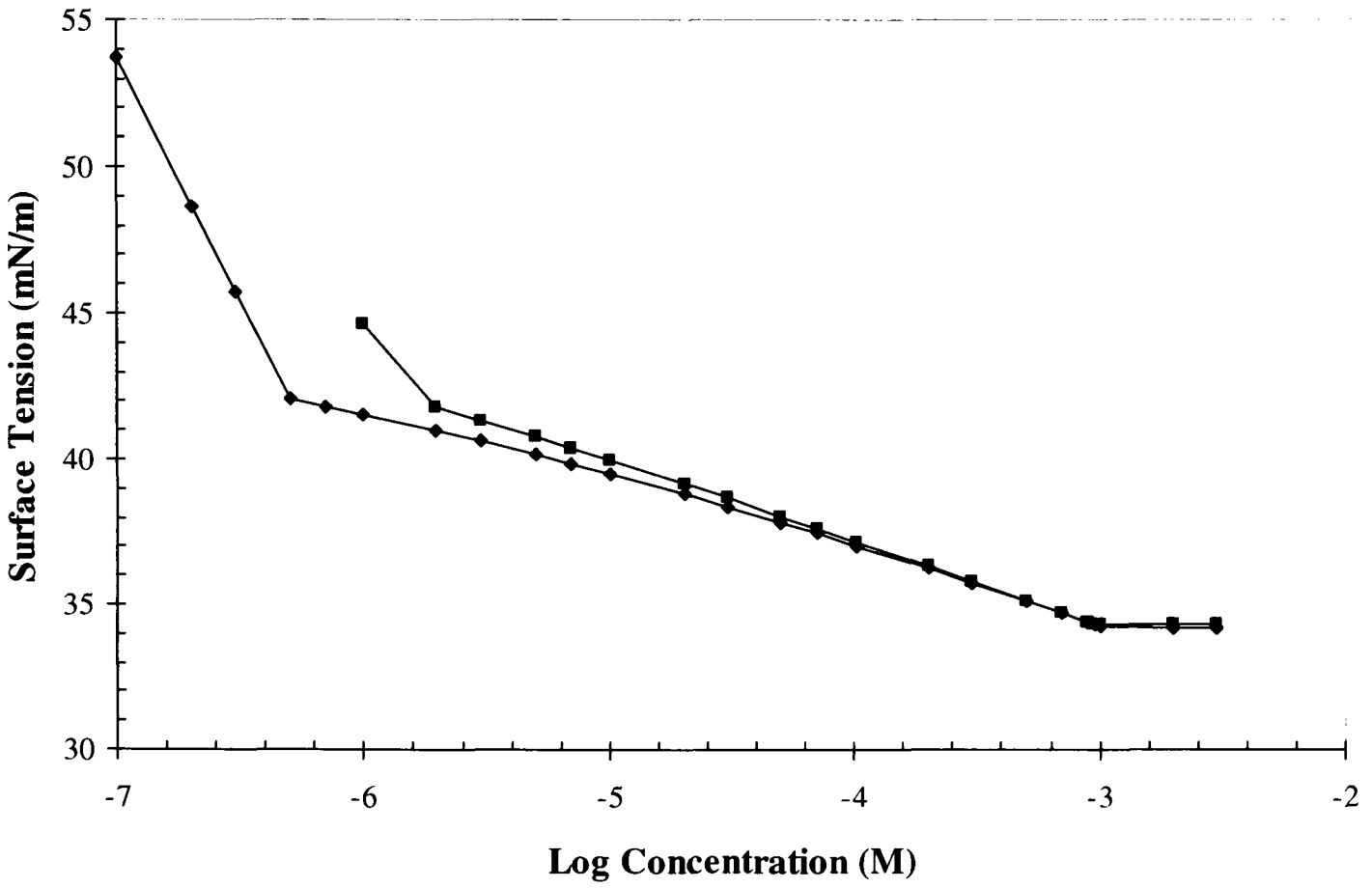


Figure 3. Surface tension against the log of concentration curves for solutions of EPE 3000-14 copolymer measured at 25°C using the Du Noüy ring, (■), and Wilhemy plate, (◆).

Figure 3 shows that above 10^{-5}M the surface tension values obtained by both techniques are consistent. The CMC value determined with the Wilhemy plate was $1x10^{-3}$M while with the Du Noüy ring it was $9.5x10^{-4}$M. The surface pressure at the CMC was 37.7mN/m with the plate and 37.4mN/m with the ring. As the bulk concentration dropped below 10^{-5}M the two techniques differed quite significantly. When using the Wilhemy plate the first break was found at a lower concentration, approx. $5x10^{-7}$M, and below this concentration, a steep increase in the slope of the curve was noted. The lack of consistency with the Du Noüy method at low copolymer concentration is believed to be related to the effect of EPE copolymer on the stability of the meniscus formed by the ring as a result of the low diffusion rate of EPE copolymers to the surface in the dilute regime. It has been reported[6,7] that a sufficiently long waiting time (sometimes hours or more) is often required to ensure an equilibrium value for the surface tension obtained in the dilute regime. At this stage, the sensitivity to the measuring technique suggests that the nature of the low-concentration breakpoint could be an experimental artefact and this will be

discussed further below. Although the two techniques perform differently at concentrations in the vicinity of the low-concentration break point, they agree well at higher concentrations.

3.3 Effect of EPE copolymer composition

Monodisperse copolymers of various molecular weights were chosen to study the effect of PPO and PEO blocks on the EPE copolymer surface activity. The surface tension data for four such EPE copolymer aqueous solutions at 25°C are plotted against the log of the copolymer bulk concentration in Figure 4. The compositions of the polymers are given in Table 2 of Chapter 2.

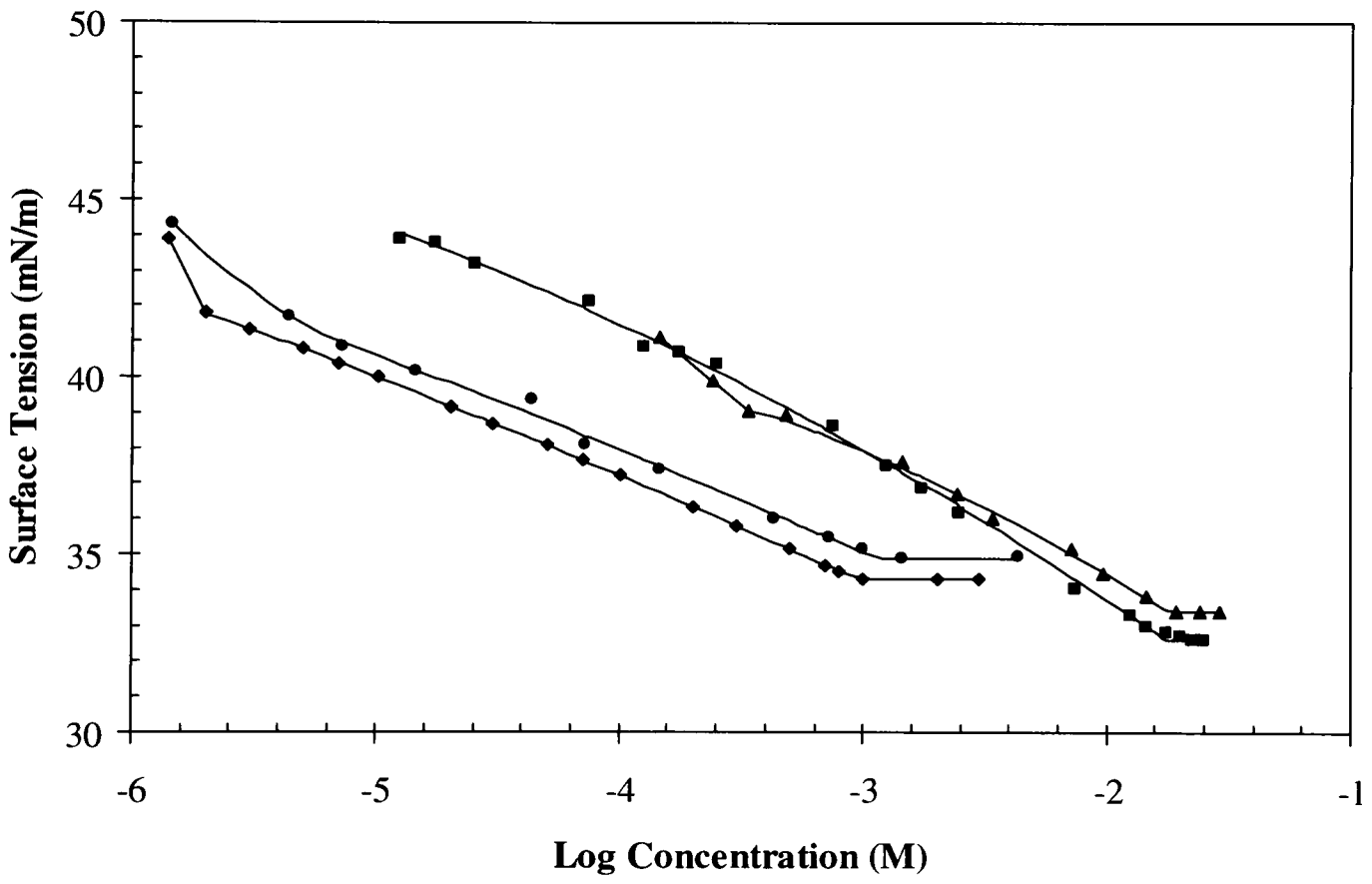


Figure 4. Surface tension against the log of log concentration curves for solutions of EPE copolymers at 25°C: EPE 1250-14 copolymer (▲); EPE 2000-14 copolymer (■); EPE 3000-21 copolymer (●); EPE 3000-14 copolymer (♦)

The values for the CMC and the maximum surface pressure, π_{max}, the surface concentration, Γ_{sat}, and the area per copolymer molecule, A, for the various EPE copolymers studied here are summarised in Table 1.

Copolymer	CMC (M)	π_{max} (mN/m)	Γ_{sat} (mol/cm^2)	A (Å^2)
EPE 3000-14	$9.5x10^{-4}$	37.7	$5.4x10^{-11}$	308
EPE 3000-21	$1.1x10^{-3}$	37.1	$4.6x10^{-11}$	362
EPE 2000-14	$1.8x10^{-2}$	39.4	$4.2x10^{-11}$	395
EPE 1250-14	$1.8x10^{-2}$	38.6	$7.5x10^{-11}$	222
Pluronic P105	$5.9x10^{-4}$	39.6	$8.0x10^{-11}$	338

Table 1. Properties of aqueous solutions of EPE copolymers obtained from surface tension measurements at 25°C.

The data show that the surface activity of EPE copolymers is very sensitive to the copolymer molecular structure. Perhaps the parameter of greatest fundamental value is the CMC, which is strongly influenced by PPO chain length, and to a much lesser extent by the PEO chain length. The CMC for a copolymer with 52 PPO blocks and 46 PEO units increases by 14% (from $9.5x10^{-4}$M to $1.1x10^{-3}$M) when the PEO block size is increased to 88 segments (50% segment number increase) at a constant PPO chain length. The number of EO units has also little effect on the CMC for C_iE_j surfactants[21]. When the same EPE copolymer with 52 units has the PPO block size reduced to 35 segments (33% segment number reduction), the CMC increases from $9.5x10^{-4}$M to $1.8x10^{-2}$M (an increase by a factor of 19). From the linear relationship between the logarithmic CMC and the number of PO units, Wanka *et al.*[8] have determined that the energy increment for the transfer of a PO group from the solution to the micelle core is about 0.2-0.3kT. This value is about 4-5 times less than the value for a CH_2 group, which is 1.2kT. This implies that the hydrophobicity of a CH_2 group is 4-5 times stronger that of a PO group, which is largely attributed to the presence of the polar oxygen atom in the PO group. A differential scanning calorimetry (DSC) study carried out by Hvidt *et al.*[9] has shown that during micellization the PPO segment undergoes an endothermic transition, whereas the PEO segment does not contribute to the transition but prevents the EPE from forming a two-phase system by keeping the PPO in solution as micelles. This observation supports the generally assumed micelle model[10] for EPE copolymers, which consist of a core of PPO

and a corona of PEO chains. Thermodynamic studies[8] on the micellization of EPE copolymers have demonstrated that the process is associated with a large endothermicity, which has been attributed to the dehydration of the PO groups. The negative entropy contribution is however the driving force for the micellization just as for traditional surfactants. The value of the CMC for EPE 1250-14 suggests that the influence of the PEO block length on the micellization becomes more pronounced as the size of PPO block exceeds the size of the PEO block. The values of CMC reported in the literature for Pluronic surfactants differ substantially and, in some instances, such as Pluronic P104[8,11], the values vary by as much as one order of magnitude. This lack of consistency is normally related to batch-to-batch variation of the Pluronic surfactants, although the sensitivity of the surface tension suggests that some of the variation could also be associated with inaccurate or no temperature control.

The area per copolymer molecule increases with the number of EO segments in molecules of EPE copolymer of the same PPO block size. In this study an increase in area per copolymer molecule was also observed with decreasing number of PO segments in molecules of the same PEO block size. The values for surface area per copolymer molecule are relatively small compared with those of nonionic surfactants with an aliphatic chain and an EO headgroup of size comparable with that of the EPE copolymer[12-14]. One might expect that, since the two PEO segments are attached to the ends of the PPO block, the PEO chains would tend to extend horizontally on the interface and therefore occupy a larger area than in the case of C_iE_j surfactants, which are anchored to the interface by their hydrocarbon tail. Such observations indicate that there is considerable folding of the polymer at the air/water interface[15] and/or protrusion of PEO segments into the water phase[16]. There is quite a large discrepancy in the values published for area per molecule for the Pluronic surfactants. In two different papers published in 1994, the area per Pluronic P104 molecule at 25°C was reported to be 310Å^2 by Wanka *et al.*[8] and 75Å^2 by Alexandridis *et al.*[5]. The difference is mainly due to which breakpoint on the surface tension curve was considered. Wanka used the second breakpoint while Alexandridis used the first one. Neutron reflection can resolve quite unambiguously any discrepancies in the areas per segment derived from surface tension data and also the causes for the low area per segment. The neutron reflection

investigations discussed in Chapter 5 and 6 show that the procedure adopted by Wanka to calculate the area per molecule is correct.

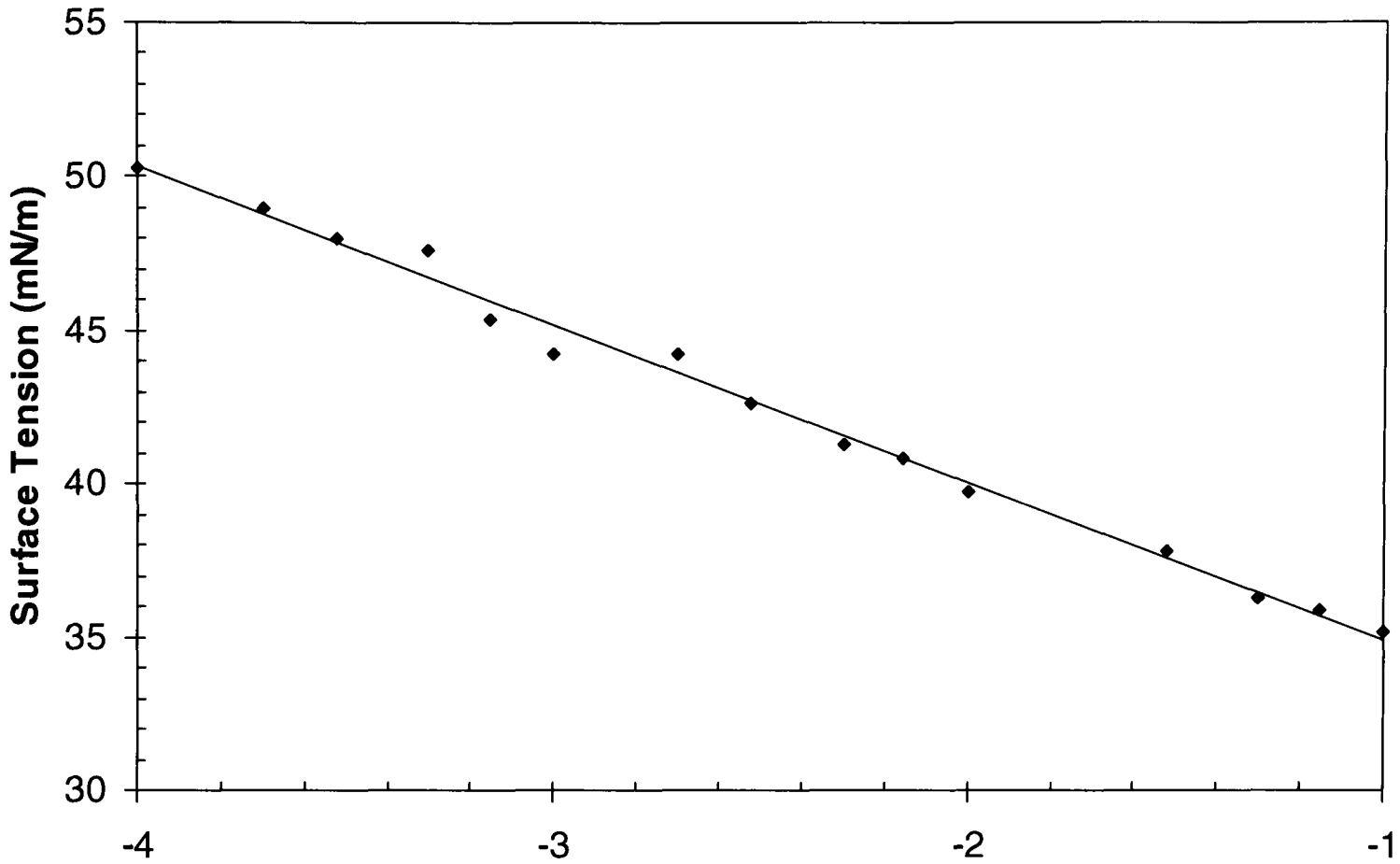


Figure 5. Surface tension against the log of concentration curve for solutions of Polypropyleneglycol MW 725 (PPG 725) measured at 25°C.

The surface tensions at the CMC are higher then the small molecule C_iE_j surfactants where values as low as 25mN/m are found[17]. Furthermore, these values of the surface tension do not seem to depend on the number of the EO groups for polymers of the same PO block size. Although the surface tension of the EPE copolymers is higher than their small molecule counterparts, there is a very large difference in the surface tension behaviour at lower concentrations. As the concentration decreases the EPE copolymers become relatively more efficient in reducing the surface tension. Thus the surface tension of solutions of EPE copolymers studied here increased by only 5-10 mN/m when the bulk copolymer concentration drops by two orders of magnitude below the respective copolymer CMC. For a series of C_iE_8 (i= 9-14) surfactants the surface tension of their solutions increases by 20-30mN/m on reducing the bulk concentration by the same range

below the CMC[20]. The surface tension curve for a water-soluble polypropylene glycol 725 (PPG 725), depicted in Figure 5, showed that it has characteristics more like those of the EPE copolymer. The surface tension for an aqueous solution of PPG 725 is reduced by approximately 10mN/m when the homopolymer bulk concentration is increased from 10^{-3} to 10^{-1}M. This behaviour can be attributed to the very large area per molecule of the EPE copolymers. The Gibbs equation then requires that the increase of surface tension with decreasing concentration is very gradual.

A clear difference between the surface tension curves presented here and those of commercial Pluronic surfactants relates to the low-concentration breakpoint. Alexandridis *et al.*[5] observed that the concentration at this breakpoint was not dependent on the copolymer composition. However Figure 4 shows that is not the case for the EPE copolymers tested here. The concentration at the first breakpoint increases on decreasing the molecular weight of the copolymer. We believe that the low-concentration breakpoint found when using the ring method is somewhat different to that obtained by the plate and reported by Alexandridis *et al.*. The low-concentration breakpoint found with the ring is always followed by a region of instability and lack of reproducibility, which we denote as "experimentally inaccessible". This behaviour may be related either to the effect of the low diffusion rate of EPE copolymers on the stability of the meniscus formed by the ring or to different levels of polydispersity at different molecular weights. In support of the first possibility, a study by Glass[18] of the adsorption properties of polyethylene oxides at the aqueous-air interface also found a decrease in adsorption rate with decreasing bulk concentration. As the Du Noüy ring is pulled, new surface area is continuously created, which is rapidly populated with surfactant molecules diffusing from the bulk. However if the diffusion process is significantly reduced, the timescale required to achieve equilibrium tension is too long for it to be possible to make a true measurement of the surface tension. Therefore when the rate of surfactant diffusion falls below some critical value, the measurement is expected to become time-dependent, unreliable and non-reproducible. The second possible explanation will be examined more closely in the next chapter, following the presentation of the results from neutron reflection.

3.4 Effect of Temperature

The surface tensions of the EPE copolymer solutions were also measured at 35°C. The surface tension curves obtained at both 25° and 35°C for each copolymer are presented in Figures 6-9. As can be seen the surface activity for the EPE copolymers is notably increased by an increase in temperature, as had also been found previously for commercial EPE copolymers[5].

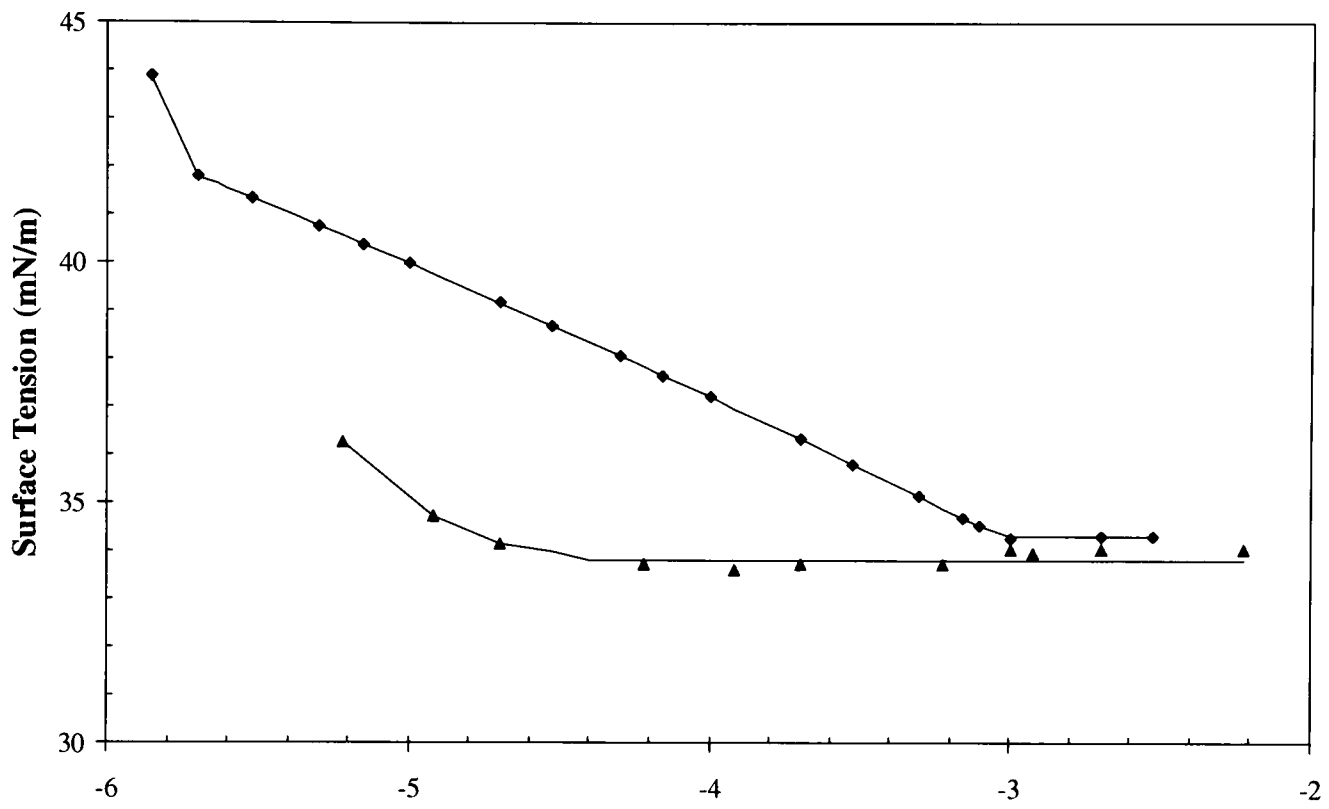


Figure 6. Surface tension against the log of concentration curves for solutions of EPE 3000-14 copolymer measured at 25°C (◆) and 35°C (▲).

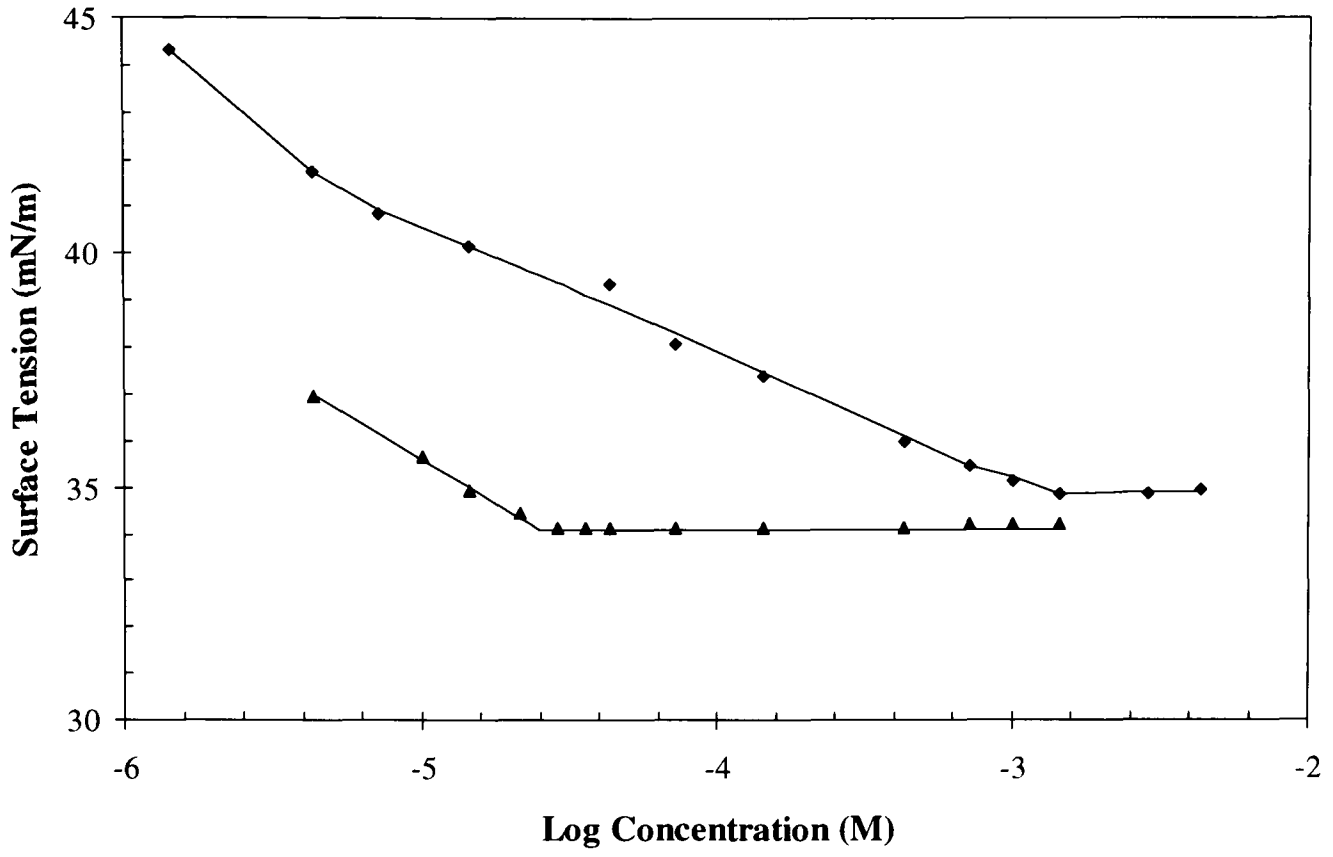


Figure 7. Surface tension against the log of concentration curves for solutions of EPE 3000-21 copolymer measured at 25°C (◆) and 35°C (▲).

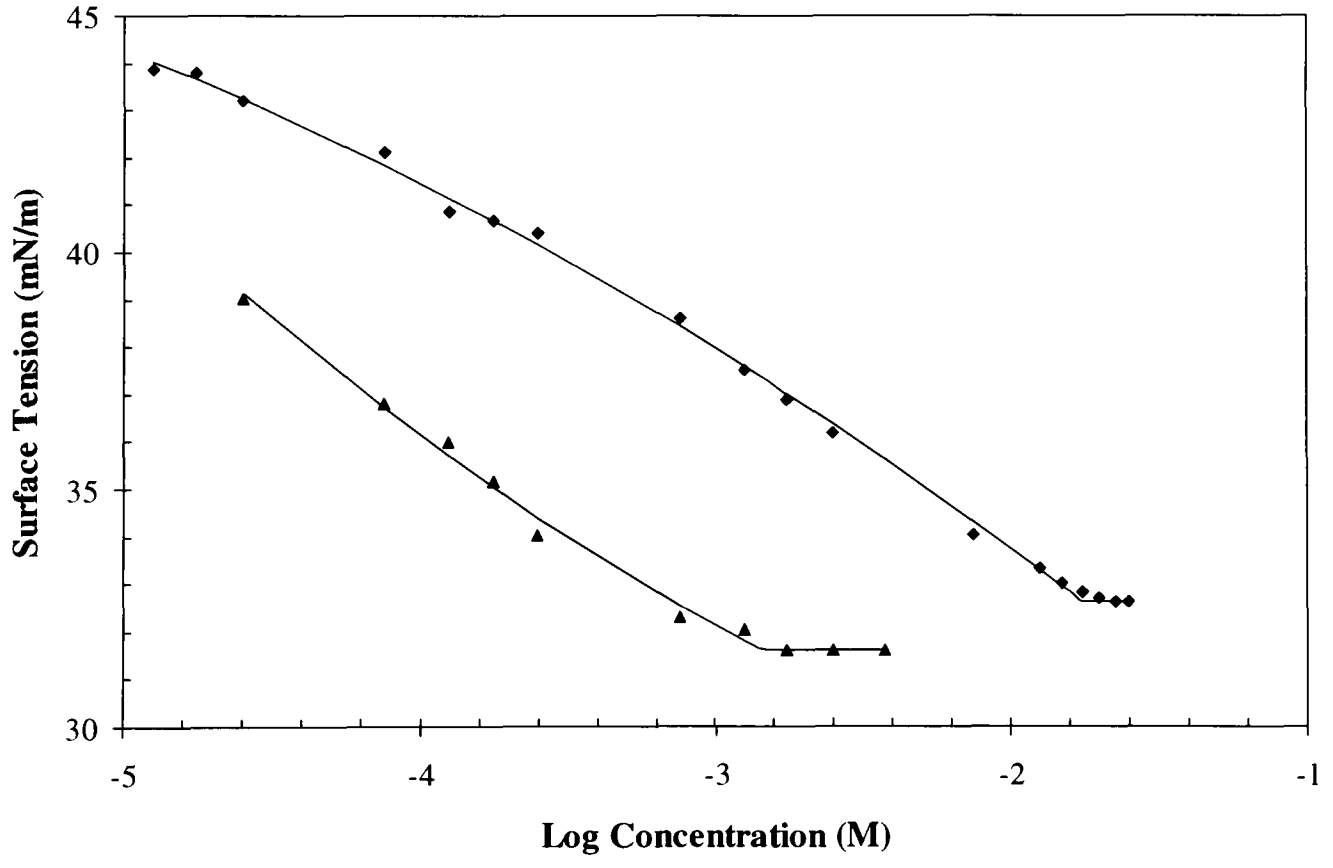


Figure 8. Surface tension against the log of concentration curves for solutions of EPE 2000-14 copolymer measured at 25°C (◆) and 35°C (▲).

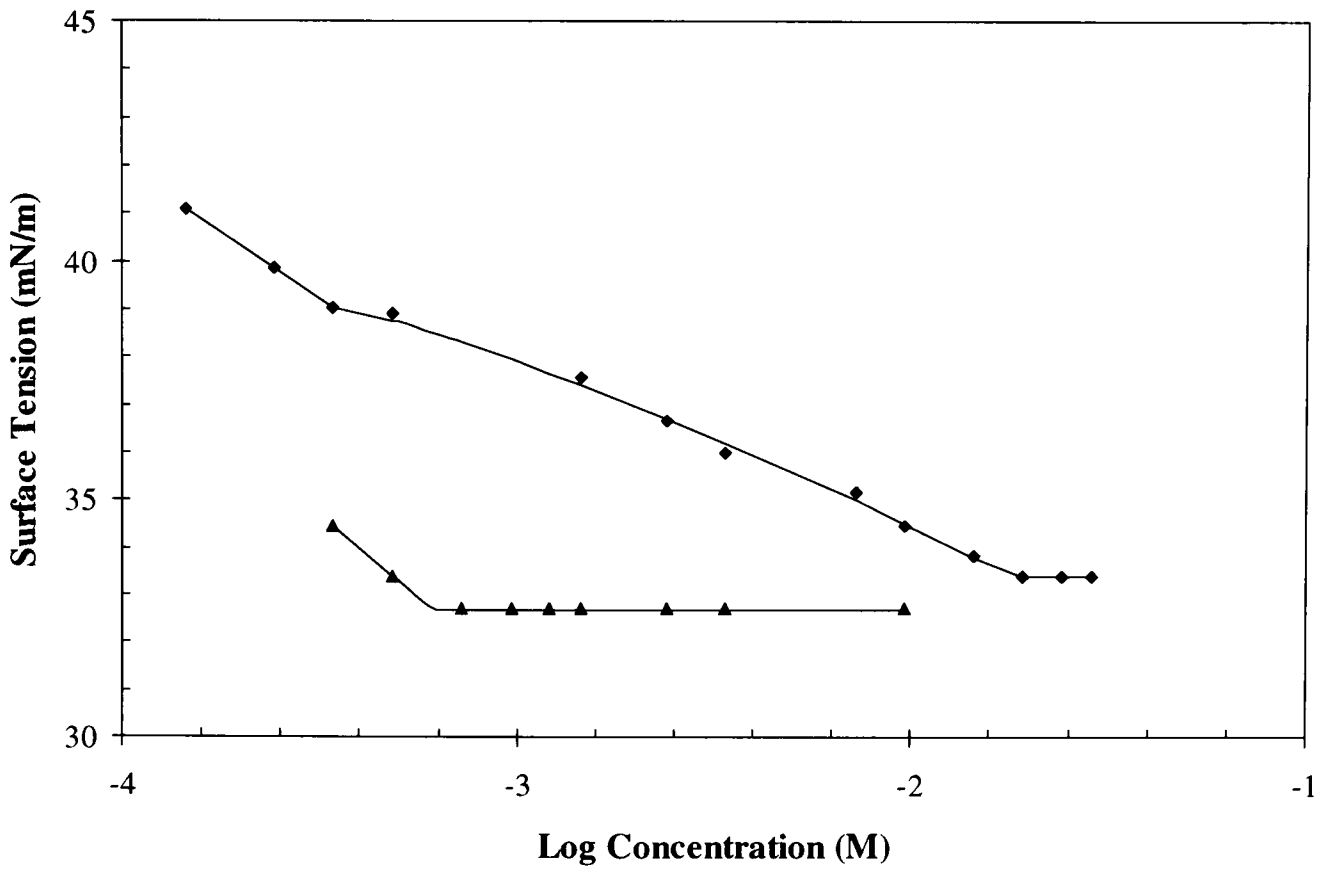


Figure 9. Surface tension against the log of concentration curves for solutions of EPE 1250-14 copolymer measured at 25°C (◆) and 35°C (▲).

The CMC, maximum surface pressure, π_{max}, surface concentration, Γ, area per molecule, A, first breakpoint concentration, C_1, and surface pressure at the first breakpoint, π_1, obtained at 35°C for the EPE copolymers studied here are given in Table 2.

Copolymer	CMC (M)	π_{max} (mN/m)	Γ_{sat} (mol/cm^2)	A (Å^2)
EPE 3000-14	2.7×10^{-5}	38.0	7.3×10^{-11}	230
EPE 3000-21	2.5×10^{-5}	37.9	6.6×10^{-11}	251
EPE 2000-14	1.4×10^{-3}	40.4	5.6×10^{-11}	295
EPE 1250-14	6.1×10^{-4}	39.3	1.2×10^{-10}	141

Table 2. Values for CMC, maximum surface pressure, π_{max}, surface concentration, Γ_{sat}, area per molecule, A, for different EPE copolymer solutions at 35°C.

The CMC values decrease by a factor of 10-45 on increasing the temperature from 25 to 35°C. As the micellization of EPE copolymers is mostly dictated by the PPO block, it is believed that increases in temperature strongly enhance the hydrophobicity of the PO blocks, which leads to an increase in the surface activity of EPE copolymers and a lower CMC. The mechanism behind this temperature dependence is still controversial. Various approaches to explain such behaviour have been based on different pair interactions, which are solvent-solvent, solute-solvent, and solute-solute. Malmsten *et al.*[19] have studied the temperature effects on the conformation of the –OCCO– segment. The increase of temperature induces a reversible conformational change in the –OCCO– segment of PO group, which assumes a less polar conformation. The solvation of this less polar PO group by the water is impaired, rendering the solute-solvent interaction less favourable. The prevalence of the solute-solute interaction over the solute-solvent one leads to the copolymer aggregation or micellization.

Such a remarkable temperature influence is special to this class of polymeric surfactants and in this respect, EPE copolymers differ greatly from C_iE_j surfactants, whose CMC values are much less affected by temperature[20]. The CMC for $C_{12}E_8$ at 15°C is $9.7x10^{-5}$M, whereas at 40°C it drops down to $5.8x10^{-5}$M [20]. The surface tension of EPE copolymers at the CMC, i.e. maximum surface pressure, appears to change only slightly with increasing temperature. However the area per copolymer molecule decreases with increasing temperature, which indicates that the molecules become more compact. This can result from either an increase in dehydration of the polymer molecule at the interface or an increase in the polymer surface concentration, or both. The effect of temperature on the monolayer structure of EPE copolymer studied by neutron reflection is described in Chapter 6.

4 Summary

The adsorption of monodisperse EPE copolymers at the air-water interface has been investigated by surface tension. The surface tension curves showed features similar to those for Pluronic surfactants published in the literature. Two breaks were observed in the surface tension vs log concentration for all tested copolymers. The high-concentration

breakpoint, above which the surface tension attains a steady value, has been attributed to the micelle formation. The concentration at which the low-concentration break occurs, is sensitive to the surface tension method used. The low-concentration breakpoint found when using the ring method is somewhat different to that obtained by the plate and reported by Alexandridis *et al.* A region of instability and lack of reproducibility, which we denote as "experimentally inaccessible", always follows the low-concentration breakpoint found with the ring. This behaviour is possibly related to the effect of the low diffusion rate of EPE copolymers on the stability of the meniscus formed by the ring. Above the low-concentration break however, the two techniques agree well. The origin of the low-concentration breakpoint found with the plate has long been a subject of controversy. Alexandridis *et al.* has argued that the break is a result of copolymer rearrangement at the surface, after ruling out other potential causes such as polydispersity, impurity and formation of monomolecular micelles, although no direct evidence was presented to support this hypothesis. The adsorption and structure of EPE copolymers at the air-solution interface can be probed directly by neutron reflection and this should therefore be the optimum technique for verifying the proposed hypothesis. The results of such a study will be present in Chapters 5 and 6.

The study on the effect of copolymer composition and temperature on the properties of aqueous solutions of monodisperse EPE copolymers produced similar results to those of commercial Pluronic surfactants. The micellization and adsorption properties of EPE copolymers are greatly influenced by the PPO chain size and its hydration level. As with C_iE_j surfactants, the PEO chain size has little effect on the CMC of EPE copolymers. The area per copolymer molecule increased with increasing PEO chain size and decreasing PPO chain size, a pattern similar to C_iE_j surfactants. EPE copolymers, however, differ greatly from C_iE_j surfactants in their high efficiency in reducing the surface tension, which has been attributed to the very large area per molecule of the EPE copolymers. It is evident that the surface activity of EPE copolymers depends strongly on their composition and the use of monodisperse material is therefore crucial for accurate characterization of EPE copolymer solution properties.

References

[1] Linse, P.; and Hatton, T.A. *Langmuir*, 13, 4066 (1997)

[2] Alexandridis, P.; Holzwarth, J. F.; and Hatton, T.A. *Macromolecules*, 27, 2414 (1994)

[3] Lopes, J.R.; and Loh, W. *Langmuir*, 14, 750 (1998)

[4] Alexandridis, P.; Athanassiou, V.; and Hatton, T.A. *Langmuir*, 11, 2442 (1995)

[5] Alexandridis, P.; Athanassiou, V.; Fukuda, S.; and Hatton, T.A. *Langmuir*, 10, 2604 (1994)

[6] Reddy, N.K.; Forster, A.; Styring, M.G.; and Booth, C. *J. Colloid Interface Sci.*, 136, 588 (1990)

[7] Yang, L.; Bedells, A.D.; Attwood, D.; and Booth, C. *J. Chem. Soc. Faraday Trans*, 88, 1441 (1992)

[8] Wanka, G.; Hoffmann, H.; and Ulbricht W. *Macromolecules*, 27, 2445 (1994)

[9] Hvidt, S.; Jorgenson, E. B.; Brown, W.; and Schillen, K. *J. Phys. Chem.*, 98, 12320 (1994)

[10] Mortensen, K. *Europhys. Lett.*, 19, 599 (1992)

[11]Schmolka, I.R.; and Raymond, A.J. *J. Am. Oil Chem. Soc.*, 42, 1088 (1965)

[12] Mysels, K.J. *Langmuir*, 2, 423 (1986)

[13] Kronberg, B.; Stenius, P.; and Thorssell, Y. *Colloid Surf.*, 12, 113 (1984)

[14] Garti, N.; and Katz, M. *J. Dispersion Sci. Technol.*, 6, 149 (1985)

[15] Nikas, Y.J.; Puvvada, S.; and Blankschtein, D. *Langmuir*, 8, 2680 (1992)

[16] Aston, M.S.; Herrington, T.M.; and Tadros, T.F. *Colloids Surf.*, 12, 113 (1984)

[17] Shinoda, K.; Yamanaka, T.; and Kinoshita, K. *J. Phys. Chem.*, 63, 648 (1959)

[18] Glass, J.E *J. Phys. Chem.*, 72, 4459 (1968)

[19] Carlsson, A.; Lindman, B.; Karlstrom, G.; and Malmsten, M. *Adv. Colloid Interface Sci.*, 32, 183 (1990)

[20] Meguro, K.; Ueno, M.; and Esumi, K. *Nonionic Surfactants: Physical Chemistry*, Marcel Dekker, New York, 109 (1987)

Chapter 5

Adsorption of EPE Copolymers at the Air-Solution Interface Studied by Neutron Reflection

1 Introduction

The investigation of adsorption of EPE copolymers at the air-liquid interface has mainly been restricted to surface tension studies of Pluronic surfactants. As discussed in the previous chapter, the surface tension studies reveal a more complex variation of interfacial adsorption with bulk concentration than would be observed for a small molecule surfactant. Specular reflection of neutrons has been shown to be an effective technique for examining polymers and surfactants adsorbed at the air-water interface[1,2], and can provide directly the amount of surfactants or polymers adsorbed at the interface. However, the use of this technique to study EPE copolymers at interfaces has been prevented by the scarcity of deuterated and well-characterised copolymers. We have used the procedure outlined by Altinok *et al.*[3], to produce monodisperse EPE and deuterated EPE copolymers for neutron reflectivity studies.

In this chapter, the results of neutron reflectivity experiments to study the adsorption of EPE copolymers at the air-water interface are presented. Experiments were carried out with copolymers of different compositions, over a range of concentrations and at two temperatures, 25°C and 35°C. The results of the neutron reflectivity measurements are related to those obtained by surface tension and the combination gives some insight into the adsorption of EPE copolymers at the air-water interface and enables us to explain ambiguities in the interpretation of earlier surface tension work.

2 Experimental Details

2.1 Materials

Two partially deuterated EPE copolymers, d-EPE 3000-14 and d-EPE 1250-14, were selected for this set of experiments. Deuterated isotopic species were prepared by reacting deuterated EO with a protonated PPO homopolymer, as described in Chapter 2. Both d-EPE 3000-14 and d-EPE 1250-14 are close matches to their respective protonated counterparts with respect to the GPC and surface tension results. For the measurements of surface excess the solutions of deuterated EPE copolymers were prepared in "null reflecting water" (NRW).

2.2 Neutron reflectivity measurement and data analysis

All the neutron reflection measurements reported in this chapter were made using the reflectometer SURF at the Rutherford Appleton Laboratory in Didcot, Oxfordshire. The characteristics and use of this instrument have already been described in Chapter 2. Measurements were made at the air-solution interface using teflon troughs mounted on an antivibration bench. The experiments were carried out at 25° and 35°C. Each solution was measured at fixed incident angles of 0.8° and 1.5°. Sample alignment was achieved as previously discussed using a laser guide. Calibration of the detector efficiency was made before each experimental session using D_2O.

The SURF reflectometer uses the time of flight method of analysis (see Chapter 2 for description) so that each measurement collects reflectivities at all values of the momentum transfer, Q, simultaneously. The exposure time of each sample was varied according to the concentration of reflecting species at the interface to ensure that in all cases, good statistics were obtained out to a relatively high Q. At high Q, the reflectivity tends toward the background level. For adsorbed surfactant monolayers, this is the case for momentum transfers of over about 0.3Å^{-1}. The component of the measured signal from the background is present in all experimental data points. However, on the SURF reflectometer, the level of background scattering is independent of momentum transfer, so that it is possible to subtract a constant background from the whole set of experimental data to obtain the true reflectivity.

2.3 Determination of Adsorbed Amounts

In this study, all the neutron reflectivity data were analysed using the Optical Matrix Method, which was described in Chapter 2. In this method, it is assumed that the interface can be described in terms of a number of discrete layers of different scattering length density and thickness. The reflectivity of the model interface can then be calculated from these parameters, compared with the measured profile and the various parameters adjusted in order to achieve a good fit between the measured data and calculated profiles. In order to determine the adsorbed amount at the air-water interface in a single surfactant system, it is often adequate to describe the interface in terms of a one-layer model containing surfactant heads and chains, solvent and air. For a surfactant in null reflecting water, the measured reflectivity of the adsorbed layer, will contain no contribution from the solvent or air and will simply be related to the adsorbed amounts of the surfactant and its scattering length by:

$$\rho\tau = \frac{b}{A} \tag{5.1}$$

where τ refers to the layer thickness, ρ is the layer scattering length density, b is the scattering length of the surfactant, and A is the area per surfactant molecule at the interface. The parameters obtained from the data fit are the scattering length density of the layer ρ, and its thickness, τ. With these data, the area per molecule can be calculated using Equation 5.1. The adsorbed amount, or surface excess, Γ, is given by

$$\Gamma = \frac{1}{AN} \tag{5.2}$$

where N is Avogadro's number.

The scattering lengths, approximate molecular volumes and calculated scattering length densities of the various species used in the neutron reflection experiments are given in Table 1.

Species	Scattering lengths (Å)	Molecular volume ($Å^3$)	Scattering length density ($Å^{-2}$)
d-EPE 3000-14	$2.19x10^{-2}$	8,000	$2.74x10^{-6}$
d-EPE 1250-14	$8.63x10^{-3}$	3,300	$2.62x10^{-6}$
d-EO	$4.40x10^{-4}$ (96%D)	64.6	$6.81x10^{-6}$
h-PO	$3.31x10^{-5}$	96.5	$0.34x10^{-6}$
H_2O	$-1.68x10^{-5}$	30	$-0.56x10^{-6}$
D_2O	$1.91x10^{-4}$	30	$6.35x10^{-6}$
NRW (8.1%v/v D_2O)	0	30	0

Table 1: Values for the various species used in the neutron reflection experiments

2.4 Determination of the surface tension-log C curve from the neutron reflectivity data

A convenient way to test the consistency of neutron reflection and surface tension techniques is to construct a γ-log *c* plot from the neutron reflection results. To construct the γ-log *c* curve, the surface excess obtained from the neutron reflection is first plotted against the logarithm of EPE copolymer bulk concentration and then fitted to a quadratic equation. This quadratic equation is subsequently integrated using Equation 5.3, which is a differential relationship between the surface tension and the surface excess for nonionic surfactants. Only a single measurement of the surface tension is used, that at the CMC, where the measurement is also usually reliable, and it avoids the large inaccuracies in determining the slope of the tangent to the γ-log *c* plot.

$$\gamma - \gamma_0 = -2.303RT \int_{\log c_0}^{\log c} \Gamma d \log c \qquad (5.3)$$

where γ is the surface tension, γ_0 is the reference surface tension at the chosen concentration c_0, Γ is the surface excess, and c is the concentration.

3 Results and Discussion

3.1 Amount of EPE 3000-14 adsorbed at the air-solution interface

The reflectivity of deuterated PEO-chain EPE 3000-14 (d-EPE 3000-14) in NRW was measured over a range of concentration at 25°C. As explained in the previous section, any specular neutron reflection from these solutions results only from EPE copolymers adsorbed at the surface. The reflectivity profiles at various d-EPE 3000-14 concentrations are shown in Figure 1. The error bars have been omitted for clarity. The continuous lines are reflectivities calculated for the single-layer model.

Figure 1 shows that the specular reflectivity decreases rapidly with increasing scattering vector, indicating that the surface layers are rather thick. The neutron reflectivity of the different d-EPE 3000-14 solutions change in both level of reflectivity and in slope as the copolymer concentration is varied. A small stepwise decrease in reflectivity level with decreasing concentration is observed when the concentration is reduced from $1.2\text{x}10^{-3}$M to $6.0\text{x}10^{-4}$M, and this is followed by a much larger drop when the concentration is reduced to $1.0\text{x}10^{-4}$M. Between $1.0\text{x}10^{-4}$M and $2.0\text{x}10^{-6}$M the reflectivity only decreases very slightly but below $2.0\text{x}10^{-6}$M it drops more sharply. The reflectivity level is approximately determined by the total scattering length density in the layer as is clear from the kinematic approximation[4], which gives the following expression for the reflectivity, R,

$$R = 16\pi^2 mh(Q)/Q^2 \qquad (5.4)$$

where m is the integrated scattering length density over the interface, $h(Q)$ is the form factor of the interface, and Q is the momentum transfer normal to the interface. Thus, the decrease in reflectivity observed with decreasing concentration corresponds to a decrease in the amount of adsorbed copolymer at the interface. The change in the slope of the curves followed a similar pattern of changes with concentration. Since the slope of each curve is related to the thickness of the adsorbed layer, the changes in the thickness of the layer parallel the changes in surface concentration.

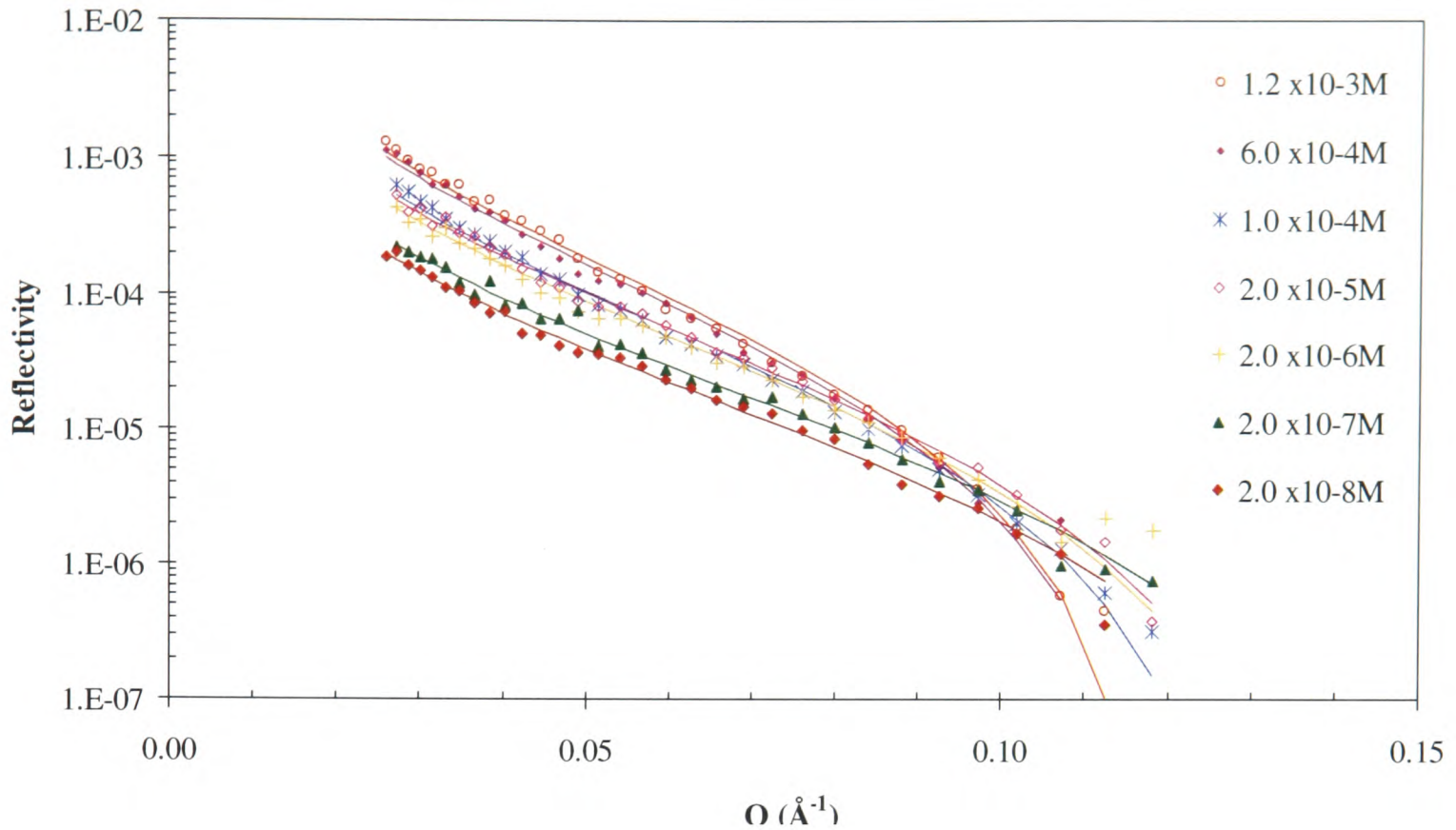


Figure 1. Neutron reflectivity profiles for d-EPE 3000-14 in null reflecting water at 25°C.

The reflectivity curves were fitted using a model of a single layer of adsorbed EPE copolymer of uniform composition using the Optical Matrix Method. Although this is not a realistic model, it is sufficient to characterise approximately the thickness and amount of adsorbed EPE copolymer. As explained in Chapter 2, the data presented here were fitted with the aid of AFIT[5] computer program. The model values of thickness, τ, scattering length density of the layer, ρ, the area per EO unit, $A_{\text{EO unit}}$, the area per copolymer molecule, $A_{\text{copolymer}}$, and the copolymer surface excess, Γ, are given in Table 2. The areas per copolymer molecule were calculated from Equation 5.1 using the values of scattering length given in Table 1. The surface excesses were then calculated from Equation 5.2. The complete set of reflectivity curves and best fits of the single layer model for each copolymer concentration are shown in Appendix 1.

Concentration (M)	τ Å	ρ x10^6 Å^{-2}	$A_{EO\ unit}$ Å^2	$A_{copolymer}$ Å^2	Γ x10^{11} mol/cm^2
1.2x10^{-3}	54±3	1.37	5.9 ±5%	297±5%	5.60±0.4
6.0x10^{-4}	54	1.30	6.3	313	5.31
2.0x10^{-4}	53	1.15	7.2	360	4.61
1.0x10^{-4}	50	1.07	8.2	410	4.05
6.0x10^{-5}	49	1.09	8.2	411	4.04
2.0x10^{-5}	47	1.08	8.7	432	3.84
2.0x10^{-6}	47	1.01	9.3	462	3.59
1.0x10^{-6}	47	0.88	10.6	530	3.13
2.0x10^{-7}	43	0.81	12.6	630	2.64
2.0x10^{-8}	44	0.70	14.3	712	2.33

Table 2. Fitted parameters using the one-layer model for adsorbed d-EPE 3000-14 at 25°C

The area per EO segment at 1.2x10^{-3}M is approximately 6Å^2, which is much less than the 11-12Å^2 per EO segment obtained for the $C_{12}E_j$ series at their CMCs[6]. The fully extended length of an EO chain increases by 3.6[7] per EO units, and the thickness of a chain containing 23 EO adducts should therefore be about 83Å. However, the total thickness obtained for the deuterated EPE 3000-14 at the 1.2x10^{-3}M is only 54Å. It should be noted that 54 Å also contains a contribution from the PPO chain, whose scattering length is not exactly zero, and therefore the true thickness of the EO chain layer should be smaller. This observation suggests that there is significant mixing or disorder within the monolayer. A similar irregularity has been found in the thickness of $C_{12}E_j$ monolayers with increasing size of the headgroups. The total monolayer thicknesses for $C_{12}E_2$, $C_{12}E_3$, $C_{12}E_4$, $C_{12}E_5$, $C_{12}E_6$, $C_{12}E_8$ and $C_{12}E_{12}$ published in the literature are 22.0, 23.0, 23.0, 24.0, 26.5, 28.0 and 31±2Å, respectively[8-10]. The average increase in thickness per EO unit in that $C_{12}E_j$ series is about 0.9Å. The structure of EPE copolymer monolayer at air-solution interface will be further examined in Chapter 6.

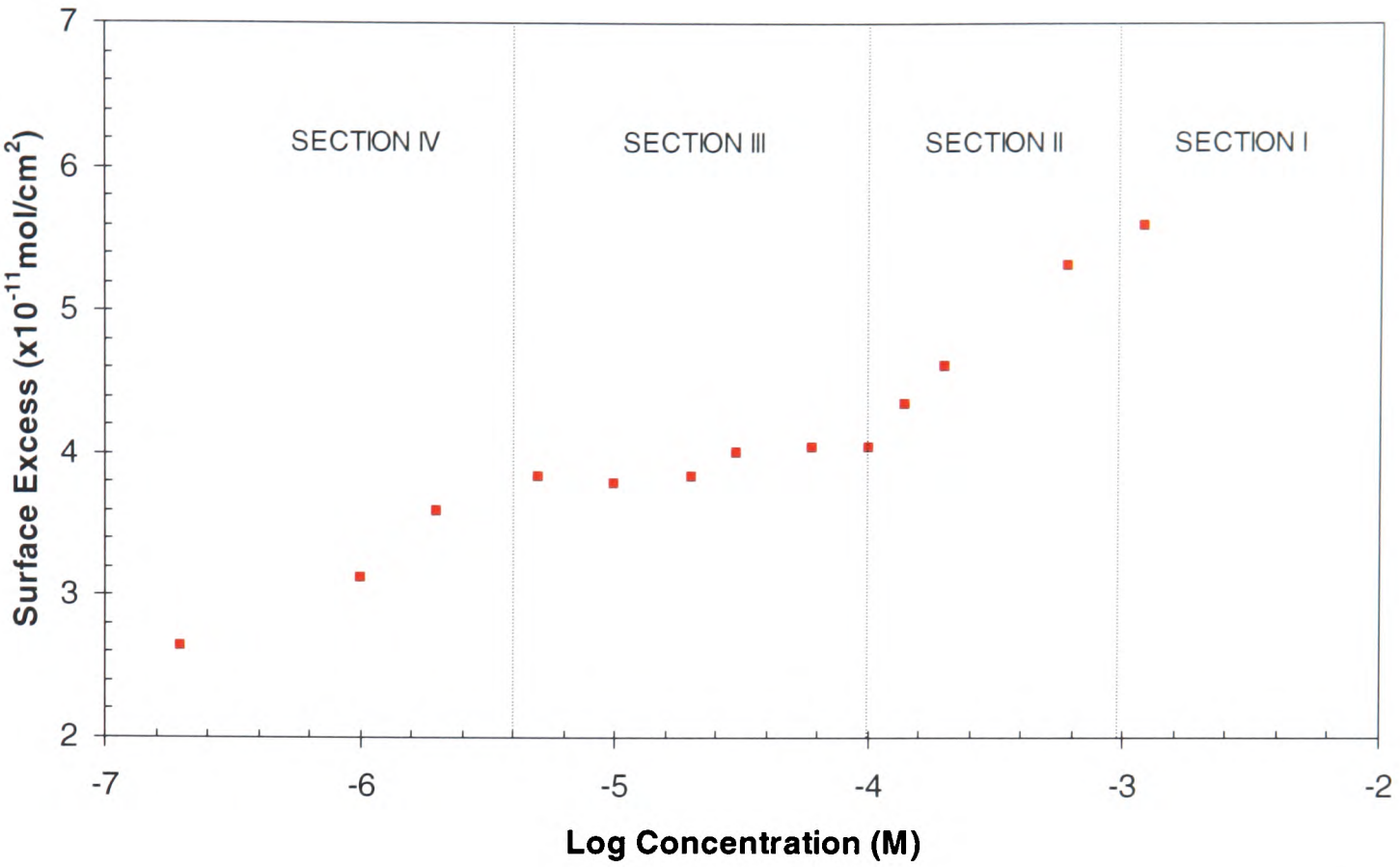


Figure 2. Adsorption isotherm of d-EPE 3000-14 at the air-solution interface at 25°C determined by neutron reflection.

The surface excess values obtained from the fitted parameters were plotted against log c and the curve is shown in Figure 2. This figure confirms the interesting pattern of adsorption anticipated from the reflectivity curves. The adsorption isotherm can be divided into four distinct sections. In section IV the surface excess decreases gradually with decreasing bulk concentration. In section III, which lies between 10^{-4} and $5x10^{-6}$M, the surface excess remains almost unchanged. This smooth variation of surface coverage with bulk concentration resembles the behaviour of poly(ethylene oxide)[11,12] and highly ethoxylated $C_{12}E_j$[6], which also show a gradual variation of surface excess with concentration. However, the behaviour of EPE 3000-14 is distinguished from these other two materials by a steep change of surface excess with concentration above 10^{-4}M in section II. Although the surface excess increases by almost 40% between 10^{-4}M and $1.2x10^{-3}$M, the thickness of the monolayer does not change significantly. This observation implies that the sudden increase in surface excess of section II results neither from bilayer formation nor from surface micellization. It is therefore probable that the sudden increase in surface excess arises from an increase in the disorder or the extent of PPO and PEO chain intermixing within the monolayer. Increased chain mixing with concentration could

possibly create space in the monolayer for further EPE molecule adsorption. This would require the orientation of EPE copolymers at the air-water interface to be more complex than the conventional inverted U orientation previously assumed. Section I is where the bulk solution is micellar. The CMC for EPE 3000-14 determined by surface tension is $9.5x10^{-4}$M at 25°C. In this section of the isotherm, although not enough data have been collected from the neutron reflection, there appears to be a much more gradual increase in the surface excess with bulk concentration.

3.2 Effect of Temperature

The reflectivity of d-EPE 3000-14 solutions was also measured at 35°C. As in the previous section, the solutions were prepared with null reflecting water. To compare the effect of temperature some of the reflectivity curves of d-EPE 3000-14 at different concentrations measured at both 25°C and 35°C are plotted together in Figure 3. The error bars have been omitted for clarity.

Figure 3 shows some interesting effects of temperature on the neutron reflectivity properties of the adsorbed monolayer of EPE 3000-14 copolymer. From the surface tension studies the CMC for this copolymer measured at 25°C is $9.5x10^{-4}$M and $2.7x10^{-5}$M at 35°C. It appears that above the CMC there is a little effect of the temperature on the level of reflectivity. As discussed above, the level of reflectivity is related to the amount of adsorbed copolymer at the interface. Consequently the amount of copolymer in the monolayer at or above the CMC is not greatly affected by increasing the temperature from 25°C to 35°C. This observation agrees with the small change in maximum surface pressure observed in the surface tension curves at both temperatures. However, below the CMC, there is a significant increase in the level of reflectivity between 25°C and 35°C without a significant change in the slope of the reflectivity curves, which implies that temperature has much less effect on the monolayer thickness than on the adsorbed amount.

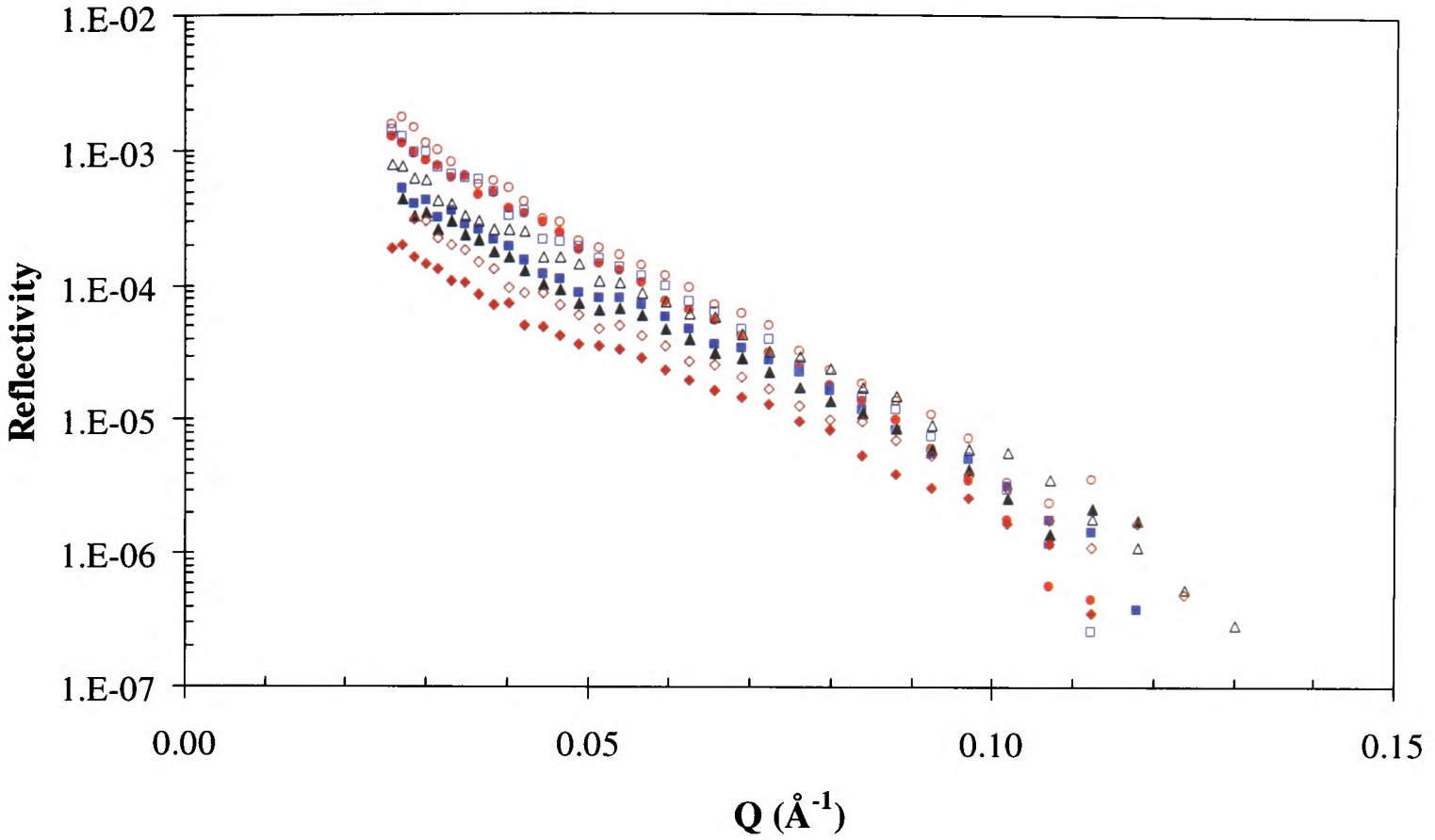


Figure 3. Neutron reflectivity profiles of d-EPE 3000-14 in null reflecting water at different concentrations: 1.2×10^{-3}M (●), 2.0×10^{-5}M (■), 2.0×10^{-6}M (▲), 2.0×10^{-8}M (♦), and at temperatures of 25°C (closed symbols) and 35°C (open symbols).

The curves were fitted into a uniform single model and the resulting values of thickness, τ, and scattering length density of the layer, ρ, are given in Table 3 together with the calculated values of the area per copolymer molecule, $A_{copolymer}$, and the copolymer surface excess, Γ. The individual reflectivity curves for each copolymer concentration measured at 35°C are given in Appendix 4.

Comparison of the results presented of Table 3 with the values given in Table 2 confirm that, while the total amount of adsorbed EPE copolymer increases with temperature, the monolayer thickness remains unchanged. As examined in the previous chapter, the surface activity of EPE copolymers is strongly dependent on the PPO chain. The remarkable effect of temperature on their surface activity has been attributed to a temperature-induced conformational change of PO and EO groups, which increases the population of less polar conformers, rendering the interactions PO-water and EO-water less favourable than the PO-EO interaction. This argument is supported by the

Flory-Huggins interaction parameters, χ_{BB}, calculated in previous studies on phase diagram of PPO-water[13] and PEO-PPO-water[14]. The $RT\chi_{polar\text{-}PO,water}$ and $RT\chi_{polar\text{-}PO,polar\text{-}EO}$ parameters are very similar, 1.7kJ/mol and 1.8kJ/mol, respectively. However, when the PO groups assume a less polar conformation the $RT\chi_{nonpolar\text{-}PO,water}$ parameter increases to 8.5kJ/mol, while the $RT\chi_{nonpolar\text{-}PO,polar\text{-}EO}$ parameter increases to a lesser extent, to 3.0kJ/mol. Hence with an increase of temperature the monolayer becomes more condensed.

Concentration (M)	τ Å	ρ x10^6 Å^{-2}	$A_{copolymer}$ Å^2	Γ x10^{11} mol/cm^2
1.2E-03	54±3	1.52	267±5%	6.21±0.4
6.0E-04	54	1.51	269	6.17
2.0E-04	51	1.57	274	6.06
2.0E-05	52	1.40	301	5.51
2.0E-06	45	1.27	384	4.33
2.0E-08	45	0.89	548	3.03

Table 3. Fitted parameters using the one-layer model for adsorbed d-EPE 3000-14 at 35°C

3.3 Effect of EPE Copolymer Composition

To study the effect of composition on the adsorption of EPE copolymers, the reflectivity of solutions of deuterated PEO-chain EPE 1250-14, abbreviated here as d-EPE 1250-14, was measured at 25°C for comparison with d-EPE 3000-14. The reflectivity profiles are shown in Figure 4. The error bars have been omitted for clarity and the continuous lines are reflectivities calculated for the single-layer model.

The reflectivity of EPE 1250-14 depicted in Figure 4 shows a similar pattern to that in Figure 1. The specular reflectivity of d-EPE 1250-14 also indicates a thick monolayer because of the rapid decrease of reflectivity with increasing momentum transfer. A similar stepwise pattern of decrease in reflectivity with decreasing concentration as for

dEPE 3000-14 is also observed. The reflectivity reduces gradually on decreasing the concentration down to about $2.3x10^{-5}$M. Between $2.3x10^{-5}$M and $2.3x10^{-7}$M the reflectivity remains unchanged, and below that range the reflectivity drops again. The flat reflectivity region is of comparable size for both copolymers, but for EPE 1250-14, the region is shifted by an order of magnitude in concentration.

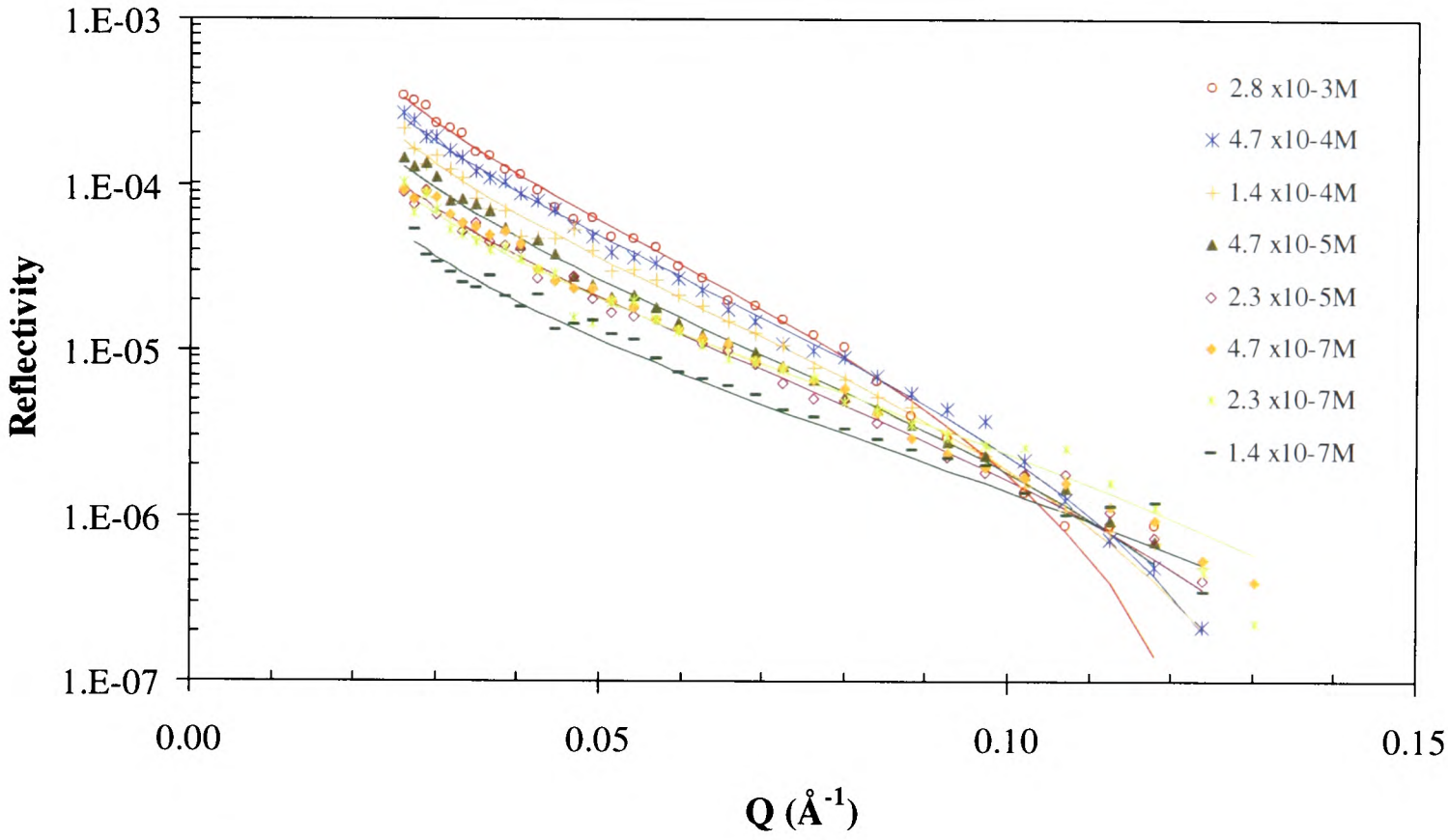


Figure 4. Neutron reflectivity profiles for d-EPE 1250-14 in null reflecting water at 25°C.

The curves were fitted to a uniform single model and the resulting values of thickness, τ, and scattering length density of the layer, ρ, are given in Table 4. The calculated values of the area per copolymer molecule, $A_{copolymer}$, and the copolymer surface excess, Γ , are also included in Table 4. The reflectivity curves are given in Appendix 3.

Concentration (M)	τ Å	ρ x10^6 Å^{-2}	$A_{copolymer}$ Å^2	Γ x10^{11} mol/cm^2
2.8E-03	49±3	0.82	215±5%	7.73±0.5
4.7E-04	45	0.77	249	6.67
3.3E-04	44	0.73	269	6.18
1.4E-04	44	0.67	293	5.67
4.7E-05	41	0.60	351	4.73
2.3E-05	39	0.55	402	4.13
2.3E-06	36	0.59	406	4.09
4.7E-07	36	0.58	413	4.02
2.3E-07	33	0.61	429	3.87
1.4E-07	32	0.47	574	2.89

Table 4. Fitted parameters using the one-layer model for adsorbed d-EPE 1250-14 at 25°C

The adsorption characteristics of EPE 3000-14 and EPE 1250-14 are compared by plotting the surface excess values obtained from the fitted parameters against log c. The result is shown in Figure 5. The CMC values for both copolymers are marked on the plot.

As anticipated from the discussion of the neutron reflectivity profiles, the adsorption of the two copolymers shows a consistent pattern. The distinct sections observed with the adsorption isotherm of EPE 3000-14 are also evident on that of EPE 1250-14. Figure 5 shows that section III, in which only a small change of surface excess with concentration occurs, is at a very similar value for the two copolymers, at about $4x10^{-11}$mol/cm^2. The steep change of surface excess with concentration in section II starts to happen at a lower concentration for the smaller copolymer. The sudden increase in surface excess in this region has previously been accounted for in terms of a reorganisation of the copolymer molecules within the monolayer. The slope of the curve in section II is similar for both copolymers.

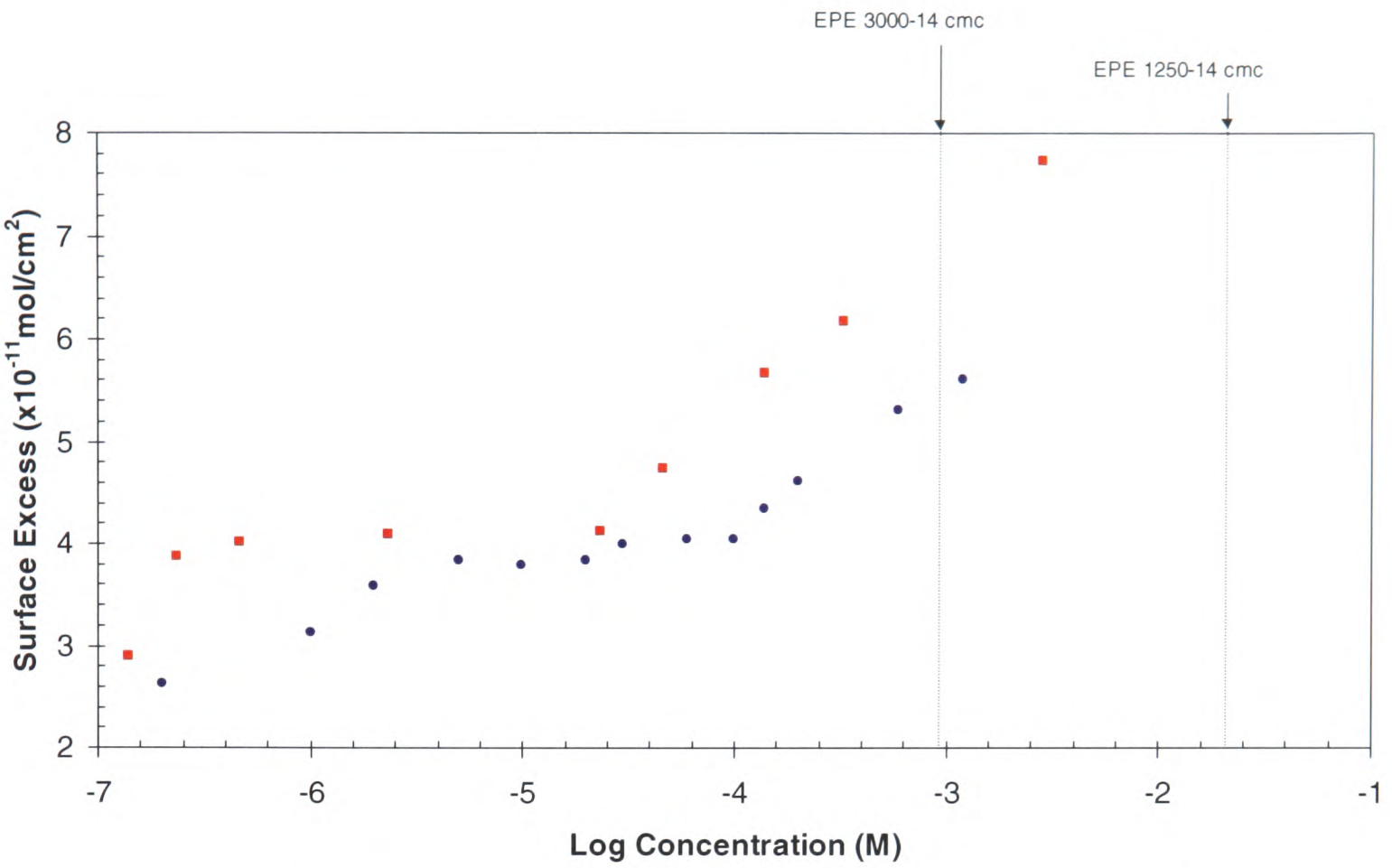


Figure 5. Air-solution interface adsorption isotherms determined by neutron reflection of d-EPE copolymers, EPE 1250-14 (■) and EPE 3000-14 (●), at 25°C.

3.4 Comparison with surface tension data

From the slope of the surface tension curve it is possible to determine the surface excess by applying Gibbs' equation. Good consistency has generally been obtained between data obtained from surface tension and neutron specular reflectivity[15]. In this section the data extracted from the neutron reflection experiments with EPE copolymers are compared with those from the surface tension measurements.

3.4.1 Surface excess and area per copolymer molecule at saturation:

To obtain the surface excess at saturation from the neutron reflection experiments, the sets of surface excess results down to 10^{-4}M at 25°C and down to $2x10^{-6}$M at 35°C, were first fitted to a quadratic function. The regression coefficients, R^2, were consistently greater than 0.999. The surface excess value corresponding to the CMC, obtained by the surface tension method, was then calculated using the quadratic equation. Good agreement between the values of surface excess for EPE 3000-14 was obtained for the

two sets of measurements at 25°C. The value obtained from the surface tension measurement at the CMC is $5.40x10^{-11}mol/cm^2$, which is close to the $5.51x10^{-11}mol/cm^2$ obtained from neutron reflectivity. The value of the area per molecule produced by neutron reflection is $301Å^2$, while by surface tension it is $308Å^2$ at the CMC. At 35°C, however, the surface excess values and area per molecule from the two techniques disagreed. At the CMC the surface excess calculated from the surface tension measurements was $7.3x10^{-11}mol/cm^2$, while from the neutron reflection it is $5.6x10^{-11}mol/cm^2$. The value of the area per molecule from the neutron reflection experiments is $297Å^2$, while from surface tension it was found to be $230Å^2$ at the CMC. Figure 6 of Chapter 4 shows that the CMC value determined by surface tension using the ring method at 35°C is very close to the "experimentally inaccessible" region, which is likely the be the reason for the lack of agreement between the two techniques at this temperature. The surface excess values obtained from neutron reflectivity are plotted against log c in Figure 6.

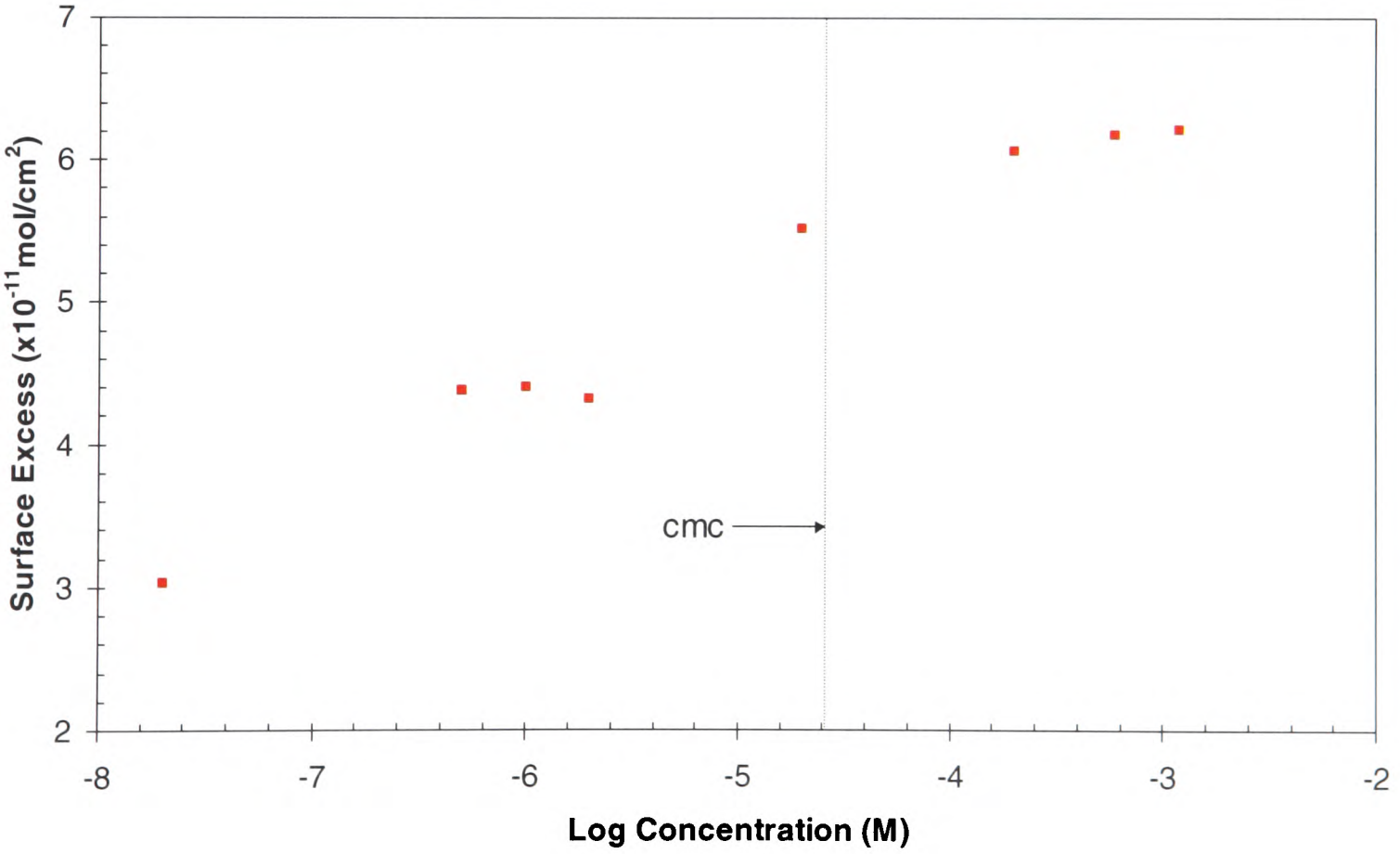


Figure 6. Adsorption isotherm of d-EPE 3000-14 at the air-solution interface at 35°C determined by neutron reflection.

3.4.2 Bulk depletion effect:

The nature of the low concentration breakpoint in the surface tension curves of EPE copolymers has long been a subject of controversy. Alexandridis *et al.*[16] suggested that the low-concentration breakpoint could originate from a rearrangement of the copolymer molecules on the surface, although no direct experimental evidence was presented. According to their proposal, at copolymer concentrations below the first break, the copolymer molecules adsorb on the air-water interface as an inverted U with the PEO chains located at the interface, oriented similarly to PEO homopolymers at the air-water interface. At the first break (approximately 10^{-3}w/v%), when the interface is fully covered with copolymer, a change in configuration takes place and the copolymer layer becomes more compact with water molecules being expelled from the monolayer and the PEO segments either dipping into the aqueous solution or folding around the PPO chain. As a result of the molecular rearrangement within the monolayer, more copolymer molecules are adsorbed in the interfacial layer causing it to become thicker. The surface tension continues to decrease with increasing bulk copolymer concentration until micellization takes place. This hypothesis is not at all consistent with the neutron reflectivity results. The adsorption isotherm of EPE 3000-14 depicted in Figure 2 shows that in Section IV of the isotherm the surface excess increases with concentration up to $4x10^{-6}$M (approx. $2x10^{-3}$%) and then there is a significant change of slope. Above this concentration, i.e. Section III of the isotherm, the surface excess hardly changes with concentration, which suggests that the monolayer is complete and undergoes no further change in Section III. Copolymer rearrangement within the monolayer only occurs above 10^{-4}M, in Section II of the isotherm, almost two orders of magnitude higher than the change suggested by Alexandridis *et al.* Thus, the interpretation of the first breakpoint as a change of the copolymer configuration at the interface is not consistent with the neutron reflectivity data.

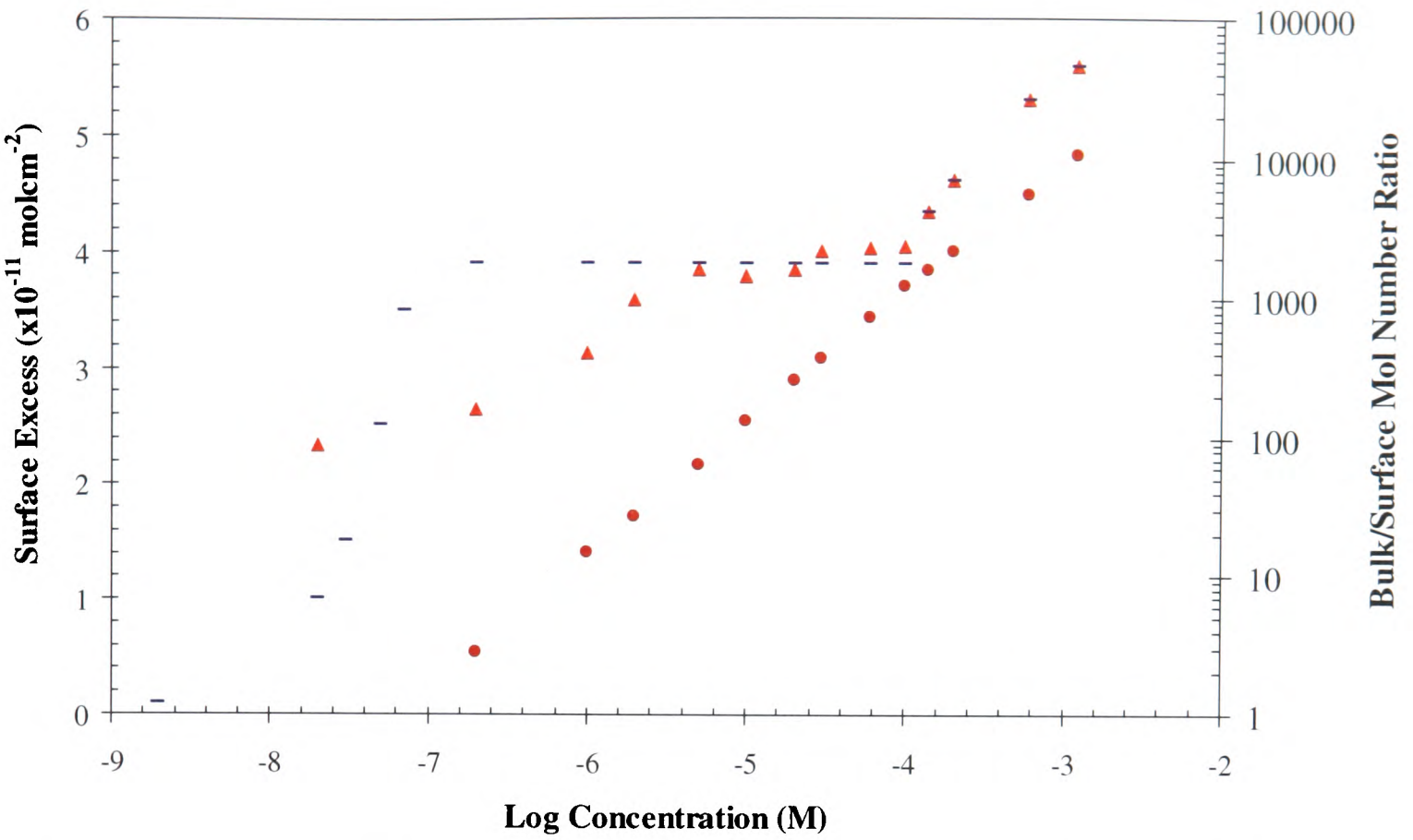


Figure 7. Surface excess as a function of the log bulk EPE 3000-14 concentration at 25°C, determined by neutron reflection, (▲), and assuming bulk depletion effect, (—). Ratio of copolymer molecule number in the bulk and at the interface, (●).

Linse *et al.*[17] have suggested that the low concentration break point results from depletion of the bulk concentration of copolymer as material is adsorbed at the surface. For EPE 3000-14 solutions at 25°C, the monolayer was complete at bulk concentration of $4x10^{-6}$M, confirming the strong surface activity of the copolymer. At extremely low concentrations, adsorption at the interface has a significant effect on the concentration of the bulk solution of copolymer molecules and this feeds back into the surface tension. Figure 7 shows the change of the ratio of EPE 3000-14 molecules in the bulk and at the interface with bulk concentration. The number of molecules in the bulk drops directly in proportion with the number of molecules at the interface, as the copolymer concentration is reduced. It becomes evident that below a certain concentration, the concentration of EPE copolymer at the surface is limited by the total amount of molecules actually present in the solution. Assuming that the EPE copolymer molecules would preferentially adsorb at the surface rather than be dispersed in the bulk, the concentration of EPE 3000-14 below which bulk depletion would have an effect is 10^{-7}M for solutions at 25°C. In

Figure 7 the curve (—) represents the calculated surface excess for EPE 3000-14 assuming preferential adsorption and hence bulk depletion below 10^{-7}M.

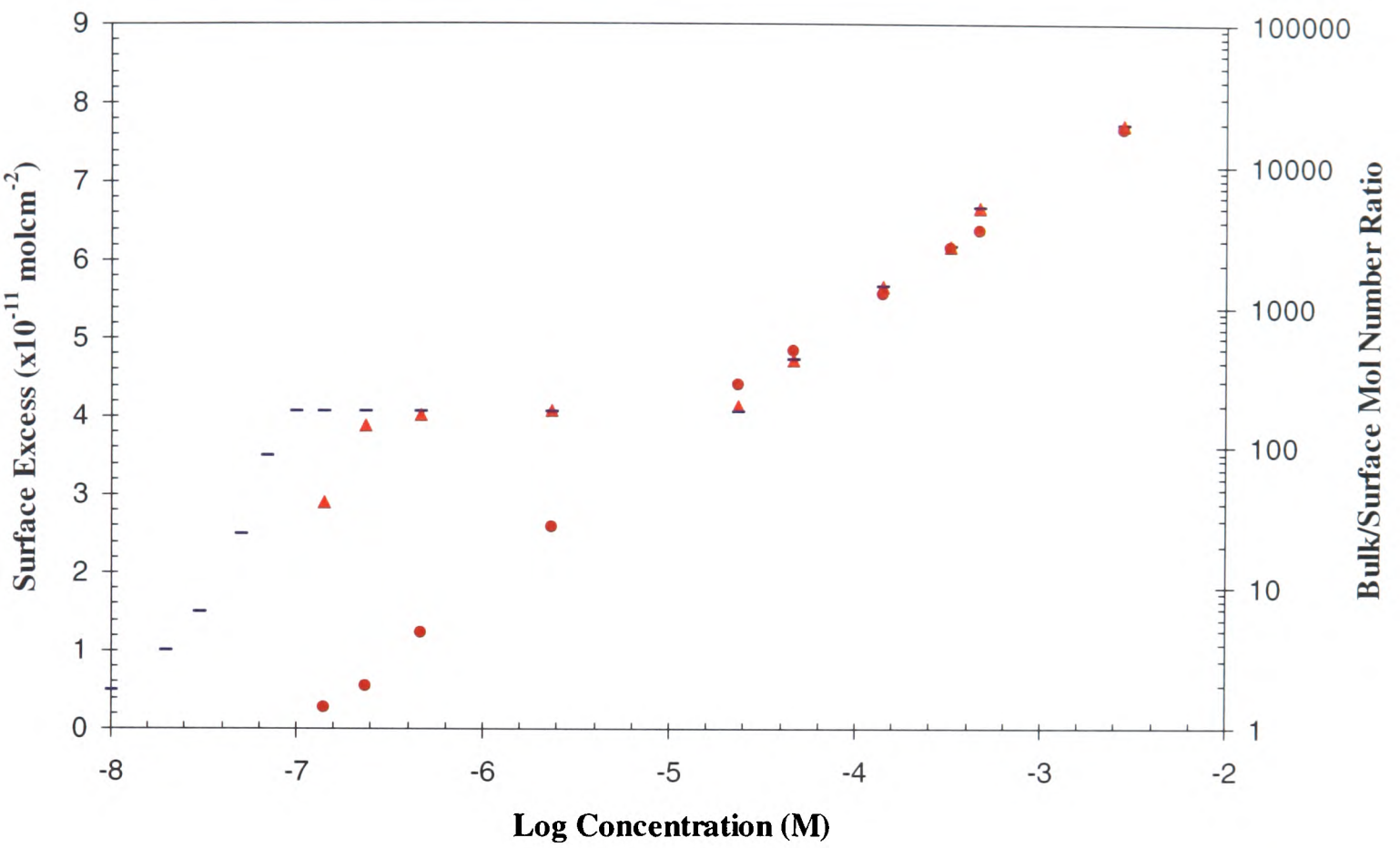


Figure 8. Surface excess as a function of the log bulk EPE 1250-14 concentration at 25°C, determined by neutron reflection, (▲), and assuming bulk depletion effect, (—). Ratio of copolymer molecule number in the bulk and at the interface, (●).

It is also interesting to analyse the effect of copolymer bulk depletion for solutions of EPE 1250-14 based on the surface excess values obtained from neutron reflectivity. Figure 8 shows that the reduction of the concentration of EPE 1250-14 molecules in the bulk follows a similar pattern to the behaviour of EPE 3000-14 in Figure 7. Making the same assumption, i.e. that the EPE copolymer molecules prefer to adsorb at the surface rather than be dispersed in the bulk, the effect of bulk depletion again takes place at about 10^{-7}M. Thus, EPE copolymer composition does not appear to affect the concentration at which the bulk depletion effect is significant.

Alexandridis *et al.* also found that the first breakpoint does not depend on the temperature. Thus the effect of temperature on the concentration at which the copolymer bulk depletion effect becomes significant was also assessed for solutions of EPE 3000-14

using the surface excess values obtained from neutron reflectivity. Figure 9 shows that once again the bulk depletion effect would take place at about 10^{-7}M. This is consistent with the observation that the surface excess at which monolayer saturation is reached is not significantly affected by temperature.

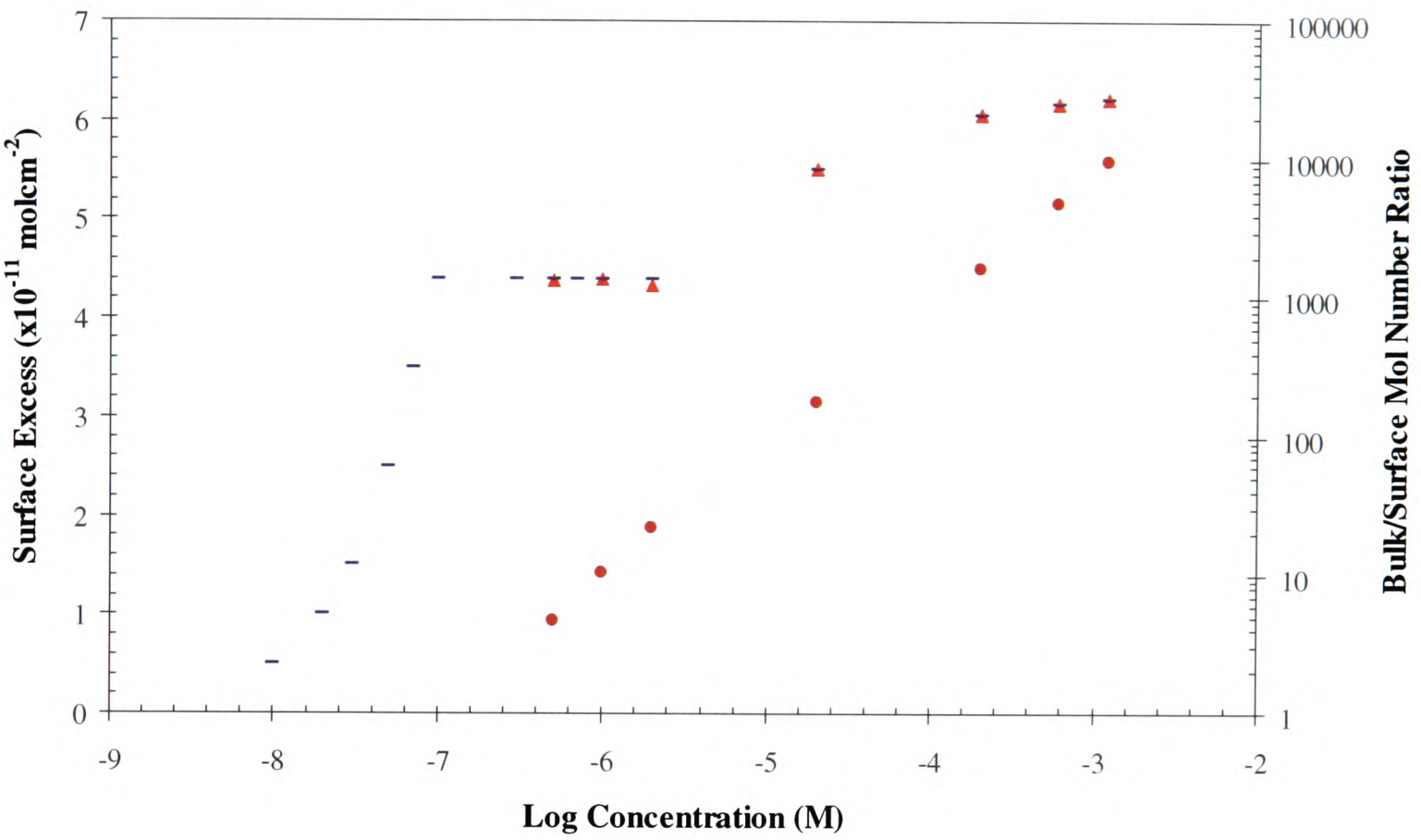


Figure 9. Surface excess as a function of the log bulk EPE 3000-14 concentration at 35°C, determined by neutron reflection, (▲), and assuming bulk depletion effect, (—). Ratio of copolymer molecule number in the bulk and at the interface, (●).

To assess the impact of bulk depletion on the surface tension behaviour of solutions of EPE 3000-14 at 25°C, the curve (—) of Figure 7, which represents the calculated surface excess values obtained from neutron reflectivity was used to calculate the bulk depletion and then incorporated into Equation 5.3. The resulting modified surface tension curve is plotted together with the surface tension curves determined by the du Noüy ring and the Wilhemy plate in Figure 10. There is a clearly good agreement down to concentrations of about 10^{-6}M. There is a steep increase in the surface tension below the low-concentration break for the curve derived from the neutron reflection and this curve is similar to that from the Wilhemy plate method. The concentration at which the break occurs is however

lower than the calculated curve. It is important to note that the surface excess values and therefore the concentration at which bulk depletion starts to occur, are very sensitive to the volume/area ratio, V/A, of the sample. Thus, different volume/area ratios should produce low-concentration breaks occurring at different concentrations and with different slopes below the break.

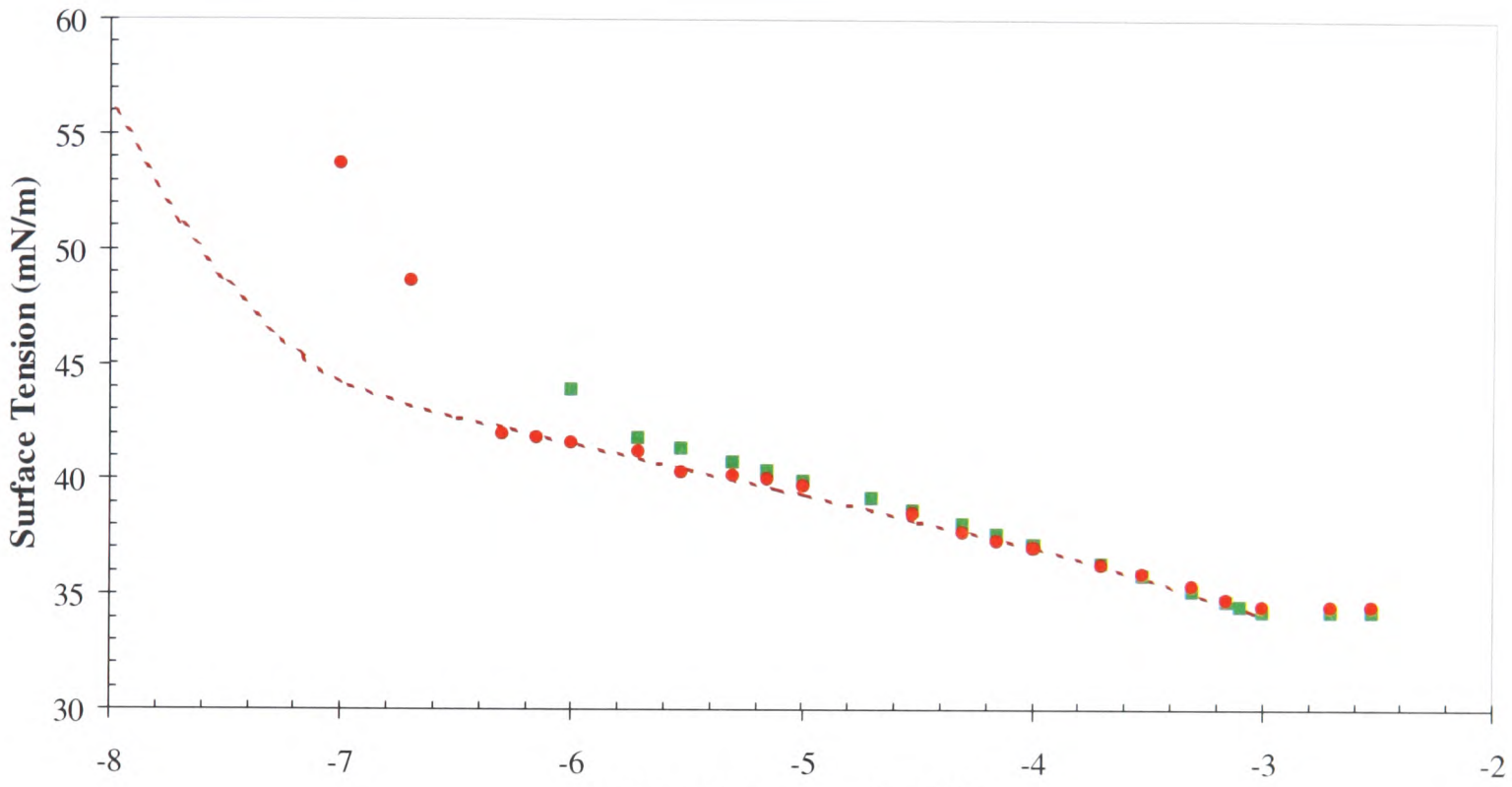


Figure 10. Surface tension as a function of log concentration for aqueous solutions of EPE 3000-14 at 25°C measured by the du Noüy ring (▪), and Wilhemy plate (●). The broken line is the surface tension calculated from the neutron reflection surface excesses assuming effects of bulk depletion.

The information obtained from the neutron reflection experiments leads to the conclusion that the origin of the low concentration breakpoint is at least in part due to the depletion of EPE copolymer molecules in the bulk of the solution. This low-concentration break is not affected by temperature nor by EPE copolymer composition and it resembles the features of the low-concentration break found with commercial Pluronic surfactants. Thus, the neutron experiments support, at least in part, the proposal of Linse *et al.*[17], based on a mean-field lattice model, that the low-concentration break is induced by the bulk depletion of EPE copolymer molecules.

3.4.3 Copolymer polydispersity effect:

The behaviour of solutions of polydisperse polymers is expected to be modified from that of monodisperse systems because of the exchange of different polymer components as the total polymer concentration is changed[18,19]. The mean-field lattice model developed by Linse *et al.* has been used to describe the effects of polydispersity on the adsorption of EPE copolymers at the air-liquid interface. According to this model, below the CMC, the higher mass fraction of a polydisperse sample, which is more surface active, governs the surface tension and the surface excess in ways similar to earlier studies of the adsorption at hydrophobic surfaces[19] and self-assembly in solution[18]. As the CMC is approached, the larger components are withdrawn from the interfacial region to form micelles. The successive replacement of larger components with smaller ones at the interface above the CMC is accompanied by a reduction in the polymer surface excess. At the CMC, the micelles are almost exclusively formed by the largest components, but as the total polymer concentration increases, the composition of the micelles approaches the overall composition of the system. These predictions of polymer fractionation by the mean-field lattice theory are based on the assumption that the system is in equilibrium.

Recently An *et al.*[20] studying the surface tension behaviour of poly (vinyl methylether) (PVME) observed that at low concentrations (below about 10^{-4}wt%) the γ–ln$c$ curve showed a sharp upturn. Similar sharp upturns have previously been observed by Eley *et al.*[21] and this was attributed to a non-equilibrium region, where the timescale required to attain equilibrium is too high for it to be possible to make a true measurement of the surface tension. In this region, measurements are expected to become time-dependent, unreliable and non-reproducible. Although the upturn of the curve obtained for PVME was approximately reproducible, there were some indications of non-equilibrium. The surface tension data calculated from the surface excesses obtained with neutron reflection showed that whereas good agreement with observed surface tensions was achieved for concentrations above from 10^{-4}wt%, for 10^{-5}wt% the results were inconsistent. An *et al.* argued that the surface tension curve upturn is almost certainly caused by changes in the kinetics of adsorption in a polydisperse system with concentration.

The model developed by An *et al.* shows that for a polydisperse sample in the higher concentration range, the higher molecular weight species of the mixture dominate the surface composition. As the concentration of polymer is lowered the effect of the Gibbs equation and the larger area of the large molecular weight species means that if all species could reach equilibrium with the surface, the lower molecular weight species would gradually be displaced from the surface as the concentration was lowered and the surface tension would remain low. However, in practice, solute species do not have time to diffuse to the surface on the time scale of the surface tension measurements when their molar concentration drops into the range 10^{-6} – 10^{-7}M. In a polydisperse sample the high molecular weight species will typically reach this condition at much higher wt% concentrations than the lower molecular weight species. Thus, as the concentration of the polydisperse sample is lowered the surface tension behaviour will be increasingly determined by the response of the lower molecular weight species, even though they are the less surface-active components of the mixture. For these species the change in surface tension with ln*c* is more rapid and hence the curve must turn upwards. An approximate model of the effect can be estimated using a model distribution for polydispersity, a model for surface mixing and a cut-off molar concentration, below which a species no longer plays any part in the surface tension behaviour and does generate a marked upturn in the γ-*lnc* plot. The sharp upturn observed in the surface tension curve of Pluronic surfactants at the low-concentration breakpoint could also be generated by such a mechanism. It is probable that the low concentration break in the surface tension curves of the EPE copolymers is then caused by a mix of three effects, i.e. bulk depletion, and polydispersity in both molecular weight and composition. The effects of the first of these can be seen in the results for our fairly well defined copolymers but the behaviour of commercial samples is likely to be dominated by the latter two effects.

4 Summary

The adsorption of highly monodisperse EPE copolymers at the air-water interface has been examined by the technique of specular neutron reflectivity. The results have clarified unsettled issues on the existence of transitions observed in the surface tension curves for such surfactants.

The experiments with EPE 3000-14 show that the area per EO segment at $1.2x10^{-3}$M is approximately 6Å^2, which is much less than the 11-12Å^2 per EO segment obtained for the $C_{12}E_j$ series at their CMCs. The monolayer thickness found for this copolymer at the same concentration was 54Å and this observation suggests a significant mixing or disorder within the monolayer, based on the argument that the thickness of a fully extended chain containing 23 EO adducts should be about 83Å. For EPE 3000-14 solutions at 25°C, the monolayer is completed at a bulk concentration of $4x10^{-6}$M, confirming the strong surface activity of the EPE copolymers. The surface excess of the saturated monolayer is about $4x10^{-11}$mol/cm^2, and does not seem to be greatly affected by temperature or copolymer composition. At low concentrations, EPE copolymers behave similarly to PEO homopolymers[11, 12].

The effect of temperature on the neutron reflectivity properties of the adsorbed monolayer of EPE copolymers has also been examined. The amount of copolymer in the monolayer at or above the CMC is not greatly affected by increasing the temperature from 25°C to 35°C. This observation agrees with the small change in maximum surface pressure observed in the surface tension curves at both temperatures. However, below the CMC, there is a significant increase in the total amount of adsorbed EPE copolymer with temperature without significant changes to the monolayer thickness. As suggested in the previous chapter, the surface activity of EPE copolymers is strongly dependent on the PPO chain. The conformational change of PO groups induced by temperature renders the PO-water interaction less favourable. Because of the reduced hydration level and the increased PEO and PPO chain intermixing, more copolymer can be accommodated in the monolayer.

Four different stages have been identified in the adsorption isotherms for EPE copolymers. At extremely low concentrations (Section IV) preferential adsorption at the interface depletes the bulk solution of copolymer molecules and therefore affects the surface tension. It becomes evident that below a certain concentration, which is determined by the volume/area ratio of the sample tested, the concentration of EPE copolymer at the surface is limited by the total amount of molecules actually present in the solution. The concentration at which this bulk depletion starts to take effect is referred

to as the low-concentration breakpoint and is believed to be of the same nature as the one found in the surface tension studies conducted by Alexandridis *et al.* The similarities between the two low-concentration breaks extend to the apparent insensitivity to temperature and EPE copolymer composition. In Section III of the isotherm, where there is almost constant surface excess, the surface tension varies linearly with log c. The surface excess at which the monolayer is saturated is hardly affected by copolymer composition and temperature and this observation explains the relative insensitivity of the low-concentration break to temperature and copolymer composition. Increasing the concentration even further, another change in the slope of the adsorption isotherm is observed (Section II), which is characterised by a steep increase of surface excess with concentration without significant increase of the monolayer thickness. It is possible that further increase in the disorder or intermixing of PPO and PEO chain within the monolayer may free some space in the monolayer for further EPE molecule adsorption. The increased adsorption with bulk concentration produces the convex curvature in the surface tension curve that is observed for the EPE copolymers studied in this work and also for the various Pluronic surfactants found in the literature. Section I of the isotherm follows micellization and there is a much lower increase in the surface excess with bulk concentration.

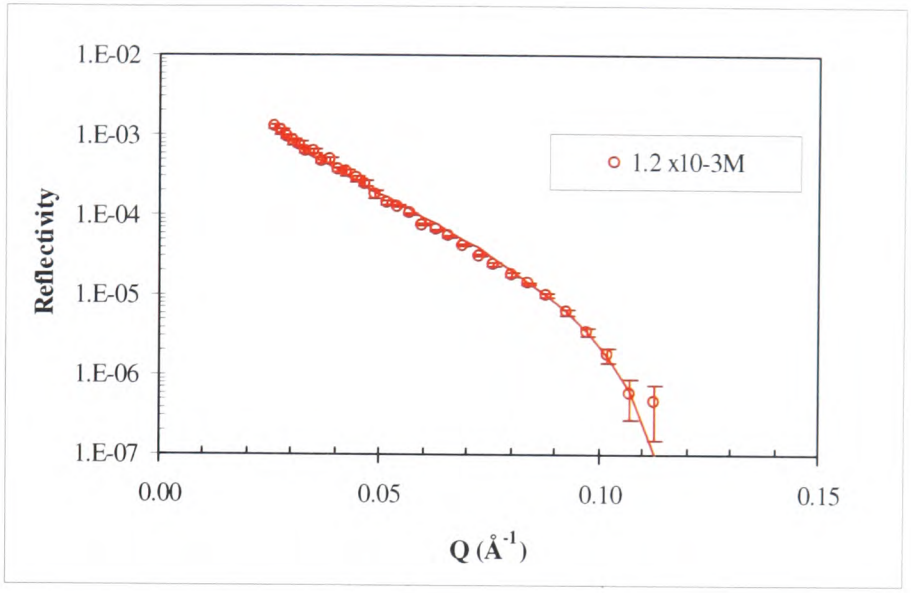
Alexandridis has proposed that the low-concentration break originates from a rearrangement of the copolymer molecules within the saturated monolayer. This proposal however is not consistent with the neutron reflectivity results. After the first breakpoint, the neutron surface excess hardly changes with concentration, which suggests that in fact the monolayer is complete. Molecular rearrangement within the monolayer and a steeper increase in surface change become apparent only at a concentration two orders of magnitude higher.

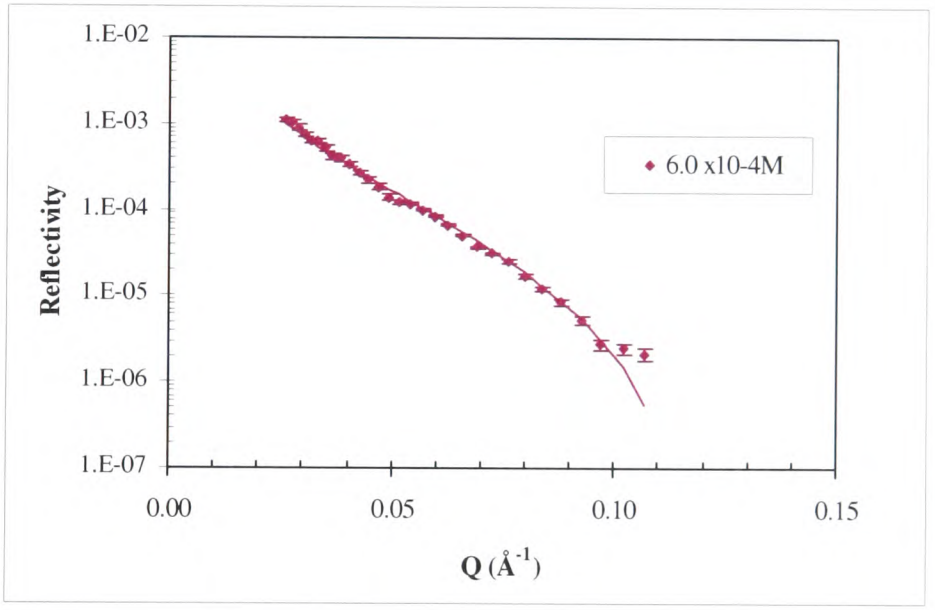
The low concentration breakpoint, particularly in commercial samples, may also be an effect of the composition polydispersity. For a polydisperse sample, the high molecular weight species of the mixture are more surface active and therefore dominate the interfacial layer composition. As the concentration of the polydisperse sample is lowered, the surface diffusion rates of the high molecular weight species drop significantly and the

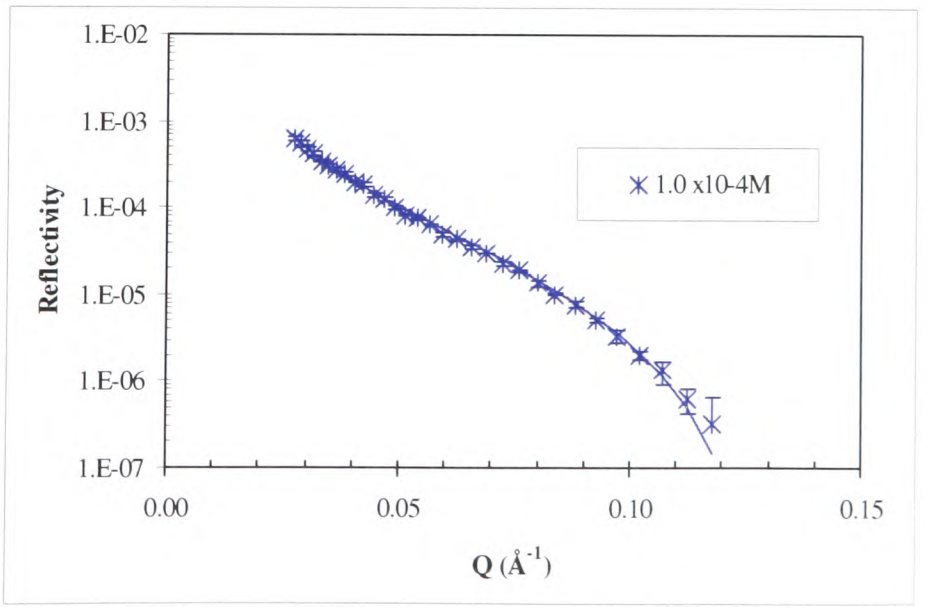
surface tension behaviour is increasingly determined by the less surface active and lower molecular weight species. This changeover in the interfacial layer composition produces a sharp upturn in the surface tension curve below a limiting concentration.

APPENDIX 3

Neutron Reflectivity curves of d-EPE 3000-14 in null reflecting water at 25°C. Continuous lines are calculated using the Optical Matrix Model for a single-layer.

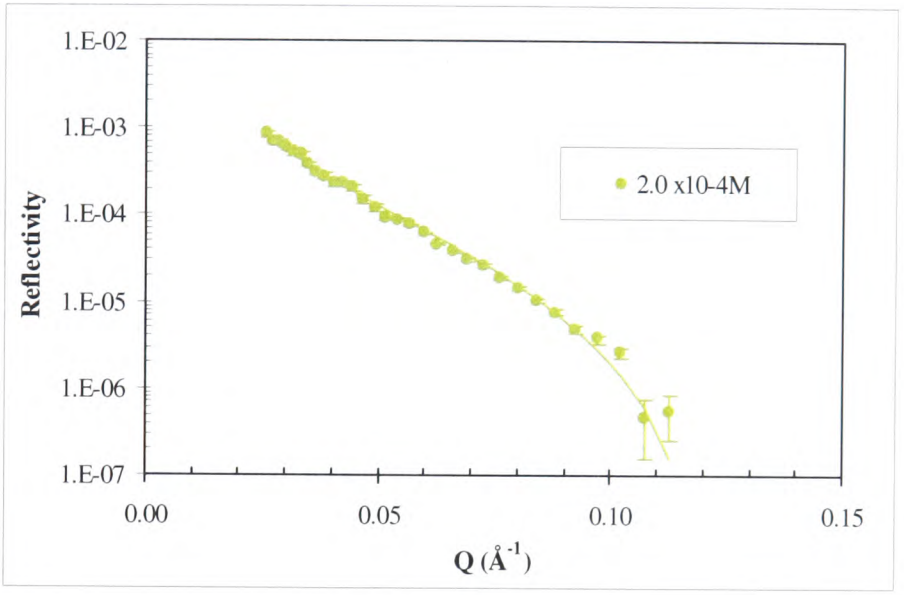


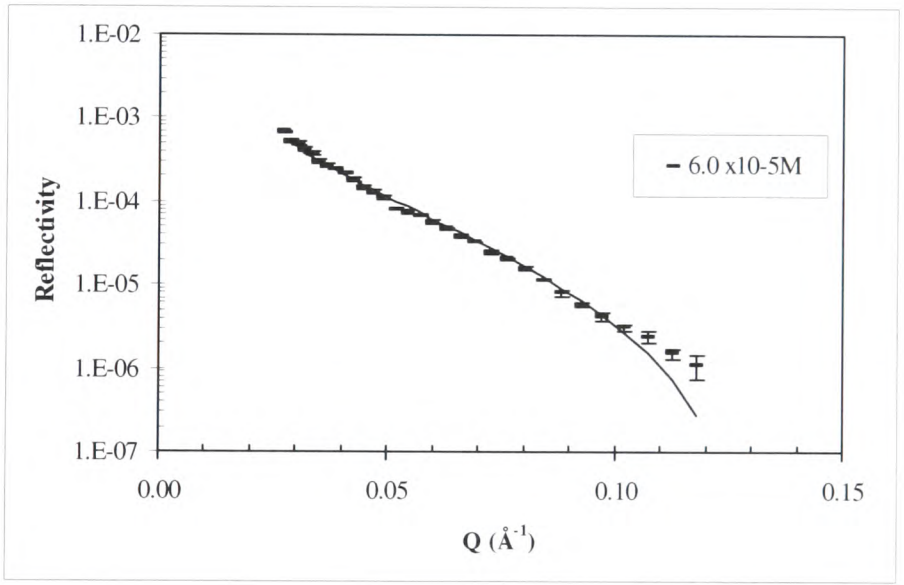


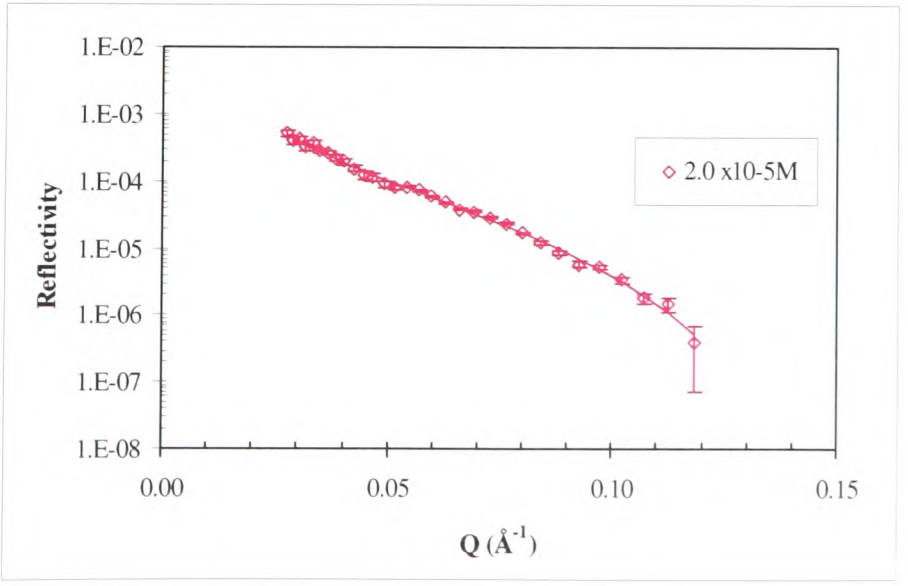


APPENDIX 3 (Cont.)

Neutron Reflectivity curves of d-EPE 3000-14 in null reflecting water at 25°C. Continuous lines are the reflectivity calculated using the Optical Matrix Model for a single-layer.

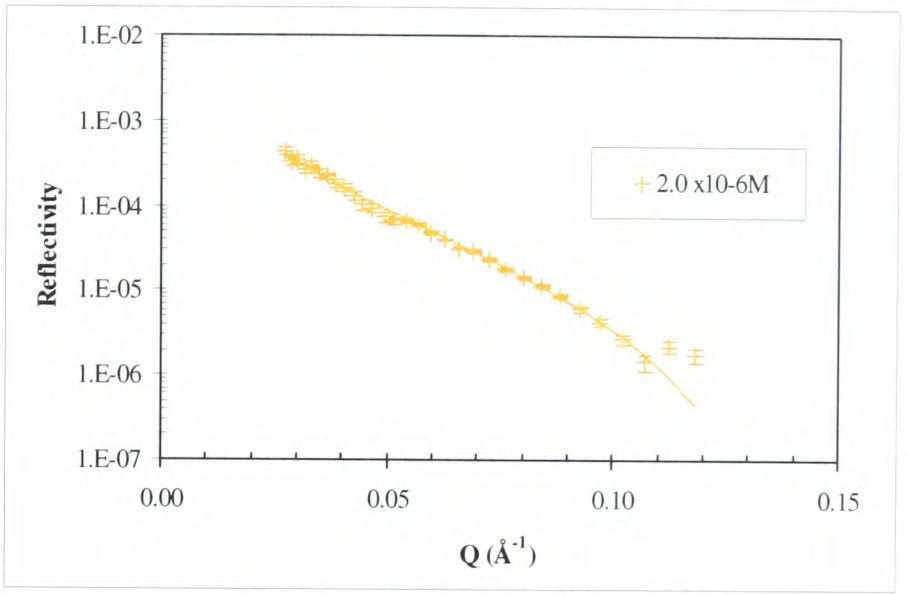


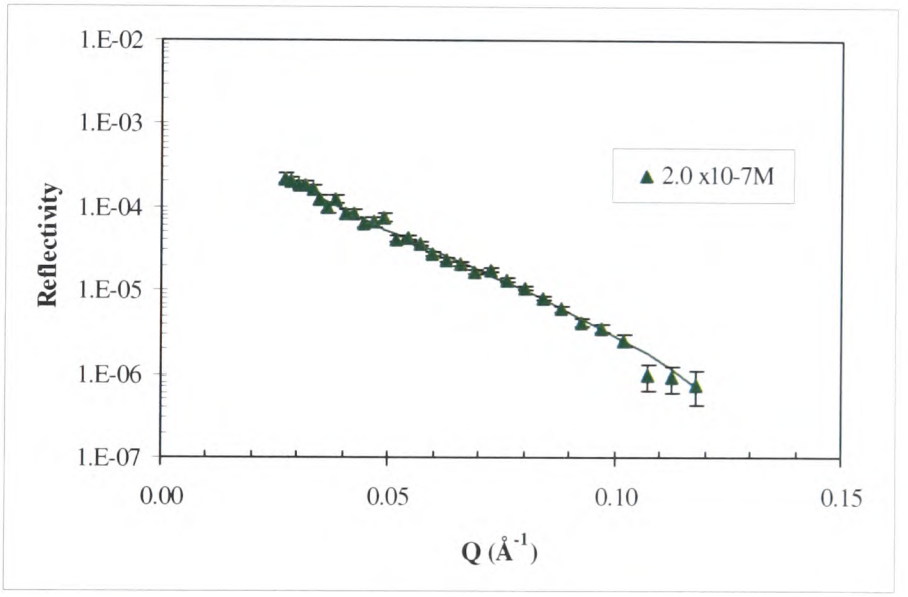


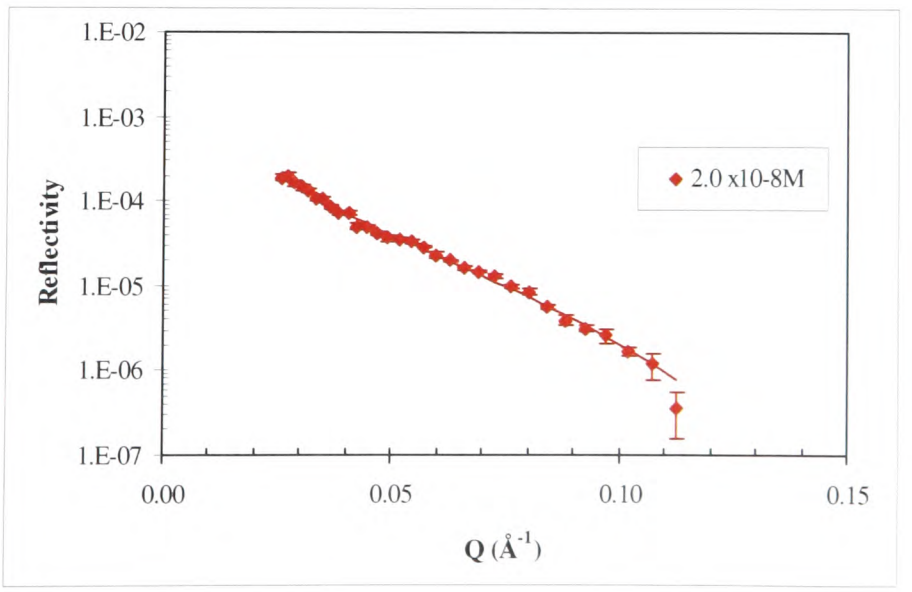


APPENDIX 3 (Cont.)

Neutron Reflectivity curves of d-EPE 3000-14 in null reflecting water at 25°C. Continuous

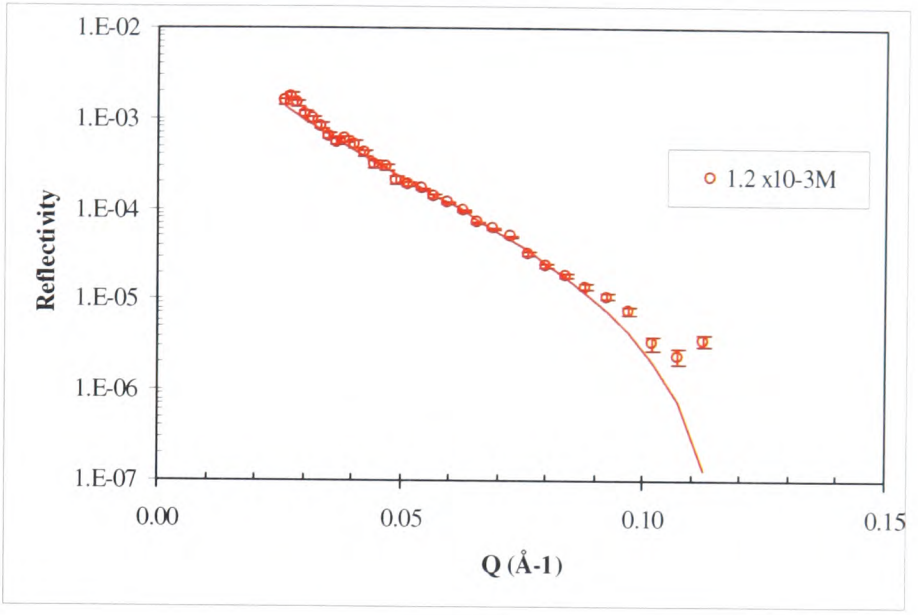


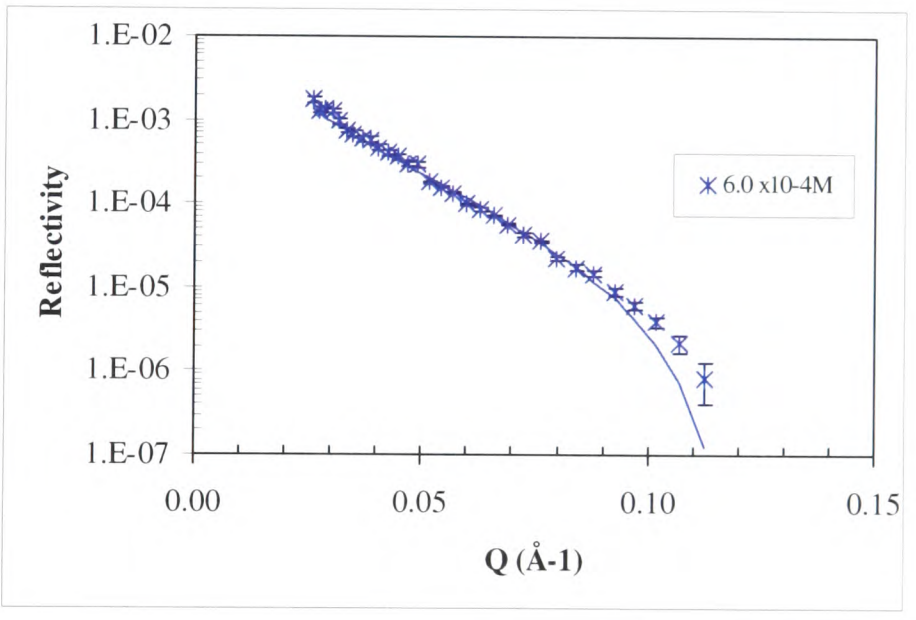


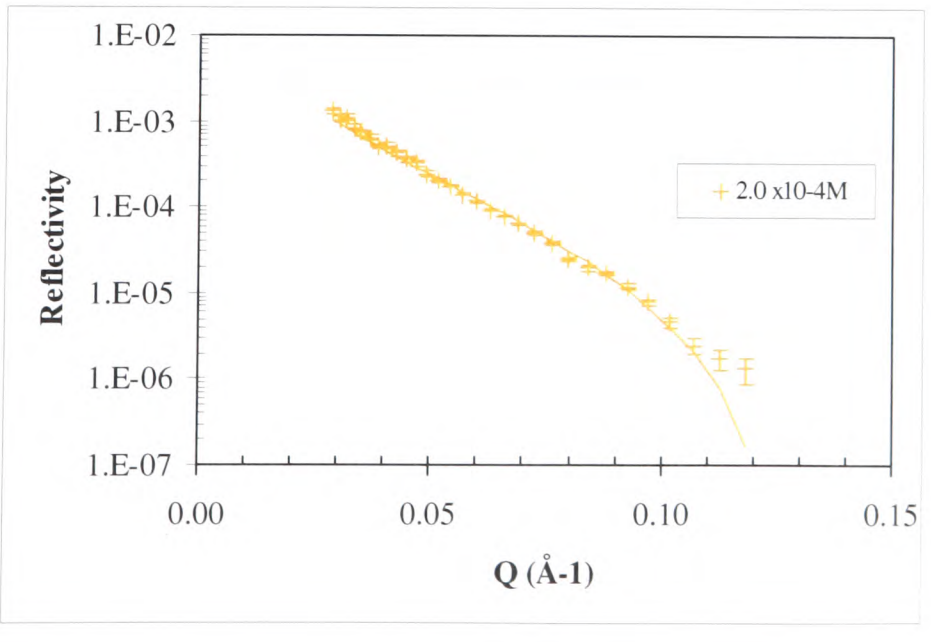


APPENDIX 4

Neutron Reflectivity curves of d-EPE 3000-14 in null reflecting water at 35°C. Continuous lines are reflectivity calculated using Optical Matrix Model for a single-layer.

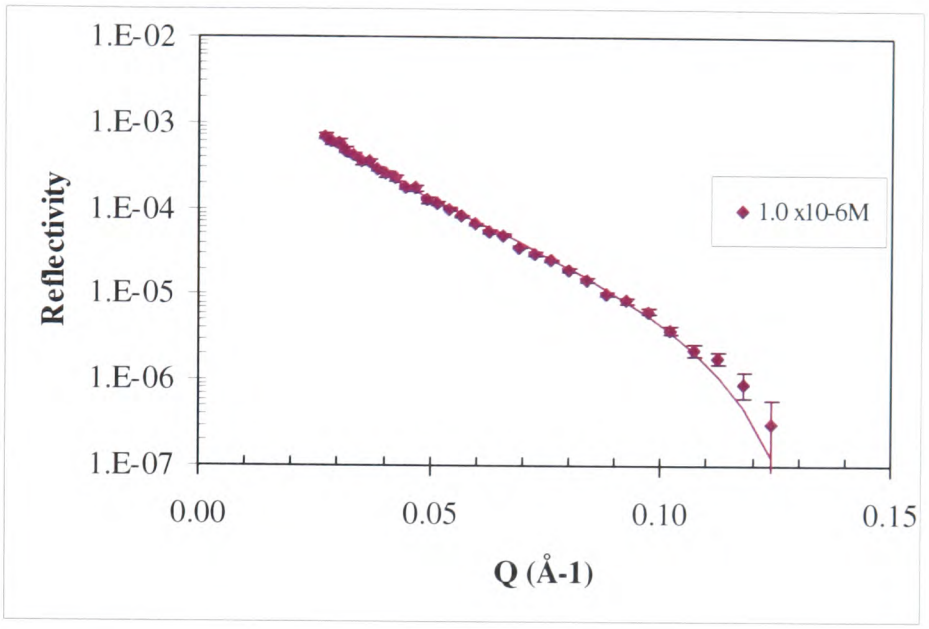


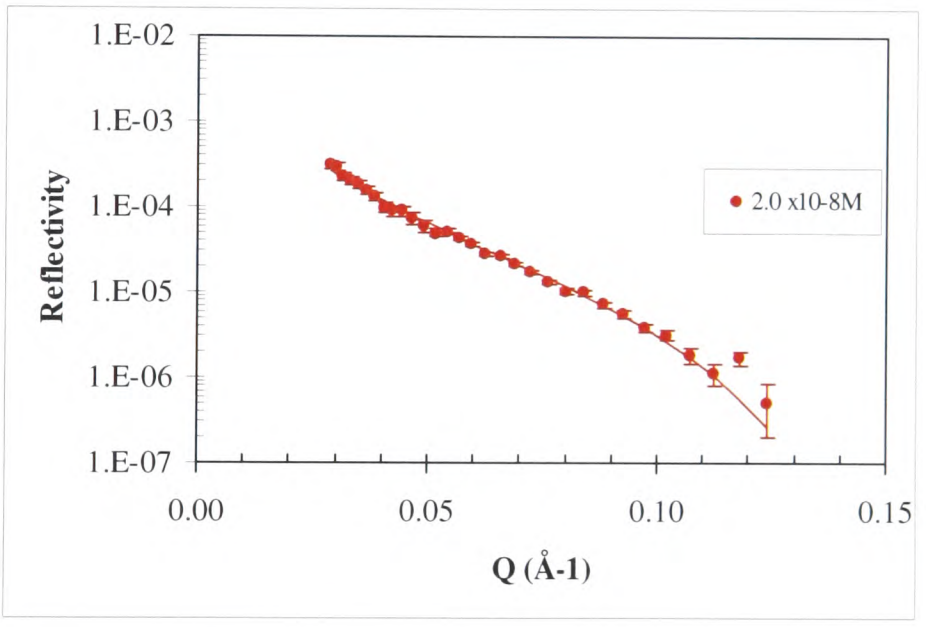




APPENDIX 4 (Cont.)

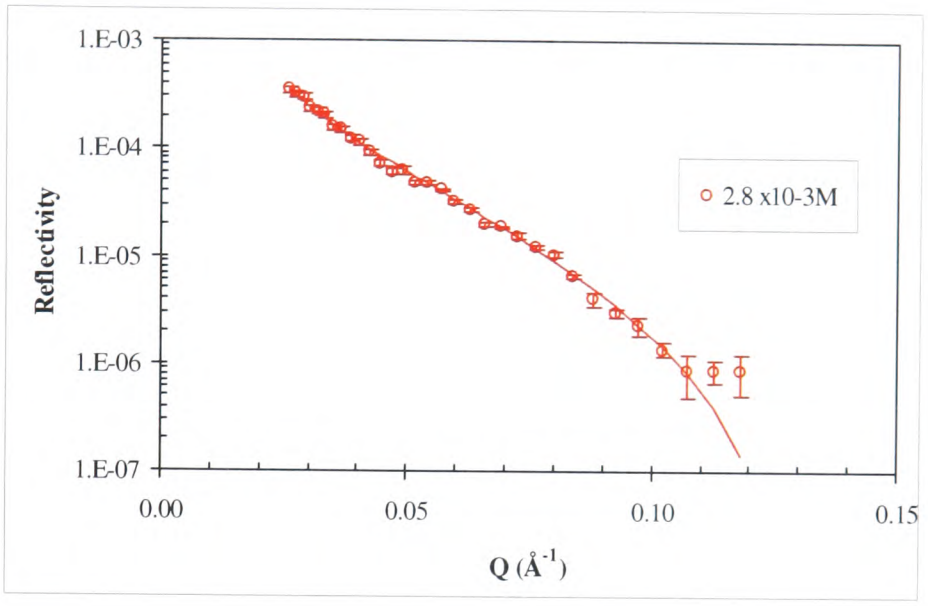
Neutron Reflectivity curves of d-EPE 3000-14 in null reflecting water at 35°C. Continuous lines are reflectivity calculated using Optical Matrix Model for a single-layer.

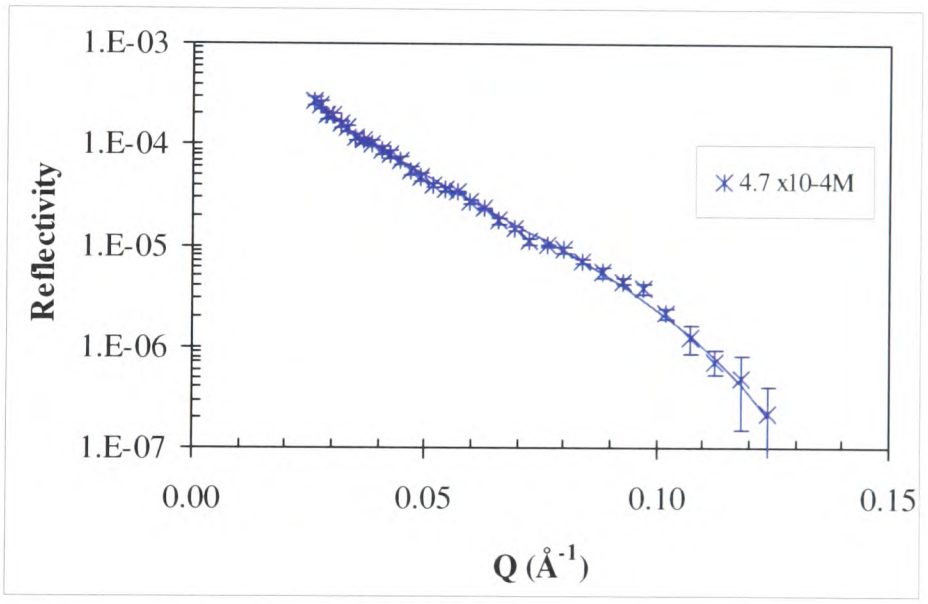


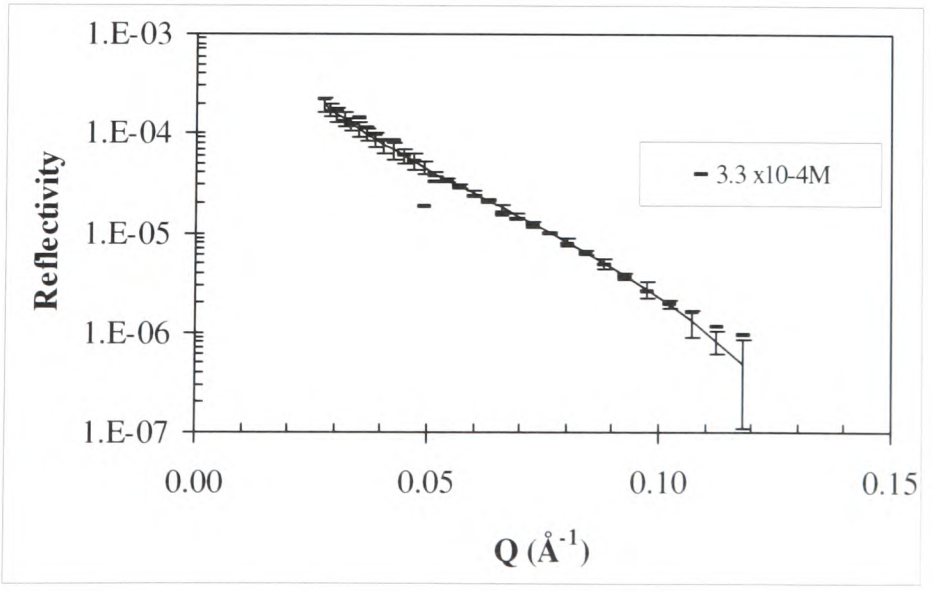


APPENDIX 5

Neutron Reflectivity curves of d-EPE 1250-14 in null reflecting water at 25°C. Continuous lines are reflectivity calculated using Optical Matrix Model for a single-layer.

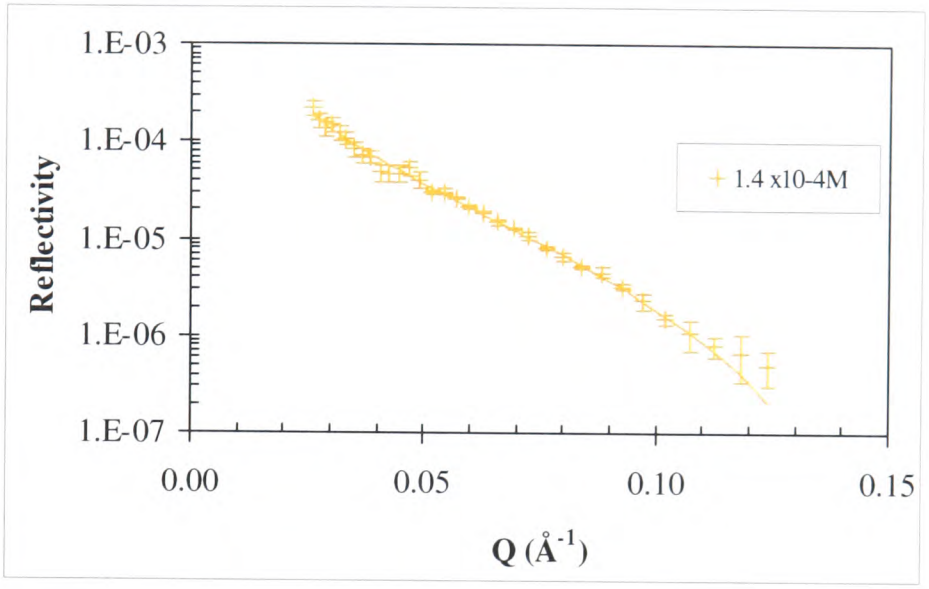


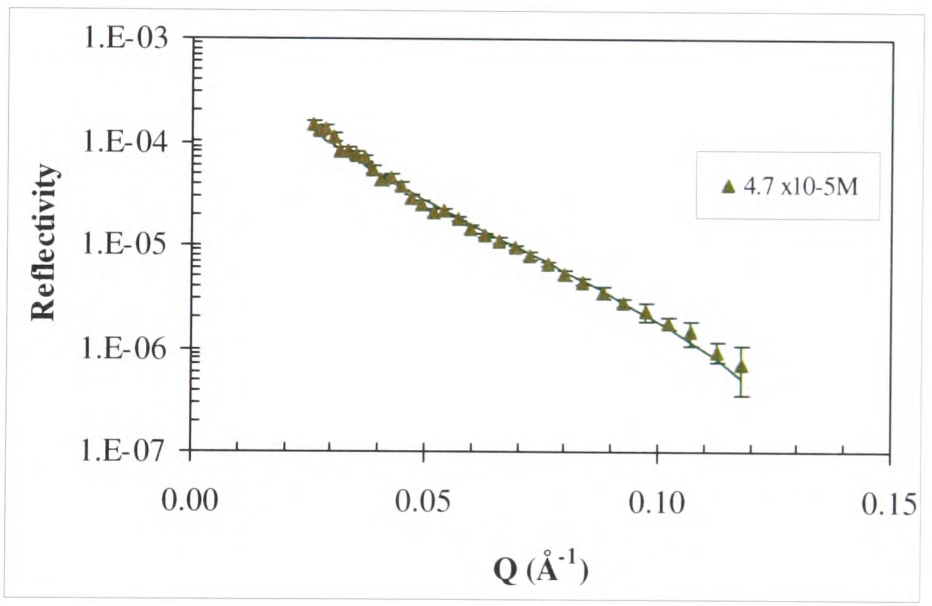


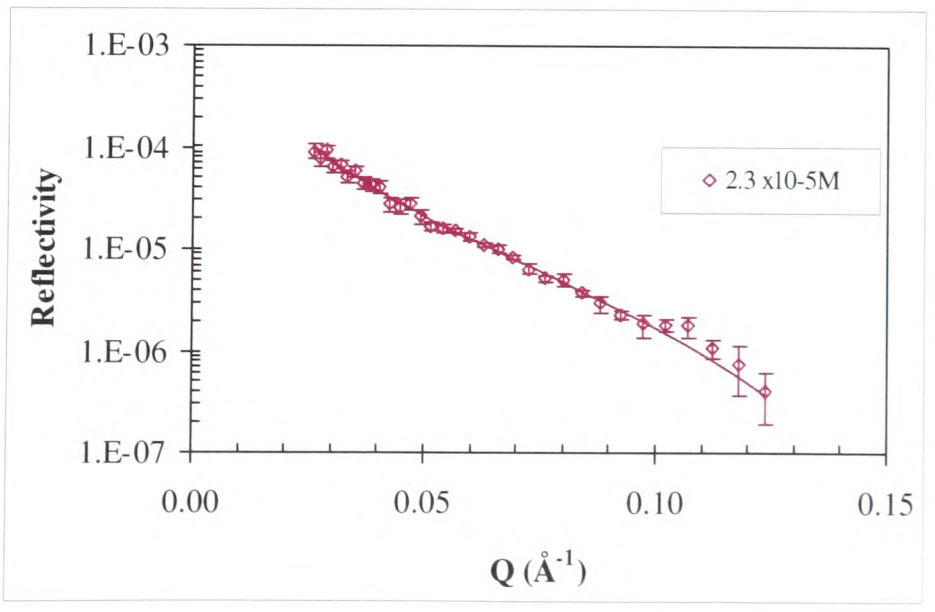


APPENDIX 5 (cont.)

Neutron Reflectivity curves of d-EPE 1250-14 in null reflecting water at 25°C. Continuous lines are reflectivity calculated using Optical Matrix Model for a single-layer.

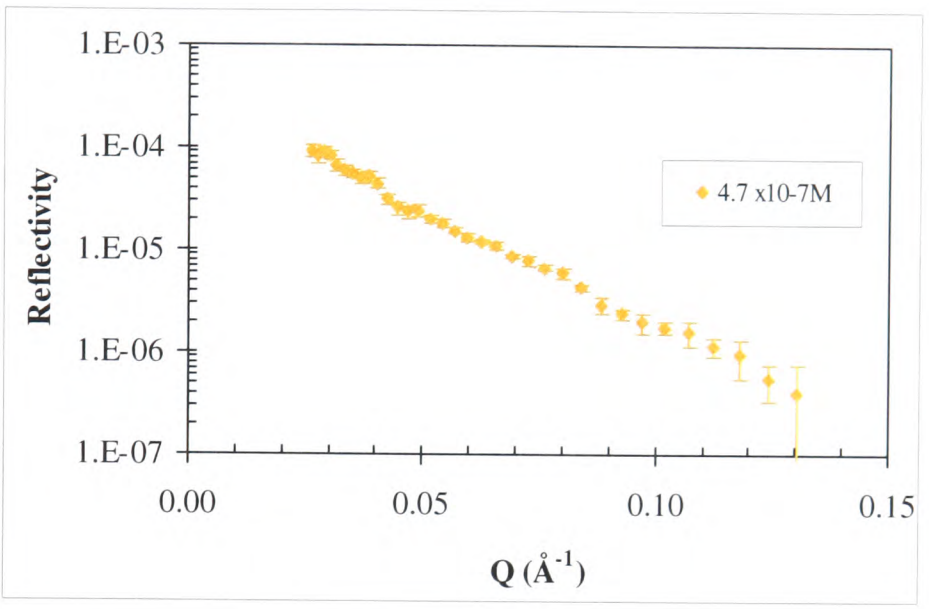


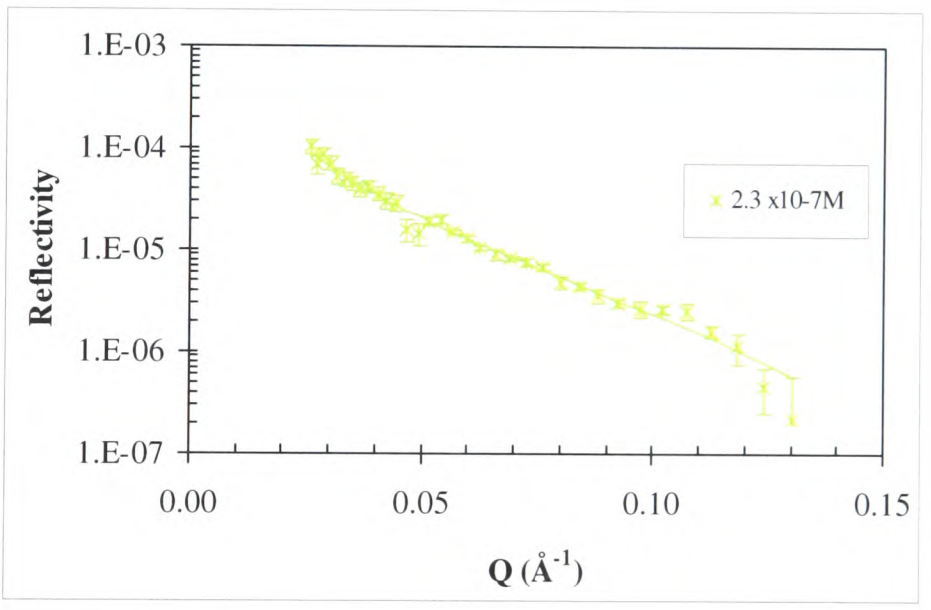


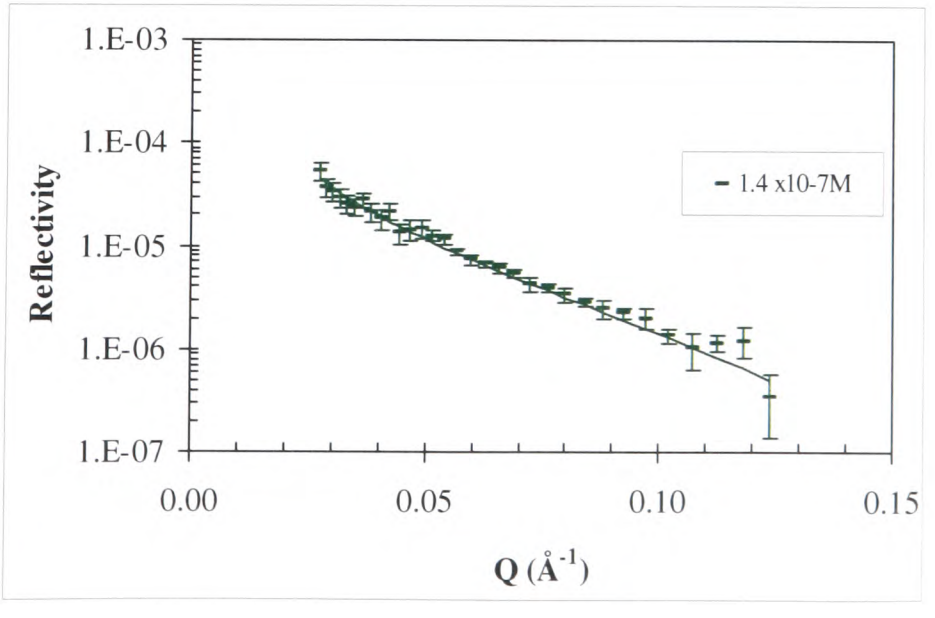


APPENDIX 5 (cont.)

Neutron Reflectivity curves of d-EPE 1250-14 in null reflecting water at 25°C. Continuous lines are reflectivity calculated using Optical Matrix Model for a single-layer.







References

[1] Rennie, A.R.; Crawford, R.J.; Lee, E.M.; Thomas, R.J.; Crowley, T.L.; Roberts, S.; Qureshi, M.S.; and Richards, R.W. *Macromolecules*, 22, 3466 (1989)

[2] Guiselin, O.; Lee, L.T.; Farnoux, B.; and Lapp, A. *J. Chem. Phys.*, 95, 4632 (1991)

[3] Atinok, H.; Yu, G.E.; Nixon, S.K.; Gorry, P.A.; Attwood, D.; and Booth, C. *Langmuir*, 13, 5837 (1997)

[4] Crowley, T.L. *Physica*, , A195, 354 (1993)

[5] Thirtle, P.N., *D.Phil. Thesis*, University of Oxford (1999)

[6] Lu, J.R.; Su, T.J.; Li, Z.X.; Thomas, R.K.; Staples, E.J.; Tucker, I.; and Penfold, J. *J. Phys. Chem.*, 101, 10339 (1997)

[7] Takahashi, Y.; Sumita, I.; and Tadokoro, H. *J. Polym. Sci.*, 11, 2113 (1973).

[8] Lu, J.R.; Li, Z.X.; Thomas, R.K.; Staples, E.J.; Thompson, L.; Tucker, I.; and Penfold, J *J. Phys. Chem.*, 98, 6559 (1994)

[9] Lu, J.R.; Su, T.J.; Li, Z.X.; Thomas, R.K.; and Penfold, J. *Langmuir*, 9, 2408 (1993)

[10] Lu, J.R.; Li, Z.X.; Thomas, R.K.; Staples, E.J.; Tucker, I.; and Penfold, J. *J. Phys. Chem.*, 97, 8012 (1993)

[11] Lu, J.R.; Su, T.J.; Thomas, R.K.; Penfold, J.; and Richards, R.W. *Polymer*, 37, 109 (1996)

[12] Henderson, J.A.; Richards, R.W.; Penfold, J.; Thomas, R.K.; and Lu, J.R. *Macromolecules* 26, 4591 (1993)

[13] Linse, P.; and Bjorling, M. *Macromolecules* 24, 6700 (1991)

[14] Malmsten, M; Linse, P.; and Zhang, K-W. *Macromolecules* 26, 2905 (1993)

[15] Simister, E.A.; Thomas, R.K.; Penfold, J.; Staples, E.; Aveyard, R.; Binks, B.P.; Cooper, P.; Fletcher, P.D.I.; Lu, J.R.; and Sokolowski, A. *J. Phys. Chem.* 96, 1383 (1992)

[16] Alexandridis, P; Athanassiou, V.; Fukuda, S.; and Hatton, T.A.; *Langmuir*, 10, 2604 (1994)

[17] Linse, P.; and Hatton, T.A. *Langmuir* 13, 4066 (1997)

[18] Linse, P. *Macromolecules* 27, 6404 (1994)

[19] Schillen, K.; Claesson, P. M.; Malmsten, M; Linse, P.; and Booth, C. *J. Phys. Chem.* 101, 4238 (1997)

[20] An, S.W.; Thomas, R.K.; Forder, C.; Billingham, N.C.; Armes, S.P. and Penfold, J. *Langmuir*, submitted

[21] Couper, A.; and Eley, D.D. *J. Polym. Sci.* 3, 345 (1948)

Chapter 6

Structure of Monolayers of EPE Copolymers at the Air-Solution Interface Studied by Neutron Reflection

1 Introduction

There is no experimental information available about the organisation of EPE copolymers adsorbed at the air-water interface. Any arguments about how such molecules are oriented within the monolayer have been based on observations mainly from surface tension measurements and correlations with studies of the configuration of poly(ethylene oxide) at the air-water interface. Alexandridis *et al.*[1] suggested that at concentrations below the first break point in the surface tension curve, the tri-block copolymer molecules adsorb on the air-water interface as an inverted U with the PEO chains located at the interface, oriented similarly to PEO homopolymers at air-water interface. At the first break (at approximately 10^{-3}w/v%), when the interface is fully covered with copolymer, a change in configuration takes place and the copolymer layer becomes more compact with water molecules being excluded from the monolayer and the PEO segments either dipping into the aqueous solution or folding around the PPO chain. These suggested structures do not fit even the simplest analysis of the neutron reflectivity as described in the previous chapter. After the first breakpoint, the neutron surface excess hardly changes with concentration suggesting that in fact the monolayer is complete and undergoes no further change in this concentration range. Molecular rearrangement within the monolayer and surface coverage changes only become apparent at a much higher concentration.

The present chapter is concerned with the application of neutron reflectivity to the determination of the configuration of EPE copolymers at the air-water interface. The effects of bulk concentration, copolymer composition and temperature on the monolayer organisation have also been examined.

2 Experimental Details

2.1 Materials

Both deuterated and protonated PEO-chain EPE copolymers were made as described in Chapter 2. The effect of composition on the monolayer organisation was studied using two partially deuterated EPE copolymers, d-EPE 3000-14 and d-EPE 1250-14. Both d-EPE 3000-14 and d-EPE 1250-14 are close matches to their respective protonated counterparts as shown by GPC and by surface tension measurements. The composition and molecular weights of the polymers are given in Table 2 of Chapter 2.

2.2 Neutron reflectivity measurement and data analysis

All the neutron reflection measurements reported in this chapter were made using the reflectometer SURF at the Rutherford Appleton Laboratory in Didcot, Oxfordshire. The procedure for making the measurements has already been described in Chapter 2. The experiments were carried out at 25° and 35°C to study the effect of temperature on the monolayer organisation. Each solution was measured at fixed incident angles of 0.8° and 1.5° and the detector efficiency was calibrated with respect to D_2O. The SURF reflectometer uses the time of flight method of analysis (see Chapter 2 for a description) so that each measurement collects reflectivities at all values of the momentum transfer, Q, simultaneously. The exposure time of each sample was varied according to the concentration of reflecting species at the interface to ensure that in all cases, good statistics were obtained out to a relatively high Q. At high Q, the reflectivity tends towards the background level. For adsorbed surfactant monolayers, this occurs at momentum transfers above 0.3Å^{-1}. The component of the measured signal from the background is present in all experimental data points. However, on the SURF reflectometer, the level of background scattering is independent of momentum transfer so that it is possible to subtract a constant background from the whole set of experimental data to obtain the true reflectivity.

2.3 Determination of surfactant configuration within the monolayer

The neutron reflectivity data were analysed using the Optical Matrix Method, which was described in Chapter 2. In the Optical Matrix Method, the model chosen for the surface

layer is divided into a number of uniform layers of different scattering length density and thickness. The Fresnel reflection and transmission coefficients are calculated for each interface from these parameters, and these coefficients are then combined to given the total reflectivity from the composite surface layer. The reflectivity of the model interface is then compared with the measured profile and the various parameters adjusted in order to achieve a good fit between the measured data and calculated profiles. The disadvantage of model fitting is that more than one model may fit a given reflectivity profile. This problem may be reduced by fitting a single model to profiles of three isotopic compositions, d-EPE in NRW and in D_2O and h-EPE in D_2O. Although the protonated PEO and PPO chains in NRW do not give much of a reflected signal, the reflectivity from D_2O solutions is very sensitive to the structure of these groups. Because the scattering length densities for PEO and PPO are only slightly greater than zero, the penetration of D_2O into the layer containing any of those two segments results in an intermediate scattering length density for the layer, to which the reflectivity is very sensitive. In consequence, the reflectivities of deuterated PEO-chain EPE copolymer in NRW and in D_2O and of fully protonated EPE copolymer in D_2O can be combined to determine the overall structure of the monolayer, although the accuracy of such an approach may vary according to the monolayer model adopted.

The monolayer model taken to fit the reflectivity profiles consisted of a multiple-layer structure, varying from four to five-layers. This was found to be the minimum number of layers that would fit all the data. The overall structure of the layers preserves the stoichiometry of the copolymer and conforms to space-filling constraints in any layer containing water. The uppermost layer was taken to comprise PO groups and air, and the remaining aqueous subphase layers contain mixtures of PO and EO groups and water at various volume fractions. The model was adjusted until the calculated reflectivities fitted all three reflectivity profiles at the different isotopic compositions using a single set of structural parameters. Each layer is characterised by its scattering length density, given by

$$\rho = \rho^{i}_{PPO} + \rho^{i}_{PEO} + \rho^{i}{}_{W} \qquad (6.1)$$

where W denotes water. The scattering length density of each component contributing to the scattering length density of each layer is calculated using the equation

$$\rho^{i}_{PPO} = \frac{n^{i}_{PO} b_{PO}}{A\tau_i} \quad \text{and} \quad \rho^{i}_{PEO} = \frac{n^{i}_{EO} b_{EO}}{A\tau_i} \tag{6.2}$$

where n^i is the number of PO/EO groups in the layer i, b is the coherent scattering length of the respective group, A is the area per copolymer molecule, and τ_i is the thickness of layer i. The scattering length density of the layer i can therefore be expressed as

$$\rho_i = \frac{n^{i}_{PO} b_{PO} + n^{i}_{EO} b_{EO} + n b_w}{A\tau_i} \tag{6.3}$$

The layer scattering length density can be written in terms of the volume fraction, ϕ_i, of the species constituting that layer

$$\rho_i = \frac{\phi^{i}_{PPO} b_{PPO} + \phi^{i}_{PEO} b_{PEO} + n b_w}{A\tau_i} \tag{6.4}$$

The area per copolymer molecule can be calculated from the equation

$$A = \frac{b_{EPE}}{\rho^{Mo}_{EPE}\tau_{Mo}} \tag{6.5}$$

where b_{EPE} is the calculated coherent scattering length of the EPE copolymer, $\rho^{Mo}{}_{EPE}$ is the scattering length density of the copolymer in the monolayer and τ_{Mo} is the total thickness of the monolayer. Finally, all structural parameters used to calculate the reflectivity profile, layer thickness, τ, layer scattering length density, ρ, and water fraction, ϕ_{water}, were adjusted to be consistent with the stoichiometry of the copolymer.

The scattering lengths, approximate molecular volumes and calculated scattering length densities of the various species used in the neutron reflection experiments are given in Table 1.

Species	Scattering lengths (Å)	Molecular volume ($Å^3$)	Scattering length density ($Å^{-2}$)
d-EPE 3000-14	$2.19x10^{-2}$	8,000	$2.74x10^{-6}$
d-EPE 1250-14	$8.63x10^{-3}$	3,300	$2.62x10^{-6}$
d-EO	$4.40x10^{-4}$ (96%D)	64.6	$6.81x10^{-6}$
h-EO	$4.14x10^{-5}$	64.6	$0.64x10^{-6}$
h-PO	$3.31x10^{-5}$	96.5	$0.34x10^{-6}$
H_2O	$-1.68x10^{-5}$	30	$-0.56x10^{-6}$
D_2O	$1.91x10^{-4}$	30	$6.35x10^{-6}$
NRW (8.1%v/v D_2O)	0	30	0

Table 1: Values for the various species used in the neutron reflection experiments

3 Results and Discussion

3.1 Structure of EPE 3000-14 monolayer

The study of the surface coverage of EPE copolymers using neutron reflectivity has given an isotherm which indicates that there are structural transitions within the layer. Four different sections were identified in which the monolayer structure and the air-water interface adsorption behaviour of EPE copolymers appeared to be changed by variation of the bulk concentration. Figure 1 shows the adsorption isotherm for EPE 3000-14 with its four distinct sections. Section IV is associated with a region where the surface coverage is affected by depletion of the copolymer in the solution, i.e. the surface excess is partly determined by the V/A ratio of the container. In Section III the surface excess is almost constant indicating that a saturated layer has been formed. In this region, the surface tension is expected to vary linearly with log c, provided that the activity coefficient of the copolymer remains unchanged. Section II is characterised by a steep increase in surface coverage without significant change in the monolayer thickness. In this region additional

adsorption should only be possible if there is a conformational change of the copolymer molecules within the monolayer. The increased adsorption with increasing bulk concentration will produce convex curvature in the surface tension curve, which is indeed the case for the EPE copolymers studied in this work and also for the various Pluronic surfactants studied in the literature. Section I is where the bulk solution is micellar, and in this region the adsorption should reach a plateau.

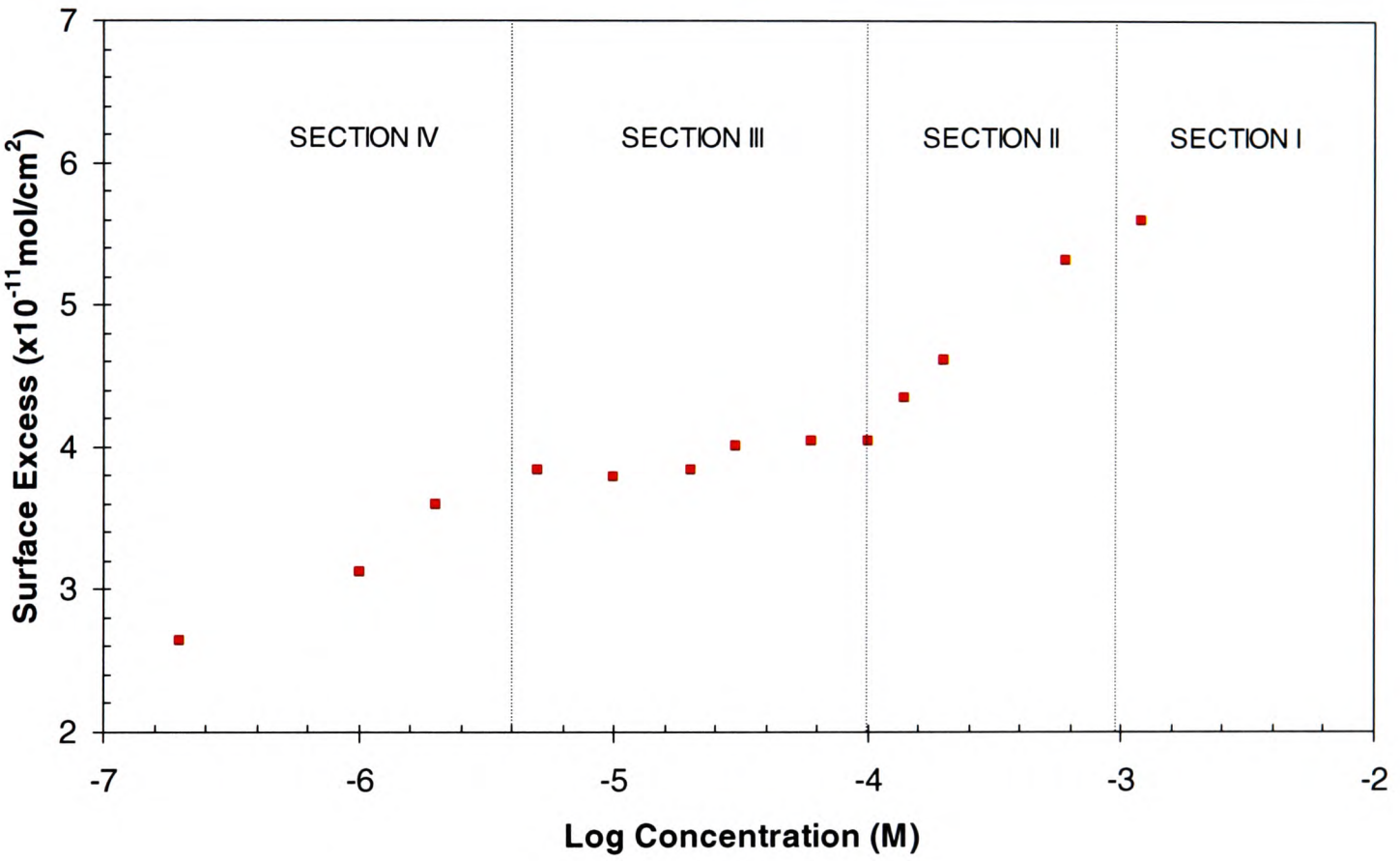


Figure 1. Adsorption isotherm of d-EPE 3000-14 at the air-solution interface at 25°C determined by neutron reflection.

The reflectivities of three isotopic compositions, d-EPE 3000-14 in NRW, d-EPE 3000-14 in D_2O, and h-EPE 3000-14 in D_2O, were measured at three different concentrations at 25°C. The concentrations used were $1.2x10^{-3}$M, $2.0x10^{-5}$M and $2.0x10^{-6}$M, which fall within sections I, III and IV respectively. The reflectivity profiles were fitted using the Optical Matrix Method (AFIT^2 computer program) taking a monolayer structure consisting of several uniform layers as explained above and using the minimum number of layers required to obtain a simultaneous fit of the three sets of isotopic data.

For the highest concentration, $1.2x10^{-3}$M, the minimum number of layers that would give a satisfactory fit to the three profiles was found to be five. The fits are shown in Figure 2.

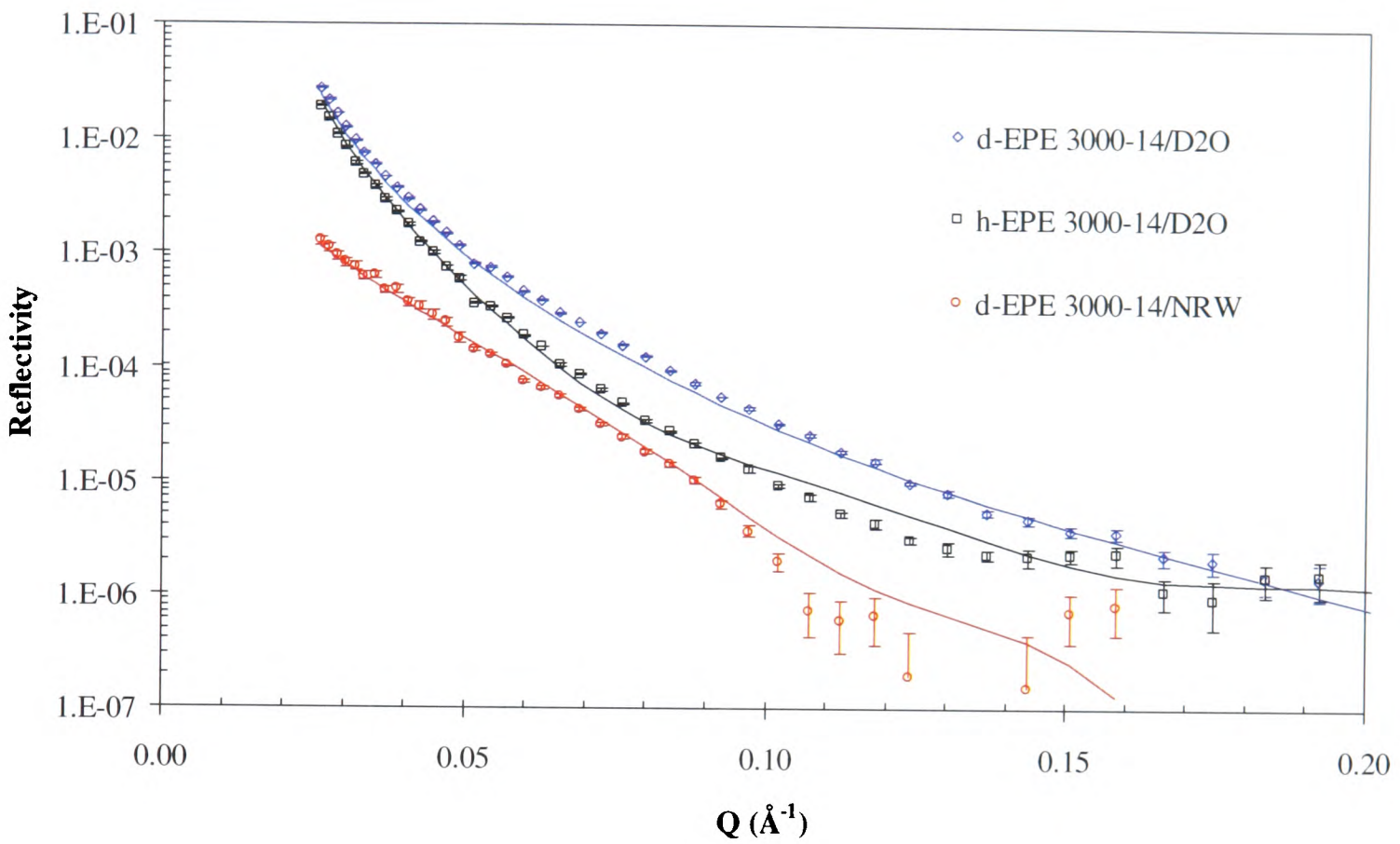


Figure 2. Neutron reflectivity profiles of $1.2x10^{-3}$M d-EPE 3000-14 in null reflecting water, (○), in D_2O, (◇), and $1.2x10^{-3}$M d-EPE 3000-14 in D_2O, (□), measured at 25°C. The best fits of a single structure to all three profiles, using the parameters in Table 2, are shown as continuous line.

For the two lower concentrations, $2.0x10^{-5}$M and $2.0x10^{-6}$M, good fits were obtained with a four-layer model. The measured and the calculated specular reflectivity profiles for those two concentrations are shown in Figure 3 and 4.

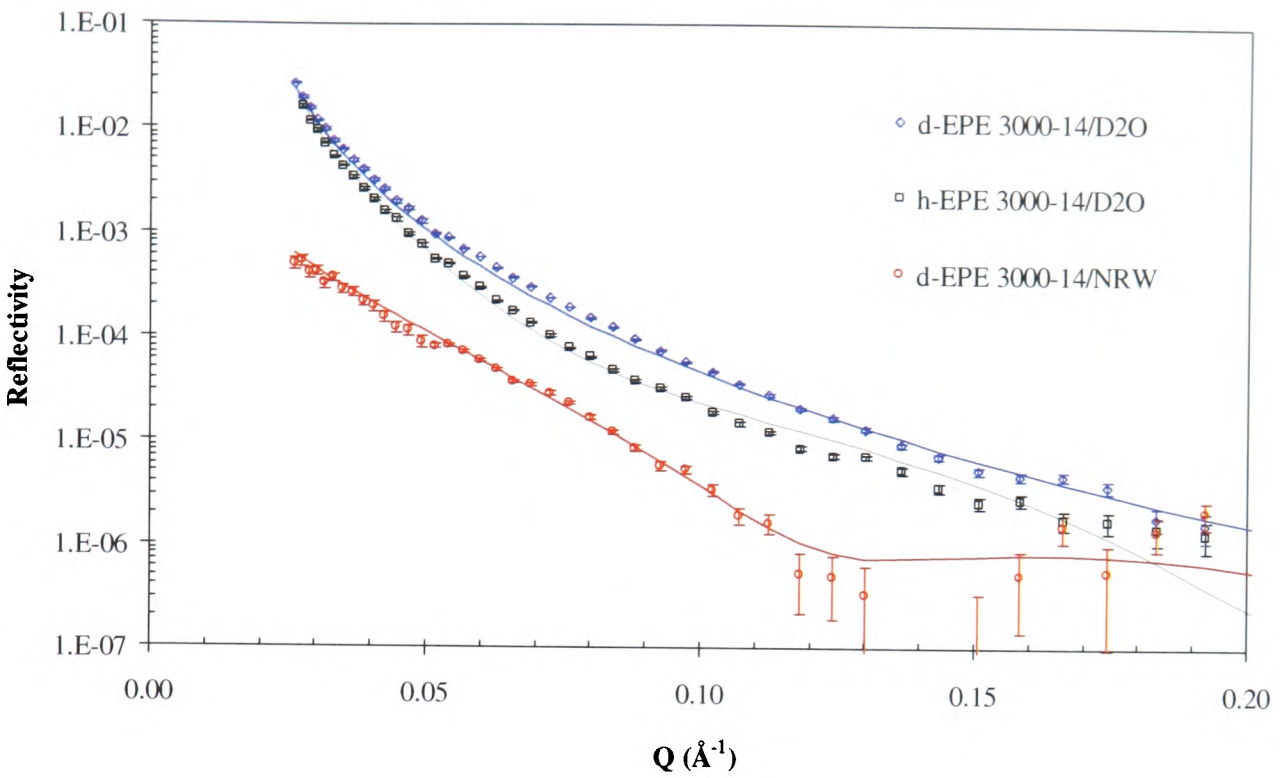


Figure 3. Neutron reflectivity profiles of 2.0×10^{-5}M d-EPE 3000-14 in null reflecting water, (○), in D_2O, (◇), and 2.0×10^{-5}M d-EPE 3000-14 in D_2O, (□), measured at 25°C. The best fits of a single structure to all three profiles, using the parameters in Table 2, are shown as continuous line.

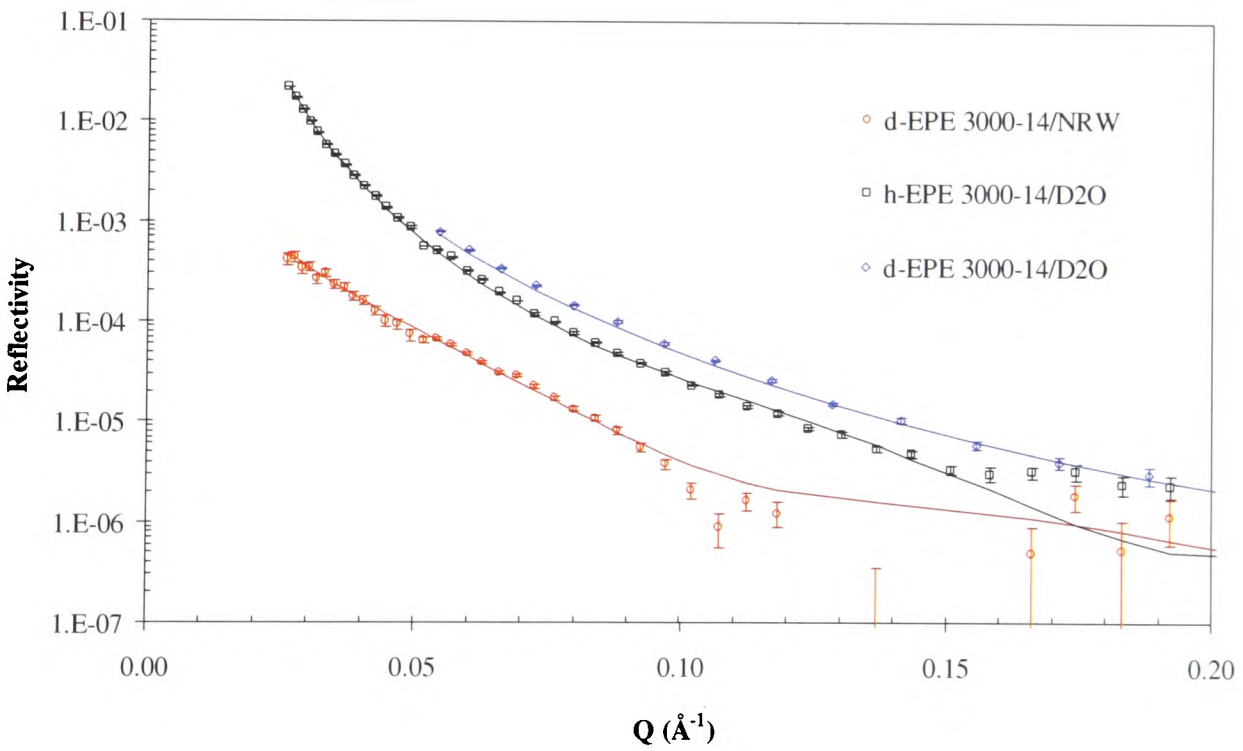


Figure 4. Neutron reflectivity profiles of 2.0×10^{-6}M d-EPE 3000-14 in null reflecting water, (○), in D_2O, (◇), and 2.0×10^{-6}M d-EPE 3000-14 in D_2O, (□), measured at 25°C. The best fits of a single structure to all three profiles, using the parameters in Table 2, are shown as continuous line.

The parameters used for the best fits are presented in Table 2.

		EPE 3000-14 Concentration (M)		
Layer	Parameters	1.2×10^{-3}	2.0×10^{-5}	2.0×10^{-6}
1	τ/Å	12±1[a]	11±1[a]	10±1[a]
	$\rho \times 10^{6}$/Å^{-2}	0.32	0.32	0.32
	ϕ_{water}	0.00	0.00	0.00
2	τ/Å	4±1	15±1	17±1
	$\rho \times 10^{6}$/Å^{-2}	2.35	4.00	4.40
	ϕ_{water}	0.05	0.60	0.65
3	τ/Å	11±1	29±2	29±2
	$\rho \times 10^{6}$/Å^{-2}	2.70	6.00	6.10
	ϕ_{water}	0.52	0.85	0.90
4	τ/Å	20±2	15±1	16±1
	$\rho \times 10^{6}$/Å^{-2}	5.35	6.40	6.40
	ϕ_{water}	0.69	0.98	0.98
5	τ/Å	25±2	-	-
	$\rho \times 10^{6}$/Å^{-2}	6.40	-	-
	ϕ_{water}	0.90	-	-
Copolymer	τ/Å	72±7	70±5	72±5
	$\rho \times 10^{6}$/Å^{-2}	1.06	0.79	0.69
	A/Å^{2}	288±20	395±30	442±40

Table 2. Structural parameters obtained from fitted profiles using the Optical Matrix Method. [a] Denotes insensitive variable in the fitting procedure.

During the fitting process, it was found that the reflectivity was not sensitive to the structure of the upper layer because of the low reflected signal from the protonated PPO groups. A more precise characterization of that particular layer would require the deuterated PPO-chain species. However, the present set of reflectivity profiles are sensitive to the remaining layers and, when the constraint of stoichiometry is included, the upper layer is well defined in terms of the total amount of PPO present. The uncertainties are in its thickness and density.

The multilayer model leads to a greater overall thickness of the layer than the single-layer model described in the previous chapter. For example, the total thickness of the five-layer monolayer at a bulk concentration of $1.2x10^{-3}$M, is 72Å, while the thickness when using just a single-layer model was found to be only 54Å. The discrepancy arises for the reason given in the previous paragraph, i.e. that the upper layer only consists of PO fragments and air, and makes little contribution to the reflectivity.

The number of layers required to obtain a satisfactory fit to the data and, more particularly, the fact that most of these layers are quite mixed, demonstrates the complex structure of the EPE copolymer monolayer at the air-water interface. The most direct way of assessing any possible structural changes with concentration is to plot the distribution of the layer components against distance normal to the surface and this is done for EPE 3000-14 at 25°C in Figures 5a-c.

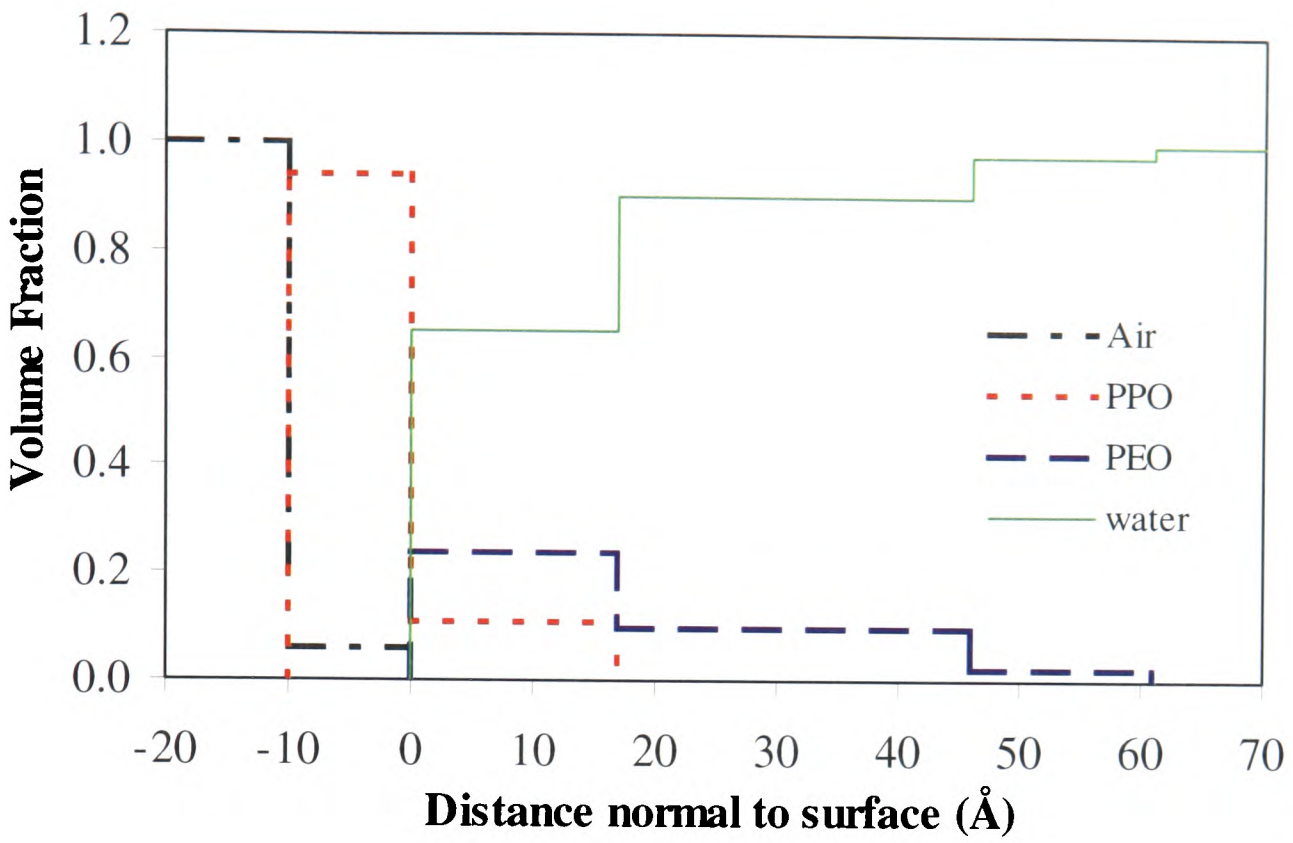


Figure 5a. Volume fraction distribution of the components at the air/water interface at 25°C for bulk concentration of 2.0×10^{-6}M EPE 3000-14 obtained from a four uniform layer model.

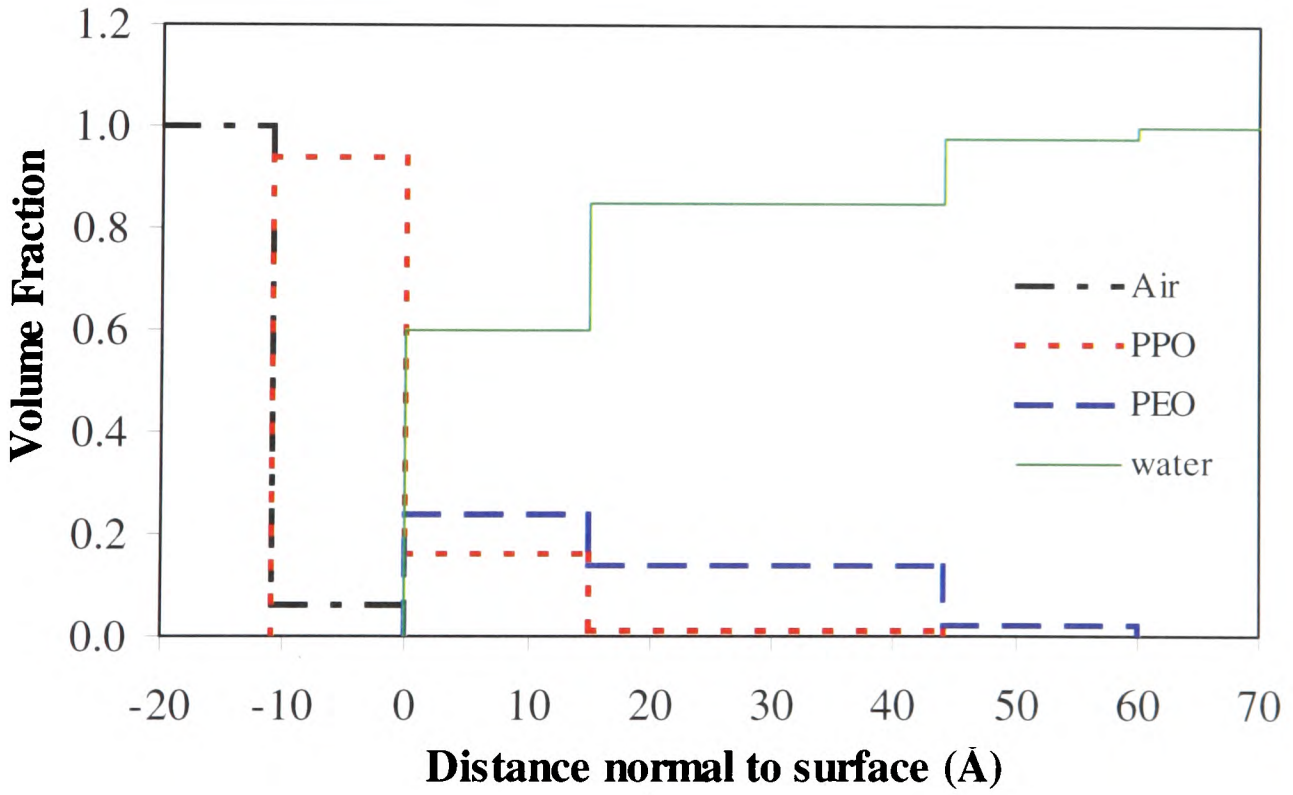


Figure 5b. Volume fraction distribution of the components at the air/water interface at 25°C for bulk concentration of 2.0×10^{-5}M EPE 3000-14 obtained from a four uniform layer model.

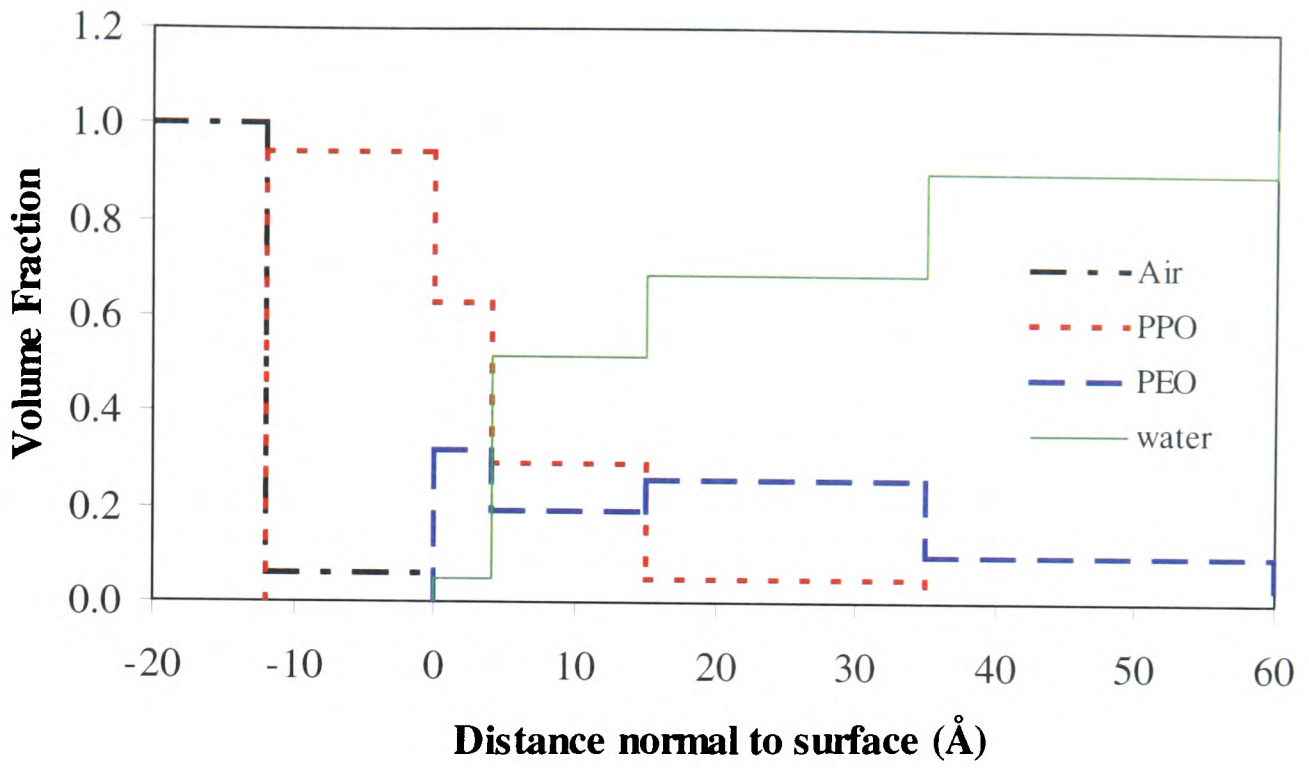


Figure 5c. Volume fraction distribution of the components at the air/water interface at 25°C for bulk concentration of $1.2x10^{-3}$M EPE 3000-14 obtained from a five uniform layer model.

These volume fraction profiles indicate that the estimated thickness of the upper layer containing PO groups remains essentially unchanged throughout the range of copolymer concentration studied. The EO groups are always found to be completely submerged in the aqueous phase, the range of penetration varying from 40-60Å depending on the copolymer concentration. The expected fully extended length for a PEO chain containing 23 EO segments would be 74Å, taking the length of an individual ethylene segment to be approx. 3.2Å. Thus the PEO must be extensively coiled in the aqueous phase. The most interesting aspect of these profiles is the change in the volume fraction of PO groups in the aqueous phase with increasing copolymer concentration. The amount of PO groups penetrating 10Å down into the aqueous subphase seems to be approximately the same at $2.0x10^{-6}$M and $2.0x10^{-5}$M. Overall the EO and PO groups appear to be well segregated at those two concentrations, but at $1.2x10^{-3}$M there is a significant increase in the width of the PO volume fraction so that it now extends 20Å down into the aqueous subphase.

The uniform layer model shown above is coarse and produces unrealistically abrupt changes in the segment distribution profile. A more realistic description of the layer

would be in terms of smoother distribution functions. We therefore refitted the data using a larger number of layers but making the variation of segment density more gradual in comparison with the minimum number of layers required to give a satisfactory fit. This gives a realistic distribution without changing the underlying simpler model and the quality of the fits to the data remains the same. The smoother distribution in term of a Gaussian volume fraction distribution was calculated assuming a series of sublayers of 10Å thickness each. From the volume fraction profile, the number of segments inside each sublayer was determined using

$$A\tau_i = \phi^i_{PPO} V_{PPO} + \phi^i_{PEO} V_{PEO} + n_w V_w \tag{6.6}$$

$$n^i_{PO} = \frac{\phi^i_{PPO} V_{PPO}}{V_{PO}} \quad \text{and} \quad n^i_{EO} = \frac{\phi^i_{PEO} V_{PEO}}{V_{EO}} \tag{6.7}$$

Retaining the assumption that the number of water molecules can be calculated by assuming all the available space in the layer is filled with water, the segment distributions shown in Figure 6a-c were obtained.

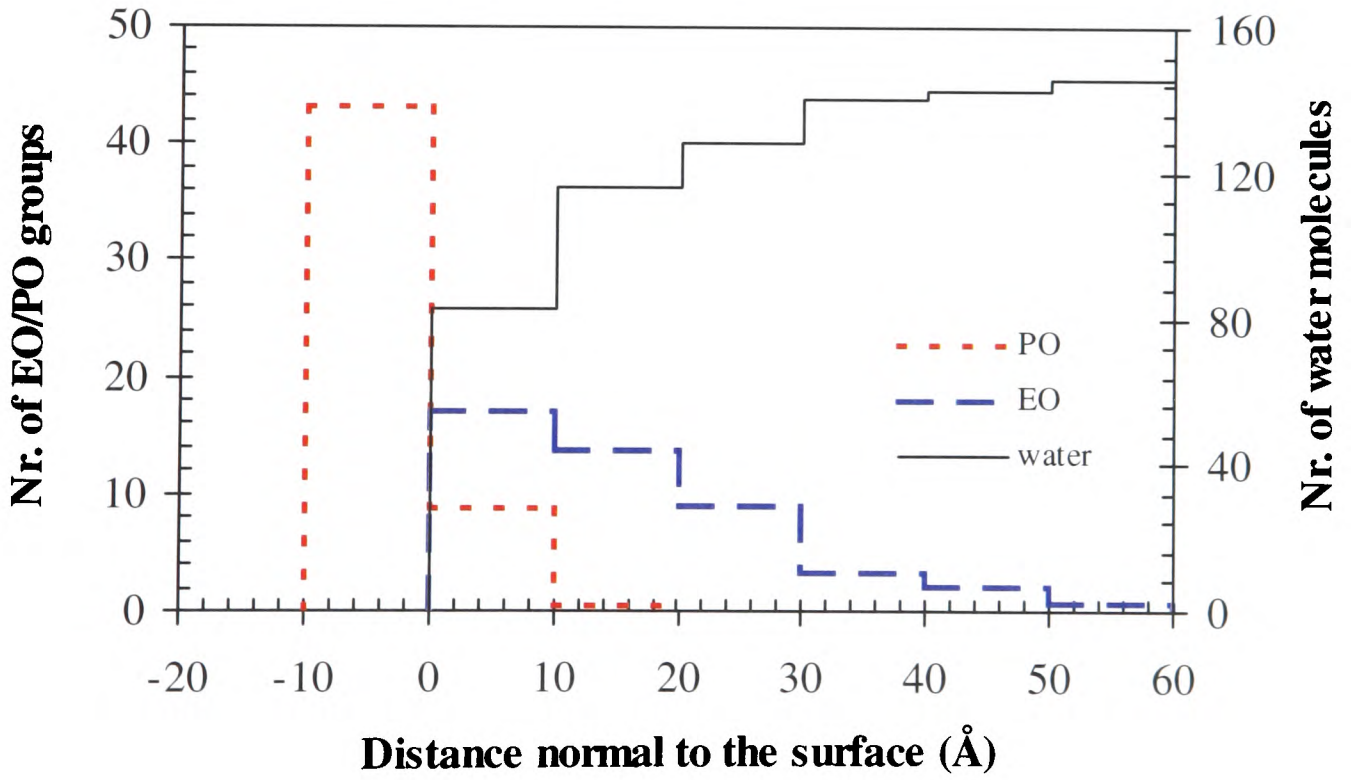


Figure 6a. Segment distribution of EPE 3000-14 at 2.0×10^{-6}M and 25°C obtained from a Gaussian profile of the volume fractions. The total number of water molecules inside the monolayer was 756.

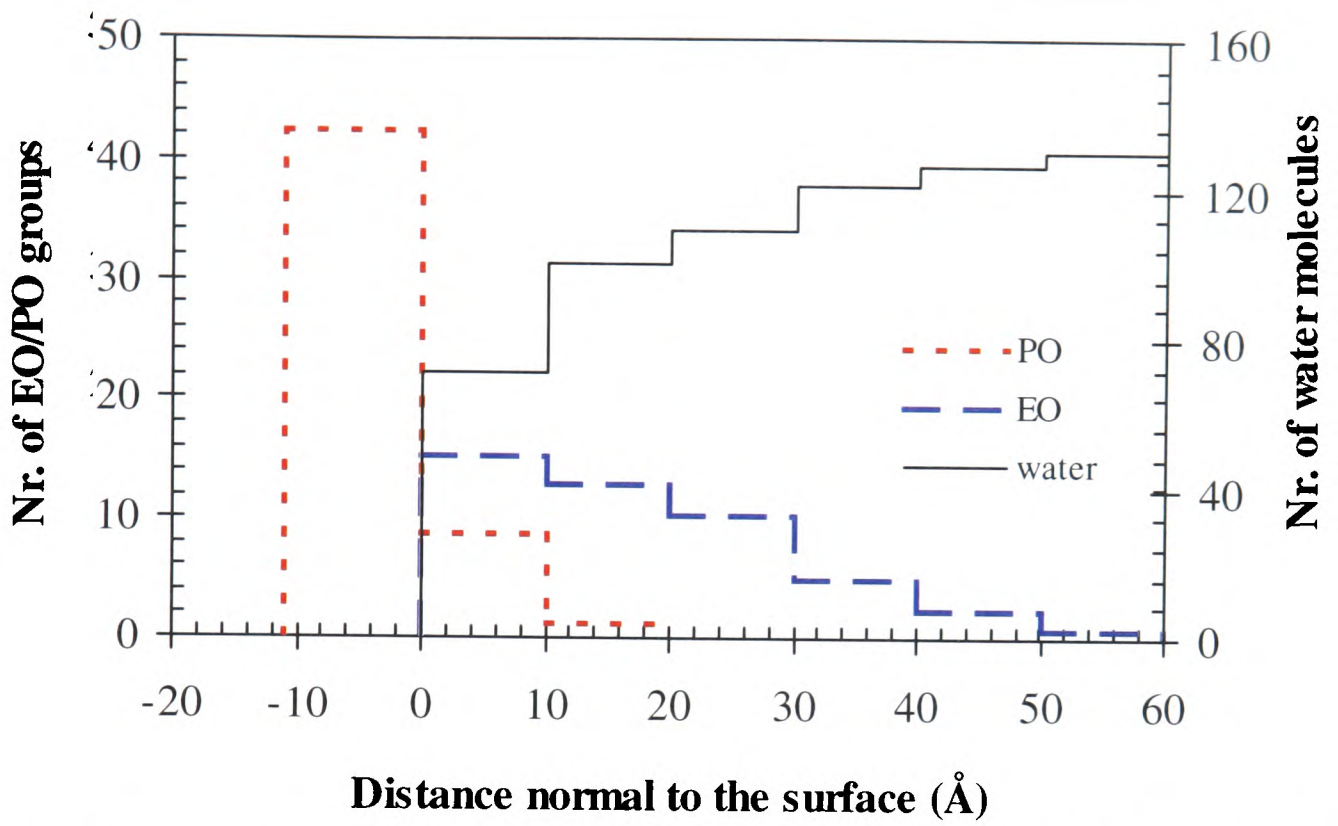


Figure 6b. Segment distribution of EPE 3000-14 at 2.0×10^{-5}M and 25°C obtained from a Gaussian profile of the volume fractions. The total number of water molecules inside the monolayer was 658.

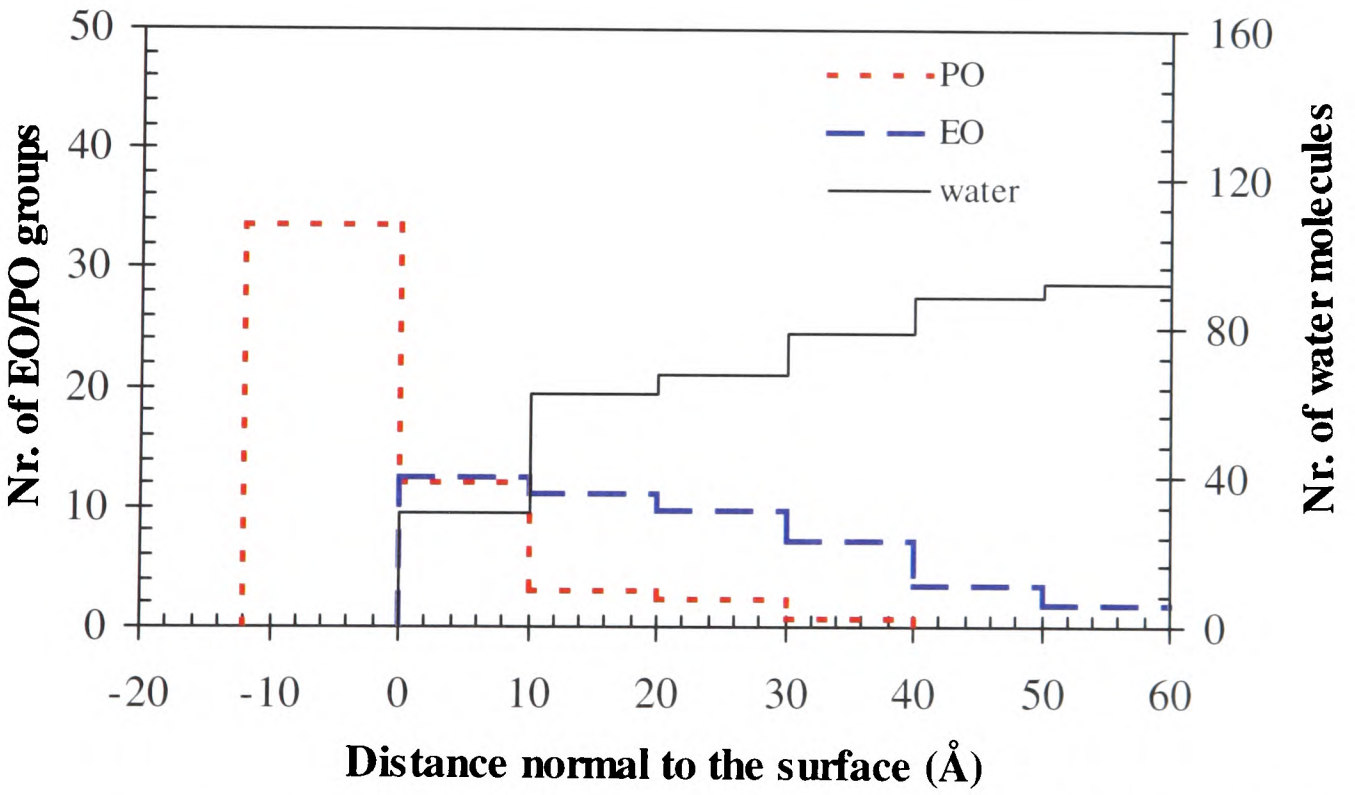


Figure 6c. Segment distribution of EPE 3000-14 at 1.2×10^{-3}M and 25°C obtained from a Gaussian profile of the volume fractions. The total number of water molecules inside the monolayer was 420.

The segment distribution profiles show that the number of PO groups in the uppermost layer remains the same for the two more diluted concentrated solutions, but at $1.2x10^{-3}M$ about 8 PO groups, originally from the upper layer, appear to become immersed in the aqueous phase. Water molecules are gradually expelled from the monolayer as the copolymer concentration increases, although in the region close to the surface the degree of dehydration seems to increase significantly. The distribution of the EO groups throughout the monolayer is not affected by the redistribution of the other species.

This observation supports the suggestion in the previous chapter concerning the rearrangement of copolymer molecules within the monolayer which takes place in Sections II and I of the isotherm of Figure 1. For EPE 3000-14 solutions above $10^{-4}M$ there is a sudden increase in surface excess which is believed to be the result of an increased disorder or intermixing of PPO and PEO chains. The volume fraction profiles indeed show that, while the PO distribution appears to be unchanged at the two lower concentrations, at $1.2x10^{-3}M$, the PO groups appear to have moved from the upper layer into the part of the aqueous phase that is rich in EO groups. The combination of PO groups being dragged down from the uppermost layer and water molecules being gradually expelled from the monolayer would lead to a more compact structure, creating some space for further EPE molecules to be adsorbed.

The monolayer structures portrayed by the volume fraction profile for both $2x10^{-6}M$ and $2x10^{-5}M$ solutions are identical. Therefore, the explanation given by Alexandridis *et al.* that the low-concentration break is a result of rearrangement of the copolymer molecules on the surface does not conform to the experimental data.

Linse *et al.*[3] have used an expanded Mean Field Lattice Model to calculate the volume fraction profile across the air-water interface for an EPE copolymer. Further details of the Mean Field Theory modified by Linse are presented in Chapter 8. A comparison between the volume fraction profile calculated for EPE 3000-14 and the volume fraction profile calculated using the Mean Field Model for a copolymer, $E_{37}P_{56}E_{37}$, shows good agreement, although the chains are longer in the compound used for the theoretical work. The volume fraction estimated by the Mean Field Model for EO groups close to the

surface is almost double that obtained from experiment. The thickness estimated for the uppermost layer, which comprises PO groups and air, was 10-12Å from experiment and about 8Å from the Mean Field Model. The functional form of the profile extending into the water subphase is similar for the experimental and theoretical distributions.

3.2 Effect of temperature on the monolayer structure

The properties of aqueous solutions of EPE copolymers have been shown to be very sensitive to temperature. The remarkable influence of temperature makes this class of polymeric surfactants quite different from the small molecule C_iE_j surfactants. The study of coverage using neutron reflectivity at 25°C to 35°C was discussed in the previous chapter. It showed that below the CMC, there is a significant increase in the total amount of adsorbed EPE copolymer with temperature without significant changes to the monolayer thickness. The strong effect could be understood on the basis of an increased disorder within the monolayer produced by a combination of reduced hydration and intermixing of PEO and PPO chains. The latter could result from a conformational change of the PO groups induced by temperature, which renders the PO-water interaction less favourable than the PO-EO interaction.

To study the effect of temperature on the structure of the monolayer, the reflectivities of three isotopic compositions, d-EPE 3000-14 in NRW, d-EPE 3000-14 in D_2O, and h-EPE 3000-14 in D_2O, were measured at 35°C with a copolymer concentration of $2.0x10^{-5}$M. The model used to account for the data at 25°C would not fit the reflectivity of the same solution at 35°C. Only with a five-layer model could the reflectivity profiles of the three isotopic species be fitted with a single set of structural parameters, as shown in Figure 7. The fitted parameters are given in Table 3.

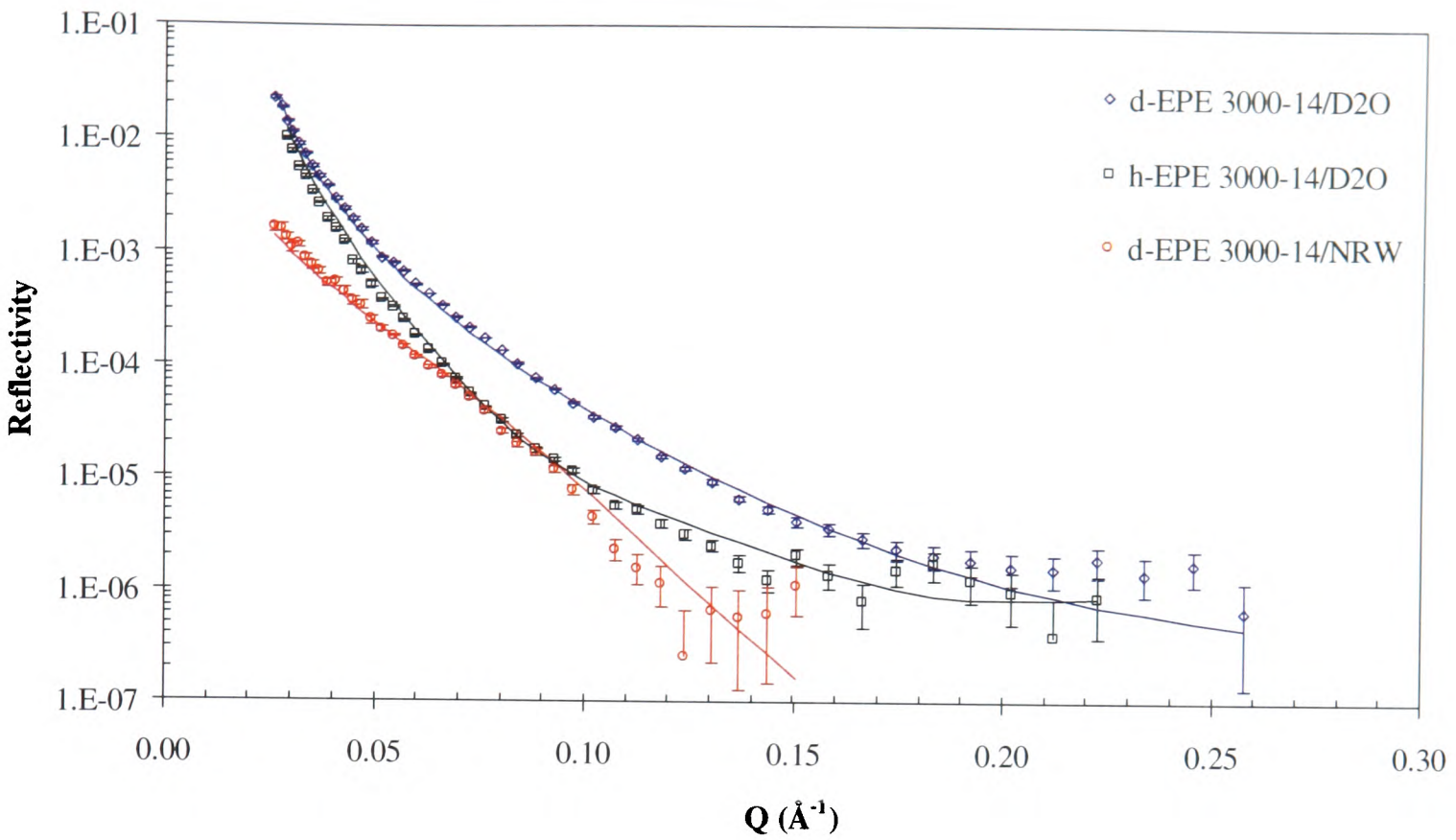


Figure 7. Neutron reflectivity profiles of $2.0x10^{-5}$M d-EPE 3000-14 in null reflecting water, (○), in D_2O, (◇), and $2.0x10^{-5}$M d-EPE 3000-14 in D_2O, (□), measured at 35°C. The best fits of a single structure to all three profiles, using the parameters in Table 3, are shown as continuous line.

The increased number of layers required for the model of the interface had no effect on the total monolayer thickness, but the thickness was again found to be greater than the one obtained with a single uniform layer model. The area per molecule was reduced significantly at the higher temperature, from 395Å^2 at 25°C down to 270Å^2 at 35°C. The copolymer scattering length density in the monolayer also increased substantially, from $0.793x10^{-6}$Å^{-2} to $1.178x10^{-6}$Å^{-2}, which implies a significant increase of the copolymer concentration in the monolayer. The increase of temperature therefore produces a considerable change in monolayer structure, with increased PEO and PPO intermixing and a reduced hydration level within the monolayer.

Layer	Parameters	2.0×10^{-5}M
1	t/Å	9±1[a]
	$\rho \times 10^6$/Å^{-2}	0.32
	ϕ_{water}	0.00
2	t/Å	13±1
	$\rho \times 10^6$/Å^{-2}	1.45
	ϕ_{water}	0.03
3	t/Å	5±1
	$\rho \times 10^6$/Å^{-2}	5.00
	ϕ_{water}	0.59
4	t/Å	21±2
	$\rho \times 10^6$/Å^{-2}	6.20
	ϕ_{water}	0.71
5	t/Å	21±2
	$\rho \times 10^6$/Å^{-2}	6.40
	ϕ_{water}	0.91
Copolymer	t/Å	69±7
	$\rho \times 10^6$/Å^{-2}	1.18
	A/Å^2	270±20

Table 3. Structural parameters obtained from fitted profiles using Optical Matrix Method. [a] Denotes insensitive variable in the fitting procedure.

To assess the structural transitions within the monolayer as the temperature is increased, the distribution of the volume fractions obtained from the uniform layer model was plotted against the distance normal to the surface.

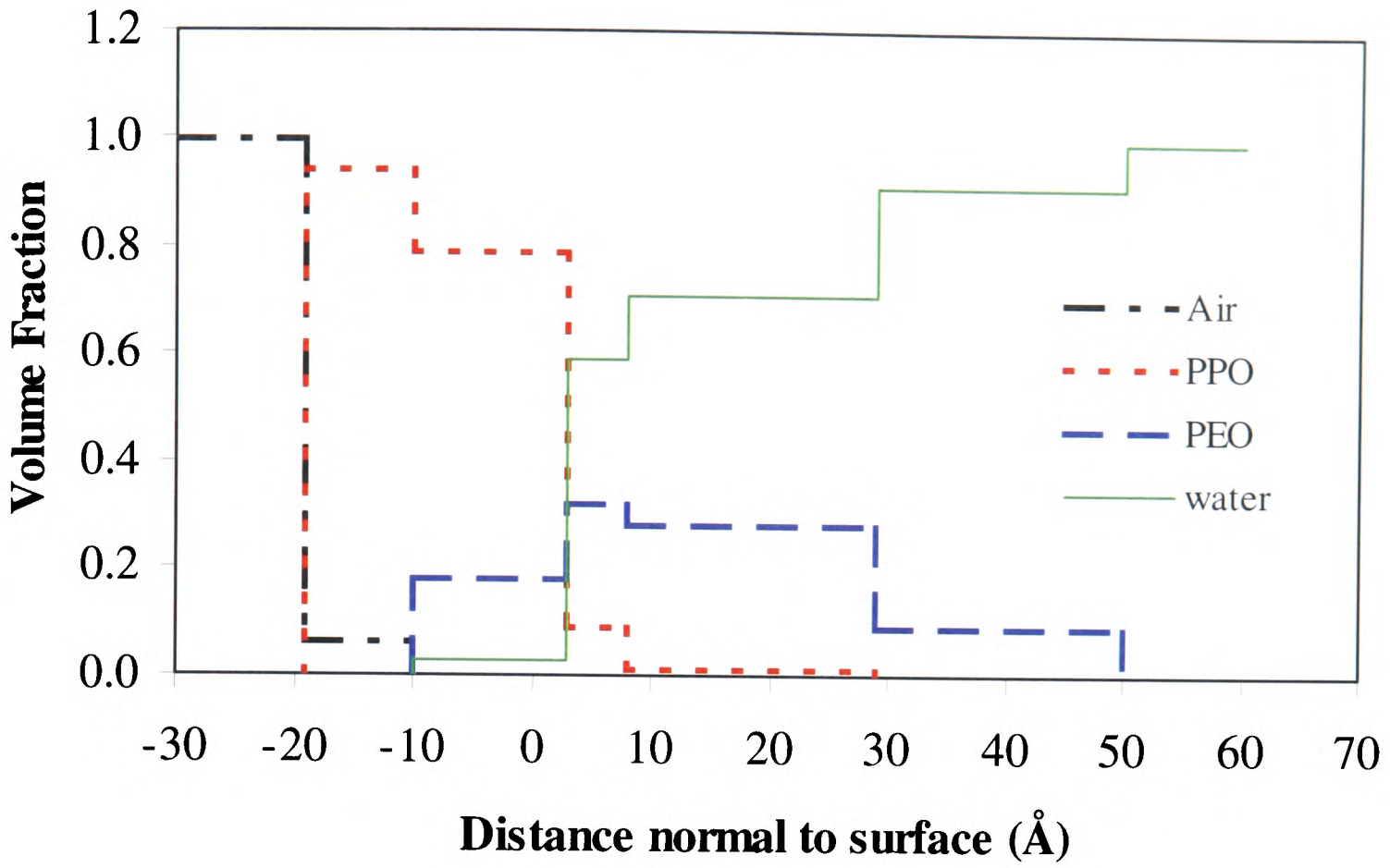


Figure 8. Volume fraction distribution of the components at the air/water interface at 35°C for bulk concentration of $2.0x10^{-5}$M EPE 3000-14 obtained from a five uniform layer model.

The volume fraction distribution at 35°C, shown in Figure 8, is compared with that from the highest surface coverage, i.e. at $1.2x10^{-3}$M, at 25°C, shown in Figure 5c. The effect of temperature is so large that at this concentration the coverage is actually similar to that at $1.2x10^{-3}$M and 25°C. Despite this similarity, there is a dramatic change in layer structure. The thickness of the upper layer above the surface, dominated by PO, doubles with the temperature increase and the extensive PO layer below the surface at 25°C has collapsed. Interestingly, a proportion of EO segments move into the uppermost layer above the surface when the temperature increases to 35°C without taking water with them. The water volume fraction profiles appear to be reasonably similar at both temperatures, although the overall hydration level of the monolayer at 35°C must be reduced given that the area per copolymer molecule decreases substantially on increasing the temperature.

The significant change of area with temperature makes it more difficult to evaluate the effect of temperature on the degree of group intermixing and level of hydration within the monolayer by analysing the volume fraction profiles. Once again dividing the Gaussian volume fraction profile into strips of 10Å thick and calculating the fragment composition inside each strip according to Equations 6.6 and 6.7 gives the segment distribution within the monolayer for 2.0×10^{-5}M EPE 3000-14 solution at 35°C shown in Figure 9.

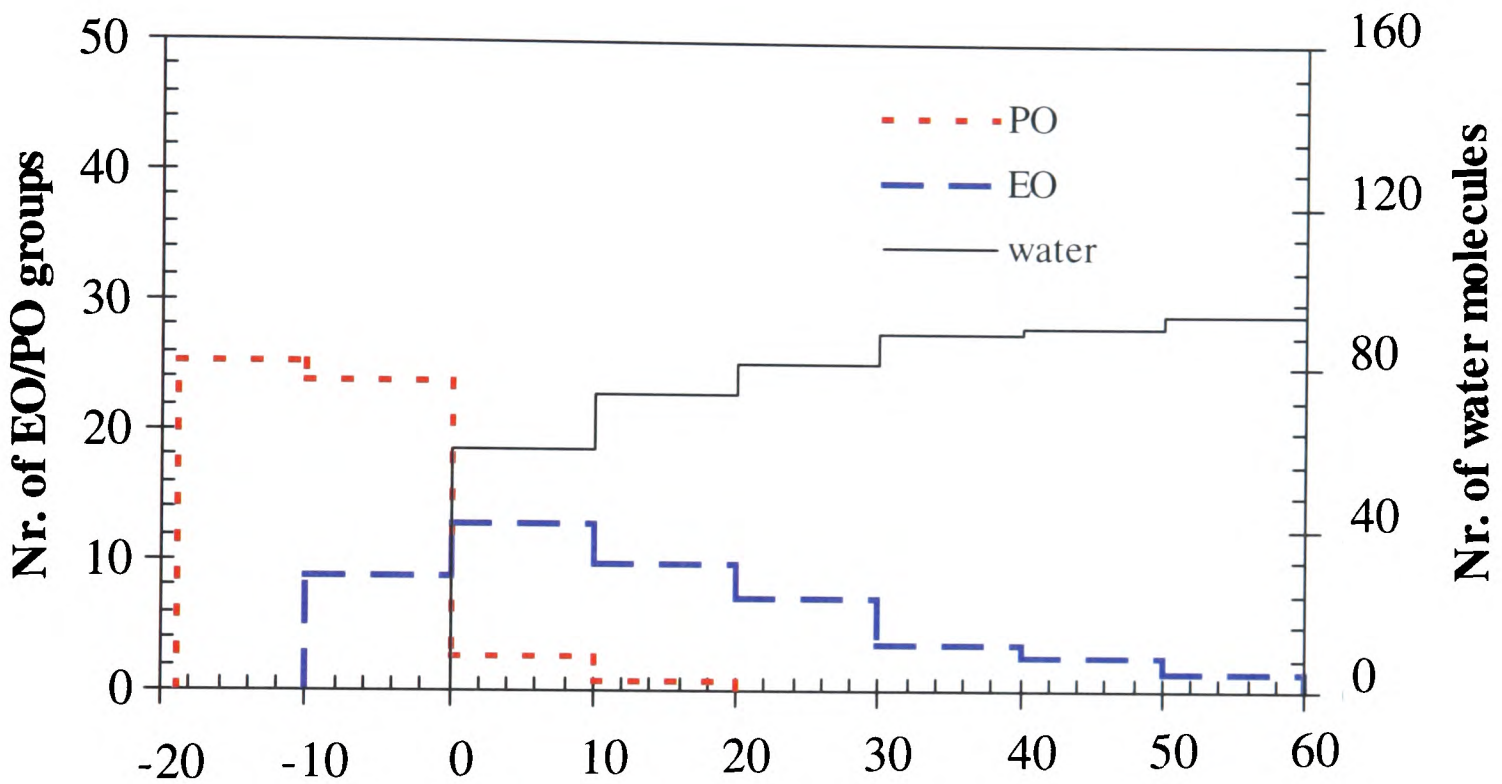


Figure 9. Segment distribution of EPE 3000-14 at 2.0×10^{-5}M and 35°C obtained from the volume fraction profile. The total number of water molecules inside the monolayer is 485.

One interesting point to observe in Figure 9 is that temperature does have a remarkable influence on the interaction between water molecules and both EO and PO groups. At 35°C the PO groups are almost entirely withdrawn into the upper layer away from the aqueous sub-phase. Around 9 EO units were found protruding into the top layer above the surface. The hydration level of the monolayer, as expected, was greatly reduced. The remarkable effect of temperature on the structure of the monolayer has been attributed to a temperature-induced conformational change of PO and EO groups, which increases the population of the less polar conformers, rendering the interactions PO-water and

EO-water less favourable than PO-EO interaction. Hence the monolayer becomes more condensed with an increase of temperature.

3.3 Effect of EPE Copolymer Composition

The coverage variation with neutron reflectivity discussed in Chapter 5 showed that similar transitions are observed in the adsorption isotherms of all the EPE copolymers, as shown in Figure 10.

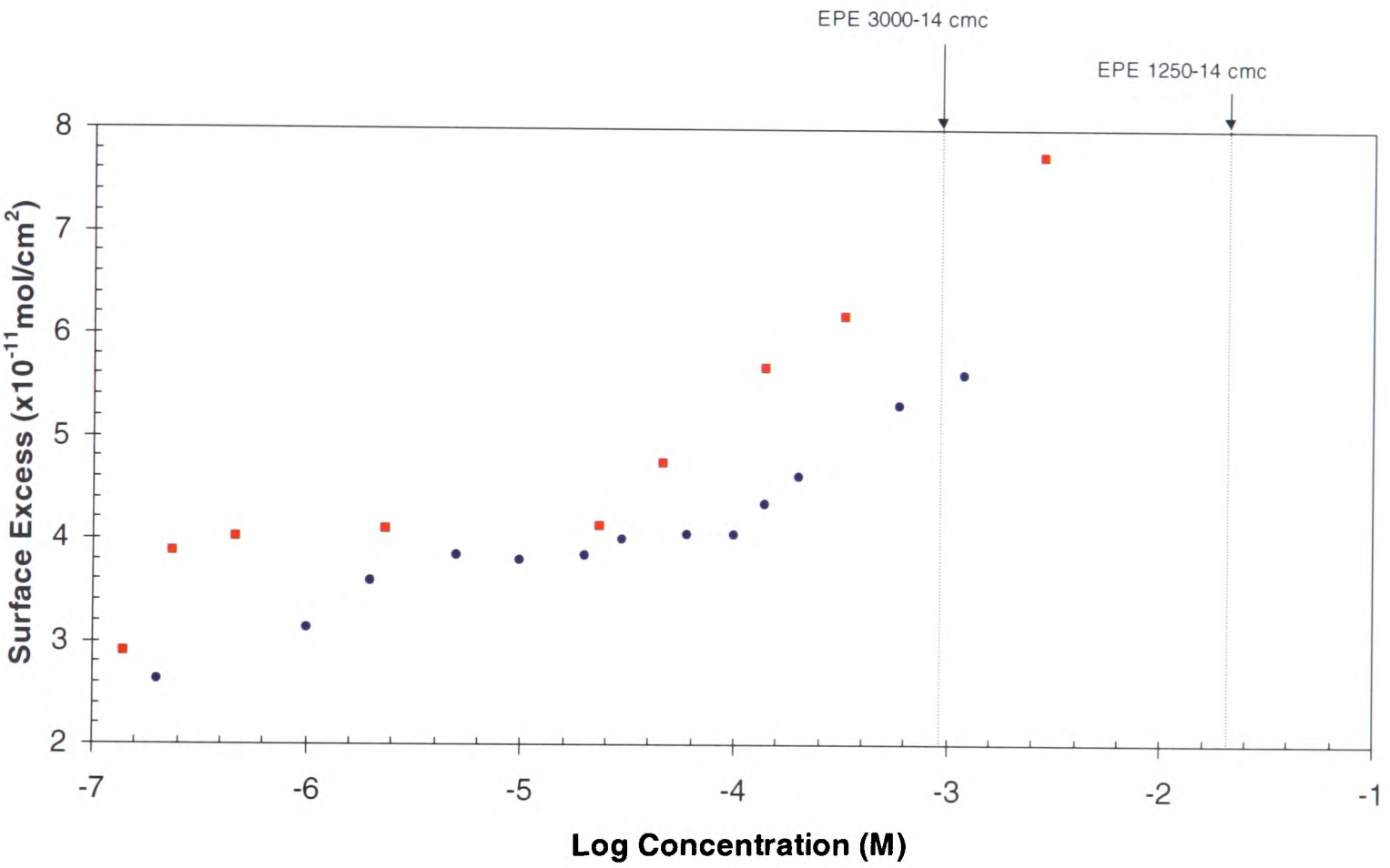


Figure 10. Air-solution interface adsorption isotherms determined by neutron reflection of d-EPE copolymers, EPE 1250-14 (■) and EPE 3000-14 (●), at 25°C.

Although the surface excesses at which the saturation of the monolayer is reached are similar for both EPE copolymers, the bulk concentration at which the structural rearrangement within the monolayer starts varies. The concentration of this point is lower for EPE 1250-14 than for EPE 3000-14. To study the effect of EPE copolymer composition on the structure of the monolayer, the reflectivities of three isotopic compositions, d-EPE 1250-14 in NRW, d-EPE 1250-14 in D_2O, and h-EPE 1250-14 in D_2O, were measured at 25°C and at two copolymer concentrations, 4.8×10^{-4}M and

$4.8x10^{-5}$M. These two concentrations are within the region (Section II) where there is a sudden increase of surface excess, associated with a structural transition within the monolayer.

The three reflectivity profiles of each copolymer concentration were fitted satisfactorily by a four uniform layer model with a single set of structural parameters. The monolayer structure used for the model was similar to that applied to EPE 3000-14. The measured and the calculated specular reflectivity profiles for the two concentrations are shown in Figures 11 and 12.

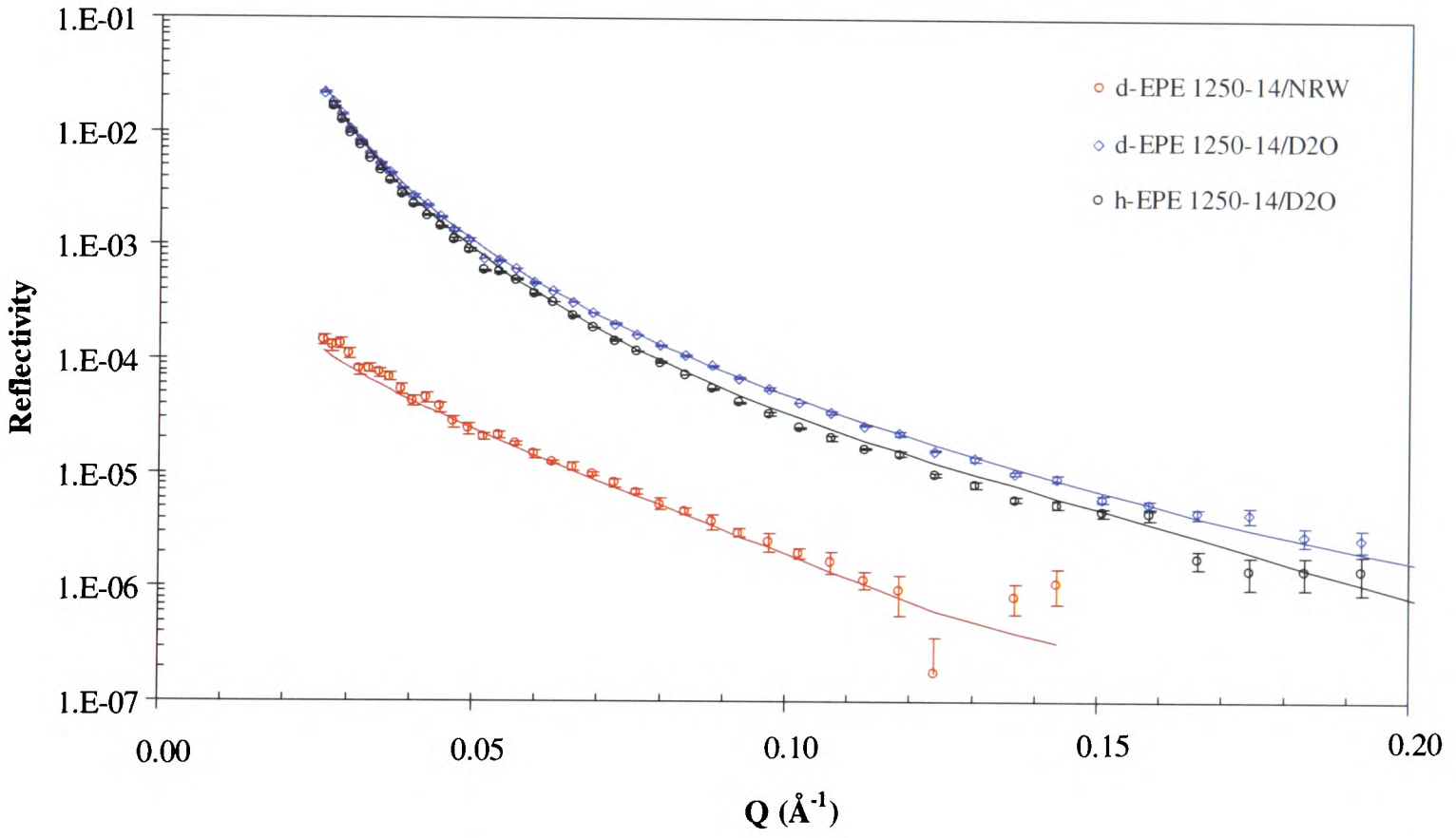


Figure 11. Neutron reflectivity profiles of $4.8x10^{-5}$M d-EPE 1250-14 in null reflecting water, (○), in D_2O, (◇), and $4.8x10^{-5}$M d-EPE 1250-14 in D_2O, (□), measured at 25°C. The best fits of a single structure to all three profiles, using the parameters in Table 4, are shown as continuous line.

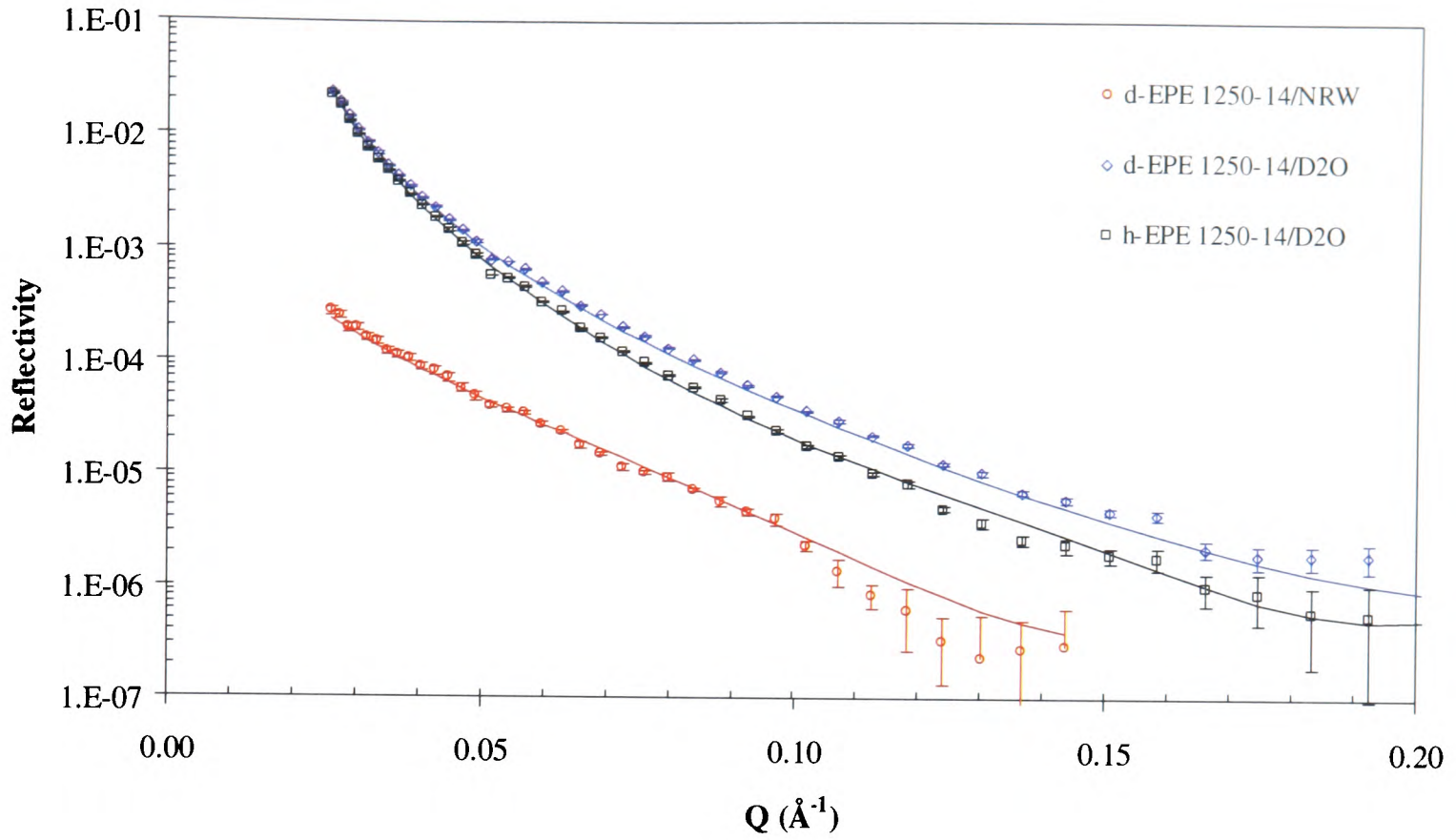


Figure 12. Neutron reflectivity profiles of $4.8x10^{-4}$M d-EPE 1250-14 in null reflecting water, (○), in D_2O, (◇), and $4.8x10^{-4}$M d-EPE 1250-14 in D_2O, (□), measured at 25°C. The best fits of a single structure to all three profiles, using the parameters in Table 4, are shown as continuous line.

The structural parameters used to calculate the reflectivity profile, i.e. layer thickness, τ, layer scattering length density, ρ, and water fraction, ϕ_{water}, were adjusted to give a simultaneous fit to the profiles of the three isotopic compositions and to the stoichiometry of the copolymer. The fitting parameters obtained are presented in Table 4.

The upper layer is once again not sensitive to the fitting parameters and, as before, the total thickness of the four-layer model appeared to be thicker than that of the single layer model described in the previous chapter. Thus, for a concentration of $4.8x10^{-4}$M, the total four-layer thickness was 50Å, while for the single-layer model it was 45Å. For the more dilute solution, $4.8x10^{-5}$M, the layer thickness was 46Å for the four-layer model, and 41Å for the single-layer. The argument that the discrepancy is due to the inadequate characterization by the single-layer model of the low reflected signal from the uppermost layer of protonated PO fragments, is what probably accounts for the difference.

Layer	Parameters	$4.8x10^{-4}$	$4.8x10^{-5}$
1	τ/Å	4±1[a]	3±1[a]
	$\rho x10^6$/Å^{-2}	0.32	0.32
	ϕ_{water}	0.00	0.00
2	τ/Å	13±1	8±1
	$\rho x10^6$/Å^{-2}	1.90	1.63
	ϕ_{water}	0.58	0.60
3	τ/Å	8±1	10±1
	$\rho x10^6$/Å^{-2}	4.30	4.20
	ϕ_{water}	0.70	0.78
4	τ/Å	25±2	25±2
	$\rho x10^6$/Å^{-2}	6.40	6.40
	ϕ_{water}	0.93	0.95
Copolymer	τ/Å	50±5	46±5
	$\rho x10^6$/Å^{-2}	0.67	0.51
	A/Å^2	259±20	368±30

Table 4. Structural parameters obtained from fitted profiles using the Optical Matrix Method. [a] Denotes insensitive variable in the fitting procedure.

The distributions of the volume fractions obtained from the uniform layer model are given in Figures 13a-b. The plots immediately show a much greater degree of disorder in the layer in that there is more extensive mixing of PO and EO groups with each other and of PO groups even with water, quite unlikely the structure of larger copolymer.

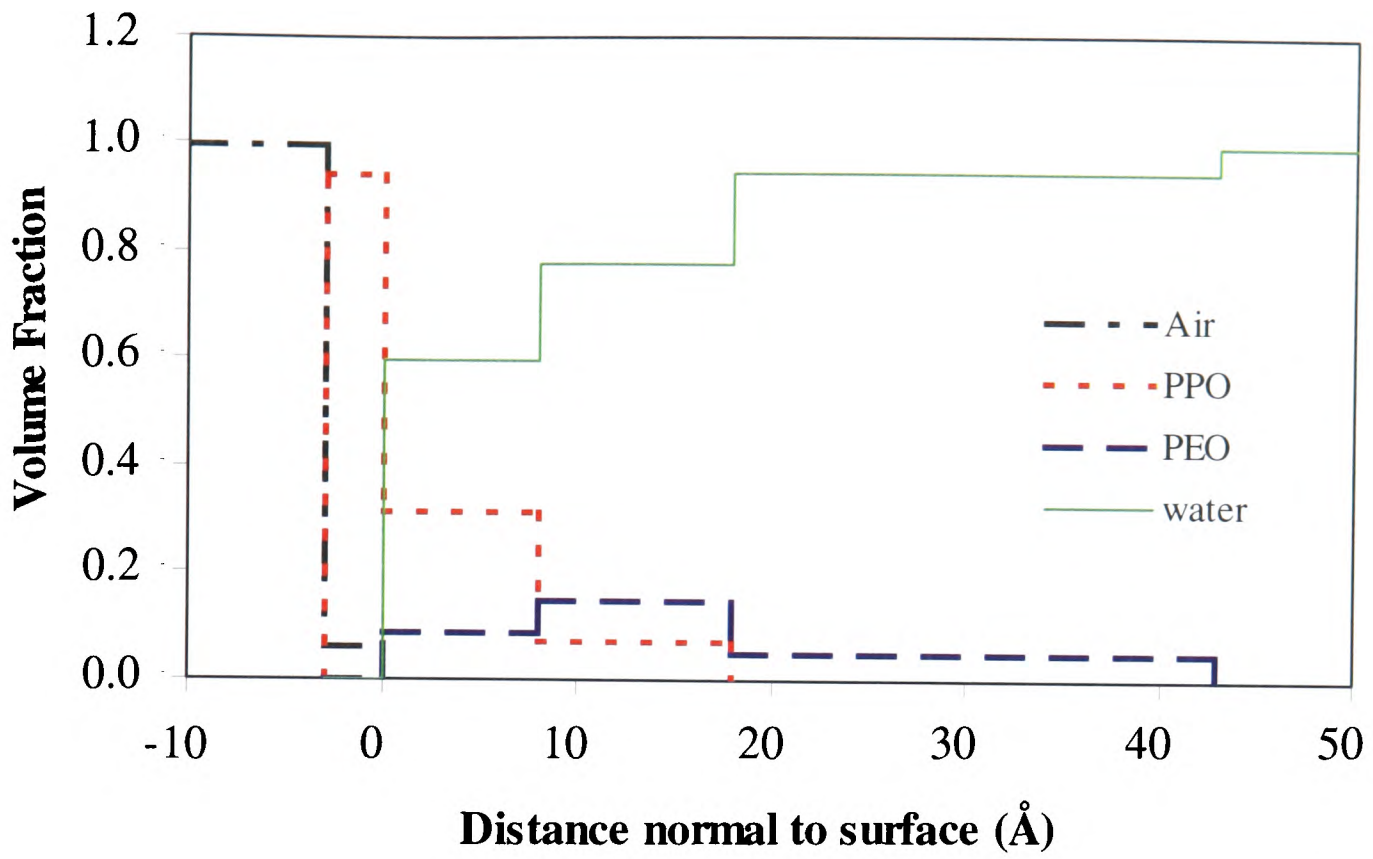


Figure 13a. Volume fraction distribution of the components at the air/water interface at 25°C for bulk concentration of 4.8×10^{-5}M EPE 1250-14 obtained from a four uniform layer model.

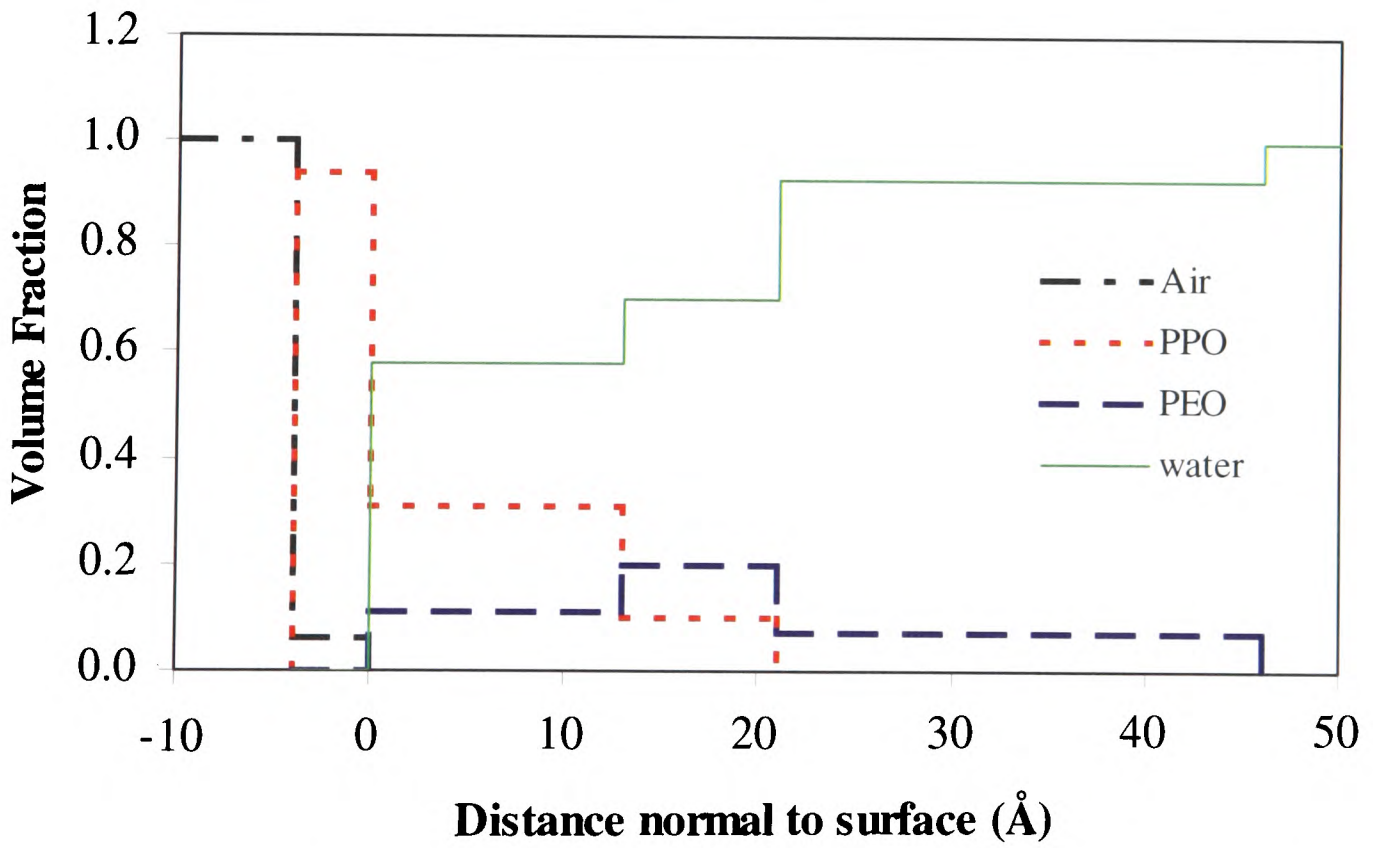


Figure 13b. Volume fraction distribution of the components at the air/water interface at 25°C for bulk concentration of 4.8×10^{-4}M EPE 1250-14 obtained from a four uniform layer model.

Once again, a clearer representation of the monolayer structure is in terms of a smoother distribution than used in the primary fitting and this is shown for both concentrations in Figure 14a-b. The fragment distribution is calculated according to Equations 6.6 and 6.7 from the Gaussian volume fraction divided into strips of 10Å thick.

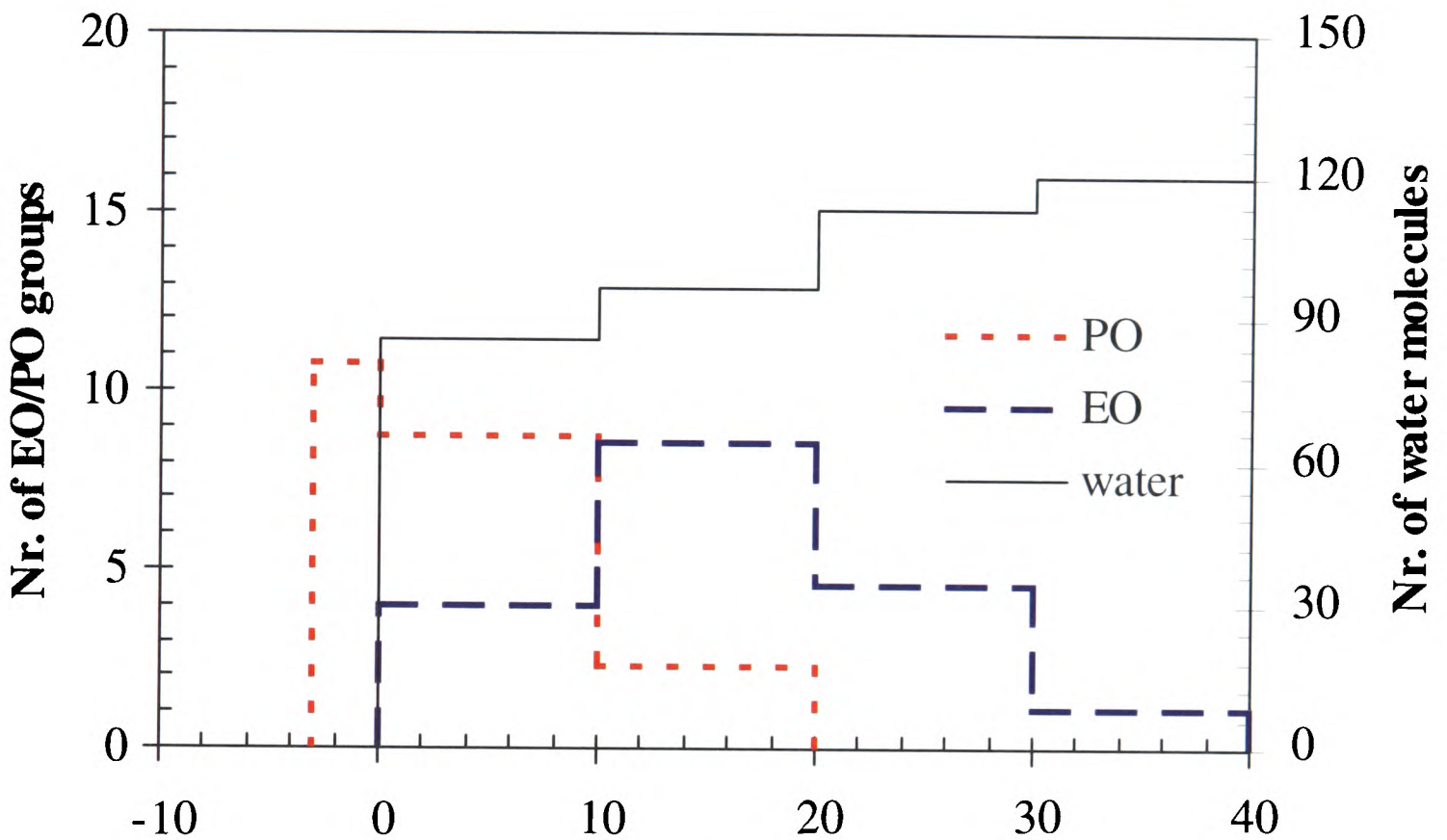


Figure 14a. Segment distribution of EPE 1250-14 at 4.8×10^{-5}M and 25°C obtained from the volume fraction profile. The total number of water molecules inside the monolayer was 418.

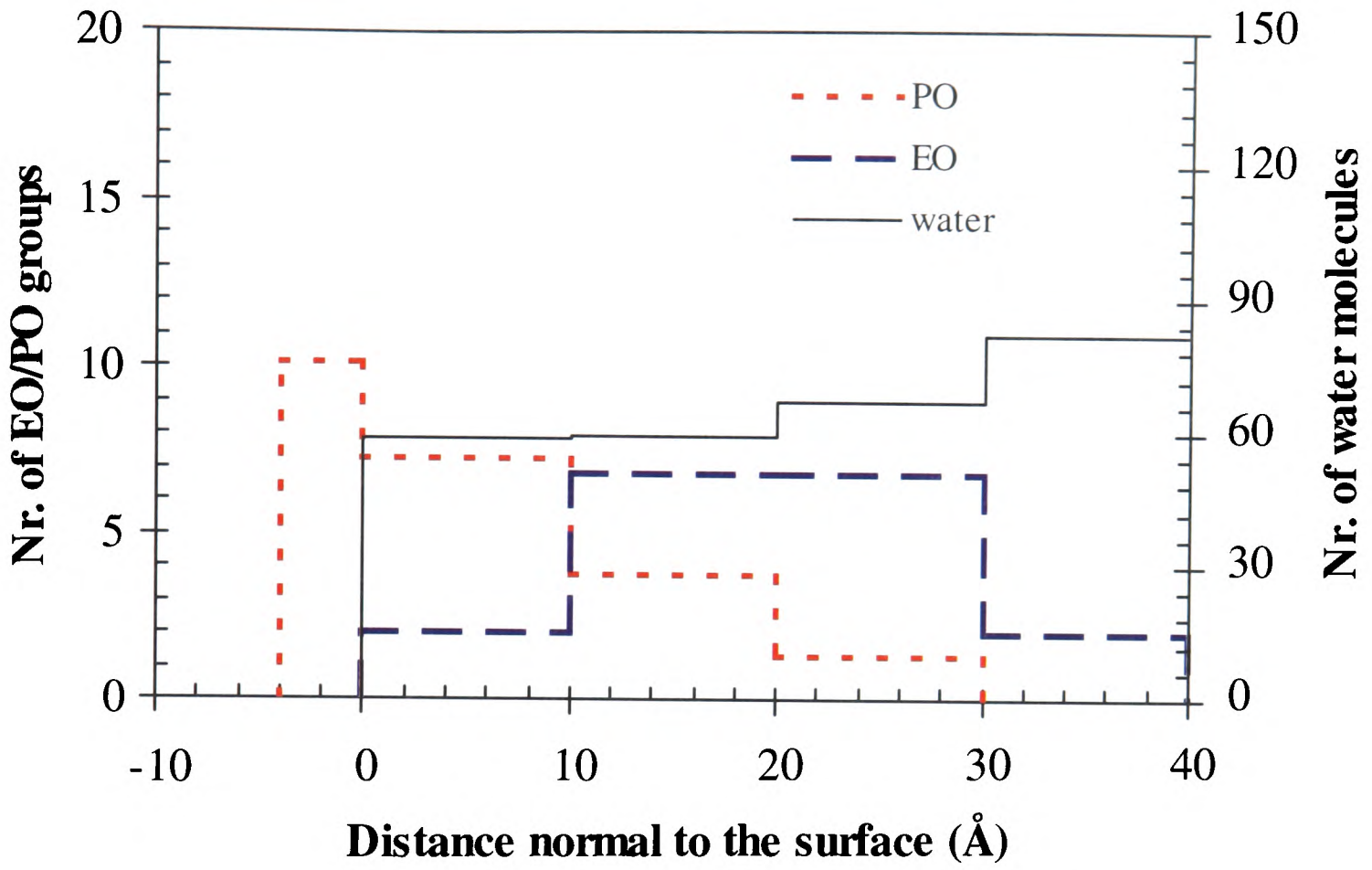


Figure 14b. Segment distribution of EPE 1250-14 at 4.8×10^{-4}M and 25°C obtained from the volume fraction profile. The total number of water molecules inside the monolayer was 268.

The segment distribution profiles show that a significant proportion of the PPO chain of EPE 1250-14 is immersed in the aqueous phase. The depth of penetration into the aqueous phase seems to increase with concentration, although the number of PO groups above the surface remains the same. The PPO layer above the surface for EPE 1250-14 is proportionally thinner than for EPE 3000-14, but when the number of PO groups in that layer are compared at a similar area per molecule segment, fewer PO groups are found for EPE 1250-14. The solution of EPE 3000-14 at 2.0×10^{-5}M with an area per molecule of 395Å contains 39 PO segments in the uppermost layer, with a thickness of 11Å. However, in the solution of EPE 1250-14 at 4.8×10^{-5}M with an area per molecule of 368Å, the uppermost layer is 4Å thick but only contains 11 PO segments. If the proportionality was retained for the number of PO groups above the surface, there should be around 17 PO units for the EPE 1250-14. The difference may be related to an increase in the interaction between the PO groups and water molecules as the PPO chain size is reduced. In fact, short chain polypropylene glycols are actually soluble in water. The

segment distribution profiles clearly indicate a large reduction of water molecules inside the monolayer as the concentration is increased. Overall the features of the monolayer structure observed for EPE 1250-14 were in agreement with those of EPE 3000-14. There is an extensive intermixing of PO and EO groups in the aqueous sub-phase near to the surface. The proportion of PPO chain of EPE 1250-14 immersed in the aqueous phase appears to be proportionally higher.

4 Adsorption Modelling for Block Copolymer

In block copolymer molecules, the properties of two or more homopolymer chains are combined; each block may retain many of the properties of the individual constituent homopolymer. If both blocks are soluble the solvent is called *non-selective*; if one block is insoluble, so that micelles may form in the solution, the solvent is denoted as *selective*.

In an adsorbed block copolymer layer, usually one block is preferentially adsorbed. We denote this as the A block or *anchor*. The other block, with lower (but not necessarily zero) adsorption affinity, is largely excluded from the surface, thereby forming a brush of freely dangling tails; we refer to this as the B block or *buoy*. The so called *brush configuration* combines two important requirements for steric stabilization whereby, on the hand, the polymer can be firmly anchored at the particle surface and, on the other, presents an elastic solvated layer around the particle which provides the repulsive steric barrier needed for stabilization.

A scaling description of the copolymer adsorption from a solution has been given by Marques and Joanny[4,5]. In a selective solvent situation, they describe the adsorbed layer structure as consisting of an anchoring layer of A blocks forming a melt at the surface, which fully wets the surface under the action of the van der Waals attraction. The buoy segments are still in a good-solvent environment and form a fully solvated layer ("brush"). In a highly selective solvent, block copolymers have a tendency to self-aggregate and form mesophases in the bulk, this self-association plays thus a major role in study of the adsorbed layer. This brush model developed by Marques and Joanny for highly selective solvent, the solvent does not penetrate the A layer, which is essentially a

molten A layer. The difficulty of applying such a model is that the structure of the layer determined by neutron reflection does not strictly support the idea that the PO blocks are acting as anchors on the surface of water. There is a significant fraction of PO penetrating the aqueous regions of the layer. The same feature is apparent in the expanded mean field lattice theory developed by Linse *et al.*

In a nonselective solvent system, they modelled a system where both blocks are still incompatible but the solvent is equally good for both blocks[6,7]. The solvent penetrates into the adsorbed anchor layer; which is a fluffy layer very similar to what is obtained in homopolymer adsorption. In particular, this anchor layer is quite dilute, and the van der Waals interaction between the polymer and the wall, which plays an important role in a highly selective solvent, is of no importance in a nonselective solvent[8]. Another important difference is the role of the mesophases in the bulk copolymer solution: in a nonselective solvent we expect mesophase formation only in semi dilute solutions. The scaling theory developed by Marques and Joanny is presented below

4.1 Marques and Joanny (MJ) scaling theory of copolymer adsorption

The mean-field theory of block copolymer adsorption[5] is expected to give a qualitatively good description of the adsorbed copolymer layer; however, it does not take into account correctly the concentration correlations induced by the excluded volume, and thus it is not expected to give quantitative results. The power law dependences are corrected to take into account the excluded volume effects. In a good solvent, the natural radius of the polymer chains is the Flory radius $R_{FA} = N_A^{3/5} a$ and $R_{FB} = N_B^{3/5} a$, N_A and N_B being the degrees of the polymerisation of the blocks and a a monomer size. The radius ratio β is the defined as

$$\beta = \frac{R_{FB}}{R_{FA}} = \left(\frac{N_B}{N_A} \right)^{3/5} \tag{6.8}$$

In the grand canonical free energy Ω' which governs the structure of the adsorbed copolymer layer[5], the free energies of both layers, F_A and F_B, is modified.

$$\Omega' = \Omega - \lambda T a^{-2}\left[\sigma - \frac{1}{N_A}\int_0^\infty \phi(z)\frac{dz}{a}\right] \tag{6.9}$$

where λ is a Lagrange multiplier, T is temperature, and ϕ is the monomer concentration. Alexander[9] has proposed a blob model to calculate the free energy of a grafted polymer brush in a good solvent. For a grafted brush with a chain density σ this leads to

$$\frac{F_B a^2}{T} \approx N_B \sigma^{11/6} \tag{6.10}$$

$$L \approx N_B a \sigma^{1/3} \tag{6.11}$$

where L is the thickness of the B layer (brush). In this section only the scaling laws of the relevant parameters N_A and N_B, and σ, are of interest, the numerical coefficients are systematically ignored. The brush size L has the same scaling behaviour as in mean field theory. The dependence of the free energy in σ is slightly modified. de Gennes[8] has proposed a modified free energy functional which explicitly takes into account correlations in an adsorbed layer. In anchor layer this is written as

$$\frac{F_A \alpha^2}{T} = -\gamma\phi_S + \int_0^\infty \frac{\alpha a^2}{\xi^3}\left[1 + \left(m\frac{\xi}{\phi}\frac{d\phi}{dz}\right)^2\right]dz \tag{6.12}$$

where ϕ_s is the surface concentration, ξ is the local correlation length (in a good solvent $\xi \sim \phi^{-3/4}$), γ is the adsorption free energy, z is the distance from the wall, and m and α are two numerical constants of order unity.

The minimization of the free energy Ω' (Equation 6.9) with respect to the chain density σ gives

$$\lambda + \frac{\mu_{ex}}{T} = N_B \sigma^{5/6} \tag{6.13}$$

with the external chemical potential μ_{ex} being a small contribution when the external solution is dilute.

The concentration profile in the anchor layer is obtained by minimization of Ω' with respect to ϕ. Close to the wall, at a distance z smaller than the layer thickness d, the Lagrange multiplier term is small in Equation 6.9, and the usual self-similar profile in an adsorbed polymer layer is obtained

$$\xi(\phi) = z \tag{6.14}$$

$$\phi(z) \approx z^{-3/4} \tag{6.15}$$

The thickness of the layer is reached when the Lagrange multiplier term $(\lambda / N_A)\int \phi dz$ becomes equal to the two terms of Equation 6.12. The thickness of the adsorbed layer is then

$$d = (N_A / \lambda)^{3/5} a \tag{6.16}$$

As in the mean-field theory, the concentration profile in the A layer is the same as in a homopolymer A adsorbed layer. The confinement of the B chains only reduces the thickness of the layer.

At distances larger than d the concentration profile of the A chains decays rapidly to zero: $\phi(z) \approx 1/\lambda^4 z^8$. It is not clear, however, whether the Cahn-de Gennes free energy of Equation 6.12 retains a meaning in this regime.

Inserting the concentration profile in the copolymer constraint[10] gives

$$N_A\sigma = 1-(a/d)^{1/3} \tag{6.17}$$

The geometrical characteristics of the adsorbed layer are given in this scaling theory by Equations 6.13, 6.16, and 6.17. Here it is considered only when the limit where the radius ratio β is smaller than $N_A^{1/2}$ for which this continuous description has a meaning

$$\sigma \approx 1/N_A \tag{6.18}$$

$$d \approx N_A^{1/2}/\beta \tag{6.19}$$

$$L \approx N_B^{2/3}\beta^{1/3} \approx N_B N_A^{-1/3} a \tag{6.20}$$

These results are quite similar to what was obtained in the mean-field approximation although the thickness of the anchor layer shows a different scaling behaviour and is somewhat larger.

The previous results are meaningful only if the adsorbed layer is continuous and may be considered locally as a semidilute solution. This requires in particular that the thickness of the A layer on the wall is much larger than a monomer size *a*. This is obviously the case when the block copolymers are moderately asymmetric but ceases to be true for very asymmetric polymers ($\beta > N_A^{1/2}$), which is now discussed. When the radius ratio β is extremely large, the adsorbed copolymer layer breaks into a patchwork of individual chains. As for homopolymer single-chain adsorption, the A block forms a flat two-dimensional pancake on the surface with a thickness d of the order of a monomer size (and decreasing with the adsorption energy γ). The radius of these pancakes is the radius of an excluded volume polymer chain in two dimensions

$$R_A = N_A^{3/4} a \tag{6.21}$$

The A chains are not close packed on the surface and form a two-dimensional dilute solution only if the A chain concentration is smaller than the overlap concentration.

$$\sigma^* = \frac{a^2}{R_A^2} = N_A^{-3/2} \tag{6.22}$$

The B blocks are dangling in the solution and form a brush as soon as $\sigma\left(R_{FB}^2 / a^2\right) >> 1$, R_{FB} being the Flow radius. If $\sigma\left(R_{FB}^2 / a^2\right) << 1$, the buoy layer is also discontinuous.

The grand canonical free energy, which governs the structure of the adsorbed layer, reads in this geometry

$$\Omega = F_A + F_B + F_{trans} - \mu_{ex}\sigma a^{-2} \tag{6.23}$$

μ_{ex} is the external chemical potential, and the external pressure contribution is here neglected. F_{trans} is the translational entropy of the chains on the surface

$$F_{trans} a^2 / T = \sigma \ln \sigma \tag{6.24}$$

F_B is the brush stretching energy given by Equation 6.10, and F_A is the adsorption free energy of the A blocks. The adsorption energy of one chain is proportional to the number of monomers N_A

$$F_A a^2 / T = -\delta \sigma N_A \tag{6.25}$$

δ being a number of order unity depending on the monomer adsorption energy γ.

When $\sigma R_{FB}^2 << 1$, the brush energy is small and

$$\sigma = \exp\left[N_A \delta + \mu_{ex} / T\right] \approx \phi_b e^{\delta N_A} \tag{6.26}$$

This is possible only when the monomer external concentration ϕ_b, is extremely small

$$\phi \prec \left(N_B^{6/5}\right)^{-1} \exp[-N_A \delta] \tag{6.27}$$

As soon as the external concentration is finite, the buoy layer B becomes continuous (although the anchor layer might be discontinuous), and the translational energy F_{trans} and the external chemical potential μ_{ex} are negligibly small in Equation 6.23. The surface density then depends strongly on the radius ratio β

$$\sigma = \beta^{-2} \tag{6.28}$$

The **A** layer forms thus a two-dimensional dilute solution if the asymmetry β is larger then $N_A^{3/4}$. When $\beta < N_A^{3/4}$ the A blocks form on the solid surface a semidilute two-dimensional layer whose properties have been discussed in details by Bouchaud and Daoud[11]. Although the **A** blocks start to form large loops and to build up the self-similar fluffy layer, the average thickness of the A layer remains of order of a monomer length. The chain density in this semidilute layer is given by Equation 6.28. The semidilute regime crosses over smoothly to the continuous regime of the previous section when $\beta = N_A^{1/2}$. In the case of adsorbed homopolymer A studied by Bouchaud and Daoud, the two-dimensional semidilute regime is obtained for extremely low bulk concentrations, which are inaccessible experimentally. The study of adsorbed diblock copolymer layers in a nonselective solvent might make this regime accessible by an accurate choice of the asymmetry of the copolymer. Finally, both in the dilute and semidilute regimes the size of the buoy layer increases with the buoy molecular mass slower than linearly

$$L = N_B^{3/5} / N_A^{2/5} a \tag{6.29}$$

Although this is much smaller than a stretched chain, it is much larger than the Flory radius of the B chains due to the N_A dependence.

When the A block is short and the B block long, the repulsion between the B blocks is a dominating feature and this determines the number of chains on the surface; the A layer

remains then undersaturated. Increasing the length of the A bock will enhance the adsorption because of a higher adsorption energy per chain, which is balanced by the lateral repulsion between the buoys. This regime is called the *buoy-dominated regime* or, for short, the *buoy regime*. On the other hand, when the A blocks are long the overlap and lateral repulsion between the buoys are weak and the number of chains is then limited by the saturation of the anchor layer. In this regime, denoted as the *anchor-dominated* or *anchor regime*, the adsorbed mass of A remains roughly constant with increasing A content. At the same time, the number of adsorbed chains and, hence, the number of B blocks decreases, as does the adsorbed amount. The transition between the buoy and anchor regimes takes place at $\beta \approx N_A$.

On the face of it, a natural model to describe the adsorbed layer structure for the EPE copolymers studied here would be the polymer brush in the anchor regime, assuming that the insoluble PO block would act as an anchor for the soluble EO chains. The values of β calculated for both copolymers are given in Table 5, however they indicate also that both copolymers are too short for such model to apply. The MJ scaling model is strictly applicable for polymers with $\beta > 1$.

	β	L (Å)	L (NR) (Å)
$E_{23}P_{52}E_{23}$	0.38	58	59±4
$E_9P_{22}E_9$	0.34	30	46±4

Table 5. Comparison of the layer thickness for two EPE copolymers adsorbed at the air-water interface predicted by the MJ model, L, with that determined by neutron reflection, $L(NR)$. The values of $L(NR)$ correspond to the thickness of layer which contains the EO groups. β is the asymmetric ratio.

Another real difficulty of applying such a model, as mentioned above, is that the structure of the layer determined by neutron reflection does not support the idea that the PO blocks are acting as anchors on the surface of water. The significant fraction of PO penetrating the aqueous regions of the layer suggests that the ends of the PO block may act as part of the extended chain in the aqueous solution. The latter may partly explain for the larger

discrepancy between the predicted and the experimental values of layer thickness for $E_9P_{22}E_9$ given in Table 5. Earlier in this chapter we have seen from the neutron reflection results that the layer for such a copolymer is very disordered with a much greater degree of overlap of PO and EO groups and even with water.

Several authors[12-15] have studied the adsorption of EPE copolymers, in particular the Pluronic series from water. The rms thickness δ_{rms} and the maximum extension δ f the profile (which should be comparable to the steric thickness δ_s) of these polymers adsorbed on polysteryrene latex have been determined by SANS[16]. The MJ van der Waals brush model would qualitatively give the same trends with increasing buoy length; quantitavely this model would predict $\delta \sim N_{EO}$, which is a stronger dependence than in the experiment. They also found that the chains were possibly too short to make the scaling approach valid.

Hydrodynamic measurements of the thickness of this type of polymer adsorbed on small silica particles have also been reported[14] for two EPE copolymers, $E_{99}P_{65}E_{99}$ and $E_{125}P_{47}P_{125}$. These two EPE copolymers were found to have very similar adsorbed amounts (≈ 0.36 mg/m^2) and virtually identical hydrodynamic thicknesses. Presumably, in this case competing effects of anchor and buoy cancel. The thickness is again of the order of the radius of gyration for the PEO block.

Results for δ_h of Pluronics on polystyrene latex have been presented by Baker *et al.*[12,13] δ_h followed a scaling law of the form $\delta_h \sim N_{EO}^{0.55}$, independent of the PPO block length. The absolute values for δ_h were comparable to those found for PEO homopolymers of a similar molecular weight, though the reported values were less than those found by others[15]. The authors claim that the PPO block lies flat at the surface.

5 Summary

Specular neutron reflectivity has been used to investigate the structure of monolayers containing monodisperse EPE copolymers at the air-water interface. The effects of

copolymer concentration, temperature and copolymer composition on the monolayer organisation have also been assessed.

The model used to describe the monolayer structure consists of an uppermost layer of PO groups and air, and further aqueous subphase layers containing mixtures of PO and EO groups and water at various volume fractions. The proposed model fitted the experimental reflectivity profiles very well and complies with the copolymer stoichiometry. A similar structure has been obtained using the expanded Mean Field Lattice Model developed by Linse *et al.* The functional forms of the volume fraction profiles between experiment and model are in good agreement.

The study of the surface coverage of EPE copolymers using neutron reflectivity has shown an isotherm with several distinct regions. Four different sections were identified between which the monolayer structure and the air-water interface adsorption behaviour of EPE copolymers appear to be sensitive to the bulk concentration. The explanation given by Alexandridis *et al.* that the low-concentration break is a result of rearrangement of the copolymer molecules on the surface, does not agree with the experimental data. The volume fraction profiles of the interface for both $2x10^{-6}$M and $2x10^{-5}$M solutions of EPE 3000-14 do not show any significant differences. Overall the EO and PO groups appear to be well segregated at those two concentrations. At a bulk concentration of $1.2x10^{-3}$M, however, the volume fraction profiles do indeed show some re-structuring within the monolayer. The PO group distribution shows some penetration into the EO rich region of the aqueous phase. This, when combined with the observation that water molecules are gradually expelled from the monolayer as a whole, produces a more compact structure, creating space for further EPE molecules to be adsorbed. This observation supports the argument that the sudden increase in surface excess, characteristic of Sections II and I of the isotherm, is a result of an increased intermixing of PPO and PEO chain in combination with dehydration of the monolayer.

Temperature has a strong effect on the interaction between water molecules and the EO and PO groups. The experiments carried out at 35°C with a solution of $2x10^{-5}$M EPE 3000-14 revealed that the PO chain is almost entirely withdrawn from the aqueous

sub-phase. The EO groups, which at 25°C are completely submerged, have about 9 units extending into the top layer above the surface. The hydration level of the monolayer is greatly reduced with increasing temperature. The remarkable effect of temperature on the structure of the monolayer can be attributed to a temperature-induced conformational change of PO and EO groups, which increases the population of the less polar conformers, rendering the interactions PO-water and EO-water less favourable than the PO-EO interaction. Hence on increase of temperature the monolayer becomes more condensed as a result of a reduced hydration level and increased PEO and PPO chain intermixing.

The study of the effect of copolymer composition showed that the overall effect of concentration for EPE 1250-14 is similar to that observed for EPE 3000-14, in terms of reduction of water inside the monolayer and extensive intermixing of PO and EO groups near the surface as the concentration is increased. However, a comparatively greater fraction of the PPO chain of EPE 1250-14 is immersed in the aqueous phase and this may be related to a more favourable interaction between the PPO chain and water molecules as the PPO chain size is reduced.

References

[1] Alexandridis, P; Athanassiou, V.; Fukuda, S.; and Hatton, T.A. *Langmuir*, 10, 2604 (1994)

[2] Thirtle, P.N. *D.Phil. Thesis*, University of Oxford (1999)

[3] Linse, P.; and Hatton, T.A. *Langmuir* 13, 4066 (1997)

[4] Marques, C.M.; Joanny, J.F.; and Leibler, L. *Macromolecules* 21, 1051 (1988)

[5] Marques, C.M.; and Joanny, J.F. *Macromolecules* 22, 1454 (1989)

[6] Broseta, D.; Leibler, L.; Ould Kaddour, L.; and Strazielle, C. *J. Chem. Phys.*, 87, 7248 (1987)

[7] Rossi, G.; and Cates, M. *Macromolecules*, 27, 1372 (1988)

[8] de Gennes, P. G. *Macromolecules*, 14, 1637 (1981)

[9] Alexander, S. *J. Phys. (Les Ulis, Fr.), 38*, 983 (1977)

[10] Dolan, A. K.; and Edwards, S. F. *Proc. R. Soc. London A*, 337, 509 (1974)

[11] Bouchaud, E.; and Daoud, M. *J . Phys. (Les Ulis, Fr.)*, 48, 1991 (1987)

[12] Baker, J. A.; Berg, J. C. *Langmuir*, 4, 1055 (1988)

[13] Baker, J. A.; Pearson, R. A.; and Berg, J. C. *Langmuir*, 5, 339 (1989)

[14] Malmsten, M.; Linse, P.; and Cosgrove, T. *Macromolecules*, 25, 2474 (1992)

[15] Alexandridis, P.; and Alan H. *Colloids and Surfaces, A: Physicochemical and Engineering Aspects*, 96, 1 (1995)

[16] Tadros, T. F.; and Vincent, B. *Journal of Physical Chemistry*, 84, 1575 (1980)

Chapter 7

EPE Copolymer-Surfactant Systems

1 Introduction

In addition to the copolymer composition and temperature, the properties of EPE copolymer solutions can be altered by the addition of other solutes, including other surfactants, electrolytes or nonelectrolytes. Such cosolutes can modify the solution properties by interacting either with the EPE copolymer molecules themselves, forming complexes, or with the water and hence varying the solvent properties.

The addition of electrolytes, such as inorganic salts, or nonelectrolytes, such as urea, is a common method for modifying the aqueous solvent quality. A number of studies have been devoted to the investigation of the aqueous solution properties of EPE copolymers in the presence of various electrolytes and nonelectrolytes. The effects of such cosolutes on the micellization and cloud point of EPE copolymer solutions have tended to be the focus of most of these studies. Most inorganic salts decrease the water solubility of organic solutes, which is referred to as the salting-out effect, while some of them have the opposite effect known as salting-in[1]. The effect of the cation type is usually smaller than that of the anion type. The salting out effect of anions at a given concentration follows the Hofmeister series. Two mechanisms have been proposed to explain this behaviour. According to one line of thought, salts affect the "solvent quality" of water; the salting-out anions being believed to be "structure-makers" while the salting-in ones are "structure-breakers". Structure makers lead to an increase in the self-hydration of water through hydrogen-bonding, and therefore a reduction in surfactant solubility. Structure breakers, on the other hand, reduce self-hydration and thereby increase the hydration of the surfactant. In an alternative interpretation, the salting-in and salting-out phenomena have an interfacial origin, ions adsorb or are depleted at the water-solute interface and modify the phase equilibrium[2,3]. The controversy between these two mechanisms has not yet been resolved. The critical micellization temperature (CMT) and cloud point (CP) of Pluronic L64 solutions in the presence of various alkali halides, NaSCN, and urea[4]

decrease in the order $Cl^- > Br^-$ and $Na^+ > K^+ > Li^+$, whereas addition of NaSCN and urea result in an increase in CMT and CP in the order NaSCN > urea. NaI appeared to be an intermediate case as it decreases the CMT but increases the CP. The effects of the salts on the solution behaviour of EPE copolymers were correlated with changes in the ion radius and the heat of solvation of the salts. The salts affect both CMT and CP to the same extent, from which it was deduced that salts affect micellization and phase separation by the same mechanism. The effect of urea on the micellization properties of EPE copolymers has been examined using the dye solubilisation method and surface tension[5]. Urea increases both the CMT and the CP and its effect diminishes as the copolymer concentration increases. The effects of urea on the properties of aqueous surfactant solutions have similarly been attributed to either an "indirect" mechanism, according to which urea acts as a "structure-breaker" and facilitates the hydration of nonpolar solutes[6,7], or a direct" mechanism, whereby urea has almost no effect on the water structure but replaces some of water molecules in the hydration shell of the solute[5].

Pandya *et al.*[8] have studied the effect of SDS on the clouding behaviour of Pluronic L64 in aqueous solution. A drastic increase in the CP was observed in the presence of SDS at concentrations much lower than its CMC. The CP increase has been attributed to the introduction of electrostatic repulsion when SDS molecules are incorporated into Pluronic micelles and the interaction between Pluronic L64 and SDS has been attributed to the formation of a complex. The clouding behaviour of mixtures containing Pluronic L64 + SDS in the presence of various potassium salts was also investigated by Pandya *et al.*. A pronounced effect of salts on the CP of L64:SDS solutions occurs even at very low salt concentrations. The CP of the L64:SDS solutions decreased on addition of salts to a value close to the CP of L64 in water. It was argued that the CP of Pluronic L64 in the presence of SDS had indeed acquired an electrostatic character, which could be effectively neutralised with addition of small amounts of salts.

The effect of conventional surfactants on the properties of EPE copolymer solutions has been little studied. Unlike electrolytes, conventional surfactants are believed to modify the solution properties of EPE copolymers by interacting with the copolymer molecules themselves. Almgren *et al.*[9] studied the aggregation behaviour of Pluronic surfactants,

Pluronic L64 and Pluronic F68 in the presence of SDS using NMR chemical shift and fluorescence quenching. They observed that while neither Pluronic grade forms micelles at 20°C, cooperative aggregation was detected when the Pluronic was mixed with SDS at a concentration as low as 1mM. The first micelles formed in these solutions are rather small and the ratio EPE:SDS in the micelle is one EPE molecule to 3 SDS molecules. As further surfactant is added the micelles remain at approximately this composition until all the copolymer molecules have been micellized. They then grow slowly to the size of normal SDS micelles, containing, on average, one EPE molecule per micelle. In systems where micelles of EPE are initially present, the addition of SDS leads to a rapid decrease in size of the micelles. The influence of surfactants on the aggregation behaviour of Pluronic has also been investigated by Hecht[10] using differential scanning calorimetry (DSC) measurements. Hecht observed that SDS, and dodecyltrimethylammonium bromide (DTAB), interact strongly with Pluronic surfactants, suppressing their micellization. SDS was found to bind to Pluronic F127 molecules and saturation is achieved at concentrations below the CMC of pure SDS. At saturation, the complex F127:SDS consists of six SDS molecules bound to one Pluronic F127 molecule. DTAB appears to interact with Pluronic F127 similarly, but saturation was only achieved at a concentration equivalent to the CMC for DTAB. In the case of DTAB, it was inferred that 17 molecules are bound to each Pluronic F127 molecule. It has been argued by both Hecht[11] and Kositza[12] that SDS would prefer binding to the PPO group, which would increase the hydrophilicity of the Pluronic and hence reduce one of the main driving forces for micellization of the copolymer. The structure of the proposed SDS:EPE copolymer complex is depicted in Figure 1. The argument for suppression of micellization was proposed to explain the disappearance of the DSC peak on addition of SDS to the solution of EPE copolymer. The proposed mechanism, however, does not agree with the SDS-induced micellization indicated by a shift of the endothermic peaks of the mixed SDS-EPE systems toward lower temperature observed in DSC thermograms presented by both Hecht[11] and Kositza[12]. The interaction between Pluronic F127 and a zwitterionic surfactant was also investigated[11]. Dimethyltetradecanamine oxide, C_{14}DMAO, was also found to suppress EPE micellization, but only at a surfactant concentration far above the CMC for C_{14}DMAO. It was therefore believed that, in this case, individual copolymer binds to the surface of the surfactant micelles.

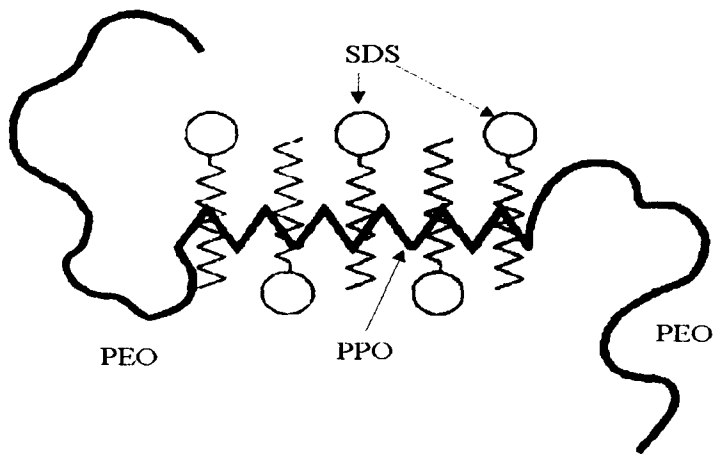


Figure 1. SDS/EPE copolymer complex structure

In this and the following chapters we discuss the solution properties of EPE copolymers mixed with various surfactants. The micellization and monolayer formation in binary mixtures of EPE copolymers and conventional surfactants was examined using existing models of surfactant mixing. Before proceeding to the experimental data, some of these models of surfactant mixing are outlined below.

2 Surfactant Mixtures

Individual surfactants vary in their ability to form aggregated structures such as micelles and monolayers. In solutions containing mixtures of surfactants, the tendency to form aggregated structures can be substantially altered from solutions containing only one of the pure surfactants. The distribution of a single surfactant in aqueous solution between the monomeric state, micelles and monolayers at the air-liquid interface depends only on the solution conditions and the concentration of the surfactant. However for a mixture of two different surfactants in aqueous solutions, the distribution of the two species between these various states depends not only on the overall solution composition and concentration, but also on the nature of the two surfactants. First, if the two surfactants have quite different free energies of micellization, then the mixed micelles would have a composition biased towards the component with the lower free energy of micellization i.e. the surfactant with the lower CMC value. The monomer concentrations would correspondingly be biased towards the component with the higher free energy of micellization. As the overall concentration is increased, the percentage of the total

surfactant present in the micellar form must also increase, and in the high concentration limit, the micelle composition must therefore tend toward the bulk composition. Since either the monomer or the micelle composition may be crucial to the behaviour of the system, the ability to predict the relative distribution of the surfactant components between monomer and micelle, given the overall solution composition, is very important.

Except for some anionic/cationic surfactant mixtures where ion pairs may be formed, the concentration of the surfactant components as monomeric species in a typical surfactant solution is so dilute that no significant interactions between surfactant monomers occur. The monomer-micelle equilibrium is therefore dictated by the tendency of the surfactant components to form micelles and the interaction between surfactants in the micelle. Prediction of monomer-micelle equilibrium reduces to modelling the thermodynamics of mixed micelle formation.

In ideal mixing the total monomer concentration of a binary mixture of two similarly structured surfactants of like charges lies between the CMCs of the individual surfactants for total surfactant concentrations at or above the CMC of the mixture. Similarly structured surfactants mix ideally because the environments for the hydrophobic and the hydrophilic groups in the mixed micelle are similar to those in the pure component micelle. For such a binary system, the mixed micelle formation can be modelled by assuming that the thermodynamics of mixing obeys the ideal solution model. Systems that exhibit ideal mixing include mixtures of n-octyl and n-decyl suphoxides[13] and mixtures of polyoxyethylene nonionic surfactants with different alkyl chain lengths or polyoxyethylene head groups, where the difference in the degree of polymerisation is not too great[14]. If, however, there are significant differences in structure between the two surfactants, the environment which each surfactant experiences within a mixed micelle will differ from that which it would experience within the single component micelle. This leads to deviations from ideal mixing and the distribution of the components between the monomeric and micellar forms is then not just a function of the free energies of micellization in the single component systems, but is influenced by the interaction between the two surfactants.

When a nonionic surfactant is inserted into a micelle composed of ionic surfactant, the nonionic hydrophilic group separates the charged ionic hydrophilic groups from each other, reducing the electrical repulsion in the Stern layer of the micelle. It therefore requires less work to insert an ionic surfactant molecule into this mixed micelle than into a pure ionic micelle due to the reduced electrical repulsion. This charge screen effect facilitates mixed micelle formation. The mixed CMC would therefore be lower than the value predicted by ideal solution theory and the system is said to exhibit a negative deviation from ideality.

In addition to electrostatic forces, another contribution to nonideality is due to the formation of oxonium salts in the hydrophilic group of the nonionic polyethoxylated surfactant. These result from the association of cations from solution with the negatively polarised ether oxygen atoms on the nonionic surfactant headgroup[15]. The resulting net positive charge of the nonionic surfactant can also contribute to the stabilization of the anionic/nonionic mixed micelles. This is likely to be the explanation for the greater deviation observed in anionic/nonionic systems compared with cationic/nonionic systems. For systems in which stabilization of the mixed micelle is very strong, the mixed CMC may even be lower than the CMCs of each of the surfactants. This has been observed in dodecyl betaine/SDS mixed systems[16]. The anionic/cationic systems exhibit the ultimate in electrostatically induced nonideality, with the oppositely charged surfactants combining to form extremely stable micelles. The deviation from ideality for binary pairs of surfactants increases in the order cationic/nonionic < anionic/nonionic < anionic/cationic.

A positive deviation from ideality is also possible and it is normally the result of physical constraints such as immiscibility of the surfactant hydrophobic groups in the micellar core, or steric effects that restrict mixing on the basis of molecular geometries of the surfactants. Binary mixtures of a hydrocarbon based surfactant and fluorocarbon based surfactant are frequently found to have higher mixed CMCs than would be expected from ideal solution theory and are said to exhibit positive deviations from ideality. The cause of this deviation is the dissimilar nature of the fluorocarbon and hydrocarbon chains, which results in the formation of the mixed micelle being disfavoured[17].

The adsorption of mixed surfactants at the air-solution interface follows a pattern similar to that of mixed micelle formation. The mixed monolayer is structured so that the surfactant hydrophilic groups adjacent to each other are oriented toward the aqueous phase while the hydrophobic groups are removed from the aqueous environment and in contact with other hydrophobic groups. Since the forces that drive micellization are of same nature as those that lead to monolayer formation, the thermodynamics and interactions between surfactant molecules are expected to be similar in both aggregation processes.

3 The Modelling of Surfactant Mixing

There has been a great deal of interest in the development of models to predict and explain mixing in surfactant systems. Early work was generally concentrated on the development of models to describe ideal mixing between surfactants, based on the thermodynamics of ideal mixing in liquids[18,19] and these have been found to be successful in predicting CMCs and monomer and micelle compositions for many ideally behaving systems. The problem of accounting for nonideal mixing has been challenging. The approach, which is most commonly used to describe and predict mixing in non-ideal systems, is that developed by Rubingh[20] from the model of ideal mixing developed by Clint[18]. In this approach Rubingh was able to account for the non-ideality of the mixing process by incorporating the Regular Solution Approximation into Clint's expressions, thus allowing there to be a non-zero enthalpy of mixing. For this reason, Rubingh's approach is generally known as the Regular Solution Model. For mixed surfactant systems, the two characteristic phenomena, mixed monolayer formation at interface and mixed micelle in solution, are often treated separately as is done below.

4 Mixed Surfactant Micelles

Models for treating mixed micellization differ in how the micellar aggregate is modelled, for example, whether counterions are taken into account, and in the way nonideality is treated. These thermodynamic models are useful for characterising some aspects of micellization but have some drawbacks. In particular they do not describe satisfactorily

the counterion binding of micelles containing ionic surfactants. Micellar aggregation of ionic surfactants is opposed by head group electrostatic repulsion, which is balanced to some extent by adsorption of counterions at the micelle surface[21-25]. Other authors[26] describe the counterion binding in terms of a continuous radial distribution function corresponding to a high counterion concentration close to the micelle and continuously decaying with increasing distance from the micelle, as predicted from Poisson-Boltzmann equation. The distinction between bound and free counterions is therefore somewhat vague, yet the stability of ionic micelles is heavily dependent on this counterion binding. The need to include the effects of counterion binding into mixed micellization when ionic surfactants are involved is important.

4.1 Pseudophase Separation Approach

The phase separation model assumes that the mixed micelles or other aggregates can be treated as a separate phase. It is clear that micelles do not constitute a thermodynamic phase, but they do mimic phase-like behaviour in the sense that they can act as both a source and a sink for surfactant species in solution. The micelles are considered to be so dilute that the interaction between them can be neglected, so the solution is treated as ideal. The drawback of the phase separation model is that micelle size becomes irrelevant. In the Pseudophase Separation Model, the effect of counterion binding can be incorporated as a form of a Charged Pseudophase Separation Model to improve the agreement between theory and experiment if the micelles contain ionic surfactants[27].

The Pseudophase Separation Approach treats mixed micellization by considering the chemical potentials of the individual surfactant components. At equilibrium the chemical potential of a particular species is the same everywhere in the system. This provides a useful link between surfactant monomers in solution and those in mixed micelles.

The chemical potential of monomeric component in the mixed micelle solution can be written as

$$\mu_i = \mu_i^0 + RT \ln C_i^M \qquad (7.1)$$

where $\mu^0{}_i$ is the standard chemical potential C_i^M and is the monomer concentration of the *ith* species, where the activity coefficient of the free monomer is assumed to be unity. In the pure *ith* component micelles, the chemical potential of *i* is given by

$$\mu_i^{Mo} = \mu_i^0 + RT \ln CMC_i \tag{7.2}$$

which depends on the CMC of the *ith* surfactant, CMC_i. In mixed micelles the chemical potential of the *ith* component can be expressed as

$$\mu_i^M = \mu_i^{Mo} + RT \ln f_i x_i \tag{7.3}$$

where the mixing behaviour is taken into account by a term containing the activity coefficient, f_i, and the mole fraction, x_i, of the component in the micelles. At equilibrium since $\mu_i = \mu_i^M$, Equations 7.1 and 7.3 can be combined to give the general result

$$C_i^M = x_i f_i CMC_i \tag{7.4}$$

At the concentration of the mixed micelle formation, CMC_{mix}, the monomer concentration of *ith* component is given by

$$C_i^M = y_i CMC_{mix} \tag{7.5}$$

Combining Equations 7.4 and 7.5

$$y_i CMC_{mix} = x_i f_i CMC_i \tag{7.6}$$

With the constraint:

$$\sum_{i=1}^{n} x_i = 1 \tag{7.7}$$

Equation 7.6 can be expressed in the generalized relationship

$$\frac{1}{CMC_{mix}} = \sum_{i=1}^{n} \frac{y_i}{f_i CMC_i} \tag{7.8}$$

This expression was derived by Clint[18]. It gives the mixed CMC in terms of the surfactant mole fractions of each component, the CMCs of the pure components, and activity coefficients in the mixed micelle.

Consideration of mass balance allows the mole fraction of the *ith* component in the micelles to be expressed as

$$x_i = \frac{y_i C - C_i^M}{C - \sum_{i=1}^{n} C_i^M} \tag{7.9}$$

where C is the total concentration of the *ith* component. If Equation 7.4 is used to substitute for C_i^M in the numerator, followed by rearrangement and the use of Equation 7.7, the generalized expression

$$\sum_{i=1}^{n} \frac{y_i C}{C + f_i CMC_i - M} = 1 \tag{7.10}$$

where M is the sum of the monomer concentrations

$$M = \sum_{i=1}^{n} C_i^M \tag{7.11}$$

Solving Equation 7.10 for the total concentration is straightforward once the activity coefficients have been calculated, and the following expressions, obtained from Equation 7.4 and 7.9, can be used to obtain individual monomer concentrations and mole fraction in the micelle respectively.

$$C_i^M = \frac{y_i f_i CMC_i C}{C + f_i CMC_i - M} \tag{7.12}$$

$$x_i = \frac{y_i C}{C + f_i CMC_i - M} \tag{7.13}$$

4.1.1 Ideal Mixing

In the case of ideal systems, the activity coefficients, f_i, are unity and the calculation of the mixed CMC according to Equation 7.8 therefore reduces to

$$\frac{1}{CMC_{mix}} = \sum_{i=1}^{n} \frac{y_i}{CMC_i} \tag{7.14}$$

4.1.2 Nonideal Mixing

From the thermodynamic point of view, nonideality in mixtures is best described using activity coefficients. By definition, such activity coefficients are equal to one for ideal mixtures or for pure components.

A generalized form for the activity coefficients in the micellar pseudophase for binary systems can be developed by considering the thermodynamics of mixing. As for liquids, the excess free energy of mixing, G^E, can be expressed

$$G^E = RT(x_1 \ln f_1 + (1 - x_1) \ln f_2) \tag{7.15}$$

If the partial derivative of Equation 7.14 is taken with respect to x_1, and some terms are eliminated with the Gibbs-Duhem relation, we obtain

$$\left[\frac{\partial G^E}{\partial x_1}\right]_{T,P} = RT(\ln f_1 - \ln f_2) \tag{7.16}$$

Combination and rearrangement of these expressions provides the binary activity coefficients as a function of the excess free energy of mixing.

$$\ln f_1 = \frac{1}{RT}\left[G^E + (1 - x_1)\frac{\partial G^E}{\partial x^1} \right] \tag{7.17}$$

The excess free energy of mixing itself is defined in terms of an excess heat (or enthalpy) of mixing H^E, and an excess entropy of mixing, S^E.

$$G^E = H^E - TS^E \tag{7.18}$$

The Regular Solution Approximation is introduced by assuming that the excess entropy of mixing, S^E, is zero. This allows the substitution of H^E in place of G^E. For binary systems this excess heat of mixing can be represented by

$$H^E = \beta^M x_1(1 - x_1)RT \tag{7.19}$$

where β^M is a dimensionless parameter. $RT\beta^M$ represents the net difference in the interaction energy between the mixed and unmixed systems. The form of expression 7.19 corresponds to the leading term in a lattice model description of liquid mixtures[28] and would predict heats of mixing symetric with respect to composition. Since H^E should be constant, the parameter will be temperature dependent. Substitution of the functional form of Equation 7.18 for G^E into the general expression for the activity coefficients directly leads to the activity coefficients of binary mixtures

$$f_1 = \exp \beta^M (1 - x_1)^2 \tag{7.20}$$

Equation 7.20 suggests a symmetrical relation between the activity coefficient and the surfactant composition of the aggregate.

The interaction parameter can alternatively be expressed in terms of the molecular interactions in the mixed micelles:

$$\beta^M = \frac{N_A z / 2(w_{11} + w_{22} - 2w_{12})}{RT} \tag{7.21}$$

where w_{11} and w_{22} are energies of interaction between the same kind of surfactant molecules in the pure micelles; w_{12} in the interaction energy between different kinds of molecules in the mixed micelles; z is the coordination number, and N_A is Avogadro number. If the value of β^M is obtained from experiment, one can discuss the mixed micellization in terms of molecular interactions. In the Regular Solution Approximation where the excess entropy of mixing is defined to be zero, the parameter β^M can be formally be interpreted as a parameter representing an excess heat of mixing. However, calorimetric measurements of excess heats of micellar mixing often show poor agreement with β^M values determined independently from CMC measurements, indicating that the assumptions of the Regular Solution Approximation do not hold for many binary surfactant mixtures[29,30]. This situation has led to the suggestion that the parameter β^M be interpreted more generally as a parameter for the excess free energy of mixing which only meets the formal criteria of the Regular Solution Approximation when the excess entropy of mixing is zero[30].

In order to solve for the activity coefficients in binary mixed micellar systems using the above form of the Regular Solution Approximation, the micellar mole fractions must first be determined. Equations 7.4 and 7.5 give

$$f_1 = \frac{y_1 CMC_{mix}}{x_1 CMC_1} \tag{7.22}$$

which, combined with Equation 7.20, gives

$$\frac{x_1^{\,2} \ln(y_1 CMC_{mix} / xCMC_1)}{(1-x_1)^2 \ln[(1-y_1)CMC_{mix} / (1-x_1)CMC_2]} = 1 \tag{7.23}$$

which can be solved iteratively for x_1. β^M can then be directly determined from

$$\beta^M = \frac{\ln(y_1 CMC_{mix} / x_1 CMC_1)}{(1-x_1)^2} \qquad (7.24)$$

Rubingh[20] has applied the Regular Solution Approximation to systems of nonideal binary mixed micelles containing ionic surfactants, and it has now been demonstrated that a number of experimental data of CMC versus monomer composition are well represented by using a single adjustable parameter β^M.

The Regular Solution treatment is useful because of its simplicity and relatively easy application to a range of phenomena. Scamehorn[30] has argued that the Regular Solution treatment is not thermodynamically valid in describing nonideal mixed micelles, but can be viewed as a useful empirical model. His arguments are

(A) The heat of mixing in micelles obtained from fitting the Regular Solution Theory to CMC data has been shown to differ substantially from that measured using calorimetry[31,32].

(B) The value of the interaction parameter β should be independent of temperature and micellar composition for the Regular Solution Theory to apply. However, β^M has been found to be substantially dependent on temperature[33] and slightly on composition[34].

(C) The excess free energy of mixing for mixed micellization can be very unsymmetrical with respect to composition, in contrast to the symmetry predicted by the Regular Solution Theory[15].

(D) If the Regular Solution Theory is applied to ionic/nonionic mixed micelles, the effective degree of counterion binding must be proportional to the mole fraction of ionic surfactant in the micelle[35], but this contrary to experimental observations[21,36,37].

5 Mixed Surfactant Monolayer Models

The adsorption of mixed surfactants at the air-liquid interface (monolayer formation) is mechanistically similar to mixed micelle formation. The mixed monolayer is oriented so that the surfactant hydrophilic groups are adjacent to each other. The hydrophobic groups

are removed from the aqueous environment and are in contact with other hydrophobic groups or air. Therefore, the forces tending to cause monolayers to form are similar to those causing micelles to form and the thermodynamics and interactions between surfactants should be similar in the two aggregation processes. The adsorption of surfactants from solution to interfaces leads to most of the practical benefits derived from mixed surfactant systems. Among the major effects observed are interfacial tension lowering and changes in the wettability of surfaces as reflected in contact angle changes. The adsorption behaviour of mixtures of soluble surfactants at interfaces and their consequent effect on interfacial properties varies significantly over a wide range of concentrations. At surfactant concentrations far below the mixed CMC, the interface is only sparsely covered by surfactant molecules and a significant amount of water remains at the interface. The adsorption density at the air-liquid interface is then so low that individual adsorbed surfactants do not interact significantly. As the concentration increases, the surface tension decreases substantially and a saturated interfacial monolayer of adsorbed mixed surfactant molecules forms. Here, the average area per molecule at the interface becomes constant and the Gibbs equation can be used to determine the molar area from the slope of surface tension versus the logarithm of surfactant concentration. With further increases in the total surfactant concentration the surface tension reaches an approximately constant value when the CMC is reached.

Below the CMC, the surfactant mixing in a monolayer composed of similarly structured surfactants approximately obeys the ideal solution theory. This means that the total surfactant concentration required to attain a specified surface tension for a mixture is intermediate between those concentrations for the pure surfactants involved. For mixtures of ionic/nonionic or cationic/anionic surfactants, below the CMC, the surfactant mixing in the monolayer generally exhibits a negative deviation from ideality, i.e., the concentration required to attain a specified surface tension is less than that predicted from ideal solution theory. Since the mechanisms leading to the nonideality of the mixed micelles are qualitatively similar for the mixed monolayer, the extent of deviation from ideality is therefore expected to be similar for the two situations[38].

As the chemical potential of surfactant molecules in the bulk solution effectively controls adsorption, a mixed surfactant model for interfaces can be viewed as a natural extension of solution models for mixed surfactant systems. At or above concentrations where the Gibbs equation holds, a surface pseudophase consisting of a saturated monolayer of adsorbed surfactant aggregate can be defined. This provides the basis for developing a generalised mixed surfactant model for interfaces.

5.1 Pseudophase Separation Approach – Regular Solution Approximation

The mixing in these monolayers has been modelled using ideal solution theory[38,39] or Regular Solution Theory. The resulting equations are similar to those already presented for mixed micelle formation.

Ingram[40] was the first to consider treating nonideal surfactant mixtures adsorbed at the interfaces using a Regular Solution Approximation similar to that used for mixed micellization for nonideality. This approach employed submicellar surface tension functions and the nonideal mixed micelle model of Rubingh[20], and utilised a nonideal surface interaction parameter.

To calculate the activity coefficients in the mixed monolayer the following expression is applied, which is the equivalent to Equation 7.20

$$f_1 = \exp \beta^s (1 - x_1)^2 \tag{7.25}$$

where β^s and x_1 are, respectively, the interaction parameter and the mole fraction of surfactant 1 in the mixed monolayer at interface. Equations corresponding to Equations 7.23 and 7.24 are

$$\frac{x_1^{\,2} \ln(y_1 C_{12} / x C_1^{\,0})}{(1 - x_1)^2 \ln[(1 - y_1) C_{12} / (1 - x_1) C_2^{\,0}]} = 1 \tag{7.26}$$

$$\beta^s = \frac{\ln(y_1 C_{12} / x_1 C_1^{\,0})}{(1 - x_1)^2} \tag{7.27}$$

where C_1^0, C_2^0, and C_{12} are the bulk phase molar concentrations of pure surfactants 1 and 2, and their mixture, respectively, required to produce the surface tension value; y_1 is the mole fraction of surfactant 1 in the mixed surfactant in the bulk solution.
The surface tension-total surfactant concentration curves for the two pure surfactants and their mixture at a fixed value y_1, the mole fraction of surfactant 1 in the total surfactant in the solution, are used to determine the molar concentrations, C_1, C_1^0, C_2, and C_2^0, required to attain same surface tension value. Substitution of these values into Equation 7.26 permits it to be solved iteratively for x_1. Equation 7.27 then gives the value of β^s from the determined x_1 and y_1 and the observed values of C_{12}, C_1^0.

An alternative approach which explicitly incorporates the force field term and extends the approach used for mixed micelles models to a range of surface pressure has been developed by Holland[41,42]. Here, nonideal mixing is treated by using a form of the regular solution approximation with a surface interaction parameter, β^s. As in the case for mixed micelles this is designed to be suitable for extension to multicomponent mixtures. Also, the derivation of this approach leads directly to the possibility of considering the effects of changes in the molar area of surfactants at the interface on mixing.

5.2 Changes in Molar Areas on Mixing

It is well known that the interfacial areas per surfactant molecules often change in going from pure to mixed systems. This is especially pronounced in the case of anionic-cationic surfactant mixtures. The importance of considering such changes in modelling mixed surfactant systems has been increasingly recognised[41-45]. For example, the Gibbs-Duhem relation can be used to demonstrate the importance of taking changes in the areas per molecule on mixing into account if thermodynamic consistency is to be maintained[43].

The model used in this thesis was developed by Holland[41,42] and his approach is based on the equilibrium chemical potentials of the surfactant species in the adsorbed mixed monolayers. The approach only considers the region where the adsorbed monolayer is saturated with surfactant and where no "bulk-like" water is present at the interface. Under these conditions the sum of the surface mole fractions of surfactant is assumed to equal

unity. While the residual solvent at the interface can clearly affect the surface free energy, it is considered that these effects are accounted for in the standard chemical potentials at the surface and in the non-ideal net interaction in the mixed pseudophase.

The chemical potential of free monomeric surfactant component *i* in solution is given by

$$\mu_i = \mu_i^o + RT \ln C_i^m \tag{7.28}$$

where μ_i^o is the standard chemical potential and C_i^m the monomer concentration of the *ith* species. For pure micelles of the *ith* component, a similar expression results

$$\mu_i^{Mo} = \mu_i^o + RT \ln CMC_i \tag{7.29}$$

which depends on the CMC of the pure surfactant, CMC_i. The chemical potential of the *ith* surfactant in the adsorbed monolayer of pure surfactant can be expressed as

$$\mu_i^s = \mu_i^{os} + \pi_i \omega_i \tag{7.30}$$

where μ_i^{os} is a standard chemical potential at the surface and $\pi_i \omega_i$ a force field term. Conveniently, both the surface pressure and the molar area can be obtained experimentally from interfacial tension measurements. Here, π_i is given by

$$\pi_i = \gamma_{H_2O} - \gamma_i \tag{7.31}$$

and the molar area, ω_i, by

$$\omega_i = -RT \frac{d \ln C_i^m}{d\gamma_i} \tag{7.32}$$

Above the critical micelle concentration (CMC_i) in a pure surfactant solution the chemical potential of the monomer is given by

$$\mu_i = \mu_i^o + RT \ln CMC_i \tag{7.33}$$

and that of surfactant species in the adsorbed pure monolayer by

$$\mu_i^s = \mu_i^{os} + \pi_i^{\max} \omega_i \tag{7.34}$$

where $\pi_i^{\max}$ is the limiting value of the surface pressure above the CMC.

At equilibrium the chemical potential of the monomeric species is equal to that in the mixed monolayer, i.e. $\mu_i = \mu_i^s$, and Equations 7.33 and 7.34 can be combined to yield the expression

$$\frac{\mu_i^{0s} - \mu_i^0}{RT} + \frac{\pi_i^{\max} \omega_i}{RT} = \ln CMC_i \tag{7.35}$$

where the term with the standard state chemical potentials is in the form of a bulk surface distribution coefficient.

In a mixed micellar system, the chemical potential can be expressed by

$$\mu_i = \mu_i^o + RT \ln f_i x_i \tag{7.36}$$

where f_i is an activity coefficient and x_i the mole fraction of the *ith* component in the micelle . Combining this expression with Equations 7.28 and 7.29 yields the monomer concentration as given in the nonideal mixed micelle model.

$$C_i^m = x_i f_i CMC_i \tag{7.37}$$

At the interface in the mixed system the chemical potential of *ith* component becomes

$$\mu_i^s = \mu_i^{os} + RT \ln f_i^s x_i^s + \pi_i^{max} \omega_i \qquad (7.38)$$

where π is the total surface pressure and ω_i' its area per mole after mixing. Nonideality in the pseudophase at the interface is accounted by the term containing an activity coefficient (f_i^s) and the mole fraction (x_i^s). As in the case of mixed micelles, the binary activity coefficients based on the regular solution theory take the form

$$f_i^s = \exp \beta^s (1 - x_i^s)^2 \qquad (7.39)$$

where β^s is a dimensionless interaction parameter analogous to that used for treating nonideal mixing in micelles.

At equilibrium, chemical potentials of the *ith* component are equal and Equations 7.35 and 7.36 can be combined to yield

$$\frac{\mu_i^{os} - \mu_i^{o}}{RT} + \frac{\pi\omega_i'}{RT} = \ln\left[\frac{f_i x_i CMC_i}{f_i^s x_i^s}\right] \qquad (7.40)$$

This expression includes a term with standard state chemical potentials in the form of a bulk-surface distribution coefficient, a force field term, and a ratio of activity coefficients and mole fractions in the micelle and monolayer.

Eliminating the bulk-surface distribution coefficient term between Equations 7.35 and 7.40 allows a generalised nonideal equation to be obtained

$$\pi\omega_i' = RT \ln\left[\frac{f_i x_i}{f_i^s x_i^s}\right] + \pi_i^{max} \omega_i \qquad (7.41)$$

This directly relates properties of the mixed surfactant system to the composition and activity coefficients in the micellar and adsorbed monolayer pseudophases and properties of pure surfactant systems.

For concentrations below the CMC, one can apply the generalised result $C_i^m = f_i x_i CMC_i$ and $C_i^m = y_i C$, which is valid below the CMC, to Equation 7.41 obtaining

$$\pi\omega_i' = RT \ln\left[\frac{y_i C}{f_i^s x_i^s CMC_i}\right] + \pi_i^{max}\omega_i \qquad (7.42)$$

Together, Equations 7.41 and 7.42 allow nonideal mixed monolayers to be treated above and below the mixed CMC by using experimentally measured properties of the pure systems and solving for mole fractions and activity coefficients in the mixed system.

To solve the model at a solution interface, either Equation 7.41 or 7.42 can be applied to each component in the system along with the constraint that mole fractions at the interface sum to unity. This allows either surface interaction parameters to be calculated from experimentally derived values of the surface pressure or given the interaction factors, surface pressures in the mixed system to be calculated.

Rosen *et al.* have recently developed an alternative to their earlier model to account for molar area change at the interface[45,46]. This incorporates a force field term as in the 2-D surface solution approach, and assumes that molar areas after mixing depend on mole fractions in the monolayer and that the ratios of partial molar areas in the mixed and pure system are constant. Their results with this method show good agreement with experimental surface tension results, and significantly improved agreement with surface mole fractions obtained using the Hutchinson method[45]. The surface interaction parameters, β^s, which result when molar areas are taken into account, differ significantly from values in their earlier model.

References

[1] Colins, K.D.; and Washabaugh, M.W. *Q. Rev. Biophy.* 18, 323 (1985)

[2] Kabalnov, A.; Olsson, U.; and Wennertrom, H. *J. Phys. Chem.*, 99, 6220 (1995)

[3] Hall, D.G. *J. Chem. Soc. Faraday Trans. 2*, 70, 1526 (1974)

[4] Alexandridis, P.; and Holzwarth, J.F. *Langmuir*, 13, 6074 (1997)

[5] Alexandridis, P.; Athanassiou, V.; and Hatton, T.A. *Langmuir*, 11, 2442 (1995)

[6] Wetlaufer, D.B.; Malik, S.K.; Stoller, L.; and Coffin, R.L. *J. Am. Chem. Soc.*, 86, 508 (1964)

[7] Frank, H.S.; and Franks, F.J. *J. Chem. Phys.*, 48, 4746 (1968)

[8] Pandya, K.; Lad, K.; and Bahadur, P. J. *Macromol. Sci: Pure Appl. Chem*, 1, 1 (1993)

[9] Almgren, M.; Stam, J.V.; Lindblad, C.; Li, P.; Stilbs, P.; and Bahadur, P. *J. Phys. Chem.*, 95, 5677 (1991)

[10] Hecht, E.; and Hoffmann, H. *Colloids Surfaces A: Physicochem. Eng. Aspects*, 96, 181 (1995)

[11] Hecht, E.; and Hoffmann, H. *Langmuir*, 10, 86 (1994)

[12] Kositza, M. J., Rees, G. D., Holzwarth, A., and Holzwarth, J. F. *Langmuir*, 16, (2000)

[13] Chu, D.Y.; and Thomas, J.K. *J. Am. Chem. Soc.*, 108, 6270 (1986)

[14] Lange, H.; and Beck, K.H. *Kolloid Z. u-Z. Polymere,* 251, 424 (1973)

[15] Nishikido, N. *J. Colloid Interface Sci.* 60, 242 (1977)

[16] Hines, J.D. *D. Phil. Thesis*, University of Oxford (1996)

[17] Smith, I.H.; and Ottewill, R.H. *Surface Active Agents*, Chem. Soc. Ind., London, p.77 (1979)

[18] Clint, J.H. *Chem. Soc. Faraday Trans 1*, 71, 1327 (1975)

[19] Shinoda, K. *Colloidal Surfactants*, Academic Press, New York, (1963)

[20] Rubingh, D.N *Solution Chemistry of Surfactants*, Mittal K.L, Ed., Plenum Press, New York, Vol. 1 (1979)

[21] Rathman, J.F.; and Scameborn, J.F. *J. Phys. Chem.*, 88, 5807 (1984)

[22] Hartland, G.V., Grieser, F.; and White, L.R. *J. Chem. Soc. Faraday I*, 83, 591 (1987)

[23] Israelachvil, J.N., Mitchel, D.J.; and Ninham, B.W. *J. Chem. Soc. Faraday II*, 72, 1525 (1976)

[24] Stigter, D. *J. Colloid Interface Sci.*, 23, 379 (1967); *J. Phys. Chem.*, 68, 3603 (1964); *J. Phys. Chem.*, 79, 1015 (1975)

[25] Beunen, J.A.; and Ruckenstein, E. *J. Colloid interface Sci.*, 96, 469 (1983)

[26] Lindman, B.; and Wennerstrom, H. *Topics Curr. Chem.*, 87, 50 (1980)

[27] Shinoda, K.; and Hutchinson, E. *J. Phys. Chem.*, 66, 577 (1962)

[28] Munster, A. *Statistical Thermodynamics*, Springer-Verlag, 2, 650, Berlin (1974)

[29] Rathman, J. F.; and Scamehorn, J. F. *Langmuir.*, 4, 474, (1988)

[30] Scamehorn, J.F. in *Phenomena in Mixed Surfactant Systems*; ACS Symposium Series 311, 1, American Chemical Society, Washington, DC (1986)

[31] Holland, P.M. in *Structure/Performance Relationship in Surfactants*, ACS Symposium Series 253, 141, American Chemical Society, Washington, DC (1984)

[32] Hey, M.J., MacTaggart, J.W.; and Rochester, C.H. *J. Chem. Soc. Faraday I*, 81, 207 (1985)

[33] Nguyen, C.M.; Scamehorn, J.F.; and Rathman, J. F. *J. Colloid Interface Sci.*, 112, 438 (1986)

[34] Kamrath, F.R.; and Franses, E.I. *Ind. Eng. Chem. Fundam*, 22, 230 (1983)

[35] Hall, D.G.; and Huddleston, R.W. *Colloids Surf.*, 13, 209 (1985)

[36] Abuin, E.B., Lissi, E.A., Nunez, R.; and Olea, A. *Langmuir*, 5, 753, (1989)

[37] Treiner, C.; and Manebach, M.H. *Colloid Polym. Sci.*, 268, 88 (1990)

[38] Zhu, B.Y.; and Rosen, M.J. *J. Colloid Interface Sci.* 99, 435 (1984)

[39] Hua, X.Y.; and Rosen, M.J. *J. Colloid Interface Sci.*, 90, 212 (1982)

[40] Ingram, B.T. *Colloid Polym. Sci.*, 25, 191 (1980)

[41] Holland, P.M. in *Phenomena in Mixed Surfactant Systems*, ACS Symposium Series 311, 102-115, American Chemical Society, Washington, DC (1986)

[42] Holland, P.M., *Colloid Surf.*, 19, 171 (1986)

[43] Holland, P.M.; and Rubingh, D.N. in *Cationic Surfactants: Physical Chemistry*, Surfactant Sciences Series 37, Marcel Dekker, Inc., New York, NY, pp 141-187 (1990)

[44] Aveyard, R., Binks, B.P., Mead, J.; and Clint, J.H. *J. Chem. Soc. Faraday I*, 84, 84 (1988)

[45] Gu, B.; and Rosen, M.J. *J. Colloid Interface Sci.*, 129, 537 (1989)

[46] Rosen, M.J.; and Gu, B. *Colloid Surf.*, 23, 119 (1987)

Chapter 8

Micellization of Binary Mixtures of EPE Copolymers and Surfactants

1 Introduction

A number of studies have been made to investigate the effect of surfactants and other solutes on the aggregation properties of EPE copolymers. Almgren *et al*[1], studying the interaction between SDS and Pluronics L64 and F68, observed that small mixed micelles formed below the nominal CMT of the pure Pluronic surfactants even at SDS concentrations below the CMC. Above the nominal copolymer CMT, larger mixed micelles are formed, but as the concentration of SDS is increased, the micelle size rapidly decreases. At high SDS concentrations, the mixed micelle size corresponds to that of a normal SDS micelle and the EPE copolymer molecules appear to be bound on the micelle surface. The ability of SDS to affect the CMT of Pluronic surfactants and ultimately completely suppress their micellization stems from an interaction between the hydrophobic tail of the SDS and the central PPO block. When the PPO block is effectively saturated with SDS molecules, the driving force for the micellization of the copolymer is suppressed. The micellization suppression mechanism was proposed to explain the disappearance of the calorimetric peak associated with the onset of micellization on addition of SDS[2,3]. However the proposed mechanism does not account for the shift of the endothermic peaks of the mixed SDS-EPE systems towards lower temperature, which is consistently observed in DSC thermograms and, which actually suggests an induced micellization of EPE copolymers in the presence of SDS. More recently Li *et al.*[4,5] have studied the interaction between Pluronic F127 and SDS using electromotive force, isothermal titration calorimetry and light scattering. They have also established that SDS binds to the micelles and monomers of the block copolymer. SDS binds to F127 micelles first forming mixed micelles, which dissociate into smaller mixed aggregates and then to monomeric F127 molecules. They have identified that SDS induces the micellization of F127 at temperatures immediately (1-4°C) below the CMT of pure F127. The precise mechanism by which SDS promotes the formation of F127 micelles was not identified. They argued that because the measurements are close to the

CMT of the pure copolymer, the SDS monomers act as a seed or nucleus for the formation of F127 micelles. Alternatively it could be that SDS monomers may affect the solvent properties of water. When solvent conditions become less favourable for the PPO blocks, the triblock copolymers aggregate to form micelles.

Dodecyltrimethylammonium bromide (DTAB) has also been found to interact strongly with Pluronic F127, suppressing its micellization. DTAB begins to bind to the F127 molecule at a concentration below its CMC, but saturation of the F127 molecule is only achieved above the CMC of DTAB[6]. Li *et al.*[7] using a combination of experiments such TTAB selective electrode (electromotive force), isothermal titration and DSC, have investigated the interaction between tetradecyltrimethylammonium bromide (TTAB) and Pluronic F127. They showed that TTAB binds to both monomeric and micellar F127. TTAB forms a polymer/micellar TTAB complex with monomeric F127. In addition, TTAB binds to F127 micelles leading to the transformation of the aggregated F127 into mixed micelles followed by a breakdown of these aggregates into smaller mixed F127/TTAB aggregates as more TTAB is added. This process continues until all the aggregated F127 is dissociated. They have also shown that TTAB can decrease the CMT of F127. The effect of zwitterionic surfactants was examined by Hecht *et al*[2], who observed that the concentration of dimethyltetradecanamine oxide (C_{14}DMAO) required to suppress the micellization of Pluronic F127 was 10 times higher than that for SDS or CTAB. It was argued that the interaction mechanism for C_{14}DMAO/EPE is different from the other two species and occurs between the micelles of C_{14}DMAO and the block copolymer.

The present chapter describes the study of the micellization behaviour of EPE copolymers in the presence of surfactants of varying ionic character using surface tension measurements. The study focuses on the application of the Pseudophase Separation Model to gain further insight into the interaction and composition of mixed micelles formed when EPE copolymers are combined with conventional surfactants, such as SDS, dodecyltrimethylammonium chloride (DTAC) and tetraethylene glycol monooctyl ether (C_8E_4). For EPE-ionic surfactant mixtures, measurements were also carried out in the

presence of 0.1M aqueous solution of NaCl to investigate the influence of the counterion on the micellization.

The Pseudophase Separation Model has been used with some success to describe the micellar mixing of many binary surfactant systems[8,9]. Since no account is taken of the degree of association of ionic surfactant species in the micelle with their counterions, and hence no inclusion of the effect of the ionic strength upon the micellar activity coefficients, the approach is only strictly applicable to nonionic surfactant mixtures. This limitation, however, has not prevented the apparently successful application of this method to many other systems, including those containing ionic surfactants[10,11]. The degree to which this success implies that electrolyte effects are unimportant in determining the net behaviour of aggregating mixtures is not clear.

2 Experimental Details

2.1 Materials

The EPE copolymer selected to study the interaction with conventional surfactants was EPE 3000-14 whose preparation and purification has been described in Chapter 2. The conventional surfactants used in this study were SDS, dodecyltrimethylammonium chloride (DTAC) and tetraethylene glycol monooctyl ether (C_8E_4) whose purification was also outlined in Chapter 2. The solutions for the surface tension measurements were prepared using ultrapure water as described in Chapter 2.

2.2 Surface tension measurements

Surface tension was measured with a Krüss K10 maximum pull tensiometer by the Du Noüy ring method. Further details of the technique can be found in Chapter 2. Before measurement, care was taken to ensure that all the glassware used was properly clean. All measurements were carried out at 25°C and a Haake water bath connected to the tensiometer was used to control the temperature. The calibration of the instrument and the cleanliness of the ring were checked by measuring the surface tension of UHQ water, which has a value of 72.0mN/m at 25°C. The measurements were repeated until a

consistent reading was attained, i.e. to within 0.1mN/m. The surface tension readings were subsequently corrected using the Harkins and Jordan correction factors (See Appendix 1 of Chapter 2). The surface tension values below the CMC were plotted against the logarithm of the surfactant bulk concentration and fitted to a quadratic equation. The regression coefficients, R^2, were consistently greater than 0.99 for all curves depicted in this chapter. The CMCs of the surfactants were calculated using the point of inflection on the γ-log c curve.

2.3 Determination of the micellar interaction parameter (β^M)

In the Pseudophase Separation Model, the CMC of an ideal binary surfactant mixture is related to the CMCs of the individual components as follows

$$\frac{1}{CMC_{mix}} = \frac{y_1}{CMC_1} + \frac{(1-y_1)}{CMC_2} \tag{8.1}$$

where y_i is the mole fraction of surfactant i in the solution, CMC_{mix} is the mixed CMC of the system, and CMC_i is the CMC of the pure surfactant i. Nonideality is incorporated by modifying the values of the CMCs by activity coefficients, f_i, for the micellar subphase

$$\frac{1}{CMC_{mix}} = \frac{y_1}{f_1 CMC_1} + \frac{(1-y_1)}{f_2 CMC_2} \tag{8.2}$$

In the Regular Solution Approximation, the activity coefficient is evaluated using the first term in a series expansion[12] to yield a single nonideality parameter, β,

$$\ln f_1 = (1-x_1)^2 \beta \quad \text{and} \quad \ln f_2 = x_1^2 \beta \tag{8.3}$$

where x_i is the mole fraction of surfactant i in the mixed micelle. Combining Equations 8.2 and 8.3 gives

$$\frac{1}{CMC_{mix}} = \frac{y_1}{\exp(1-x_1)^2 \beta CMC_1} + \frac{(1-y_1)}{\exp(x_1)^2 \beta CMC_2} \tag{8.4}$$

The numerical value of the interaction parameter, β^M , in the mixed micelle may be found by iterative solution of the following pair of equations

$$\frac{x_1^2 \ln(CMC_{mix} y_1 / CMC_1 x_1)}{(1-x_1)^2 \ln[CMC_{mix}(1-y_1)/CMC_2(1-x_1)]} = 1 \qquad (8.5)$$

$$\beta^M = \frac{\ln(CMC_{mix} y_1 / CMC_1 x_1)}{(1-x_1)^2} \qquad (8.6)$$

The mixed CMC and the mixed micelle composition of a binary mixture can be calculated as a function of the solution composition, knowing the CMCs of the individual components, and the interaction parameter, by solving numerically both Equations 8.5 and 8.6.

3 Results and Discussion

3.1 Micellization in the SDS/EPE 3000-14 system

Figure 1 shows the plot of surface tension against the log of the concentration for pure SDS and EPE 3000-14 together with mixtures at two SDS:EPE 3000-14 molar ratios, 90:10 and 80:20.

Comparison of the surface tension curve of EPE 3000-14 with the curve for SDS shows that there is a striking difference in surface activity. The surface tension of EPE 3000-14 changes less than 10mN/m over the three orders of magnitude of concentration shown in Figure 1, in comparison with about 30mN/m for SDS in less than one order of magnitude of concentration. EPE 3000-14 also has a much lower free energy of micellization, with a CMC at 9.5×10^{-4}M, compared with that of SDS which is 7.9×10^{-3}M.

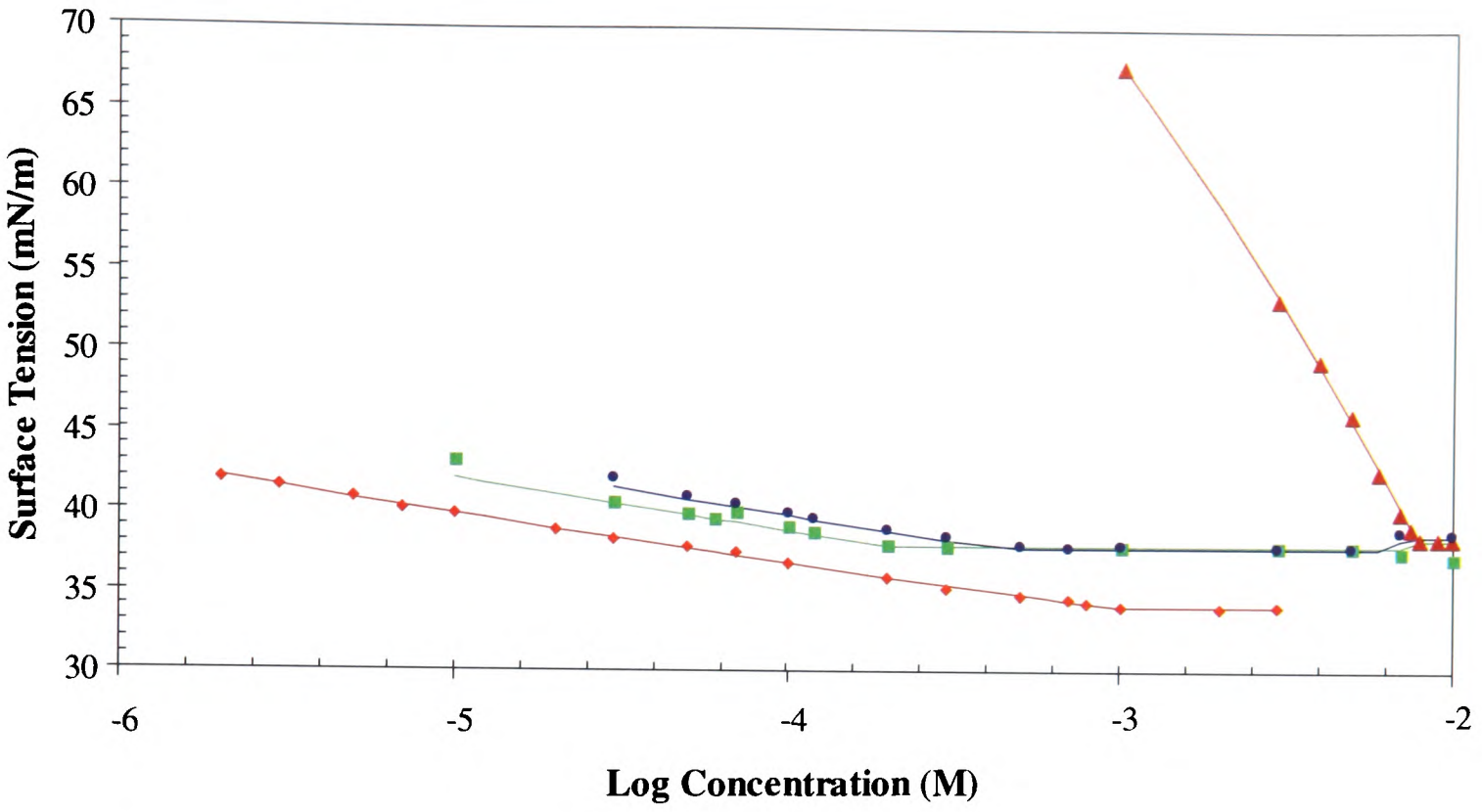


Figure 1. Surface tension against the log of the concentration of SDS, (▲), EPE 3000-14, (♦), and mixtures at y_{SDS}=0.9, (●), and y_{SDS}=0.8, (■) measured at 25°C.

The surface tension curves of both mixtures show some interesting features. The surface activity of the sub-micellar solutions is dominated by EPE 3000-14. The mixed CMC occurs at a surface tension close to that of SDS at the CMC. The CMCs of the mixtures at both SDS:EPE 3000-14 ratios are lower than those of the individual components, indicating a cooperative interaction between the two surfactants. The general interpretation from earlier calorimetric studies suggests that interactions of hydrophobic chain of SDS molecules with the central PPO block of the copolymer lead eventually to a suppression of its micellization due to the electrostatic repulsion[6,13,14]. The surface tension measurements here show that the presence of SDS actually promotes EPE 3000-14 micellization. Thus, the nature of the interaction between EPE copolymers and ionic surfactants is far from understood.

The structures of SDS and EPE copolymers are significantly different and non-ideal mixing of the two species in the mixed micelle would therefore be expected. To interpret the deviation from ideality shown by the mixed CMC, the Regular Solution Approximation was used. The interaction parameter, β^M, was calculated for each mixture by iterative solution of Equations 8.5 and 8.6. Table 1 gives the measured values of the

CMCs for the pure components and the mixtures, the mole fraction of SDS in the mixed micelle, x_{SDS}, and the calculated β^M values.

System	CMC (M)	x_{SDS}	β^M
SDS	7.9×10^{-3}	-	-
EPE 3000-14	9.5×10^{-4}	-	-
80:20 SDS:EPE 3000-14	3.0×10^{-4}	0.47	-9.7
90:10 SDS:EPE 3000-14	5.0×10^{-4}	0.50	-8.8

Table 1. Measured CMCs for SDS, EPE 3000-14 and their mixtures, and calculated mixed micelle composition and interaction parameters.

Using Equations 8.4 and 8.5, the mixed CMC and the micelle composition for SDS/EPE 3000-14 systems were then calculated as a function of the SDS mole fraction in the solution, y_{SDS}. The curves are shown in Figure 2.

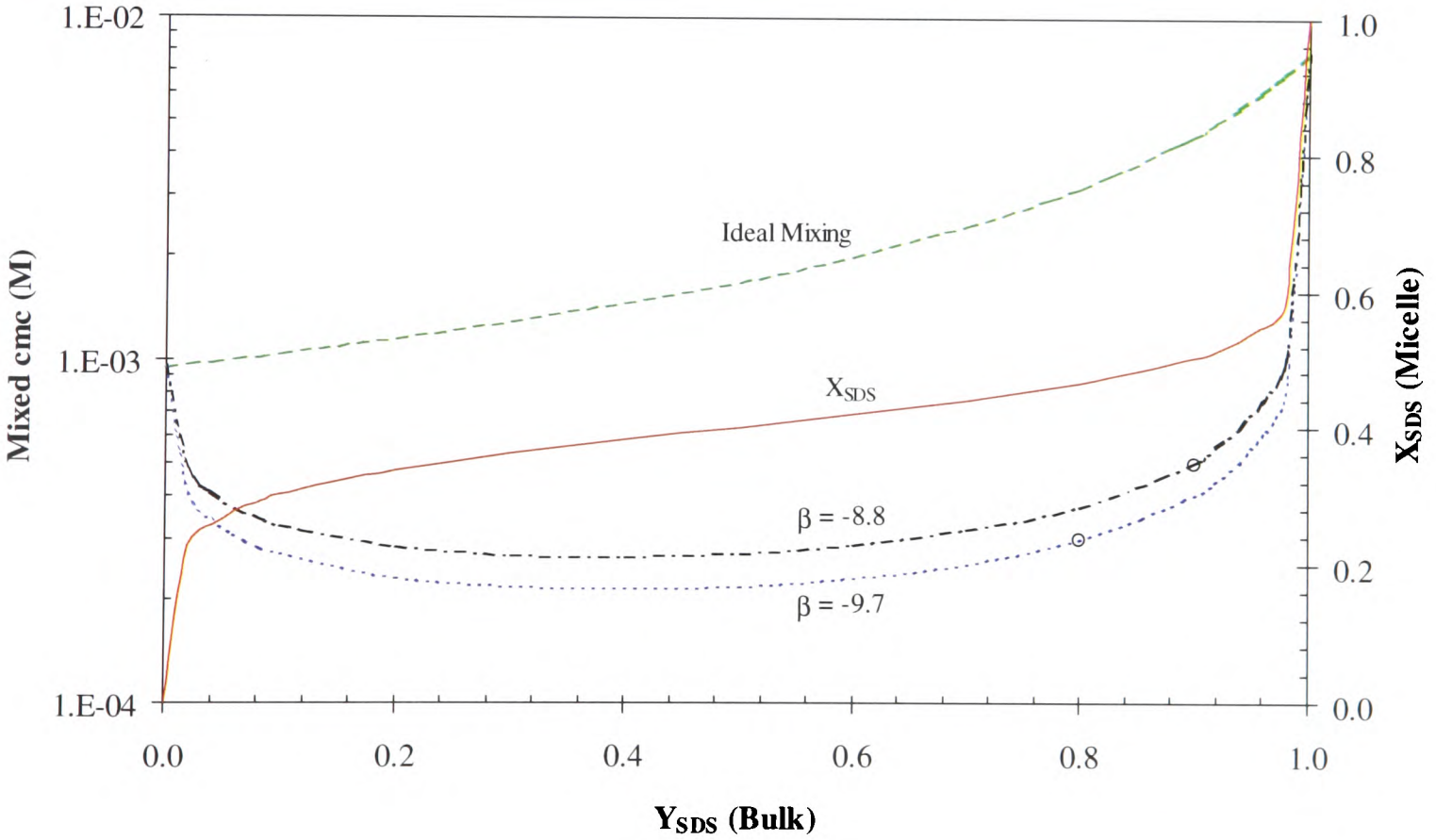


Figure 2. CMC and the micellar composition, x_{SDS}, for mixtures of SDS and EPE 3000-14 over the solution composition range, y_{SDS}, calculated assuming ideal and nonideal mixing. (○) indicates the observed CMC for the two compositions studied.

Where a system is well described by the Pseudophase Separation Model, the value of β^M should be invariant with the bulk composition, so all points should fall on the same line. The interaction parameter varied with the solution composition, for a solution of y_{SDS}=0.8, β^M is -9.7, whereas for y_{SDS}=0.9 it is –8.8. The effect of this variation in the nonideality parameter upon the predictive capability of the model is shown in Figure 2, where the value of the CMC is calculated for all bulk phase compositions. Such a variation in β^M with solution composition has been reported elsewhere. Penfold *et al.*[15] have reported variations in β^M with solution composition for mixtures of SDS:$C_{12}E_6$. The variation has been explained in terms of the increase in non-zero excess entropy of mixing, due to the greater interaction between SDS molecules within the micelles, resulting in greater packing constraints and the possibilities of changes in hydration. Variations of β^M with solution composition and temperature were also reported by Hines *et al.*[16] from the application of the Pseudophase Separation Model to the surface tension data from strongly interacting mixtures of SDS and C_{12}-betaine, and the variations have been attributed to changes in hydration. An important consideration in assessing the variation of interaction parameter with composition, which is relevant to the systems studied here, is the sensitivity of the mixed CMC determination. Small errors in the surface tension values can result in large errors in the interaction parameter and, hence, the composition curves, as discussed elsewhere[17,18]. It can be seen in Figure 2 that at both extreme of y_{SDS} range, small variations in the measured mixed CMC value can produce quite large variations in the interaction parameters.

Despite the shortcomings of the model, the consistently large negative values of the nonideality parameters indicate a strong net attractive interaction between SDS and EPE 3000-14. The interaction is much stronger than that for other SDS/conventional nonionic systems, the interaction parameter for a SDS/$C_{12}E_8$ system being only -4.1[19]. Surprisingly the values for β^M obtained here are of the same order as those for the strongly interacting SDS/zwitterionic systems studied by Hines[20], who obtained a β^M value of –9.1 for a SDS/C_{12}betaine 80:20, and by Tajima[21], who obtained a β^M value of -14.1 for a SDS/C_{12}glycine. In general, the nonideal behaviour of SDS/C_iE_j systems has been attributed to the additional micelle stabilization resulted from the screening of the repulsive interaction between the negatively charged SDS headgroups by the C_iE_j

headgroups[22]. There is also an additional strong electrostatic interaction between SDS and PEO groups. This is attributed to the formation of an oxonium salt, resulting from the association of Na^+ with the negatively polarised oxygen atoms of the nonionic PEO groups. Thus the PEO chains would gain a slightly cationic character and their interaction with an anionic surfactant would be magnified[23,24]. Penfold *et al.*[15] have studied the departure of SDS/$C_{12}E_6$ from ideal mixing using SANS and observed no strong correlation with micelle size or with structure. The overall structure and size of the SDS/$C_{12}E_6$ mixed micelles showed no marked changes with composition or concentration. Although the Regular Solution Model parameterises the experimental measurements well, it is not predictive, and because it does not consider the molecular structures of the surfactants explicitly, it cannot give detailed insight into the mixing properties at a molecular level. Applying the molecular-thermodynamic model, Shiloach and Blankschtein[25] showed that the synergism in the SDS/$C_{12}E_6$ mixed micelle is indeed predominantly electrostatic. The steric contribution to mixed micelle formation in such a system is insignificant. The nonideality of a mixed surfactant system is dictated not only by the interaction forces between surfactant molecules, but also by other structural characteristics, such as differences in the sizes of the surfactant heads or the lengths of the surfactant tails. We believe that the strong attractive interaction between EPE copolymers and SDS stems from a combination of electrostatic forces and structural characteristics, such as molecular size and micellar structure.

The structure of EPE copolymer micelles have been investigated on several occasions[6,26-29]. Recent studies by Goldmints *et al.* and Yang *et al.* have shown that the micelles possess a hydrophobic core consisting mainly of the PO blocks and some water, which is surrounded by the outer shell, the corona, consisting of the hydrated EO blocks. Although Goldmints *et al.* obtained excellent fits to their data, the micelle structure model has a segment and water distribution that is not at all similar to what we have observed at the air/water interface (see Chapter 6). The inconsistency of their model also becomes more evident when one considers the interaction parameters (χ) among the species. The Flory-Huggins interaction parameters between pairs of species in the different equilibrium states, $\chi_{AA'}$, are compiled in Table 2.

Species	$kT\chi_{AA'}$ (kJmol^{-1})				
	PO (nonpolar)	PO (polar)	EO (nonpolar)	EO (polar)	water
PO(nonpolar)	-	1.4[b]	-2.0[c]	3.0[c]	8.5[b]
PO(polar)	1.4[b]	-	0.5[c]	1.8[c]	1.7[b]
EO(nonpolar)	-2.0[c]	0.5[c]	-	1.3[a]	5.6[a]
EO(polar)	3.0[c]	1.8[c]	1.3[a]	-	0.7[a]
Water	8.5[b]	1.7[b]	5.6[a]	0.7[a]	-

Table 2. Flory-Huggins interaction parameters ($\chi_{AA'}$) of the relevant pairs of species in the different equilibrium states. [a] From references 30 and 31. [b] From reference 32. [c] From reference 33.

Polar PO groups are expected to interact equally with water and polar EO groups, but they interact preferably with nonpolar EO groups. In the case of nonpolar PO groups, they are likely to interact more favourably with polar EO groups rather than with water and very attractively with nonpolar EO groups. There it would be reasonable to anticipate some mixing of EO and PO groups, at least in some parts of the micelle, as they do at the air/water interface. One would also expect that there would be some points of similarity between the structure adopted at the air/water interface and that in the micelle. At the air/water interface there is very little contact between PO segments and water whereas there is some mixing of PO and EO segments, especially at the higher surface coverage, which could be considered as being thermodynamically closer to the micelle. We have recently found it possible to reinterpret the SANS data published by Goldmints *et al.* to give an alternative micellar structure more in line with that observed at air/water interface[34]. In this work the micellar structure was described in terms of four layers, similarly to the surface layer. The part that could be regarded as approximately equivalent to the core of the model of Goldmints *et al.* consists of a core of 14Å radius containing 80% by volume PO, 6% EO and 14% water, and a second shell of thickness 14Å containing 51% PO, 5.7% EO and 43.3% water. The two structures are compared in Table 3.

	radius, Å±1	Volume fractions ±0.01			number of units per polymer in micelle		
		ϕ_{PO}	ϕ_{EO}	ϕ_{water}	n_{PO}/N±0.5	n_{EO}/N±0.5	n_{water}/N±0.5
Shell 1	14	0.80	0.06	0.14	4.5	0.5	2.5
Shell 2	28	0.51	0.057	0.43	20.0	3.5	55
Shell 3	40	0.055	0.055	0.89	4.5	7.0	240
Shell 4	66	0.01	0.05	0.94	4.5	35.0	1360
Core[a]	35.4±	0.37	0	0.63	34.0	0	185
Corona[a]	56±	0	0.11	0.89	0	46.0	780

Table 3. Best fit of a four-shell model to small angle scattering data for $E_{23}P_{34}E_{23}$ at 41°C. N is the aggregation number of the micelle and is equal to 21. [a]Model used by Goldmints *et al.*[26]

Despite the difference in the interpretation of the micelle structure, the two models agree that the micellar core contains a significant amount of water. The retention of water molecules inside the micelle core should lead to some degree of PPO chain ordering, which in turn would imply an entropy penalty for micellization. Evidence of PPO chain ordering upon micellization has been found in the study of ^{13}C chemical shifts of methyl carbons in the PPO blocks conducted by Almgren *et al.*[1]. Their results showed a progressive shift upfield in the transition from the large Pluronic L64 micelles to neat polypropylene glycol and to PPO blocks of Pluronic in the monomeric state. The upfield shifts were argued to be the result of a change from a highly extended conformation in the large micelles to a completely coiled conformation in the monomeric state and in the neat polypropylene glycol. The hindrance to micellization resulting from hydration could also explain the results obtained by Wanka *et al.*[35] for the energy increment for the transfer of a PO group from solution to the micelle core. They observed that the transfer energy increment is about 4-5 times lower than that for a CH_2 group, which implies that the hydrophobicity of a PO group is 4-5 times weaker than that of a CH_2 group. The hydration of the copolymer micelle core may indeed be an important contribution to the origin of the large nonideality of SDS/EPE 3000-14 mixtures.

Upon the co-micellization of SDS and EPE 3000-14, SDS molecules are likely to penetrate inside the micelle and to be distributed within Shell 2 and 4, with their headgroups close to the micelle surface and the hydrophobic tails located within the hydrated Shells 2 and 3. This argument is supported by the study of mixed monolayer formation with mixtures of SDS and EPE 3000-14, to be described in Chapter 9, where we find that the SDS molecules are mainly adsorbed into the layers just below the almost pure PPO layer outside the water. Baglioni *et al.*[36] have used electron spin-echo modulation of an x-doxylstearic acid spin probe to investigate the positions of the SDS headgroups relative to the ethylene oxide region of the nonionic surfactant in mixed micelles of SDS/$C_{12}E_6$. They showed that the SDS headgroup is located in the hydrophilic region close to the micelle surface. Therefore we expect that the introduction of the SDS hydrocarbon tails in hydrated shells of the micelle would involve the removal of water retained in the micellar core. In fact, the release of the associated water of hydration from the micelle core could lead to a substantial gain in entropy favouring the mixing of the two surfactants. Micelle dehydration and changes of PPO chain conformation upon mixing with surfactants are evident in the study by Almgren *et al.*[1]. They examined the aggregation behaviour of Pluronic L64 and F68 in the presence of SDS using fluorescence quenching and NMR. They observed that when a micellar solution of Pluronic is mixed with increasing amounts of SDS there is a rapid decrease in micelle size. Similar results were found for micellar solutions of Pluronic F127[2]. The ^{13}C chemical shift for the methyl carbons in the PPO blocks is again shifted upfield in the transition from the large Pluronic L64 micelles to the small mixed ones.

The dehydration of EPE copolymer micelles upon mixed micellization with SDS allows a completely different interpretation of the calorimetric study results carried out by Hecht *et al.*[2,6] and Kositza *et al.*[3]. The thermograms depicted in Figures 3 and 4 show the endothermic peaks related to the micellization of Pluronic surfactants. Addition of SDS progressively reduces the peak size up to a point when it disappears entirely. The effect has been attributed to the binding of SDS to the more hydrophobic PPO block, which increases its hydrophilicity up to a point when it completely suppresses the micellization of copolymer. Similar effects have been observed with other types of surfactants, like DTAB, CTAB and C_{14}DMAO, but to different extents. Endothermicity is known to be

associated with dehydration of the copolymer molecules during micellization[35]. Thus the effect may be related to the formation of increasingly dehydrated SDS/copolymer mixed micelles, as the surfactant concentration is increased.

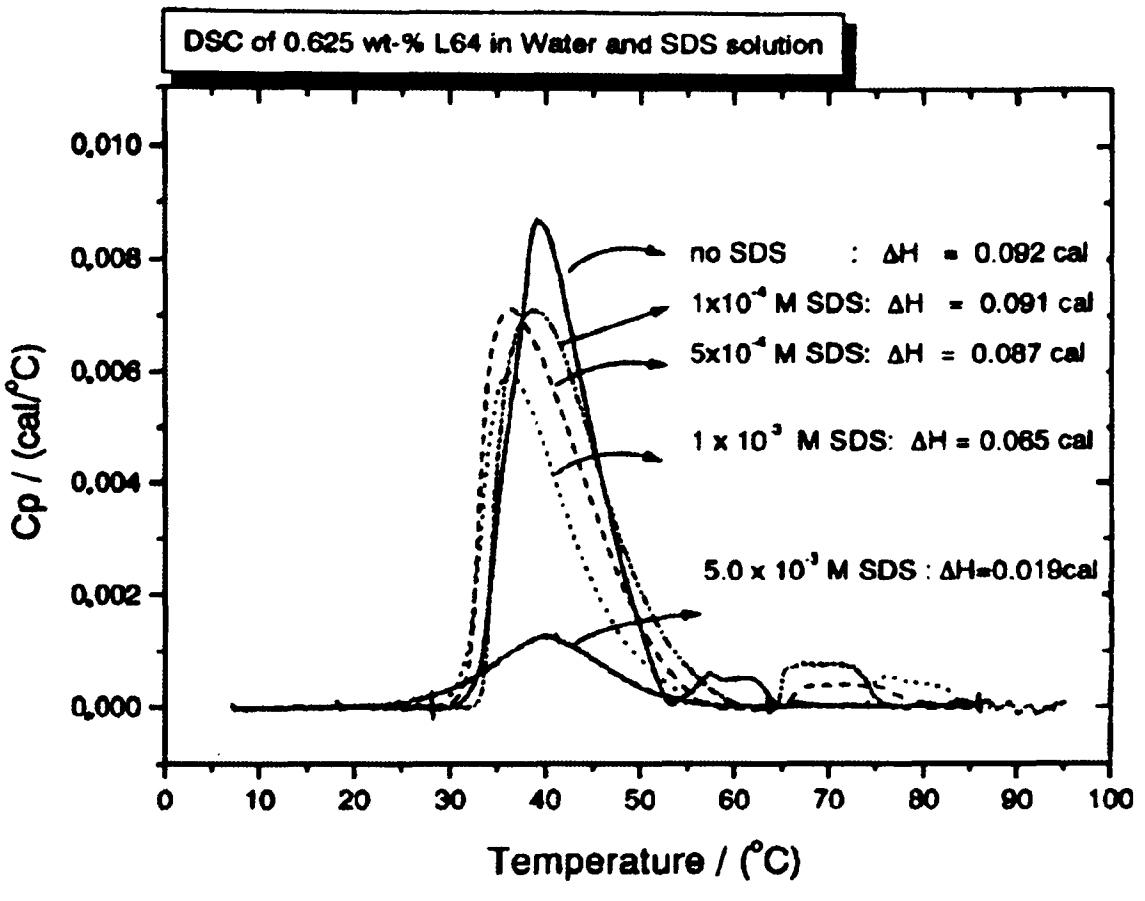


Figure 3. DSC thermograms showing endothermic peaks of Pluronic L64 solutions as function of SDS concentration[3].

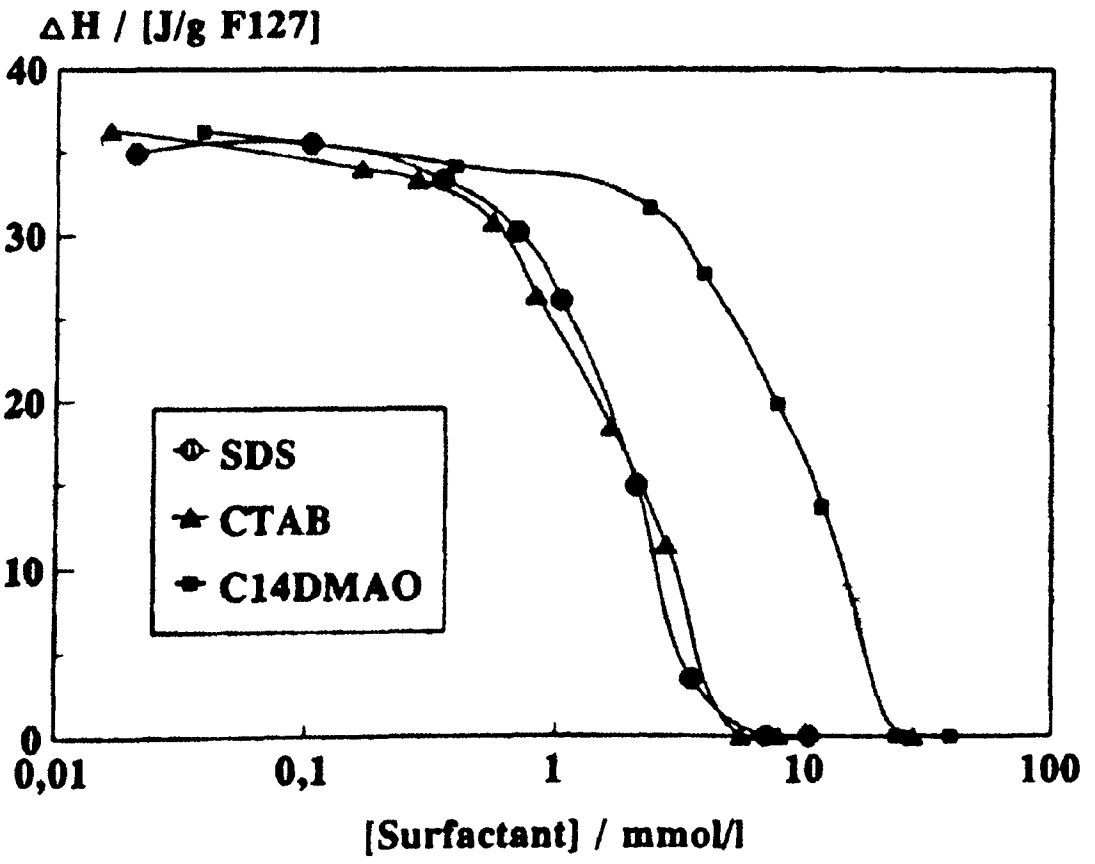


Figure 4. Micellization enthalpy of 1%w/w Pluronic F127 as a function of surfactant concentration measured by DSC[2].

To study the effect of electrolyte on the interaction between SDS and EPE 3000-14, the surface tension of the systems studied above was also measured in the presence of 0.1M NaCl. The surface tension curves are shown in Figure 5.

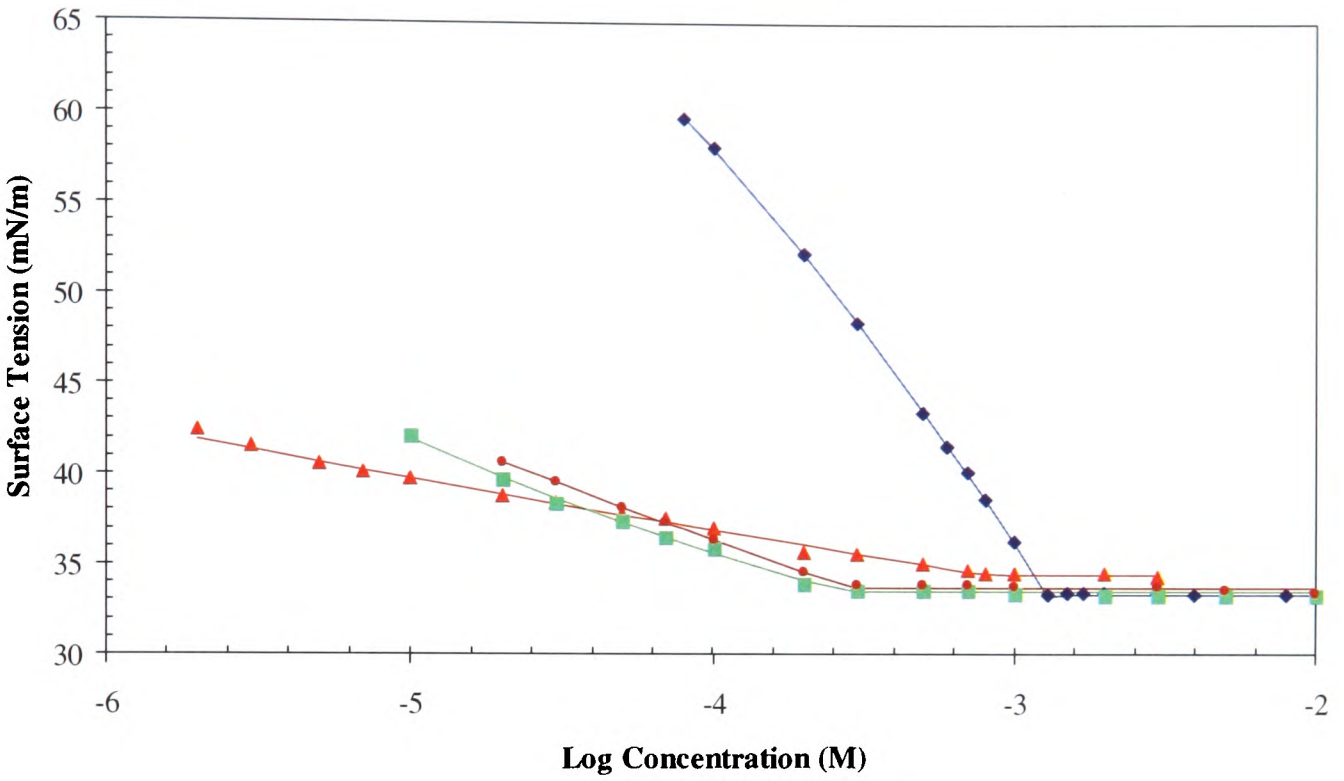


Figure 5. Surface tension against the log of concentration of SDS, (♦), EPE 3000-14, (▲), and mixtures at y_{SDS}=0.9, (●), and y_{SDS}=0.8, (■) in 0.1M NaCl solutions measured at 25°C.

As can be seen from Figure 5, the surface activity of pure EPE 3000-14 is weakly affected by the presence of salt, its CMC being reduced from $9.5x10^{-4}$M to $8.2x10^{-4}$M in a background of 0.1M NaCl. This is a typical effect for nonionic surfactants and has been attributed mainly to the salting-out of the hydrophobic groups in aqueous solution by the electrolyte[37]. Conversely, the surface activity of anionic surfactants, like SDS is significantly changed in the presence of electrolyte. The depression of CMC observed with addition of NaCl is due mainly to the decrease in the thickness of the electrical double layer surrounding the ionic headgroups and the consequent decrease in the electrostatic repulsive interactions between the SDS headgroups in the micelle. The addition of electrolyte creates an interesting feature in the SDS/EPE 3000-14 system. Comparison of the surface tension curves of both surfactants given in Figure 5 indicates that, while EPE 3000-14 has lower free energy of micellization, SDS has now become more effective in reducing the surface tension. The mixtures of the two surfactants result

in systems with lower values of the CMC and a surface tension reduction equivalent to SDS in a background of 0.1M NaCl. These results show the potential advantages of utilising non-ideal mixtures to develop synergistic surfactant systems.

The composition of mixed micelles at the CMC and the interaction parameters for SDS/EPE 3000-14 mixtures in the presence of NaCl were calculated using Equations 8.5 and 8.6 and the results are given in Table 4.

System	CMC (M)	x_{SDS}	β^M
SDS	1.3×10^{-3}	-	-
EPE 3000-14	8.2×10^{-4}	-	-
80:20 SDS:EPE 3000-14	2.4×10^{-4}	0.55	-6.6
90:10 SDS:EPE 3000-14	2.9×10^{-4}	0.60	-6.8

Table 4. Measured CMCs for SDS, EPE 3000-14 and their mixtures in the presence of 0.1M NaCl, with calculated mixed micelle composition and interaction parameters.

The addition of electrolyte reduces the magnitude of the negative value of the interaction parameter, which is consistent with the behaviour of other ionic-POE nonionic mixtures reported in the literature[38]. The decrease in magnitude implies a decrease in the net attractive interaction between the two surfactants. In the case of SDS/C_iE_j mixtures, the decrease has been attributed to the added electrolyte reducing the SDS headgroup repulsion, consequently reducing the impact of the screening effects of the C_iE_j molecules. Although the β^M values indicate a weakening of the interaction between SDS and EPE 3000-14 with addition of NaCl, the effect of the electrolyte on the actual CMC values of the mixtures is nevertheless still to lower them below the corresponding values in the absence of electrolyte. Figure 6 shows the variation of the CMC values with composition assuming both ideal and nonideal mixing. The nonideal mixing curves were calculated from the experimental surface tension results for a mixture of 80:20 SDS/EPE 3000-14.

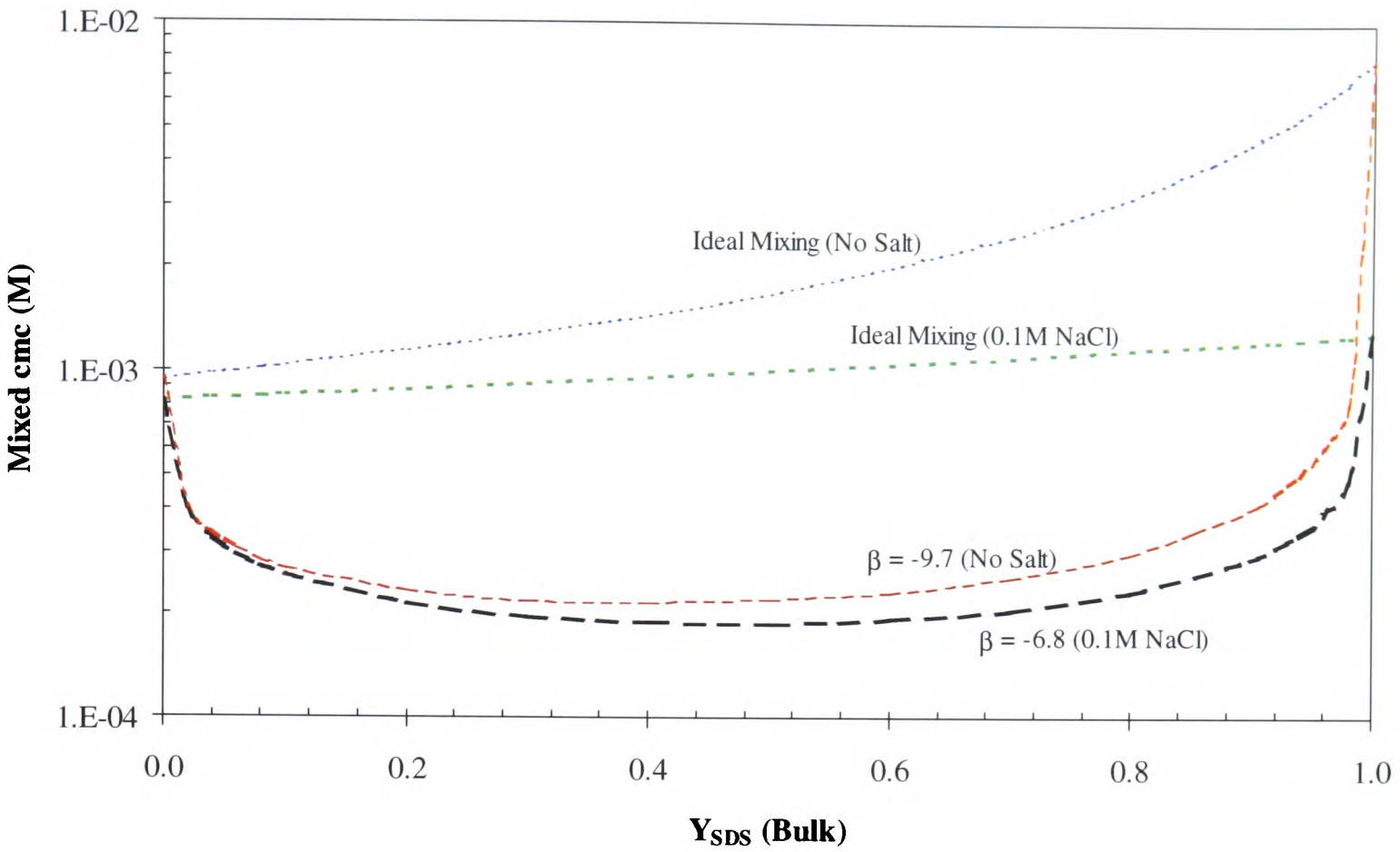


Figure 6. CMC for mixtures of SDS and EPE 3000-14 over the solution composition range, y_{SDS}, calculated assuming ideal and nonideal mixing.

In the Regular Solution Model the parameter β measures the extent to which nonideal mixing departs from ideality, which is a function of the CMC values for each component. Figure 6 shows that even though the nonideal curve for the mixtures in NaCl is shifted to a slightly lower CMC, the reference ideal curve for the system is shifted to a greater extent in the same direction. It is also evident from the relatively small effect of the salt on the CMC of the mixtures that, unlike in SDS/C_iE_j mixtures, the electrostatic screening effect plays only a minor role in the process of mixed micelle formation between SDS and EPE 3000-14. The dehydration mechanism and the electrostatic attractive interaction between SDS and PEO groups appear to be the parameters that contribute most to the nonideality in the mixed micellization of SDS and EPE 3000-14.

3.2 Micellization in the DTAC/EPE 3000-14 system

While mixtures of Pluronic surfactants and SDS have been previously investigated to a significant extent, studies on the aggregation properties of EPE copolymers in the

presence of cationic surfactants are scarce. Hecht *et al.*[6] have used calorimetry to examine the interaction between Pluronic F127 and DTAB. They observed that DTAB begins to interact with F127 molecules at a concentration close to its CMC. Although surface tension is a very widely used technique to characterise the aggregation properties of mixed surfactants system, it has never been applied to study the interaction between EPE copolymers and cationic surfactants.

To study the effect of cationic surfactants on the aggregation properties of EPE copolymers, a mixture of dodecyltrimethylammonium chloride (DTAC) and EPE 3000-14 was used. The surface tension of the solutions was measured as a function of the total amount of surfactant. Figure 7 shows the plot of surface tension against the log of the concentration for pure DTAC and EPE 3000-14 together with that for the 90:10 DTAC:EPE 3000-14 mixture.

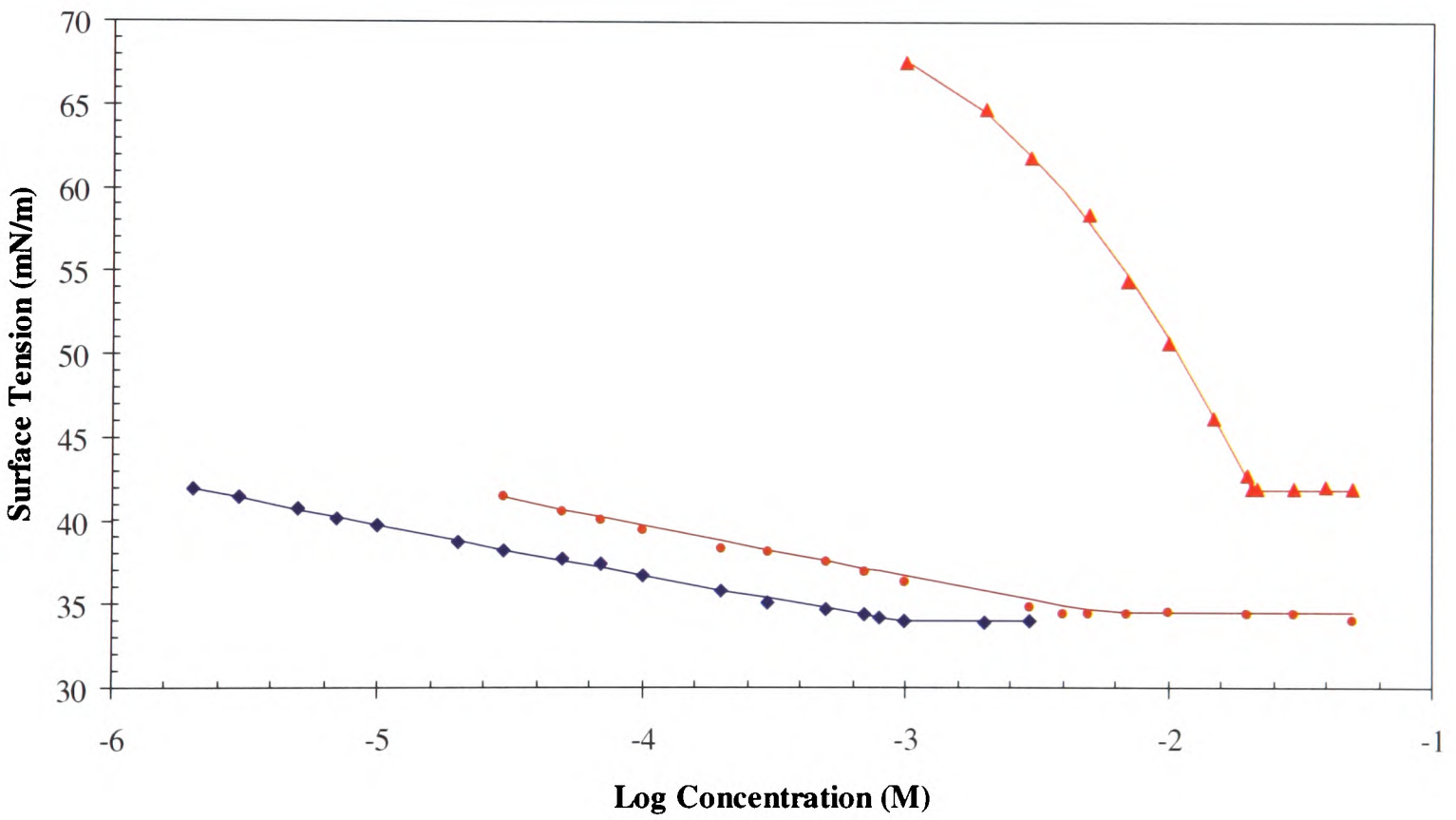


Figure 7. Surface tension against the log of the concentration for DTAC, (▲), EPE 3000-14, (♦), and mixtures at y_{DTAC}=0.9, (●), measured at 25°C.

The value of the β^M parameter calculated from the experimentally determined CMC values for each individual component and the mixture is presented in Table 5.

System	CMC (M)	X_{DTAC}	β^M
DTAC	2.1×10^{-2}	-	-
EPE 3000-14	9.5×10^{-4}	-	-
90:10 DTAC:EPE 3000-14	3.6×10^{-3}	0.41	-2.7

Table 5. Measured CMCs for DTAC, EPE 3000-14 and their mixture, and the calculated mixed micelle composition and interaction parameter.

The value of –2.7 obtained for the DTAC/EPE 3000-14 mixtures is somewhat larger than the interaction parameters measured for other cationic/nonionic systems[38]. It is generally agreed that the negative deviations from ideality exhibited by ionic/nonionic surfactant mixtures are largely a result of the reduced repulsion between ionic head groups in the micelle upon addition of nonionic molecules. However, in contrast to the anionic/nonionic mixtures, the interaction between cationic and nonionic surfactants is much weaker. This is attributed to the lack of electrostatic attraction between cationic surfactants and POE groups. The DTAC bulky headgroup is also likely to hinder the interaction with the triblock copolymer.

It was proposed that the nonideality of SDS/EPE 3000-14 mixtures could be a process driven by the desolvation of the micelle core with the incorporation of SDS hydrocarbon tails. However SDS and DTAC have the same hydrocarbon chain and according to the Regular Solution Approximation, the mole fraction of DTAC, x_{DTAC}, is 0.41 for a solution composition of y_{DTAC}=0.9. Therefore DTAC would be expected to cause dehydration of the core to a similar extent to that caused by SDS. The reason for the reduced dehydration effect observed with the mixture of DTAC and EPE 3000-14 is likely to be related to the structure of the mixed micelle.

In the study conducted by Baglioni *et al.* to investigate local packing in mixed micelles of SDS/$C_{12}E_6$ and DTAC/$C_{12}E_6$, it was found that, unlike SDS, the DTAC headgroup is located close to the hydrophobic core. In our study of mixed monolayer formation with mixtures of DTAC and EPE 3000-14 (See Chapter 9), it will be shown that DTAC prefers to be located mainly into the uppermost PPO-rich layers. Upon the co-micellization of DTAC and EPE 3000-14, DTAC molecules are expected to have their hydrophobic

chains located in Shell 2 and their headgroups at the interface between Shell 2 and 3. In such a configuration there would be fewer water molecules in contact with the hydrophobic chains of DTAC, and therefore, the dehydration effect is likely to be reduced.

The addition of salt to the SDS/EPE 3000-14 mixture affected the surface activity but the attractive interaction remained strong in a way consistent with the dehydration mechanism. Similarly to SDS/EPE 3000-14 mixture the effect of salt on the interaction between DTAC and EPE 3000-14 was also examined. The surface tension curves for each component, DTAC and EPE 3000-14, and a 90:10 DTAC:EPE 3000-14 mixture were measured in a background of 0.1M NaCl and the curves are shown in Figure 8.

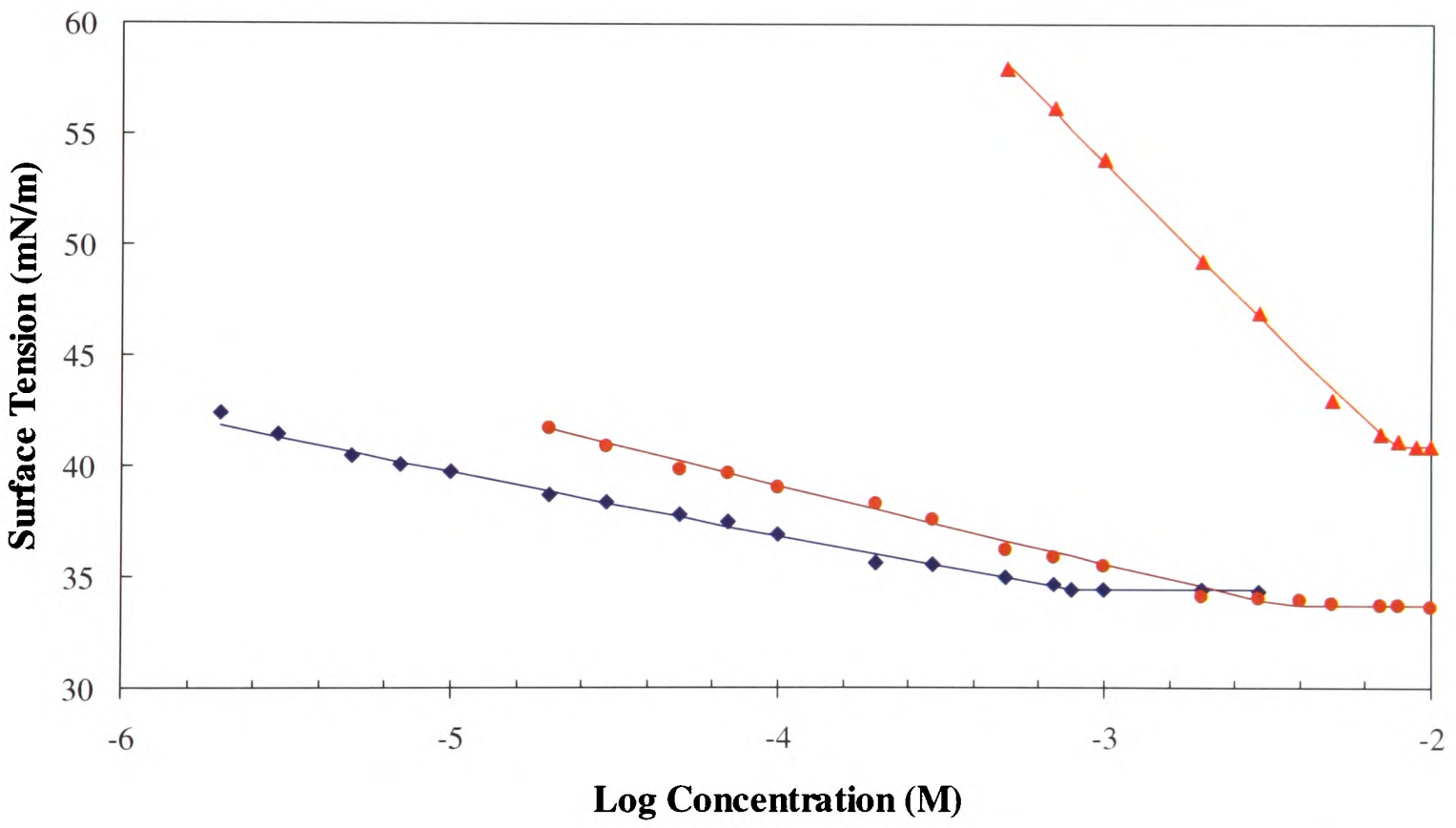


Figure 8. Surface tension against the log of the concentration for DTAC, (▲), EPE 3000-14, (♦), and mixtures at y_{DTAC}=0.9, (●), in 0.1M NaCl solutions measured at 25°C.

It appears from the comparison of the curve of Figure 8 with the curves in pure water shown in Figure 7, that the presence of the salt produces little change in the overall properties of the system. The DTAC surface activity is much less affected by the presence

of salt than SDS, its CMC being reduced slightly from $2.1x10^{-2}$M to $7.8x10^{-3}$M with addition of 0.1M NaCl. The surface activity of the mixture was also slightly affected. The CMC was decreased from $3.6x10^{-3}$M to $2.8x10^{-3}$M, and some reduction of the surface tension at the CMC was also observed.

System	CMC (M)	X_{DTAC}	β^M
DTAC	$7.8x10^{-3}$	-	-
EPE 3000-14	$8.2x10^{-4}$	-	-
90:10 DTAC:EPE 3000-14	$2.8x10^{-3}$	0.49	-1.6

Table 6. Measured CMCs for DTAC, EPE 3000-14 and their mixture, and the calculated mixed micelle composition and interaction parameter.

The interaction between the two surfactants in the presence of salt was then evaluated according to the Regular Solution Approximation. The value of the β^M parameter based on the experimentally determined CMC values for the individual components and the mixture, is presented in Table 6.

Similarly to SDS, the addition of salt alters the balance of the surface activity of the two components and increases the surface activity of the mixture. The relatively small effect of the salt on the CMC of the mixtures also indicates that the contribution of the electrostatic screening effect to the process of mixed micellization between DTAC and EPE 3000-14 is insignificant. The negative value of interaction parameter obtained with the DTAC/EPE 3000-14 mixture in the presence of salt indicates a synergistic behaviour consistent with the dehydration mechanism. Penfold *et al.*[39] have studied mixtures of $C_{16}TAB/C_{12}E_6$ in electrolyte and they showed that the mixture behaves as though it is ideally mixing in the micelles. For a solution mixture of 70/30 $C_{16}TAB/C_{12}E_6$ they observed a slightly greater variation in the micelle composition than in the other studied compositions, consistent with a slightly negative interaction parameter. The micelles formed at composition richer in $C_{12}E_6$ are closer to the composition corresponding to the minimum energy micelle formation and show little or no variation in composition with concentration. Despite the ideal mixing behaviour of $C_{16}TAB/C_{12}E_6$, the mixed micelles

showed pronounced growth with increasing surfactant concentration and mole fraction of $C_{12}E_6$ in solution.

3.3 Micellization in the C_8E_4/EPE 3000-14 system

In spite of the vast number of investigations on the interaction in mixed surfactant systems, very little has been done with mixtures of nonionic surfactants. One of the reasons is that nonionic mixtures would be expected to behave ideally and are therefore deemed to be uninteresting. Systems that exhibit ideal mixing include mixtures of n-octyl and n-decyl suphoxides[40] and mixtures of polyoxyethylene nonionic surfactants with different alkyl chain lengths or polyoxyethylene head groups, where the difference in the degree of polymerisation is not too great[41]. In these cases, where the deviations from ideality are small, the thermodynamic description of the mixed micellization process of nonionic surfactants by means of the Pseudophase Separation Approach[42] has been particularly successful. Non-ideality in nonionic mixtures may result from packing constraints caused by differently structured surfactants, and can be observed for example for mixtures of hydrocarbon or fluorocarbon surfactants with like charge.

In a recent study, Couderec *et al.*[43] have investigated the interaction between hexaethylene glycol mono-n-decyl ether ($C_{12}E_6$) and Pluronic F127 using isothermal titration calorimetry and DSC measurements. They showed that $C_{12}E_6$ and F127 do form mixed micelles and that there is a synergistic interaction between the two surfactants. The addition of $C_{12}E_6$ to a fixed amount of F127 leads to a significant shift of the endothermic peak of the mixed $C_{12}E_6$:F127 systems to a lower temperature particularly when the concentration of $C_{12}E_6$ exceeds its CMC, as shown in Figure 9. Reduction of the onset temperature associated with the micellization endothermic transition, which is related to the critical micellization temperature (CMT), has been also observed with mixtures of SDS and F127, but to a much smaller extent, not more than 3°C[2,3,5]. It is interesting to note that the onset temperature for the $C_{12}E_6$:F127 mixture is reduced to a temperature close to that associated with an endothermic transition of pure $C_{12}E_6$.

In comparison with other surfactants studied previously, the interaction between $C_{12}E_6$ and F127 appears to be very different as demonstrated in Figure 10. The values of the micellization enthalpy of Figure 10 were extracted from references 2 and 40 and are replotted as a function of the surfactant concentration after normalization to their respective CMC values. ΔH_{mic} results for the $C_{12}E_6$/F127 mixtures were normalized only to the F127 concentration despite the fact that ΔH_{mic} contains contributions from both $C_{12}E_6$ and F127. Figure 10 shows that ΔH_{mic} values for the $C_{12}E_6$/F127 mixtures are lower than those for the other surfactant mixtures which may be related to a variation in the composition of Pluronic F127 or even different methodologies applied to test the samples.

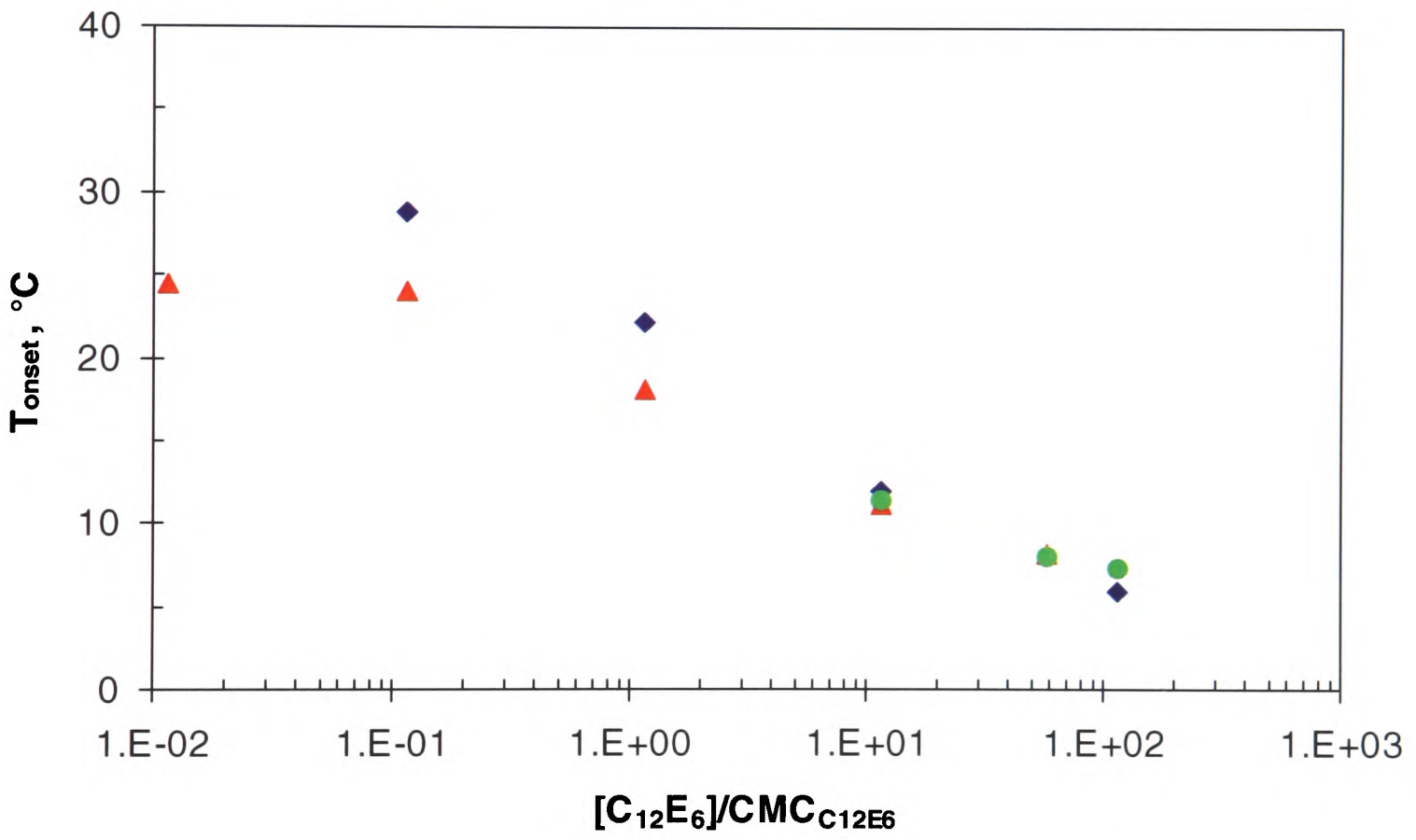


Figure 9. Onset temperature of micellization for Pluronic F127at 0.05% w/v (♦), 0.5% w/v (▲) and 5.0% w/v (●) as a function of surfactant concentration normalized to its CMC[43].

Ionic surfactants, SDS and DTAB, and the zwitterionic C_{14}DMAO interact with F127, suppressing the ΔH associated with the mixed micellization formation. The extent to which ΔH_{mic} is suppressed varies with the surfactant. The suppression starts at a surfactant concentration equivalent to one-tenth of the CMC value for SDS and to about

the CMC value for DTAB. The suppression in the mixture with C_{14}DMAO only becomes evident at a concentration approximately 50 times higher than CMC of C_{14}DMAO. In case of $C_{12}E_6$ the mixed micellization process appears not to be affected up to a concentration 100 times higher than the CMC of $C_{12}E_6$. On contrary, there is slight increase in ΔH when the concentration of $C_{12}E_6$ exceeds 10 times its CMC value, but it may be related to the contribution of $C_{12}E_6$ micellization to the enthalpy change of the system. It suggests therefore that the mechanism that drives the mixed micelle formation between $C_{12}E_6$ and F127 is very different from the one that operates in the mixtures with ionic and zwitterionic surfactants.

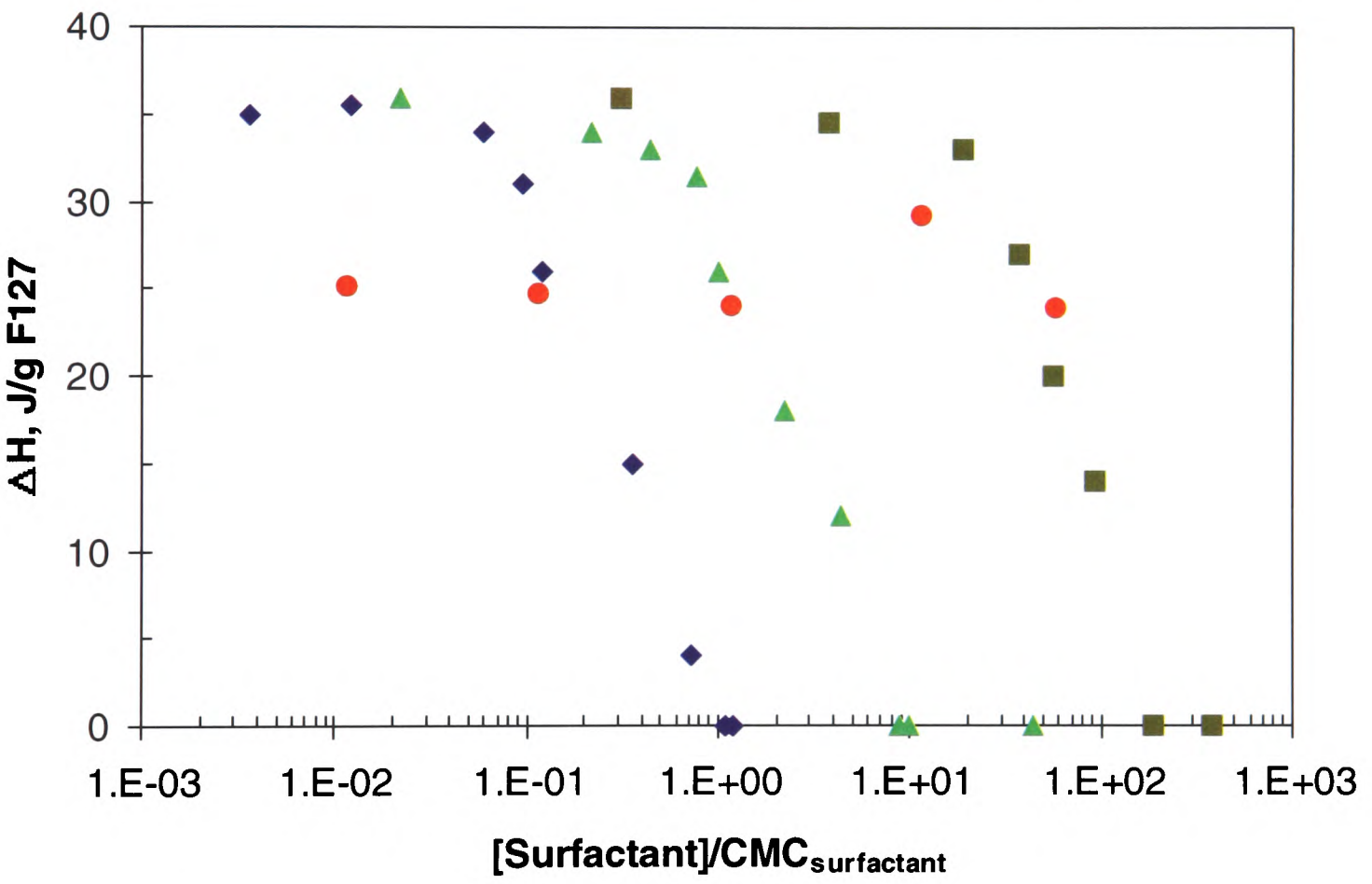


Figure 10. Micellization enthalpy of 1wt% Pluronic F127 + SDS (♦)[2], 1wt% Pluronic F127 + CTAB (▲)[2], 1wt% Pluronic F127 + C_{14}DMAO (■)[2], and 0.5%w/v Pluronic F127 + $C_{12}E_6$ (●)[43] measured by DSC.

To complete our investigation on the aggregation behaviour of EPE 3000-14 in the presence of conventional surfactants, we selected a nonionic surfactant that would have a

free energy of micellization comparable to SDS and DTAC. The chosen nonionic was C_8E_4 whose CMC value is $6.3x10^{-3}$M and whose cloud point is at 37.4°C[44].

The plots of surface tension against the log of the total surfactant concentration are shown in Figure 11. For this mixture the composition studied was 90/10 C_8E_4/EPE 3000-14. The CMCs were calculated from the plots using the criterion of maximum adsorption and the point of inflection on the curve of γ/log c, and the values are given in Table 7.

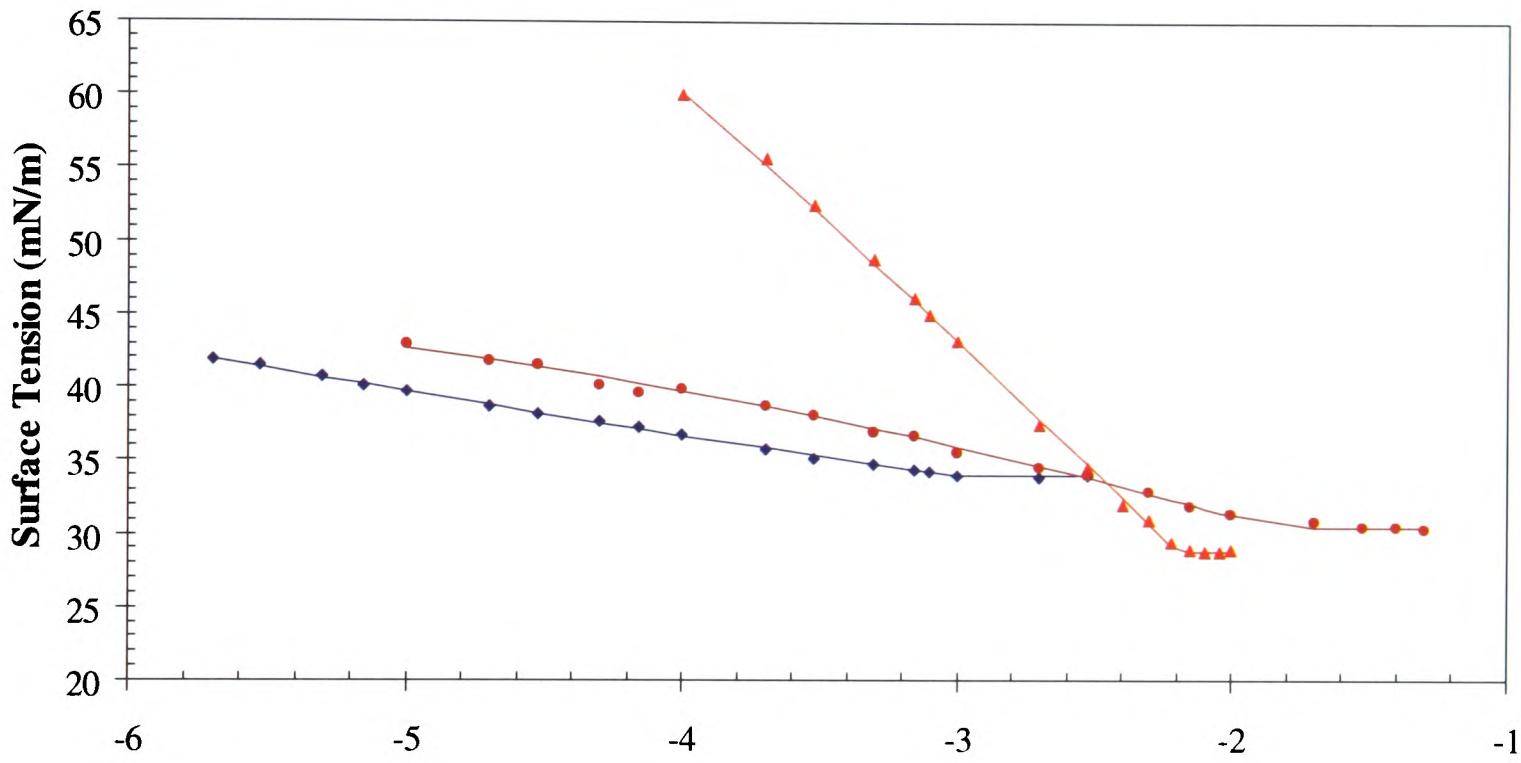


Figure 11. Surface tension against the log of the concentration for C_8E_4, (▲), EPE 3000-14, (♦), and mixtures at y_{C8E4}=0.9, (●), measured at 25°C.

Figure 11 shows some intriguing behaviour for the mixture. The surface tension at the mixed CMC lies in between the surface tension at saturation for pure components, which is expected for ideal mixing. However, the value of the mixed CMC is appreciably higher than that of either pure C_8E_4 or EPE 3000-14, indicating strong repulsive interaction with a significant deviation from ideality.

The value of the nonideality parameter, β^M, for micellar mixing calculated iteratively from Equations 8.5 and 8.6 is given in Table 7, together with the mole fraction of C_8E_4 in

the mixed micelle, x_{C8E4}, and the measured values of the CMCs for the pure components and the mixture. The values in italics are the values calculated for ideal mixing.

System	CMC (M)	X_{C8E4}	β^M
C_8E_4	$6.3x10^{-3}$	-	-
EPE 3000-14	$9.5x10^{-4}$	-	-
90:10 C_8E_4:EPE 3000-14	$2.1x10^{-2}$	0.47	+6.5
90:10 C_8E_4:EPE 3000-14	*$4.0x10^{-3}$*	*0.57*	*0.0*

Table 7. Measured CMCs for C_8E_4, EPE 3000-14 and their mixture and the calculated mixed micelle composition and interaction parameter.

C_8E_4 and EPE 3000-14 have quite different structures, and some departure from ideality might be expected. Attractive interactions between nonionic surfactants have been previously reported[38]. Rosen *et al.*[23] obtained a value for β^M of –0.4 for a mixture of $C_{12}E_3/C_{12}E_8$. As shown in Table 7, the CMC value of $2.1x10^{-2}$M measured for a 90/10 C_8E_4/EPE 3000-14 mixture is well above the value of $4.0x10^{-3}$M, which is the CMC for an ideal mixture. Consequently, the calculated interaction parameter has the remarkably high value of +6.5.

The formation of mixed micelles is normally explained by the spontaneous self-association of surfactant molecules due to the "hydrophobic effect", which favors the formation of surfactant aggregates with the hydrophobic chains in the interior of the aggregate, leaving the hydrophilic head groups at the surface in contact with the aqueous solution. However, there are other effects which can make comparable contributions to the overall energy balance. Nagarajan[38] has identified seven basic sources, viz. (i) transfer free energy of the surfactant tails, (ii) deformation free energy of the surfactant tails, (iii) core-water interfacial free energy, (iv) headgroup steric interactions, (v) headgroup dipole interactions, (vi) headgroup ionic interactions, and (vii) free energy of mixing of surfactant tails. This range of possibilities makes it difficult to determine unambiguously the source of the deviation from ideality in the present system. Repulsive free-energy contributions associated with micellization have been described elsewhere, and they are normally driven by separate steric, interfacial, and electrostatic

contributions[45-48]. It seems unlikely, however, from the nonionic character and the structures of both C_8E_4 and EPE 3000-14 that any such repulsive interactions could be the source for the antagonism observed.

The calorimetry studies discussed above show that the mechanism that drives the mixed micellization of $C_{12}E_6$ and F127 must be quite different from that in the mixtures with SDS and CTAB. An increase in CMC is a phenomenon which has been observed for conventional surfactant systems in the presence of non-surfactant additives and this has been attributed to the modification by the additive of the solvent quality of water. The solvent quality is a controlling factor in the self-assembly of block copolymers[49] and the addition of cosolutes or cosolvents to water for particular applications has been long exploited by the industry[49,50]. Recently the micellar structure of Pluronic P105 in mixed solvents consisting of water and various polar cosolvents has been studied using small-angle neutron scattering (SANS)[51-56]. P105 forms micelles in all the cosolvent-water mixed solvents examined, but the CMC and CMT varied according to the cosolvent type and content. Micelles are formed at higher concentrations when ethanol, propylene glycol or formamide are added to water, indicating that ethanol-water, propylene glycol-water and formamide-water mixed solvents offer better solvent conditions for the block copolymer. On the contrary, the addition of glycerol or glucose promotes the formation of micelles and shifts the micellization boundary to lower concentrations. The micelle core and corona radii and the micelle association number decrease upon the addition of ethanol, propylene glycol or formamide, and there is an accompanying decrease of the polymer volume fraction in the micelle core and corona. The addition of glycerol or glucose, however, increases the micelle association number and reduces the corona thickness, and there is a substantial increase in the polymer fraction in the corona. The effects of the cosolvents on the micellar structure were explained in terms of the polarity and the affinity of the cosolvent to the different segments of the block copolymer. Judging from their octanol/water partition coefficients (log P), ethanol, propylene glycol and formamide, although both miscible with water, are hydrophobic compared with the PEO blocks, and they have higher affinity than water for the hydrophobic PPO blocks. Thus, the addition of ethanol, propylene glycol or formamide in water results in better solvent conditions for the block copolymer and leads to an increase of the solvent content in both

micelle core and the corona. Glycerol and glucose have the most negative values for log *P* among the cosolvents studied, which indicates that they have a strong affinity to water. In the presence of glycerol or glucose, the amount of water hydrating the PEO corona decreases. In those studies the *reduction* of CMC values for EPE copolymers have been associated with the formation of dehydrated micelles, which is exactly the same conclusion we reached above for explaining the mechanism that drives the micellization of SDS/EPE and DTAC/EPE mixtures. However an *increase* in the CMC value resulting from better solvent conditions, leads to the formation of more hydrated micelles. In the case of the mixture C_8E_4/EPE 3000-14 we believe that the explanation of the effective repulsive interaction is similarly a result of an increase in micelle hydration.

The mixed micelle composition calculated for the mixture of C_8E_4/EPE 3000-14 using the Regular Solution Approximation shows that X_{C8E4} for a β^M of +6.5 is 0.47. One might therefore expect the co-micellization of C_8E_4 and EPE 3000-14 to lead to significant changes in the micellar structure. The effects of cosolvents on the microstructure of Pluronic micelles, which we have discussed above, were related to changes in the block copolymer interfacial area, the preference of the different cosolvent for different microdomains, and the ability of the cosolvent to modify the interfacial curvature by swelling different blocks of the copolymer to different extents. PEO-resembling cosolvents, such as glycerol and glucose, will prefer to be located in the polar microdomains, which are mainly occupied by the PEO segments of the copolymer and water. They will therefore not contribute to the swelling of the PEO blocks as shown by the decrease in the interfacial area in the micelle. PPO-resembling cosolvents, such as ethanol and propylene glycol, will prefer to be in the apolar domains, i.e. in the region mainly occupied by PPO blocks. When propylene glycol or ethanol is added, they therefore swell both PEO and PPO blocks resulting in the observed increase in interfacial area. They therefore provide better solvency conditions for the whole copolymer molecule and decrease its hydrophobicity.

We expect that C_8E_4, which consists of an octyl hydrophobic chain with only four EO segments, to be overall more hydrophobic than the PEO block and therefore to mix preferentially with the PPO block. This is also supported by the study of mixed

monolayer formation with mixtures of C_8E_4 and EPE 3000-14 (See Chapter 9), where we find preferential adsorption of C_8E_4 molecules in the uppermost, PO-rich part of the interfacial layer. However, in the recent study by Couderec *et al.*, $C_{12}E_6$ was also found to interact with Pluronic F127, but in a synergistic way. This is surprising because, in terms of their tendencies to interact with PO blocks, $C_{12}E_6$ and C_8E_4 might be expected to be rather similar. The explanation for the quite different behaviour lies in a combination of hydrophobic chain size and hydration.

$C_{12}E_6$ has the same hydrophobic chain length as SDS and DTAC. As argued above the chains of these two surfactants would be expected to cause dehydration of the core, much of it in Shell 2 and 3. $C_{12}E_6$ can be expected to do something similar except that it will probably penetrate a little further into Shell 1, but some of the $C_{12}E_6$, or a fraction of the $C_{12}E_6$ hydrophobic chains would remain in Shell 2 where they could cause some dehydration. It should therefore have a synergistic effect. C_8E_4, on the other hand, could not only fit into the core (Shell 1) but also would maintain or increase the level of hydration by the incorporation of the solvated headgroups. In this respect it would behave more like ethanol and propylene glycol and would therefore destabilize the micelle. This is a very dramatic effect of size on the aggregation properties, which results from a combination of molecular size and micellar structure. No comparable effect could be expected from conventional surfactant mixtures.

3.4 Comparison of mechanisms of interaction in systems containing ionic surfactants/polyglycol ethers and ionic surfactants/EPE copolymers

There is a considerable literature on the interactions between polymer and surfactant molecules in solution. For systems where significant binding occurs, such as poly-(ethylene oxide) (PEO) with sodium dodecyl sulfate (SDS) it is well documented[57-60] that the presence of the polymer acts as a nucleation site for micelle formation at concentrations well below the surfactant's normal critical micelle concentration (CMC). The concentration marking the onset of polymer/surfactant binding is known as the critical aggregation concentration (CAC) and is independent of polymer concentration and molecular weight. The polymer/surfactant complex has been described[61] as a "pearl necklace" structure where polymer wraps itself around surfactant micelles. As the

concentration of surfactant is increased, the polymer becomes saturated with surfactant micelles and then solution micelles form. The critical micelle concentration in the presence of polymer therefore depends on the polymer concentration. In the studies of the binding of SDS by PEO of various molecular weights by surface tension method, the binding ratio found was 0.3mol SDS per base mole PEO[62].

In viewing polymer/surfactant association, it is pertinent first to consider the self-association, or micellization, of a typical ionic surfactant, such as SDS, in water. The chief driving force for association is a reduction of the hydrocarbon/water contact area of the alkyl chains of the dissolved surfactant. The process of micellization of the ionic surfactant represents a delicate balance between several forces favoring and resisting aggregation. One of the main forces resisting aggregation is the crowding together of the ionic headgroups at the periphery of the micelle. The consequently high charge density in this zone favors the tight binding of counterions which diminishes the electrical potential and headgroup repulsion. If one considers the spherical model of the micelle, which describes the dilute properties of a typical anionic surfactant such as SDS, on a molecular scale there is a considerable distance between the headgroups at the periphery, if only for geometrical reasons of packing. Some of this space will accommodate counterions, but most will comprise areas of the hydrocarbon chain exposed to water – an obviously unfavorable situation. Early NMR data[63] indicated that the first three or four carbons of micellized molecules of SDS are in intimate contact with water. Accordingly, any change brought about to diminish either one of these unfavorable conditions will promote micellization. The proposed necklace configuration for the PEO/SDS complex would include several features already observed, such as (1) a more favorable free energy of association, as manifested in a lowered CMC; (2) increased ionic dissociation of the aggregates[64]; and (3) an altered environment of the CH_2 groups of the surfactant near the headgroups, as seen in the ^{13}C-NMR data of Cabane[65]. Since the balance of forces leading to surfactant aggregation is changed in the presence of the polymer, it is not surprising that the aggregation number may change.

Several factors have a direct influence on polymer/surfactant association[66]. In most cases it is clear that some of them do affect the association in the same way as they do the

micellization of the surfactant, confirming the similarity of the two processes. Concerning the polymer, a minimum molecular weight of polymer is apparently required to ensure "complete" interaction with the surfactant. Schwuger[67] investigated the influence of PEO molecular weight on the surface tension behaviour of SDS solutions. For a molecular weight of 600, association was relatively weak, but for a molecular weight of 1550 it was pronounced, and beyond 4000, it was found to be strong and largely independent of molecular weight. Another factor expected to influence the interaction is the hydrophobicity of the polymer. The higher hydrophobicity lowers the molecular weight limit required for interaction. One infers that a driving force for association is a reduction of the polymer hydrophobic segment/water interfacial area by contacting of such areas with exposed hydrophobic areas of developing surfactant aggregates. For polypropylene oxide (PPO) where one is limited to molecular weights below 1000 for water-solubility reasons, the interaction was pronounced for the member of molecular weight 600, but the high surface activity of this polymer complicated the interpretation of surface tension data[67].

The binding of SDS to monomeric EPE copolymer molecules, was studied by Li *et al.*[4,5] using a SDS surfactant selective electrode via electromotive force (EFM), isothermal titration calorimetry (ITC), and light scattering. They found that SDS interacts with the unassociated EPE copolymer molecules in a similar way as found for SDS/nonionic polymer systems[68]. In the ITC experiments with fixed concentration of EPE copolymer and varying concentration of SDS, they found that as the concentration of SDS increases a T_1 point is attained which signifies the onset of the formation of SDS micelles on the polymer. T_1 is independent of the polymer concentration[69,70] and molecular weight but depends on the temperature following the same trend as the CMC of the surfactant[66,71]. The binding process proceeds with increasing SDS concentration until a second point is reached, T_2, when the unassociated EPE copolymer molecules is fully saturated with bound SDS micelles. T_2 is independent of molecular weight, varies little with temperature, and increases with increasing polymer concentration. The comparison of the values of the binding parameter T_1 for unassociated EPE copolymer monomers and those for PEO and PPO show that T_1 for SDS/EPE copolymer is much lower than the corresponding ones for PEO[72,73] and PPO[72,74]. Therefore the attractive interaction between

bound SDS micelles and EPE copolymer is more facile resulting in more stable bound micelles relative to those in the PPO/SDS and PEO/SDS complexes. This is achieved by the stronger EPE copolymer/SDS attractive interactions reducing the headgroup repulsion in the surfactant aggregate and therefore stabilizing the bound micelles. These results demonstrate that the covalent binding between PEO and PPO blocks in EPE copolymers give rise to a more efficient binding with SDS than the individual polymers can provide. Indeed the almost one order of magnitude decrease in T_1 for the block copolymer clearly demonstrates the phenomenon of synergy in the relation of the surfactant binding properties of EPE copolymer when compared to the individual oligomers[4]. Li *et al.*[5] have also found that SDS can bind to the micelles of EPE copolymers. The initial part of the binding involves the formation of mixed EPE copolymer/SDS micelles and as further SDS is added, the EPE copolymer-rich mixed micelles start breaking down to smaller aggregates. The breakdown process continues until the point when all the EPE copolymer molecules are dissociated to monomers. A third interaction of SDS with EPE copolymers involves the promotion of EPE copolymer micelles at concentrations up to 3°C below the critical micellar temperature of pure EPE copolymer solution. The exact mechanism which describes how SDS promotes the formation of EPE copolymer micelles is not clear at present. One could argue that because the measurements are close to phase boundaries, the single SDS monomers act as a seed or nucleus for the formation of EPE copolymer micelles. On the other hand it could be that SDS monomers added at concentrations or temperatures just before the appearance of EPE copolymer micelles may affect the solvent properties of water by the disturbance of its hydrogen bonds. It is well-known that the solubility of the PEO blocks is much better in water than that of PPO blocks. When solvent conditions become unfavorable for the PPO blocks, the EPE copolymer molecules will aggregate to form micelles. On this basis one could argue that when SDS monomers induce EPE copolymer micelles, such unfavorable conditions for the solubility of single EPE copolymers exist. In this work we have attributed the synergistic interaction between SDS and EPE copolymers stems partly from a substantial gain in entropy associated with the dehydration of the core of the mixed micelle.

Several authors allude to the fact that interaction between uncharged water-soluble polymers is much more stronger with anionic surfactants than with cationics. Nagarajan

and Kalpakci[75] found only feeble indications of interaction of dodecylammonium chloride and dodecylammonium bromide with PEO, as judged by viscosity criteria. Complex formation using cationic surfactants is strongly influenced by the nature of the counterions and increases in the order $Cl^- < Br^- < I^- < SCN^-$[76]. This is an intriguing finding and several explanations have been advanced for the origin of this difference. The first and most popular one is that the large headgroups of the cationic surfactants reduce the access of the polymer to the surface of the cationic micelles, and this mechanism has been modelled theoretically by Nagarajan[77] and Ruckenstein *et al.*[78] As discussed above the association between ionic micelles and polymers usually leads to a stabilization of the micelles, which is apparent from the reduced values of the CMC. The stabilization is thought to be originated from a stabilization of the interface between the hydrocarbon core and water[75,79] at which the polymer resides[65]. However, in the case of cationic surfactants, the bulky head groups already shields most of the core from contact with water[80], and furthermore, steric repulsions between headgroups and polymer segments may produce an unfavorable contribution to the free energy of formation of polymer-bound micelles. Therefore, only sufficiently hydrophobic polymers will interact with cationic surfactant micelles, because of the additional reduction in free energy due to the transfer of polymer segments from the aqueous phase to the micellar surroundings. Recently, it has been found that the loss in electrostatic repulsion among the headgroups upon formation of the smaller polymer-bound micelles constitutes another important contribution to the reduction of the free energy of micellization and, the reduction in CMC[81]. The size of the surfactant headgroup may have a certain influence on the interaction with polymer, but is only part of the explanation as to why anionic surfactants interact more strongly than cationic ones with uncharged polymers. In another explanation of the difference between anionic and cationic surfactants, a fractional positive charge on the polymer molecules has been invoked, which is thought to originate from protonation of the ether oxygens in the case of polyethers. The very low pK_a value of an ether, however, raises serious doubts about the importance of protonation at neutral pH. A third explanation proposed by Witte and Engberts[82], suggests that there is a difference in the interactions of cations and anions with the hydration shell of the polymer, which would favor the interaction of anionic surfactants. It has been also suggested that the solvent molecules orient at the polymer surface to create a weak

surface charge density around the polymer, which would favor binding of an oppositely charged surfactant[83].

The interaction between cationic surfactant and EPE copolymers was also investigated by LI et al using a combination of experiments involving electromotive force measurement, isothermal titration calorimetry (ITC), and light scattering[5]. As discussed above cationic surfactants are more selective and only interact weakly with those polymers which have specific hydrophobic groups. If we consider the separate EO and PO blocks of EPE copolymers, SDS interacts strongly with PPO and PEO whereas tetradecyltrimethylammonium bromide (TTAB) only interacts weakly with PPO[66]. On the other hand, a preliminary DSC measurement showed that cationic surfactants readily form mixed micelles with Pluronic surfactants and also moderate its micellar properties[3]. In the ITC and EFM experiments Li *et al.* investigated the binding characteristics of TTAB to unassociated Pluronic F127 molecules. They found that T_1 (critical aggregation concentration) is independent of the copolymer concentration and that T_2 (when the unassociated copolymer molecules is fully saturated with bound TTAB micelles) increases as the polymer concentration increases. This is exactly the type of behaviour that is expected when ionic surfactants bind to neutral polymers. The comparison of the values of T_1 and T_2 measured for TTAB/F127 and SDS/F127 demonstrates conclusively that EPE copolymers interact much more strongly with SDS than TTAB, first in stabilizing the bound aggregates (lower T_1), and also the maximum capacity for Pluronic F127 to bind SDS aggregates is about 4 times greater than that for TTAB aggregates. AT T_2, the SDS/F127 complex contains on average four bound SDS micelles per polymer[4,5]; for TTAB/F127, the complex contains one TTAB micelle per F127 polymer molecule.

The interaction between TTAB and Pluronic F127 takes place via the methyl substituent on the PPO blocks of the F127 chain and the TTAB micelles and is hydrophobic in the sense that it involves the removal of the hydrocarbon contact with water. Specifically, the interaction involves direct contact between the CH_3- groups in the PPO blocks and the area between the headgroups on the micellar surface where the hydrocarbon chains are in contact with water. This interaction also involves the removal of bound water from the

micellar surface and possibly from hydrated parts of the polymer and results in a reduction of the micelle/water interfacial tension[77]. In comparison with SDS/F127, these interactions are less facile because of the bulky headgroups in the TTAB micelles. For SDS/F127 there is also an additional strong electrostatic attraction between SDS micelles and both PEO and PPO blocks of F127 involving the etheric oxygen linkage[84] in the chain and the SO_4- headgroup; the exact nature of this interaction however is still a subject of debate[85]. This interaction involves the removal of bound water from the micellar surface and the chain.

The interaction between TTAB and micellar F127 has also been studied by Li *et al.* and they found that like with SDS, the addition TTAB breaks down the F127 micelles first into smaller aggregates and eventually into F127 monomers. They claim that in the mixed micelles these ionic surfactants bind to the aggregated PPO blocks which make up the hydrophobic core of the F127 micelle, and with the PEO blocks. The reasons given for that were the following. (1) The hydrated PEO blocks which form the outer corona of the F127[26,29] are not aggregated, because they are still fully hydrated. These so-called hydrophilic headgroups are relatively free PEO chains, and for an ionic surfactant to bind to such PEO chains the monomer ionic surfactant must reach the critical concentration of T_1 (EO). The binding of SDS and TTAB to F127 micelles takes place well before this critical monomer concentration T_1 is reached[4,68]. (2) In general, cationic surfactants such as TTAB have little or no affinity for PEO chains[66,72] and certainly less than SDS[85]. The disruption of F127 micelles by ionic surfactants must also be influenced by the charged headgroup of the surfactants. It may very well be that when the charge density in the hydrophobic core of the F127/ionic surfactant mixed micelles reaches a certain critical value, the headgroup repulsion dominates to such an extent that it destabilizes the mixed micelles.

The DSC experiments carried by Li *et al.* also showed that TTAB, like SDS, promotes the formation of F127 micelles by lowering the CMT by up to 3°C and the CMC. This means that the interaction between ionic surfactants and EPE copolymers in the mixed micelles are favorable and that synergistic behaviour occurs, which was the case found in our studies.

3.5 Considerations on Thermodynamic Modelling for Nonideal Mixing of EPE Copolymers in Micellar Solution

Nonideal micelle formation is most commonly modelled by regular solution theory. As discussed in Chapter 7, all the effects that result in the nonideality upon surfactant mixing can be included in the component activity coefficients in the micelles. If the surfactant mixing in the micelle obeys regular solution theory, the following relationships are valid for a binary surfactant system

$$\Delta H^E = \Delta G^E = \beta^M x_1 x_2 RT \tag{8.7}$$

where ΔH^E is the heat of mixing in the micelle and ΔG^E is the excess free energy of mixing in the micelle. In the regular solution approximation where the excess entropy of mixing is defined to be zero, the parameter β^M can be physically interpreted as the parameter representing an excess heat or enthalpy of mixing. There is substantial evidence that regular solution theory is not valid in describing the nonideal mixed micelles apart from those demonstrated in this chapter with the mixtures of EPE copolymers. The heat of mixing obtained from fitting regular solution model to CMC data has been shown to differ greatly from that measured by calorimetry[86,87]. The excess free energy of mixing upon mixed micelle formation can be very unsymmetrical with respect to composition[24], contrary to the prediction of Equation 8.7. The value of β^M should be independent of temperature and micellar composition. We have found to be slightly dependent on composition for the mixtures SDS/EPE 3000-14 and similar discrepancies have been previously reported[88]. Another physical interpretation for β^M also based explicitly on the regular solution approximation expressed in terms of the molecular interactions in the mixed micelles is given by:

$$\beta^M = \frac{N_A\left(w_{11} + w_{22} + 2w_{12}\right)}{RT} \tag{8.8}$$

where w_{11} and w_{22} are the self-interaction energies, w_{12} is the distinct interaction energy and N_A is the number of molecules in the system. The physical interpretation of β^M in

terms of Equation is not a pre-requisite in the use of a single fitting parameter for activity coefficients, but merely an attempt to ascribe physical meaning to β^M. However, a real system in which the nonideality is not predominantly enthalpic in origin may not be well described by this approach.

Regarding the mixtures of EPE copolymers and surfactants, the deviation from regular solution approximation implies that there must be a non-zero TS^E contribution to the excess free energy of mixing. In fact there are evidences described above of substantial gain in entropy upon mixed micelle formation in mixtures with EPE copolymers. Nevertheless, when surfactants with different molecular structures are mixed, like the ones we studied, the nonideality of mixing reveals an eminent irregular nature. In other words the nonideal behaviour of mixing does deviate from regular solution types of behaviour in many cases. It follows that the key issue is that the basic presumption for the regular solution theory is that different molecules should have a similar size and shape before and after mixing[89]. Evidently as one of the most important parameters to characterize the nonidealities, β^M loses its "regular" physical identity and consistency in these systems. Consequently, the interaction parameter β^M reduces to an empirical one[23]. To solve this fundamental problem alternative models have been developed.

Osborne-Lee *et al.*[90] have proposed an alternative pseudophase separation model for nonionic/anionic mixtures which that accounts for the additional contributions to the excess entropy, the non-random arrangement of the surfactants in the mixed micelle and the conformational entropy changes of the long-chain polyoxyethylene surfactants. The former contributions must always be significant since reduction of charge density by arranging anionic surfactants interspersed among nonionics is thought to be the primary mechanism responsible for the strong interaction. Because the arrangements will tend to increase the number of contacts between unlike surfactant molecules, the entropy in such mixed micelles is, then, less than that for micelles which result from random mixing. The mixing process of a long-chain polyoxyethylene surfactant and an anionic surfactant involves more than simple relocation of the head on the surface of the micelle. That is, there will be an increased number of allowable conformations for long polyoxyethylene chain. This leads to an increase in the entropy of each chain upon mixing. The latter

contributions will be significant for longer ethylene oxide chains. The two effects have been considered separately by using the lattice and conformational partition functions. The free energy of mixing is equal to the sum of the contributions from these partition functions. The micellar activity coefficients of surfactants derived from the excess free energy can be calculated provided one knows the interaction parameter β^M, the coordination number z, and the surface density of the long-chain polyoxyethylene hydrophilic groups in the micelle. This model has been shown to describe satisfactorily the mixed CMC and the micellar composition for the mixtures of an alkylbenzene sulfonate and two ethoxylated nonylphenol surfactants[89]. For long polyoxyethylene chains (> 50 groups) the predictions of the proposed model are not so good indicating that additional factors must be incorporated into the free energy expression. These additional terms are believed to be related to the changing hydration of ethylene oxide chains with changing temperature. We expect that the lack of accountability for hydration changes in the proposed model would impair its suitability for the mixtures with EPE copolymers. As discussed in previous chapters the micellization of EPE copolymers is strongly influenced by temperature. The remarkable effect of temperature has been attributed to a temperature-induced conformational change of PO and EO groups, which increases the population of less polar conformers, rendering the interactions PO-water and EO-water less favourable. Hence with an increase of temperature the PPO block becomes increasingly more hydrophobic and therefore less hydrated.

Ruckenstein, Rao, Nagarajan, Blankschtein, and so forth[25,38,45,91] have also developed some molecular thermodynamic models to describe mixed micellization by predicting the excess Gibbs free energy of the mixing process. In particular, Ruckenstein and Rao[45,91] have developed an isotherm model to predict the interfacial tension of oil-brine system in the presence of surfactant and cosurfactant, by taking into account the different sizes of the solute molecules as well as the solute-solvent and solute-solute interactions in the interfacial phase.

We believe that the nonideality upon mixing between EPE copolymers and anionic surfactants arises partly also from characteristics of the micelle structure that result from the nature and behaviour of EPE copolymers in a micellar solution. It has been shown that

the architecture of the EO/PO copolymer and the internal degrees of freedom for both EO and PO groups play a significant role in its micellization behaviour[92]. A number of approaches to modelling micelle formation in solutions of block copolymers have been suggested by a number of researchers over the past decade. Leiber *et al.*[93], Noolandi and Hong[95], Munch and Gast[95], and Nagarajan and Ganesh[96] computed the free energy of micelle formation assuming uniform copolymer segment concentrations in the core and corona regions, respectively. Scaling theories for polymeric micelles with an insoluble core and an extended corona were developed by Halperin[97], Marques[98], Semenov[99], and Zhulina and Birshtein[100]. In a third approach, van Lent and Scheutjens[101], Linse[102,103], and Hurter *et al.*[92,104] used a self-consistent mean-field theory to determine the detailed segment density profiles within a micelle, making no a priori assumptions as to the locations of the micellar components. The micelle structures determined from this model have been confirmed recently by Monte Carlo simulations[105], and show that the interfacial region between the core and corona of the micelle is diffuse and not sharp as is assumed in the other modelling approaches. Here we provide a shorter account of the mean field lattice theory adapted to spherical micelles. A more extended theoretical description of the lattice theory can be found elsewhere[32,101,106].

3.5.1 Mean-field lattice theory of EPE copolymer micellization

The micellization of EPE copolymers was modelled on the basis of a mean-field lattice theory for multicomponent mixtures of copolymers with internal degrees of freedom occurring in heterogeneous systems[102,103]. The conformations of the polymer chains are described as random walks on a spherical lattice. The space is divided into lattice cells, each being able to contain one polymer segment or a solvent molecule. The interaction extends only to segments or solvent molecules in adjacent lattice cells. The random-mixing (mean-field) approximation is applied within each layer separately, and thus it is possible to obtain and describe radial concentration profiles.

The computation involves a self-consistent determination of the state distributions (i.e. the distributions of the polar and nonpolar states of the EO and PO species in each layer) and the segment density distributions (i.e., the radial distribution of each polymer segment and

of water molecules). The state distributions are derived from the partition function and are given by the following implicit set of non-linear equations[32]

$$P_{ABi} = \frac{X_{AB}}{\sum_{B} X_{AB}} \tag{8.9}$$

where

$$X_{AB} \equiv g_{AB} \exp\left[-\beta U_{AB} - \sum_{A'} \sum_{B'} \chi_{AB} \langle P_{A'B'i} \phi_{A'i} \rangle \right] \tag{8.10}$$

valid for all species (EO, PO, and water, collectively labelled *A*), states (polar and nonpolar conformation in the case of EO or PO, collectively labelled *B*), and layers (*i*). In Equation 8.9, P_{ABi} denotes the fraction of species *A* in layer *i* which is in state *B*. In Equation 8.10 U_{AB} is the internal energy of state *B* of species *A* (arising from different internal energy of the polar and nonpolar conformations), g_{AB} is the degeneration factor of state *B* of species *A* (arising from different number of polar and nonpolar conformations), $\beta = (kT)^{-1}$, where *k* is the Boltzmann constant and *T* is the absolute temperature, ϕ_{Ai} is the volume of species *A* in layer *i*. The angular brackets indicate an averaging over three adjacent layers. Moreover, χ_{AB} is the Flory-Huggins interaction parameter representing the interaction energy between species *A* and *B*, which is given by

$$\chi_{AB} = (\delta_A - \delta_B)^2 v_B / kT \tag{8.11}$$

where δ_A is the solubility parameter for the specie A, and v_B is the molar volume of specie *B*. A priori the χ parameter is a purely energetic term. Thus, a state is favoured by a high degeneration, a low internal energy, and a favourable interaction (small χ) with its neighbouring segments.

The species volume fraction ϕ_{Ai} needed in Equation 8.10 is simply related to n_{xsi}, the number of sites in layer i occupied by segments of rank s (the sth segment in a chain) belonging to component x according to

$$\phi_{Ai} = \frac{1}{L_i} \sum_{x} \sum_{s=1}^{r_x} \delta_{A,t(x,s)} n_{xsi} \tag{8.12}$$

where L_i is the number of sites in layer i and r_x the number of segments in component x. Finally, the Kronecker delta selects only those segments of rank s of component x if they are of type A.

The expression for the segment distribution is more complex, since the correct weight of all conformations and the connectivity of the chains have to be taken into account. Again starting from the partition function, n_{xsi} is obtained by a matrix method and is given by[32]

$$n_{xsi} = C_x \left\{ \Delta_i^T . \left[\prod_{s'=r_x}^{s+1} \left(W^{t(x,s')} \right)^T \right] . s \right\} \left\{ \Delta_i^T . \left[\prod_{s'=2}^{s} W^{t(x,s')} \right] . p(x,1) \right\} \tag{8.13}$$

where C_x is a normalization factor related to the bulk volume fraction of component x, $W^{t(x,s)}$ a tridiagonal matrix comprising elements which contain factors describing the lattice topology and weighting factors for segment of rank s belonging to component x, $p(x,1)$ a vector describing the distribution of the first segment of component x among the layers, and Δ and s being elementary column vectors. The weighting factor G_{ai} for species A in layer i entering W is given by

$$G_{Ai} = \exp(-\beta u_{Ai}) \tag{8.14}$$

where the species potential u_{Ai} can be divided into two parts according to

$$u_{Ai} = u_i^{\cdot} + u_{Ai}^{\text{int}} \tag{8.15}$$

If the species potentials are defined with respect to the bulk solution, i.e., if $u_A^b = 0$, then the two terms are given by

$$\beta u_i' \equiv \alpha_i + \sum_x \frac{\phi_x^b}{r_x} + \frac{1}{2}\sum_{A'}\sum_{A''}\sum_{B'}\sum_{B''}\phi_{A'}^b P_{A'B'}^b \chi_{B'B''} P_{A''B''}^b \phi_{A''}^b \tag{8.16}$$

$$\beta\mu_{Ai}^{\text{int}} \equiv \sum_B \left[P_{ABi}\left(\beta U_{AB} + \ln\frac{P_{ABi}}{g_{AB}}\right) - P_{AB}^b\left(\beta U_{AB} + \ln\frac{P_{AB}^b}{g_{AB}}\right)\right] + \sum_{A'}\sum_B\sum_{B'}\chi_{BB'}\left(P_{ABi}\langle P_{A'B'i}\phi_{A'i}\rangle - P_{AB}^b P_{A'B'}^b \phi_{A'}^b\right) \tag{8.17}$$

The species-independent term u_i', which is related to the lateral pressure in a continuous model, ensures that the space is completely filled in layer i by a suitable choice of α_i. In Bulk u' becomes zero. The species-dependent term u_{Ai}^{int} has two contributions, the internal free energy for species A in layer i being diminished by the corresponding quantity in bulk and the mixing energy for species A in bulk. In both cases, averages are taken over the relevant state distributions. At distances far away from the center of the aggregate, P_{ABi} approaches P_{AB}^b, ϕ_{Ai} approaches ϕ_A^b, and hence u_{Ai}^{int} becomes zero. Since u_{Ai} is needed for obtaining ϕ_{Ai} through Equations 8.12 – 8.14 and since u_{Ai} itself depends on ϕ_{Ai} according to Equations 8.15 and 8.17, Equations 8.12 – 8.17 have to be solved self consistently. Furthermore, the state distribution has to fulfil Equation 8.10.

The micellar solution is (hypothetically) divided into spherical subsystems (cells), each of which contains one micelle and its accompanying solution. The volume of the cell V_s is simply the inverse micellar number density. The excess free energy A_s of a cell contains two parts: A^σ, which is the free energy associated with the formation of a micelle fixed in space in contact with the bulk solution, and the mixing entropy, as given by[101]

$$\beta A_S = \beta A^\sigma + \ln(V_m / V_s) \tag{8.18}$$

where V_m is the volume of the micelle. A necessary requirement for stable micelles ay equilibrium is that the positive A^σ be balanced by the favourable mixing entropy of the

micelle, implying that A_s =0. Given that the equilibrium state and the segment distributions are determined, A^{σ} is obtained from by

$$A^{\sigma} = A - A^{*} - \sum_{x} n_x \left(\mu_x - \mu_x^{*}\right) \tag{8.19}$$

where A-A^{*} is given by

$$\beta\left(A - A^{*}\right) = \beta\left(A_{\text{int}} - A_{\text{int}}^{*}\right) - \ln\frac{\Omega}{\Omega^{*}} + \beta\left(U - U^{*}\right) \tag{8.20}$$

The first term denotes the contribution arising from the internal degrees of freedom, the second term is the mixing entropy, and the third is the mixing energy. The total internal free energy arising from the internal states becomes

$$\beta A_{\text{int}} = \sum_{i}\sum_{A} n_{Ai} \sum_{B} P_{ABi}\left[\beta U_{AB} + \ln\frac{P_{ABi}}{g_{AB}}\right] \tag{8.21}$$

where Σ_i denotes the sum over layers, Σ_A the sum over species (segment types), and Σ_B the sum over the states of species A, n_{Ai} is the number of sites in layer i occupied by segments of type A. The mixing entropy arises from the difference between the configuration degeneration of the system and of the reference state. When self-exclusion at a mean-field level is taken into account and the contributions of all the conformations of all components are included, the mixing entropy of the system can be expressed as

$$\ln\frac{\Omega}{\Omega^{*}} = -\sum_{x}\sum_{c} n_{xc} \ln\frac{n_{xc} r_x}{w_{xc}} \tag{8.22}$$

where n_{xc} denotes the number of chains of component x in conformation c and where W_{xc}, which is related to the degeneration of component x in conformation c, is given by

$$w_{xc} = L_{k(x,c,1)} \prod_{s=2}^{r_x} \lambda_{k(x,c,s-1),k(x,c,s)} \tag{8.23}$$

where $k(x,c,s)$ is the number of the layer in which the segment of rank s of the component x in the conformation c is located, $L_{k(x,c,1)}$ indicates the number of possibilities for the position of the first segment, being consistent with conformation c, and the product λ elements representing the probability of the remaining s-1 segments, likewise being consistent with conformation c. Finally, within the mean-field approximation the interaction energy is given by

$$\beta U = \frac{1}{2}\sum_{i=1} L_i \sum_{A}\sum_{A'}\sum_{B}\sum_{B'} \phi_{Ai} P_{ABi} \chi_{BB'} \left\langle P_{A'B'i} \phi_{A'i} \right\rangle \tag{8.24}$$

where $\left\langle x_i \right\rangle \equiv \sum_{i'=1}^{M} \lambda_{ii'} x_i$, in the case of nearest-neighbour interaction only, the sum over i' in the definition of $\langle x_i \rangle$ contains at most three terms. In expression 8.24, the state summation variable B is always associated with the species summation variable A, B' summed with A', etc.

In Equation 8.19, $\mu_x - \mu_x^*$ denotes the difference between the chemical potential of component x in bulk and in the reference state, which is by

$$\beta(\mu_x - \mu_x^*) = r_x \sum_{A}\sum_{B} \phi_{Ax}^* \begin{Bmatrix} P_{AB}^b \left[\beta U_{AB} + \ln \dfrac{P_{AB}^b}{g_{AB}} \right] \\ -P_{AB}^* \left[\beta U_{AB} + \ln \dfrac{P_{AB}^*}{g_{AB}} \right] \end{Bmatrix} + \ln \phi_x^b + 1 - r_x \sum_{x'} \frac{\phi_{x'}^b}{r_{x'}} - \frac{r_x}{2} \sum_{A}\sum_{A'}\sum_{B}\sum_{B'} \begin{bmatrix} (\phi_A^b - \phi_{Ax}^*) P_{AB}^b \chi_{BB'} P_{A'B'}^b (\phi_{A'}^b - \phi_{A'x}^*) \\ +\phi_{Ax}^* \phi_{A'x}^* \chi_{BB'} \left(P_{AB}^* P_{A'B'}^* - P_{AB}^b P_{A'B'}^b \right) \end{bmatrix} \tag{8.25}$$

where ϕ_x^b denotes the volume fraction of component x and ϕ_{Ax}^* the volume fraction of species A in component x. An important quantity is the excess number of segments of component x in the cell, defined as

$$\Gamma_x = \sum_{i=1}^{M} L_i \left[\left(\sum_{s=1}^{r_x} \phi_{xsi} \right) - \phi_x^b \right] \tag{8.26}$$

where $\phi_{xsi} = n_{xsi} / L_i$. The excess number of polymer molecules will be referred to as the aggregation number of micelle, $N_{agg} = \Gamma_{polymer} / r_{polymer}$. Given $\Gamma_{polymer}$, the micelle volume is approximated by

$$V_m = \frac{\Gamma_{polymer}}{\phi_{polymer,i=1} - \phi^b_{polymer}} \tag{8.27}$$

Finally, the total volume fraction of component x in the cell, $\phi_{x,tot}$ (equal to the stochiometric concentration of x in the micelle solution), is the sum of the excess and bulk volume fractions according to

$$\phi_{x,tot} = \Gamma_x / V_s + \phi^b_x \tag{8.28}$$

Thus, on the basis of a selected bulk composition, the numerical procedure involves the computation of the equilibrium state and segment distributions according to Equations 8.12 - 8.15, and 8.17 and the excess free energy of the cell from Equation 8.19. Equation 8.26 is then used to compute the amount of excess polymer, Equation 8.27 to obtain the micellar volume, and Equation 8.18 to obtain the volume of the cell, with the total composition being calculated finally from Equation 8.28. Any change in the bulk composition leads to a change in the total concentration, with concomitant change in the micellar structures, or possibly to there being no micelles formed at all. The lowest total polymer concentration at which stable micelles exist (which requires $A^\sigma > 0$ and $\partial A^\sigma / \partial N_{agg} < 0$) is referred to as the critical micelle concentration (CMC).

In contrast to many other thermodynamic descriptions of the micellization process[96,102], the present approach does not assume neither a constant polymer density in the aggregates nor a confinement of the species in different regions. On the contrary, the variation of the polymer density within the aggregates and the distribution of the EO and PO segments are quantities directly obtained from the calculations on the model system. The results presented by Linse[102,103] have shown that the theory is able to qualitatively predict essential parts of the phase diagram of EPE copolymers in aqueous solution. In particular,

the occurrence of the monomeric solution, micellar solution, solution of rodlike aggregates, and phase separation at increasing temperature was obtained. Moreover, the theory is able to predict the radial segment distribution of the different types of segments. The coarse simplifications in the mean-field lattice theory preclude a fully quantitative agreement with experimental results. Some weaknesses of the model have been identified, and possible extensions have been indicated. The strength of the present approach is that one obtains, at least, a qualitatively correct description and a deeper understanding of the phenomena occurring in polymer solution by using a unified, but versatile, approach.

So far, the lattice theory for polymers with internal states has been applied for describing phase behaviour[33], adsorption to solid surfaces[107,108], self-aggregation[102,109], as well as protein partitioning in polymer two-phase systems[110] with polymers containing EO and PO, and good agreement with experimental data was found.

Linse *et al.*[111] have used an expanded mean field lattice theory to model the adsorption properties of EPE copolymers at the air/water interface. In chapter 6 we showed that the volume fraction profile across the air/water interface for an EPE copolymer determined by neutron reflection is in agreement with that calculated by Linse. We believe that the mean-field theory could possibly be modified to describe the mixed micellization between EPE copolymers and surfactants. Linse *et al.* have applied the mean-field model extended with internal degrees of freedom to study the mixed micellization of aqueous solutions containing mixtures of di- and tri-block EO/PO copolymers[112], triblock EPE copolymers of different molecular weights[113], and also the solubilisation of hydrocarbons in EPE copolymer micelles[92,114]. The effect of hydrocarbon on the micelle structures was modelled by incorporating the interaction parameters among hydrocarbon, the polymer components and water. The predictions of model regarding the changes in the micelle structure compare favourably with published light scattering results[115,116]. The lattice theory has thus been successful in elucidating the underlying structural effects which result from the mixing of EO/PO copolymers of different architecture and the solubilisation of organic solutes inside the copolymer micelles. For mixtures of EPE copolymers and ionic surfactants some further modifications to the mean-field model extended with internal degrees of freedom to allow the theory to describe the electrostatic

contributions to mixed micellization. There have been some studies using an extended Flory-Huggins theory adapted for charged polymers to investigate the effects of electrostatic interactions on the polymer solubility and miscibility. Khokhlov and Nyrkova[117] have shown that the mixing entropy of the counterions could be dealt within the standard Flory-Huggins theory by a renormalization of the number of polymer segments. Independently, Nilsson[118,119] and later Johansson *et al.*[120] numerically solved models based on an extended version of the Flory-Huggins theory, where the counterions were explicitly included as a separate component on the same level as the solvent and the chain molecules. Gottschalk *et al.*[121] have adapted the the mean-field model extended with internal degrees of freedom for charged copolymers using the sama approach taken by Nilsson to account for the electrostatic contributions. The approach involves the explicit inclusion of the counterions and any potential salt components in the model on an equal balance as the solvent and the polymeric components. The effects of the electrostatic interaction among the charges were included by imposing electroneutral phases. Hence the extended model does not contain any explicit terms describing the electrostatic energy contribution to the free energy of the system. However electrostatic interactions are the most significant source of mixing nonidealities in most surfactant mixtures that include ionic surfactants. Therefore the theory will require further extensions to account for the electrostatic free energy contributions by introducing, for example, the Poisson-Boltzmann equation.

4 Summary

To study the aggregation behaviour of EPE copolymers in mixed surfactant systems, the surface tension of various combinations of surfactants (SDS, DTAC, and C_8E_4) has been measured at the air/liquid interface. For the SDS/EPE 3000-14 and the DTAC/EPE 3000-14 systems, the effects of electrolytes, in this case 0.1M NaCl, on the mixed micelle formation were also investigated. Values of the mixed critical micelle concentrations were obtained and the results were analysed in the framework of the Pseudophase Separation Model.

For SDS/EPE 3000-14 mixtures, a strong attractive interaction between SDS and EPE 3000-14 was observed. For a mixture of 90:10 SDS/EPE 3000-14 a value of -8.8 for β^M was obtained, which is significantly higher than for SDS with conventional nonionic surfactants. The synergistic interaction in the system is attributed to a substantial gain in entropy associated with the dehydration of the core of the mixed micelle. The addition of salt alters the balance of the surface activity of the two components and therefore increases the surface activity of the mixture but the attractive interaction remains strong in a way that would not be expected for small molecule systems but which is consistent with the dehydration mechanism.

In comparison with the SDS/EPE 3000-14 system, a much reduced interaction parameter was obtained for the DTAC/EPE 3000-14 mixtures. The value of –2.7 for β^M obtained for the 90:10 DTAC/EPE 3000-14 mixture seems somewhat larger than the interaction parameters measured for other cationic/nonionic systems, which can be attributed to the same dehydration mechanism as proposed for SDS.

The mixture of C_8E_4/EPE 3000-14 shows very peculiar behaviour. The interaction parameter obtained for a 90:10 C_8E_4/EPE 3000-14 mixture is +6.5. This is attributed to a similar mechanism as for the charged surfactants except that the additional penetration possible with such a small hydrophobic chain causes a reversal of the dehydration effect. This is contrasted with the synergistic interaction of the larger $C_{12}E_6$ with Pluronic surfactants.

References:

[1] Almgren, M.; Stam, J.V.; Lindblad, C.; Li, P.; Stilbs, P.; and Bahadur, P. *J. Phys. Chem.*, 95, 5677 (1991)

[2] Hecht, E.; and Hoffmann, H. *Langmuir*, 10, 86 (1994)

[3] Kositza, M. J., Rees, G. D., Holzwarth, A., and Holzwarth, J. F. *Langmuir*, 16, (2000)

[4] Li, Y.; Xu, R.; Bloor, D.M.; Holzwarth, J.F.; and Wyn-Jones, E. *Langmuir*, 16, 10515 (2000)

[5] Li, Y.; Xu, R.; Couderec, S.; Bloor, D.M.; Wyn-Jones, E.; and Holzwarth, J.F. *Langmuir*, 17, 183 (2001)

[6] Hecht, E.; and Hoffmann, H. *Colloids Surfaces A: Physicochem. Eng. Aspects* , 96, 181 (1995)

[7] Li, Y.; Xu, R.; Couderec, S.; Bloor, D.M.; Holzwarth, J.F. and Wyn-Jones, E.; *Langmuir*, 17, 5742 (2001)

[8] Rubingh, D.N *Solution Chemistry of Surfactants*, Mittal K.L, Ed., Plenum Press, New York, Vol. 1 (1979)

[9] Rosen, M.J., and Hua, X.Y. *J. Colloid Interface Sci.*, 90, 212 (1982)

[10] Rosen, M.J., and Hua, X.Y. *J. Am. Oil Chem. Soc.*, 59, 582 (1982)

[11] Rosen, M.J., and Zhu, B.Y *J. Colloid Interface Sci.*, 99, 427 (1984)

[12] Guggenheim, E.A. *Trans. Faraday Soc.*, 33, 151 (1937)

[13] Alexandridis, P.; and Holzwarth, J.F. *Langmuir*, 13, 6074 (1997)

[14] Pandya, K.; Lad, K.; and Bahadur, P. J. *Macromol. Sci: Pure Appl. Chem*, 1, 1 (1993)

[15] Penfold, J.; Staples, E.; Thompson, L.; Tucker, I.; Hines, J.; Thomas, J.K.; Lu, J.R.; and Warren, N. *J. Phys. Chem.*, 103, 5204 (1999)

[16] Hines, J.; Thomas, J.K.; Garrett, P.R.; Rennie, G.K.; and Penfold, J. *J. Phys. Chem. B*, 101, 9215 (1997)

[17] Penfold, J.; Staples, E.; Thompson, L.; Tucker, I.; Hines, J.; Thomas, J.K.; and Lu, J.R. *Langmuir*, 11, 2496 (1995)

[18] Hoffmann, H.; and Poesnecker, G. *Langmuir*, 10, 381 (1994)

[19] Rosen, M.J., and Zhao, F. *J. Colloid Interface Sci.*, 95, 443 (1983)

[20] Hines, J.; Thomas, J.K.; Garrett, P.R.; Rennie, G.K.; and Penfold, J. *J. Phys. Chem. B*, 102, 8834 (1998)

[21] Tajima, K.; Nakamura, A.; and Tsutumi, T. *Bull. Chem. Soc. Jpn.* 52, 2060 (1979)

[22] Warren, N. *PhD Thesis*, Oxford University (1999)

[23] Rosen, M.J., and Hua, X.Y. *J. Colloid Interface Sci.*, 86, 164 (1982)

[24] Nishikiko, N. *J. Colloid Interface Sci.*, 60, 242 (1976)

[25] Shiloach, A; and Blankschtein, D. *Langmuir*, 14, 1618 (1998)

[26] Goldmints I.; Yu, G.; Booth, C.; Smith, K.; and Hatton, T.A. *Langmuir*, 15, 1651 (1999)

[27] Mortensen, K.; and Pedersen, J.S. *Macromolecules*, 26, 805 (1993)

[28] Goldmints I.; von Gottberg.; Smith, K.; and Hatton, T.A. *Langmuir*, 13, 3659 (1997)

[29] Yang, L.; Alexandridis, P.; Steytler, D. C.; Kositza, M. J., and Holzwarth, J. F. *Langmuir*, 16, 8555 (2000)

[30] Karlstrom, G. *J. Phys. Chem.*, 89, 4962 (1985)

[31] Bjorling, M.; Linse, P.; and Karlstrom, G. *J. Phys. Chem.*, 94, 471 (1990)

[32] Linse, P.; and Bjorling, M. *Macromolecules*, 24, 6700 (1991)

[33] Malmsten, M.; Linse, P.; and Zhang, K-W. *Macromolecules*, 26, 2905 (1993)

[34] Vieira, J.B.; Li, Z.X.; Thomas, R.K.; and Penfold, J. *J. Phys. Chem. B*, 106, 10641 (2002)

[35] Wanka, L.; Hoffmann, H.; and Ulbricht, W. *Macromolecules*, 27, 2445 (1994)

[36] Baglioni, P.; Dei, L.; Rivara-Minten, E.; and Kevan, L. *J. Am. Chem. Soc.*, 115, 4286 (1993)

[37] Harned, R.S.; and Owen, B.B.; *The Physical Chemistry of Electrolytic Solutions*, 3rd. edition Reinhold, New York (1958)

[38] Holland, P.; and Rubingh, D. *Mixed Surfactant Systems*, ACS Symposium Series 501, Washington (1992)

[39] Penfold, J.; Staples, E.; Cummins, P.; Tucker, I.; Thomas, J.K.; Simister, E.A.; and Lu, J.R. *J. Chem. Soc. Fraraday Trans.*, 92, 1773 (1996)

[40] Chu, D.Y.; Thomas, J.K. *J. Am. Chem. Soc.*, 108, 6270 (1986)

[41] Lange, H.; Beck, K.H. *Kolloid Z. u-Z. Polymere,* 251, 424 (1973)

[42] Clint, J.H., *J. Chem. Soc. Faraday I*, 71, 1327 (1975)

[43] Couderec, S.; Li, Y.; Bloor, D.M.; Holzwarth, J.F.; and Wyn-Jones, E. *Langmuir*, 17, 4818 (2001)

[44] Glatter, O.; Fritz, G.; Lindner, H.; Popela, J.; Mittelbach, R.; Strey, R.; and Egelhaaf S.U. *Langmuir*, July (2000)

[45] Puvvada, S.; and Blankschtein, D. *J. Chem. Phys.*, 92, 3710 (1990)

[46] Nagarajan, R.; Ruckenstein, E. *J. Colloid Interface Sci.*, 71, 580 (1979)

[47] Nagarajan, R.; Ruckenstein, E. *Langmuir*, 7, 2934 (1991)

[48] Eriksson, J.C.; and Ljunggren, S. *Prog. Colloid Polym. Sci.*, 76, 188 (1988)

[49] Alexandridis, P.; and Spontak, R.J. *Curr. Opin. Colloid Interface Sci.*, 4, 130 (1999)

[50] Alexandridis, P. *Curr. Opin. Colloid Interface Sci.*, 2, 478 (1997)

[51] Alexandridis, P.; and Yang, L. *Macromolecules*, 33, 5574 (2000)

[52] Holmqvist, P.; Alexandridis, P.; and Lindman, B. *Langmuir*, 13, 2471 (1997)

[53] Holmqvist, P.; Alexandridis, P.; and Lindman, B. *Langmuir*, 30, 6788 (1997)

[54] Ivanova, R.; Lindman, B.; and Alexandridis, P. *Langmuir*, 16, 3660 (2000)

[55] Alexandridis, P.; Ivanova, R.; and Lindman, B. *Langmuir*, 16, 3676 (2000)

[56] Ivanova, R.; Lindman, B.; and Alexandridis, P. *Langmuir*, 16, 9058 (2000)

[57] Jones, M. *J. Colloid Interface Sci.*, 23, 36 (1974)

[58] Chari, K.; Antalek, B.; Lin, M. Y.; and Sinha, S. K. *J. Chem. Phys.*, 100, 5294 (1994)

[59] Kang, Y. S.; and Kevan, L. *J. Phys. Chem.*, 98, 7624 (1994)

[60] Brown, W.; Fundin, J.; and Miguel, M. D. *Macromolecules*, 25, 7192 (1992)

[61] Shirama, K. *J. Biochem.*, 75, 309 (1974)

[62] Goddard, E. D.; and Hannan, R. B. *J. Colloid Interface Sci.*, 55, 73 (1976)

[63] Saunders, F. L. *J. Phys. Colloid Interface Sci.*, 28, 475 (1968)

[64] Muto, S.; Ino, T.; and Meguro, K. *J. Am. Oil Chem. Soc.*, 49, 437 (1972)

[65] Cabane, B. *J. Phys. Chem.*, 81, 1639 (1977)

[66] Goddard, E. D.; and Ananthapadmanabhan, K. P. in *Interactions of Surfactants with Polymers and Proteins*, CRC Press, Boca Raton, Fl. (1993)

[67] Schwuger, M. J.; and Lange, H. *J. Phys. Colloid Interface Sci.*, 46, 528 (1974)

[68] Ghoreishi, S.M.; Fox, G.A.; Bloor, D.M.; Wyn-Jones, E.; and Holzwarth, J.F. *Langmuir*, 15, 5474 (1999)

[69] Ghoreishi, S.M.; Li, Y.; Bloor, D.M.; War, J.; and Wyn-Jones, E. *Langmuir*, 15, 4380 (1999)

[70] Blandamer, M.J.; Cullis, P.M.; and Engberts, J. B. F. N. *J. Chem. Soc., Faraday Trans.*, 94, 2261 (1998)

[71] La Mesa, C. *J. Chem. Phys.*, 94, 323 (1990)

[72] Wang, G.; Olofsson, G. *J. Chem. Phys. B*, 102, 9276 (1998)

[73] van Stam, J.; Brown, W.; Fundin, J.; Almgren, M.; and Lindblad, C. *ACS Symposium Series*, 532, 194 (1993)

[74] Bloor, D.M.; Wan-Yunus, W.M.Z.; Wan-Badhi, W.A.; Li, Y. Xu, R.; Wyn-Jones, E.; and Holzwarth, J.F. *Langmuir*, 11, 3395 (1995)

[75] Nagarajan, R.; and Kalpakci, B. Polym. *Prep. Chem. Soc. Div. Polym. Chem.*, 23, 41 (1982)

[76] Saito, S.; and Yukawa, M. *J. Phys. Colloid Interface Sci.*, 30, 211 (1969)

[77] Nagarajan, R. *J. Chem. Phys.*, 90, 1980 (1989)

[78] Ruckenstein, E.; Huber, G.; and Hoffmann, H. *Langmuir*, 3, 382 (1987)

[79] Goddard, E.D. *Colloid Surf.*, 19, 255 (1986)

[80] Tabony, J. *Mol. Phys.*, 51, 975 (1984)

[81] Brackman, J. C.; Engberts, J. B. F. N. *Langmuir*, 7, 2097 (1991)

[82] Witte, F.M.; and Engberts, J.B.F.N. *J. Org. Chem.*, 53, 3085 (1988)

[83] Samii, A.; Karlstrom, G.; and Lindman, B. *Langmuir*, 7, 653 (1991)

[84] Chu, B. *Langmuir*, 11, 414 (1995)

[85] Wang, Y.L.; Han, B.X.; Yan, H.; Cooke, D.J.; Lu, J.R.; and Chu, B. *Langmuir*, 11, 414 (1995)

[86] Holland, P.M. in *Structure/Performance Relationship in Surfactants*, ACS Symposium Series 253, 141, American Chemical Society, Washington, DC (1984)

[87] Hey, M.J., MacTaggart, J.W.; and Rochester, C.H. *J. Chem. Soc. Faraday I*, 81, 207 (1985)

[88] Kamrath, F.R.; and Franses, E.I. *Ind. Eng. Chem. Fundam*, 22, 230 (1983)

[89] Fowler, R.; and Guggenheim, E.A. in *Statistical Thermodynamics*, Cambridge University Press, London (1960)

[90] Scamehorn, J.F. in *Phenomena in Mixed Surfactant Systems*; ACS Symposium Series 311, 1, American Chemical Society, Washington, DC (1986)

[91] Ruckenstein, E.; and Rao, I.V. *J. Colloid Interface Sci.*, 117, 104 (1987)

[92] Hurter, P.N.; Scheutjens, J.M.H.M.; and Hatton, T.A. *Macromolecules*, 26, 5030 (1993)

[93] Leiber, L.; Orland, H.; and Wheeler, J.C. *J. Chem. Phys.*, 79, 3550 (1983)

[94] Noolandi, J.; and Hong, K.M. *Macromolecules*, 16, 1443 (1983)

[95] Munch, M.R.; and Gast, A.P. *Macromolecules*, 21, 1360 (1988)

[96] Nagarajan, R.; and Ganesh, K. *J. Chem. Phys.*, 90, 5843 (1989)

[97] Halperin, A. *Macromolecules*, 20, 2943 (1987)

[98] Marques, C.M. *Macromolecules*, 21, 1051 (1988)

[99] Semenov, A.N. *Sov. Phys. JETP*, 61, 733 (1985)

[100] Zhulina, Y.B.; and Birshtein, T.M. *Polym. Sci. USSR*, 12, 2880 (1986)

[101] van Lent, B.; and Scheutjens, J.M.H.M. *Macromolecules*, 22, 1931 (1989)

[102] Linse, P. *Macromolecules*, 26, 4437 (1993)

[103] Linse, P. *J. Chem. Phys.*, 97, 133896 (1993)

[104] Hurter, P.N.; Scheutjens, J.M.H.M.; and Hatton, T.A. *Macromolecules*, 26, 5592 (1993)

[105] Wang, Y.; Mattice, W.L.; and Napper, D.H. *Langmuir*, 9, 66 (1993)

[106] Scheutjens, J.M.H.M.; and Fleer, G.J. *J. Chem. Phys.*, 84, 178 (1980)

[107] Tiberg, F.; Malmsten, M.; Linse, P.; and Lindman, B. *Langmuir*, 7, 2723 (1991)

[108] Malmsten, M.; Linse, P.; and Cosgrove, T. *Macromolecules*, 25, 2474 (1992)

[109] Linse, P.; and Malmsten, M. *Macromolecules*, 25, 5434 (1992)

[110] Calsson, M.; Linse, P.; and Tjerneld, F. *Macromolecules*, 26, 1546 (1993)

[111] Linse, P.; and Hatton, T.A *Langmuir*, 13, 4066 (1997)

[112] Linse, P. *Macromolecules*, 27, 2685 (1994)

[113] Linse, P. *Macromolecules*, 27, 6404 (1994)

[114] Svensson, M.; Alexandridis, P.; and Linse, P. *Macromolecules*, 32, 5435 (1999)

[115] Al-Saden, A.A.; Florence, A.T.; Morrison, H.; and Whateley, T.L. *J. Pharmacol. Suppl.*, 31, 81 (1979)

[116] Al-Saden, A.A.; Florence, A.T.; and Whateley, T.L. *J. Colloid Interface Sci.*, 90, 303 (1982)

[117] Khokhlov, A.R.; and Nyrkova, I.A. *Macromolecules*, 25, 1493 (1992)

[118] Piculeil, L.; Ilioupolos, I.; Linse, P.; Nilsson, S.; Turquois, T.; Viebke, C.; and Zhang, W. in *Gums and Stabilisers for the Food Industry*, Oxford University Press, Oxford (1994)

[119] Piculeil, L.; and Lindman, B. in *Adv. Colloid Interface Sci.*, Elsevier Science Publisher B.V., Amsterdam (1992)

[120] Johansson, H.O.; Karlstrom, G.; Matiasson, B.; and Tjerneld, E. *Bioseparation*, 5, 269 (1995)

[121] Gottschalk, M.; Linse, P.; and Piculeil, L. *Macromolecules*, 31, 8407 (1998)

Chapter 9

Adsorbed Layers of Binary Mixtures of EPE Copolymers and Surfactants

1 Introduction

Although there have been several previous studies of the bulk properties of solutions of EPE copolymer/surfactant mixtures, mixed monolayer formation involving these polymers at interfaces has been neglected. This may result in part from the lack of well-characterized samples of EPE copolymers, in contrast to polydisperse Pluronic or related commercial equivalents, and in part from a lack of experimental techniques capable of exploring the problem in detail.

Hecht *et al.* [1] have studied binary mixtures of Pluronic F127 and SDS by measuring the surface tension of solutions containing fixed amount of Pluronic as a function of the SDS concentration. The surface tension curve profile was very complex, as shown in Figure 1. To explain the effect of SDS concentration they divided the curve into four different regions. In Region I, which corresponds to SDS concentration below 0.5mM, the surface tension remains almost flat. It was argued that in Region I monomeric SDS and EPE molecules would compete for adsorption at the surface. In this region, EPE copolymer is substantially more surface active than SDS and should therefore dominate the surface adsorption. One interesting feature of this region, which was either not explained or not observed in the original paper, is revealed when the surface tension of this flat region is compared with the surface tension of pure Pluronic F127 solution. The surface tension of Region I is approx. 39mN/m while for the pure F127 solution it is 44mN/m, which indicates that the interaction between SDS and Pluronic F127 is already significant in this region. With increasing SDS concentration, the SDS molecules bind to the EPE monomers forming less surface-active complexes, and as a result block copolymer would tend to desorb from the surface and cause the surface tension to increase (Region II). In Region III the block copolymer molecules are believed to be entirely saturated with SDS

molecules and further increase in the SDS concentration would then lead to an increased SDS adsorption at the interface, which lowers the surface tension. When the free SDS concentration becomes high enough to form micelles the surface tension should remain approximately constant, as observed in Region IV.

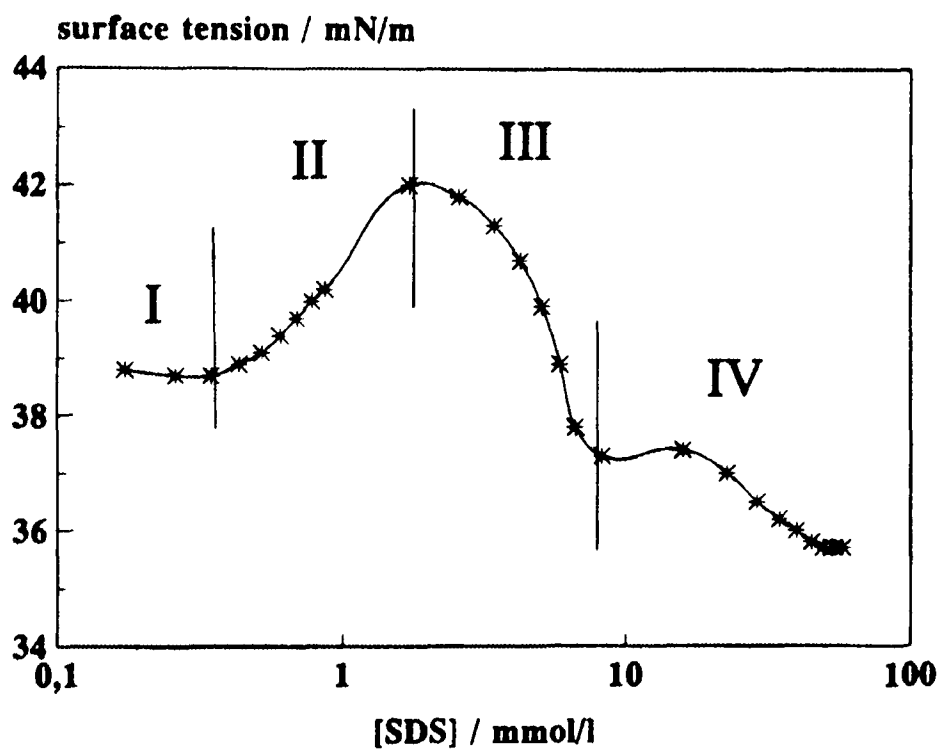


Figure 1. Surface tension as a function of SDS concentration for 10^{-3}wt% Pluronic F127 solution measured at 25°C.

The present chapter describes the study of the formation of mixed monolayers at the air-water interface from binary systems containing SDS, dodecyltrimethylammonium chloride (DTAC) and tetraethylene glycol monooctyl ether (C_8E_4) using surface tension measurements. For EPE-ionic surfactant mixtures, measurements were also carried out in the presence of 0.1M aqueous solution of NaCl to investigate the influence of the swamping electrolyte on the surface activity of the mixtures.

The Regular Solution Model is applied to calculate the monolayer composition and to gain further insight into the interaction between surfactant and copolymer at the interface. In this chapter we also explore the applicability of the Pseudophase Separation Model by comparison of the predicted mixed monolayer compositions with those measured directly by neutron reflection of the mixtures. Neutron reflection is now a well-established technique for probing adsorbed layers. It is particularly well suited to the study of

mixtures in which by isotopic substitution, neutrons can be made sensitive to only one adsorbed species at a time[2-4]. Surface excesses directly measured by neutrons may be integrated according to the Gibbs equation to yield the value of the surface tension lowering at any given concentration[5]. Comparison with the observed value of the surface tension at a concentration where there are fewer uncertainties in the surface tension, e.g. at the CMC, provides an essentially model independent check for consistency.

2 Experimental Details

2.1 Materials

The surfactant partners selected for EPE 3000-14 in this study were sodium dodecylsulfate (SDS), dodecyltrimethylammonium chloride (DTAC), and tetraethylene glycol monooctyl ether (C_8E_4). The preparation and purification of protonated and deuterated analogues of surfactant mixture components have already been described in Chapter 2 and the preparation of the solutions for surface tension measurements in Chapter 8.

2.2 Surface tension measurements

Surface tension measurements were carried out exactly as described in Chapter 8.

2.3 Determination of the surface interaction parameter (β^s)

Mixing in layers adsorbed at interfaces has been treated by the Pseudophase Separation Models developed by both Rosen[6,7] and Holland[8,9], which are described in Chapter 7. In the Pseudophase Separation Model, the molar concentration required to attain a given surface tension in a solution of an ideal binary surfactant mixture is related to the molar concentration of the individual components required to attain the same surface tension as follows

$$\frac{1}{C_{12}} = \frac{y_1}{C_1} + \frac{(1-y_1)}{C_2} \qquad (9.1)$$

Deviations from ideality are generally measured as a function of their effects on the properties associated with the lowering of the surface tension. The nonideality is incorporated by modifying the values of the concentrations by activity coefficients, f_i, of the surfactants in the interface.

$$\frac{1}{C_{12}} = \frac{y_1}{f_1^s C_1} + \frac{(1-y_1)}{f_2^s C_2^0} \tag{9.2}$$

In the Regular Solution Approximation, the activity coefficient is evaluated using the second-term of the Margules expansion approximations[10] to yield the nonideality parameter, β^s,

$$\ln f_1^s = (1-x_1)^2 \beta^s \quad \text{and} \quad \ln f_2^s = x_1^2 \beta^s \tag{9.3}$$

where x_i is the mole fraction of surfactant i in the mixed monolayer.

The numerical value of the interaction parameter, β^s , in the mixed monolayer may be found by iterative solution of the following pair of equations

$$\frac{x_1^2 \ln(C_{12} y_1 / C_1 x_1)}{(1-x_1)^2 \ln[C_{12}(1-y_1)/C_2(1-x_1)]} = 1 \tag{9.4}$$

$$\beta^s = \frac{\ln(C_{12} y_1 / C_1 x_1)}{(1-x_1)^2} \tag{9.5}$$

The surface composition and the interaction parameter of a binary mixture can be calculated by solving numerically both Equations 9.4 and 9.5, knowing the solution phase molar concentrations of the individual components required to achieve the surface tension value

2.4 Neutron reflectivity measurement and data analysis

All the neutron reflection measurements reported in this chapter were made using the reflectometer SURF at the Rutherford Appleton Laboratory in Didcot, Oxfordshire. The procedure for making the measurements has already been described in Chapter 2. The experiments were carried out at 25°C. Each solution was measured at fixed incident angle of 1.5°. The detector efficiency was calibrated with respect to D_2O. The data obtained were reduced by applying the scale factor before further analysis.

2.5 Determination of surface excess by neutron reflectivity

In this study, all the neutron reflectivity data were analysed using the Optical Matrix Method, which was described in Chapter 2. In this method, it is assumed that the interface can be described in terms of a number of discrete layers of different scattering length density and thickness. For the determination of the surface excess of one surfactant in a mixture at the air-solution interface, the reflectivity is measured for a mixture where one surfactant is deuterated and the other protonated in NRW. The measured reflectivity of the adsorbed layer will therefore result almost entirely from the deuterated surfactant. The procedure for determining the surface concentration is to fit this reflectivity profile by comparing it with a profile calculated using the optical matrix method from the fitting parameters, i.e. the scattering length density of the layer and its thickness. It is often adequate to describe the interface in terms of a one-layer model containing surfactant heads and chains, solvent and air. From the fitting parameters, the scattering length density of the layer, ρ, and its thickness, τ, the area per molecule, A, and the adsorbed amount, or surface excess, Γ, can be calculated by

$$A = \frac{b}{\rho\tau} = \frac{1}{\Gamma N} \tag{9.6}$$

where N is Avogadro's number.

The scattering lengths of the various species used in the neutron reflection experiments are given in Table 1.

It is straightforward to extend Equation 9.6 to the determination of surface excess for binary mixtures, when it becomes

$$\rho = \frac{1}{\tau}\left[\frac{b_1}{A_1} + \frac{b_2}{A_2}\right] \tag{9.7}$$

Ideally, the evaluation of the adsorbed amounts should be made with the nondeuterated surfactant having zero scattering length because Equation 9.7 then becomes identical with Equation 9.6. In practice it is more convenient to use the protonated form, and this will give rise to a small contribution to the reflectivity (see Table 1). In this case we use three isotopic combinations, which are: dA/hB, hA/dB, and dA/dB, where dA and hA denote deuterated and protonated surfactant A respectively, all in NRW. The fitting of each isotopic combination yields a set of values for layer thickness, τ, and scattering length density, ρ. Each set of fitting parameters is subsequently substituted in Equation 9.7 to produce three equations, which are solved simultaneously to give A_1 and A_2. From the area per molecule, the surface excess of each surfactant component, Γ_i, may be calculated using Equation 9.6.

Species	Scattering lengths x10^5 (Å)
d-EPE 3000-14	2,194.44
h-EPE 3000-14	360.88
d-SDS	276.23
h-SDS	15.98
d-DTAC	253.91
h-DTAC	-6.34
d-C_8E_4	248.98
h-C_8E_4	-21.68
H_2O	-1.68
D_2O	19.14
NRW (8.1%v/v D_2O)	0.00

Table 1: Values for the various species used in the neutron reflection experiments

3 Results and Discussion

3.1 Mixed Monolayer Formation in the SDS/EPE 3000-14 system

As discussed in the previous chapter binary mixtures of EPE 3000-14 and SDS are already known to depart widely from ideality in the micellar pseudophase. The strong deviation observed was however attributed to a significant dehydration of the micellar core. The surface tension of solutions of pure SDS and EPE 3000-14, and of the mixtures at two SDS:EPE 3000-14 molar ratios, 90:10 and 80:20, already shown in Chapter 8, are shown again here for convenience in Figure 2.

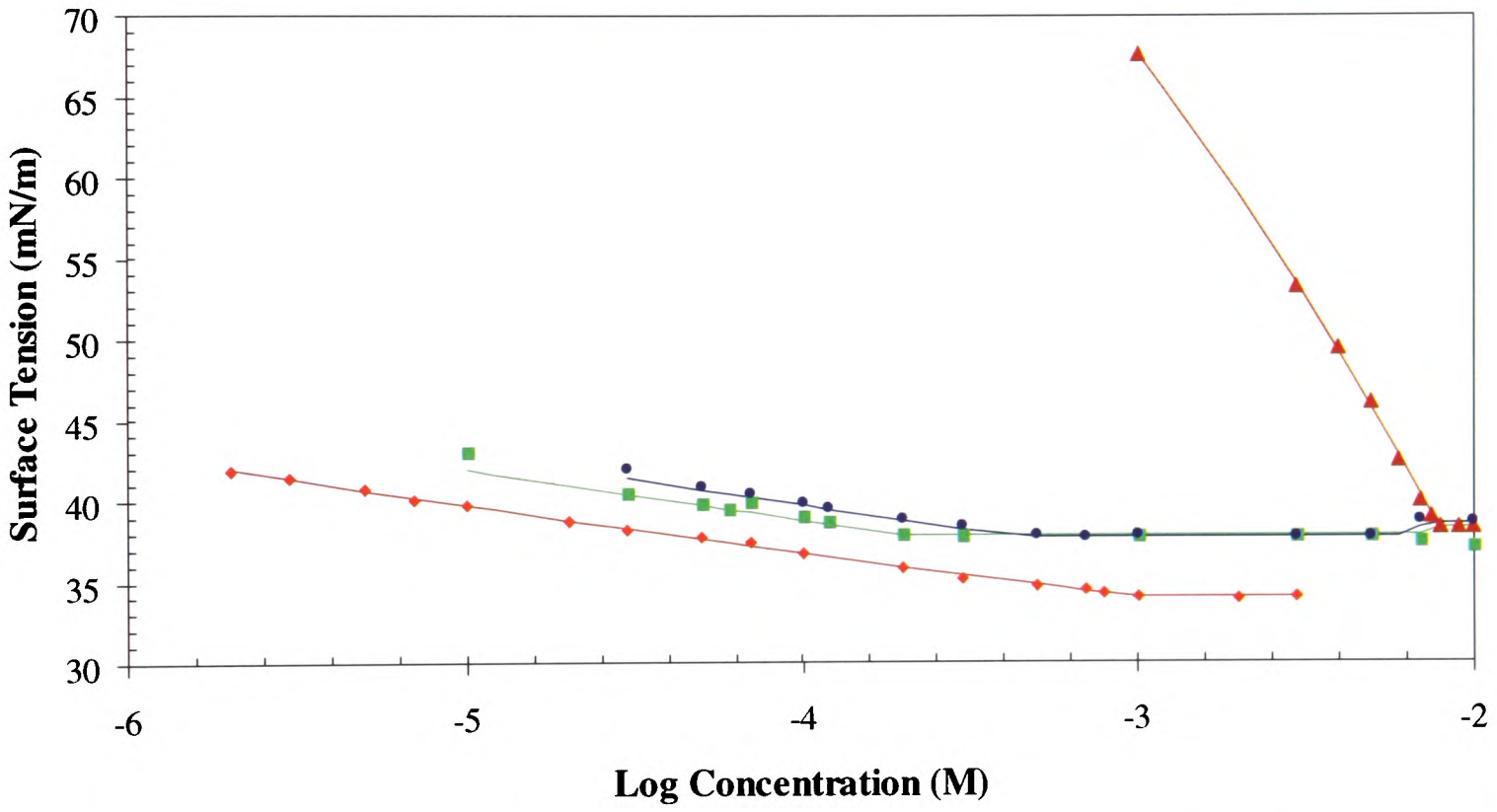


Figure 2. Surface tension against the log of the concentration for SDS, (▲), EPE 3000-14, (♦), and mixtures at y_{SDS}=0.9, (●), and y_{SDS}=0.8, (■) measured at 25°C.

Figure 2 shows that EPE 3000-14 is much more surface active than SDS. As consequence, the surface activity of their mixtures below the CMC is therefore dominated by EPE 3000-14. The limiting surface tensions of the mixtures at the CMC are given in Table 2.

Surfactant System	CMC (M)	π^{max} (mN/m)
SDS	$7.9x10^{-3}$	33.7
EPE 3000-14	$9.5x10^{-4}$	38.8
80:20 SDS/EPE 3000-14	$3.0x10^{-4}$	34.2
90:10 SDS/EPE 3000-14	$5.0x10^{-4}$	34.2

Table 2. The limiting surface pressure values obtained at 25°C.

The ideality of mixing can be assessed using the Pseudophase Separation Model, from which the concentration required to attain a specific surface pressure of the mixture is estimated from the concentrations required to achieve the same surface pressure value for each individual mixture components, in this case SDS and EPE 3000-14. Mixtures for which the predicted concentration does not agree with the experimental values are then said to be nonideal. Nonideality in mixed adsorbed layers is treated in much the same way as micelles by the introduction of activity coefficients into the appropriate thermodynamic surface equations of state[6-8]. Table 3 shows the results of the Pseudophase Separation Model analysis of the interfacial layer for the two bulk compositions studied here at various surface pressures.

Surface Pressure (mN/m)	80/20 SDS/EPE 3000-14			90/10 SDS/EPE 3000-14		
	$C_{SDS:EPE}$ (M)	β^s	x_{SDS}	$C_{SDS:EPE}$ (M)	β^s	x_{SDS}
32.3	$5.0x10^{-5}$	0	0.01	$1.0x10^{-4}$	0	0.01
33.8	$1.5x10^{-4}$	0	0.02	$3.0x10^{-4}$	0	0.03

Table 3. Surface composition of SDS/EPE 3000-14 solutions at 25°C

It is immediately clear that there is a considerable apparent difference between the interaction parameters obtained for the mixed monolayer formation and those obtained for micellar mixing. However, the apparently ideal behaviour of SDS/EPE 3000-14 mixtures at the interface is just the result of the dominance of the surface activity of the copolymer, which masks the true situation. In Figure 3 the surface tension against the concentration

of SDS/EPE 3000-14 mixture is replotted. At each concentration point, the resulting surface tension of the mixture is compared with those values of surface tension for the pure component taken at the concentration they are present in the mixture. Therefore in Figure 3, at a concentration of 10^{-3}M, for instance, the surface tension of the mixture at this concentration is compared with the values of surface tension for pure SDS at $9x10^{-4}$ and for pure EPE 3000-14 at 10^{-4}. At sub-micellar concentrations of the mixed systems the amount of SDS available at the air-solution interface is insignificant, and the resulting surface activity of the mixture is solely determined by the EPE 3000-14 concentration. It is known that a large difference in the surface activity of the two components makes it very difficult to determine the β^s parameter.

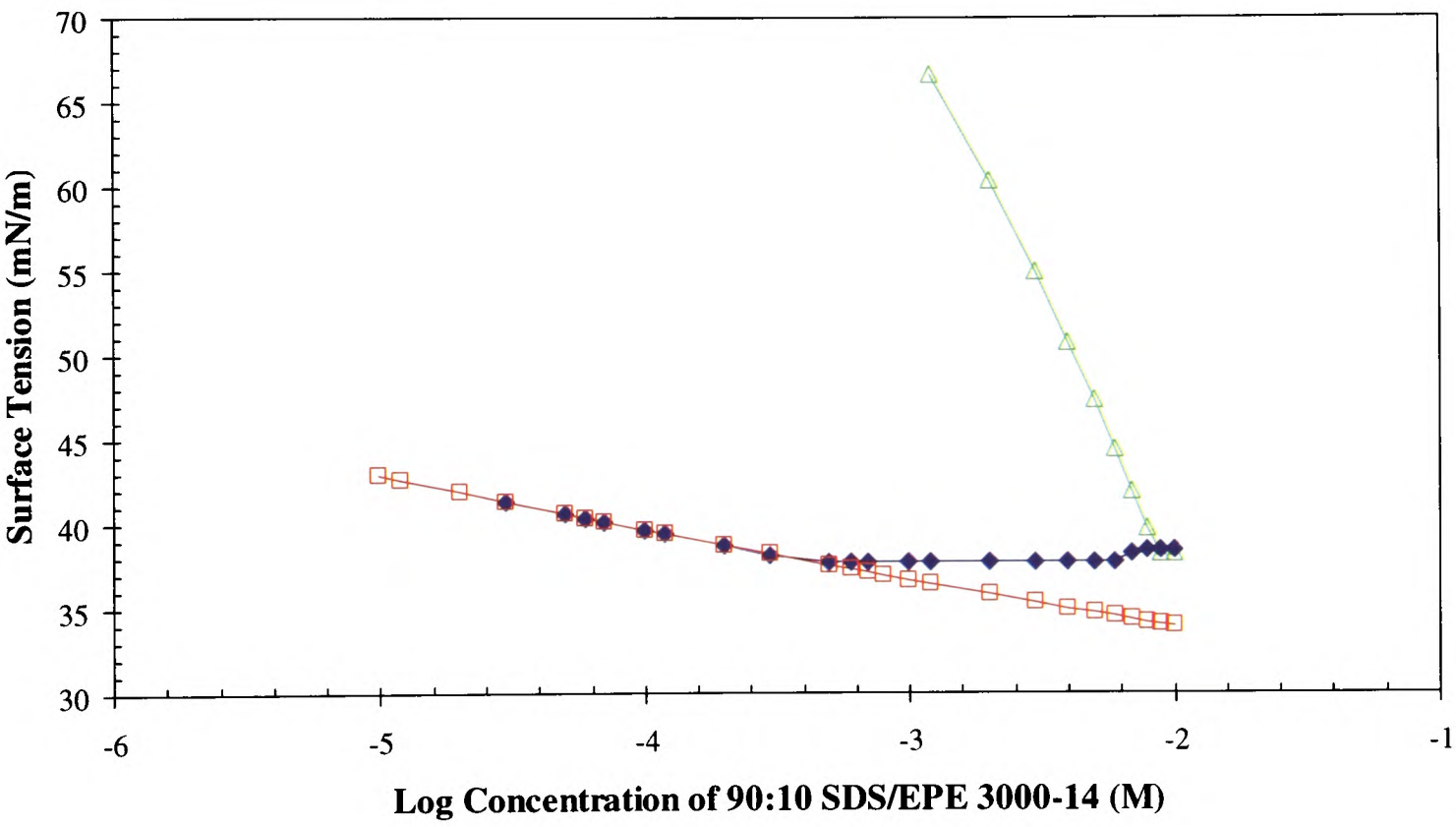


Figure 3. Surface tension against the log of the concentration for the SDS/EPE 3000-14 mixture at y_{SDS}=0.9, (♦). Curves with open symbols represent the surface tension of pure SDS, (△), and EPE 3000-14, (□), at each concentration point of the studied mixture

It has been shown previously that excellent agreement can be obtained between surface tension measurements and integrated surface excesses derived from neutron reflection data[5,11]. The advantage of neutron reflection is that it is a direct method for the determination of surface excess and composition and is more accurate than the results from the application of the Gibbs equation to surface tension measurements. Figures 4-7

show neutron reflectivity measurements for mixtures of SDS and EPE 3000-14 in the bulk mole ratio of 90:10, all in null reflecting water (NRW). For each mixture at each surfactant concentration, three isotopic contrasts were used, d-SDS/h-EPE 3000-14, h-SDS/d-EPE 3000-14, and d-SDS/d-EPE 3000-14, so that the individual excesses of each adsorbed species, as well as the total surface excess, could be determined.

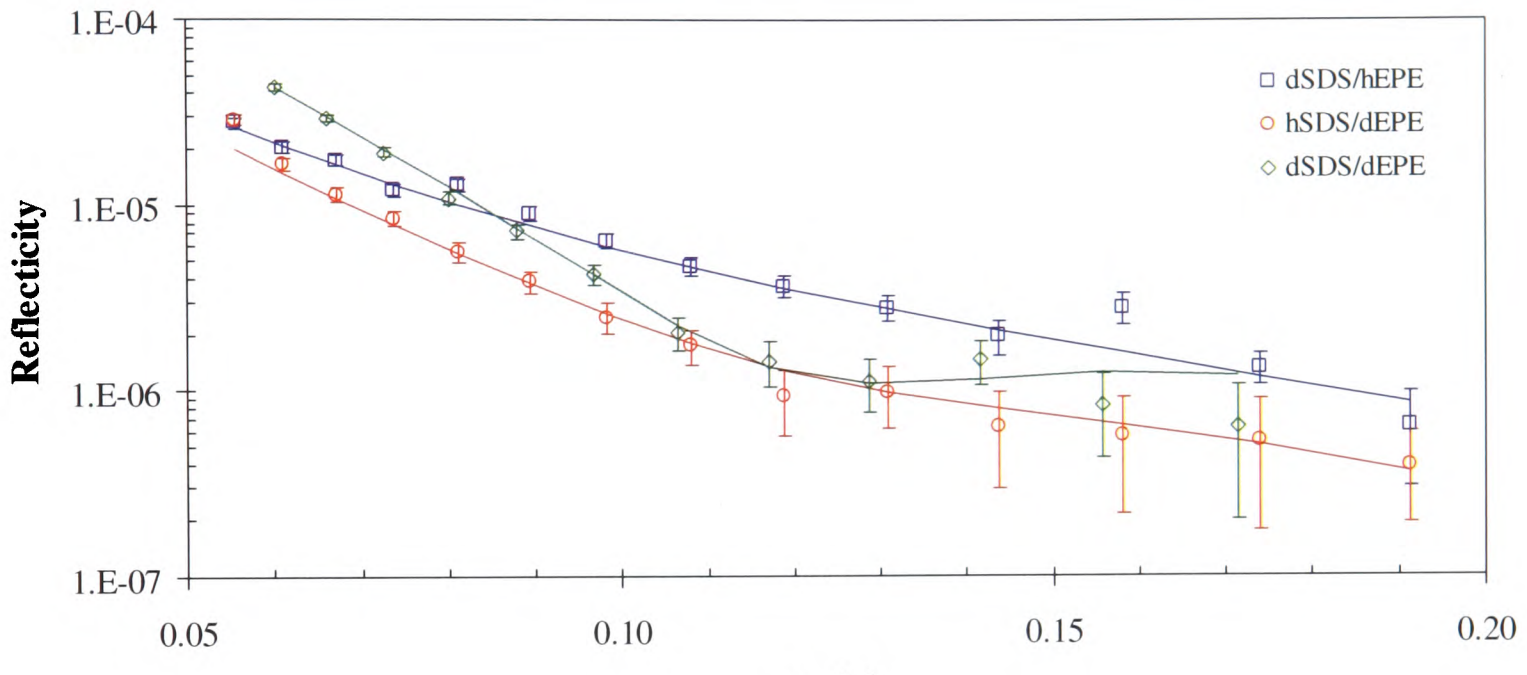


Figure 4. Neutron reflectivity profiles for 90/10 SDS/EPE 3000-14 mixtures at a bulk concentration of $7x10^{-3}$M. The continuous lines are best fits to the data.

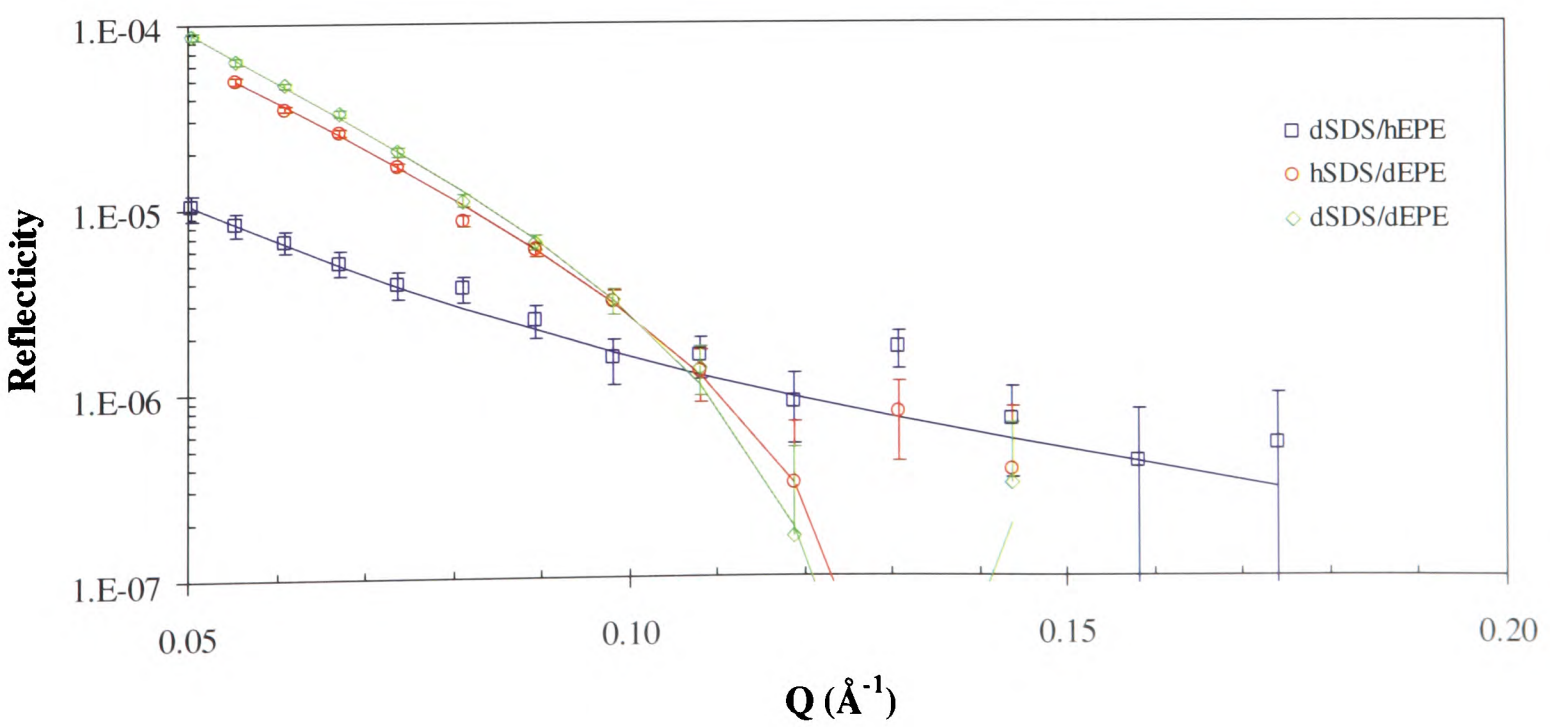


Figure 5. Neutron reflectivity profiles for 90/10 SDS/EPE 3000-14 mixtures at a bulk concentration of $1x10^{-3}$M. The continuous lines are best fits to the data.

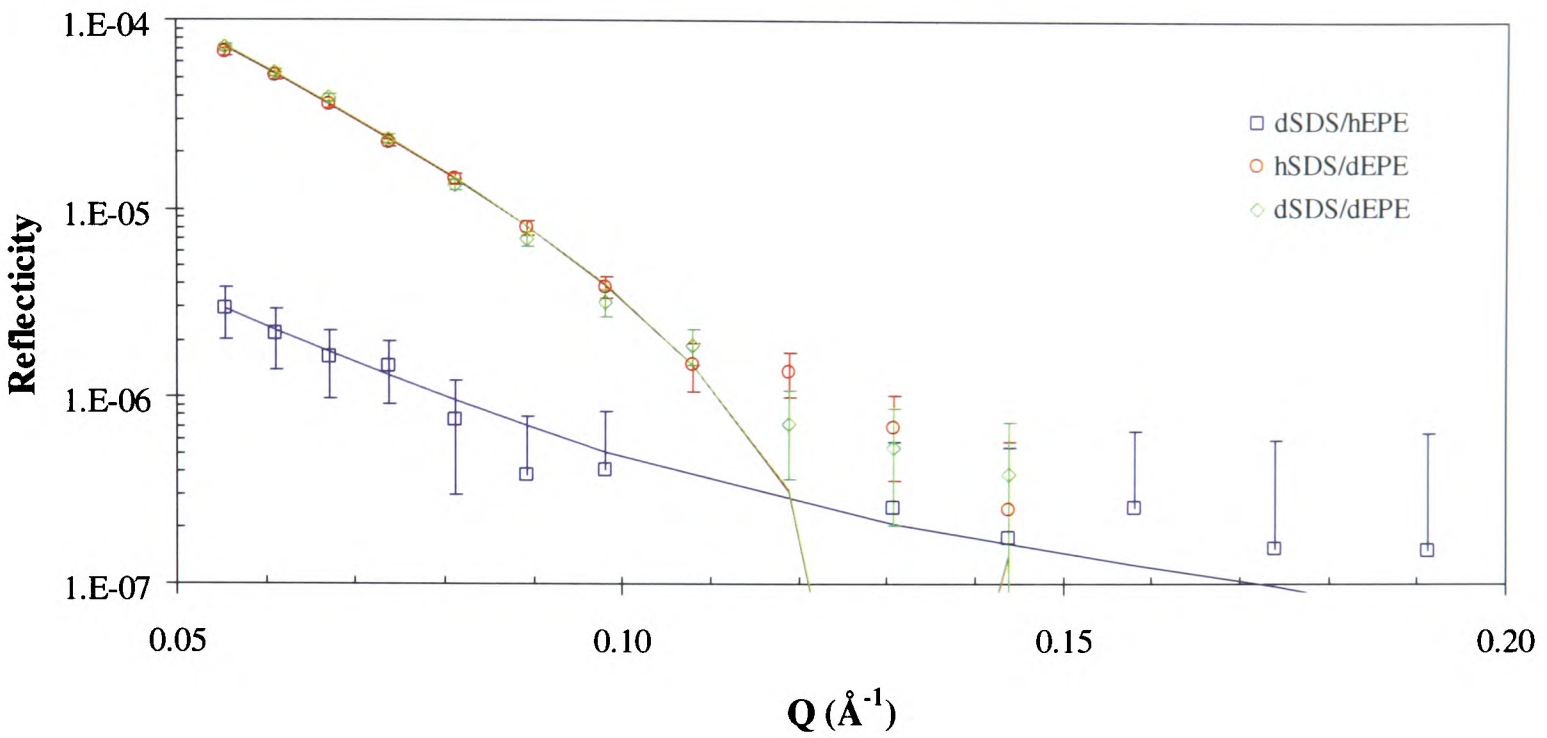


Figure 6. Neutron reflectivity profiles for 90/10 SDS/EPE 3000-14 mixtures at a bulk concentration of $3x10^{-4}$M. The continuous lines are best fits to the data.

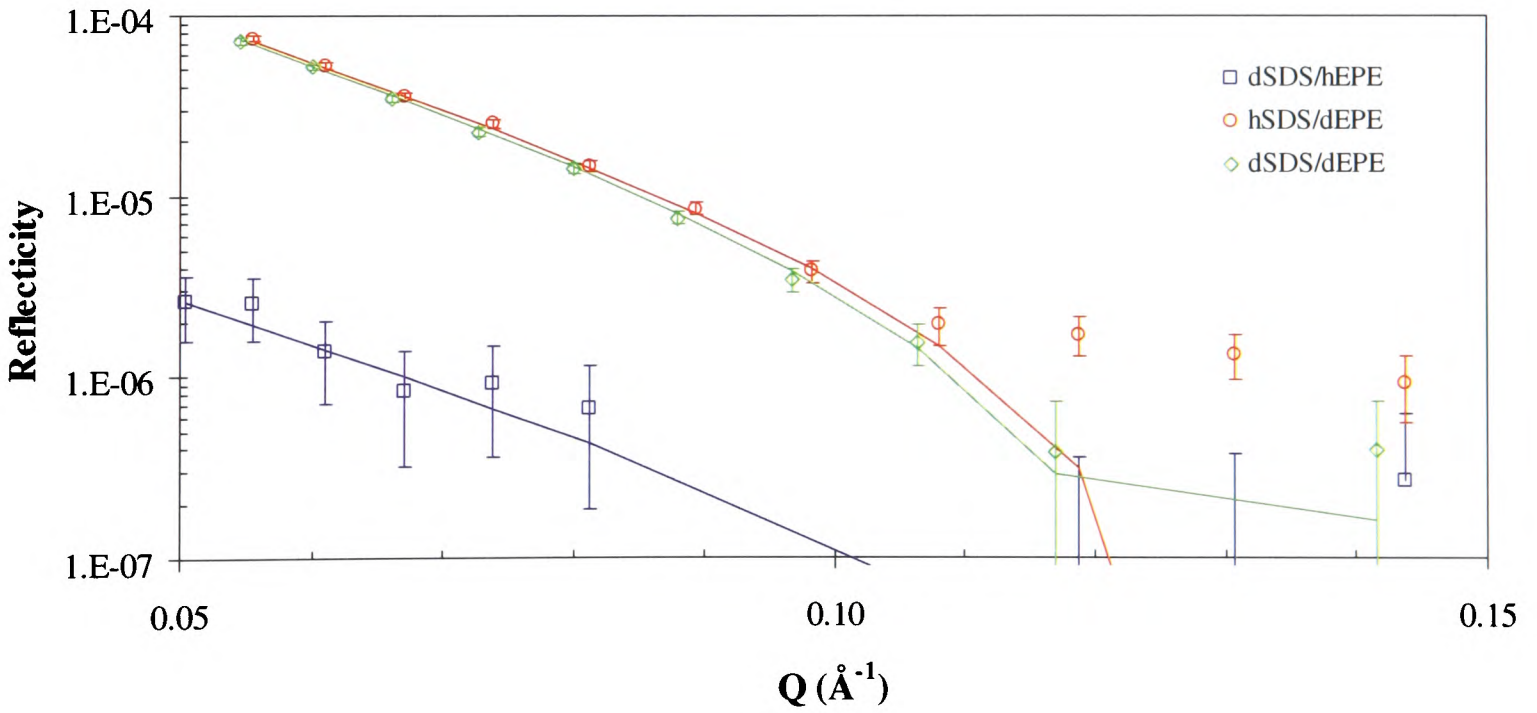


Figure 7. Neutron reflectivity profiles for 90/10 SDS/EPE 3000-14 mixtures at a bulk concentration of $1x10^{-4}$M. The continuous lines are best fits to the data.

Concentration (M)		$7x10^{-3}$			$1x10^{-3}$			$3x10^{-4}$			$1x10^{-4}$		
Layer	Parameters	dS/hE	hS/dE	dS/dE	dS/hE	hS/dE	dS/dE	dS/hE	hS/dE	dS/dE	dS/hE	hS/dE	dS/dE
1	τ/Å	20±2	20±2	46±4	20±2	48±4	48±4	19±2	48±4	48±4	19±2	48±4	49±4
	$\rho x10^6(Å^{-2})$	1.20	0.29	0.93	0.65	0.88	1.01	0.39	1.06	1.07	0.34	1.06	1.04
2	τ/Å	26±2	26±2		28±2			29±2			30±2		
	$\rho x10^6(Å^{-2})$	0.02	0.23		0.02			0.06			0.06		
Total	τ/Å	46±4	46±4	46±4	48±4	48±4	48±4	48±4	48±4	48±4	49±4	48±4	49±4
	$\rho x10^6(Å^{-2})$	0.53	0.53	0.93	0.28	0.88	1.01	0.19	1.06	1.07	0.17	1.06	1.04

	A ($Å^2$)	$\Gamma x10^{10}$ (mol/cm^2)	A ($Å^2$)	$\Gamma x10^{10}$ (mol/cm^2)	A ($Å^2$)	$\Gamma x10^{10}$ (mol/cm^2)	A ($Å^2$)	$\Gamma x10^{10}$ (mol/cm^2)
SDS	138±10	1.20±0.10	410±30	0.41±0.05	-	0	-	0
EPE 3000-14	950±80	0.17±0.05	525±40	0.32±0.05	432±30	0.38±0.05	430±30	0.39±0.05
SDS/EPE 3000-14		1.38±0.10		0.77±0.05		0.38±0.05		0.39±0.05

Table 4. Parameters and surface excesses obtained from the neutron reflectivity of three isotopic combinations dSDS/hEPE 3000-14 (dS/hE), hSDS/dEPE 3000-14 (hS/dE), dSDS/dEPE 3000-14 (dS/dE), at different bulk concentrations.

The data are fitted to a model using just two parameters, the thickness of the interfacial layer and its scattering length density. This model is fitted to the sets of isotopic data in such a way as to give a consistent area per molecule of each surfactant species. Up to the bulk concentration of 10^{-3}M a single-layer model was suitable to fit the reflectivity curves for both isotopic combinations of h-SDS/d-EPE 3000-14 and d-SDS/d-EPE 3000-14. Although the single-layer model would also fit the reflectivity curve for d-SDS/h-EPE 3000-14 combination, a two-layer one was applied in order to yield values of area per surfactant species consistent with the other isotopic combinations. The results obtained by this method of fitting together with the individual coverages calculated from areas per molecule using Equation 9.6 are given in Table 4. It shows that below the mixed CMC, the surface concentration of SDS is indeed negligible. However as the bulk concentration exceeds the mixed CMC, there is a substantial increase in the SDS mole fraction at the interface and the surface composition tends towards the bulk composition in agreement with the Regular Solution Model. The evolution of the surface composition to that of the bulk has been observed previously[2,3] and it is consistent with systems where the interactions between the monomers are independent of geometry and packing constraints.

C^{bulk} M	C^{bulk}/CMC	x_{SDS}	Γ_{EPE} x10^{10} mol/cm^2	$\tau_{EPE:SDS}$ Å	τ_{EPE} Å
$1x10^{-4}$	0.20	0.00	0.39	49	47-49
$3x10^{-4}$	0.60	0.08	0.38	48	47
$1x10^{-3}$	2.00	0.56	0.32	48	47
$7x10^{-3}$	14.00	0.87	0.17	46	43-44

Table 5. Mixed monolayer mole fraction of SDS, x_{SDS}, EPE 3000-14 surface excess, Γ_{EPE}, and monolayer thickness, $\tau_{EPE:SDS}$, for SDS:EPE 3000-14 90:10 at a range of bulk concentration normalised to the mixed CMC value. τ_{EPE} is the monolayer thickness for pure EPE 3000-14 equivalent to the copolymer surface coverage in the mixture.

The reflectivity fitting parameters given in Table 4 provide some interesting features of the structure of the mixed monolayer. In Chapter 6 it has been demonstrated that the monolayer structure of pure EPE at the air-liquid interface comprises an uppermost layer,

which extends outside the water and contains only PO groups, and a layer in the aqueous phase that contains few PO and all EO groups. The single-layer model used to fit the reflectivity profile of the partially deuterated EPE 3000-14 was, however, shown to be generally insensitive to the protonated PO groups due to its low scattering density. The contribution to the reflectivity of the partially deuterated EPE 3000-14 was almost entirely from the deuterated PEO groups buried inside the aqueous phase. A comparison between the layer thickness for the d-SDS/d-EPE 3000-14 mixtures and that for pure EPE 3000-14 obtained using the single-layer model is shown in Table 5. When the actual surface excess of the copolymer is considered, the results of layer thickness for both mixtures and pure copolymer up to 10^{-3}M are in fact equivalent, within ±1Å. This implies that the distribution of EO groups inside the mixed monolayer appears to be same as in that for pure copolymer. This is as would be expected, at least for the two most dilute concentrations of the mixture, i.e. 10^{-4} and $3x10^{-4}$M, as the surface concentrations of SDS in both solutions are negligible. However at a bulk concentration of 10^{-3}M, the molar ratio of SDS in the monolayer, x_{SDS}, measured by neutron reflection has substantially increased to 0.56. The values of thickness obtained from the data fitting for both isotopic combinations h-SDS/d-EPE 3000-14 and d-SDS/d-EPE 3000-14 were however the same, 48Å, which implies that the greater fraction of the deuterated tails of SDS must be located inside the aqueous phase and mixed together with the EO groups. Baglioni *et al.*[12] have investigated the positions of the SDS headgroups relative to the ethylene oxide region of the nonionic surfactant in mixed micelles of SDS/$C_{12}E_6$. From the analysis of the results of electron spin echo modulation of doxylstearic acids in mixed micelles, they concluded that the SDS headgroup is located in the hydrophilic region close to the micelle surface. In the case of the thick SDS/EPE 3000-14 monolayer, for the SDS headgroups to be located close to the main aqueous part of the overall layer-solution interface, the SDS hydrophobic tails would also have to be mostly adsorbed in the hydrated layer. At $7x10^{-3}$M (14.0CMC), the concentration is far in excess of the mixed CMC value and the structure of the mixed monolayer appears to be more complex. A two-layer model was used to fit the reflectivity curves for the h-SDS/d-EPE 3000-14 and d-SDS/h-EPE 3000-14 combinations. This suggests that the fragment distribution within the mixed monolayer is substantially changed at this concentration. The surface excess of the copolymer is reduced to $0.17x10^{-10}$ mol/cm^2. The same copolymer coverage in a

solution of pure EPE 3000-14 would be distributed in a monolayer 43-44Å thick, which is thinner than the 46Å measured for the combination of d-SDS/d-EPE 3000-14. This increase of the monolayer thickness may now be the result of the penetration of a fraction of the deuterated chains of SDS into the low scattering layer of PPO outside the water.

The study of the interaction between SDS and EPE 3000-14 has been complicated by the large difference in the surface activity of the two components. However the surface activity of ionic surfactants can be considerably modified in the presence of electrolytes. To study the effect of electrolyte on the interaction between SDS and EPE 3000-14 in the interfacial layer, the surface tension of the systems studied above was measured in the presence of 0.1M NaCl. The surface tension curves, already shown in Chapter 8, are shown again in Figure 8 for convenience.

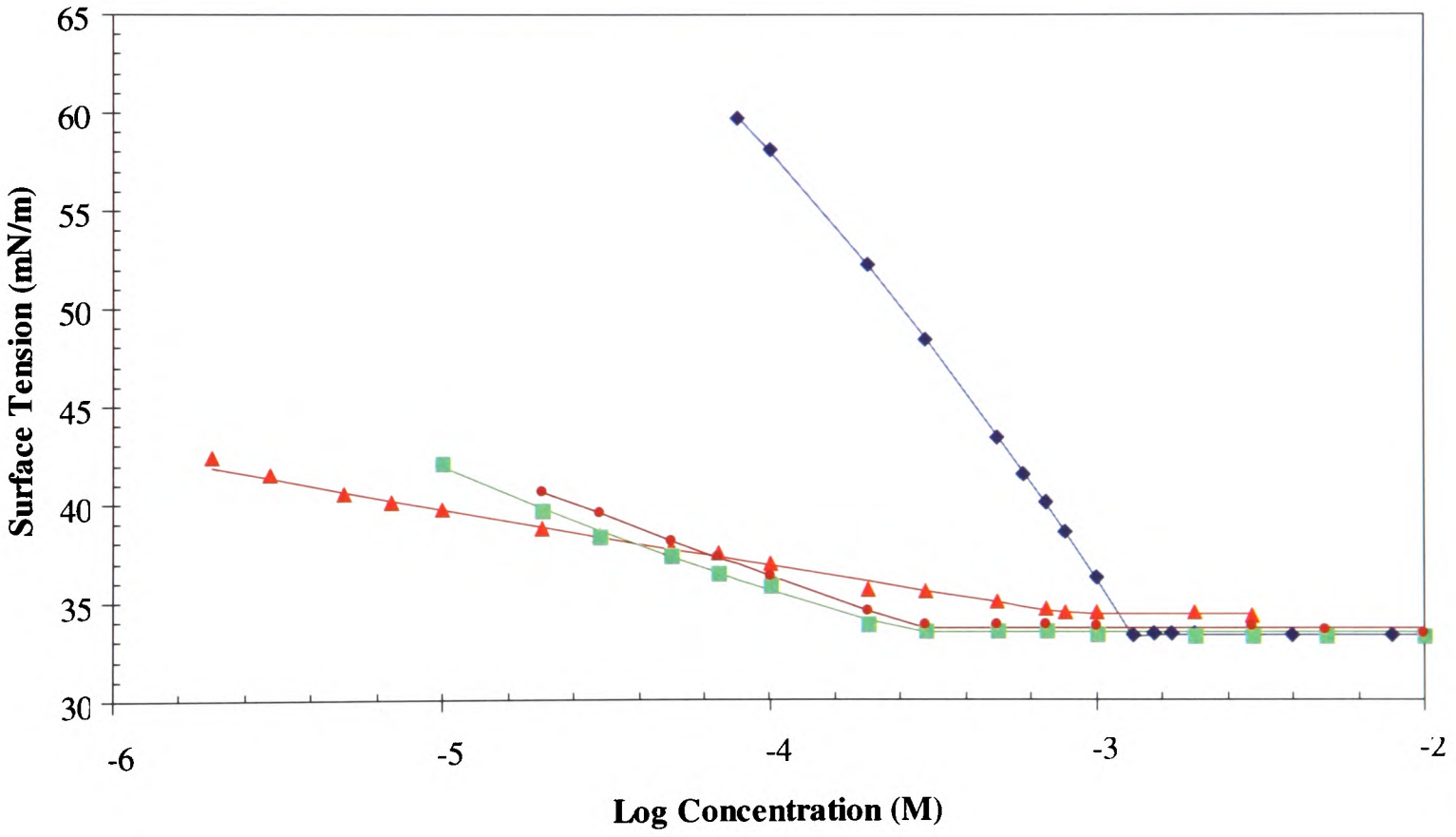


Figure 8. Surface tension against the log of the concentration for SDS, (♦), EPE 3000-14, (▲), and mixtures at y_{SDS}=0.9, (●), and y_{SDS}=0.8, (■) in 0.1M NaCl solutions measured at 25°C.

The effect of NaCl on the surface activity of SDS is attributed mainly to the decrease in the thickness of the electrical double layer surrounding the ionic headgroups and the

consequent decreased electrostatic repulsive interactions between the SDS headgroups. As can be seen from Figure 8, the surface activity of pure SDS is greatly increased, whereas that of EPE 3000-14 is only weakly affected in a background of 0.1M NaCl. Figure 2 showed that the surface tension curve of SDS/EPE 3000-14 mixtures in pure water is similar to that of pure EPE 3000-14. However in the presence of salt, the curves combine features of both SDS and EPE 3000-14. Mixtures of the two surfactants in the presence of salt results in enhanced interaction with low values of the CMC and a surface tension reduction. The values for the limiting surface pressures obtained from the plots in Figure 8 are given in Table 6.

Surfactant System	CMC (M)	π^{max} (mN/m)
SDS	$1.3x10^{-3}$	38.7
EPE 3000-14	$8.2x10^{-4}$	37.6
80:20 SDS/EPE 3000-14	$2.4x10^{-4}$	38.5
90:10 SDS/EPE 3000-14	$2.9x10^{-4}$	38.3

Table 6. Values of the limiting surface pressure values obtained at the CMCs at 25°C.

Surface Pressure (mN/m)	80/20 SDS/EPE 3000-14			90/10 SDS/EPE 3000-14		
	$C_{SDS:EPE}$ (M)	β^s	x_{SDS}	$C_{SDS:EPE}$ (M)	β^s	x_{SDS}
32.5	$2.4x10^{-5}$	-5.3	0.32	$3.0x10^{-5}$	-6.1	0.38
34.7	$5.5x10^{-5}$	-6.9	0.44	$7.0x10^{-5}$	-7.2	0.48
35.7	$8.0x10^{-5}$	-7.2	0.47	$1.0x10^{-4}$	-7.5	0.52

Table 7. Surface composition of SDS/EPE 3000-14 solutions in the presence of 0.1M NaCl at 25°C.

Nonideality in the mixed monolayer has been treated by the Pseudophase Separation Model developed by Rosen[6,13] using the surface tension measurements. The derived values of the interaction parameter, β^s at each composition are given in Table 7 together

with values of the predicted monolayer composition. The results show when the surface activity of SDS is increased by the addition of salt, the mixing in the interfacial layer becomes nonideal and the strong attractive interaction is of a similar magnitude to those observed in the mixed micelles described in the previous chapter. The values of the interaction parameter, β^M, for mixed micelle formation found for SDS/EPE 3000-14 in pure water were -9.7 for a composition of y_{SDS}=0.8, and –8.8, for a composition of y_{SDS}=0.9. In the presence of 0.1M NaCl, the β^M values were –6.6 and -6.8, respectively.

The values of β^s vary with surface pressure in the manner expected given the nature and composition of the interfacial layer. Variations of β^s with surface pressure were also reported by Hines *et al.*[14] from the application of the Pseudophase Separation Model to the surface tension data from strongly interacting mixtures of SDS and C_{12}-betaine. At high surface pressures, the interface is highly concentrated in surfactant species and areas per adsorbed molecule typically approach those calculated for close packing. As the surface pressure is decreased, however, the surface excess concentrations of adsorbed species are reduced (reaching a limit of zero when the surface pressure is zero). At this point, the interfacial concentration and composition is identical to that in the bulk, where the interactions become ideal due to the low concentrations of surfactant monomer in aqueous solution. Thus the value of β^s must approach zero as π approaches zero. In the case of SDS/EPE 3000-14 systems the difference in the surface activity between the two species at very low concentrations is also likely to contribute to the variation of β^s.

The suitability of the Pseudophase Separation Model to describe the surface composition for SDS/EPE 3000-14 systems can be assessed by comparing the predicted surface compositions with those compositions derived directly by neutron reflection. Figures 9-12 show neutron reflectivity measurements from the binary mixtures of SDS and EPE 3000-14 in the bulk mole ratio of 90:10, where three different isotopic compositions have been studied. All solutions were in null reflecting water. The curves were fitted to a suitable model to yield a value of area per molecule of each surfactant consistent within the set of isotopic combinations. The results obtained from fitting the data together with the calculated coverages are tabulated in Table 8.

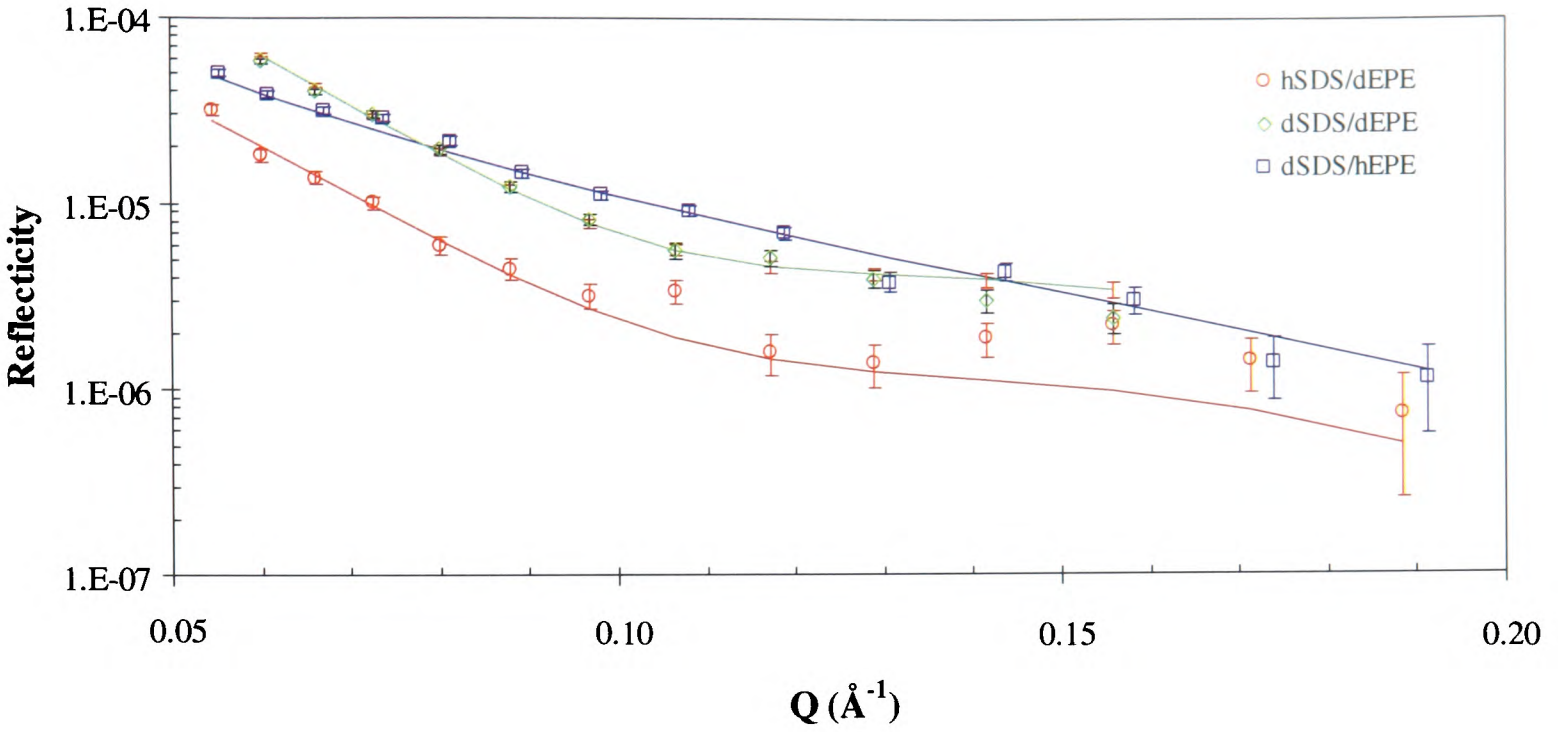


Figure 9. Neutron reflectivity profiles for 90/10 SDS/EPE 3000-14 mixtures at a bulk concentration of $3x10^{-3}$M and in the presence of 0.1M NaCl. The continuous lines are best fits to the data.

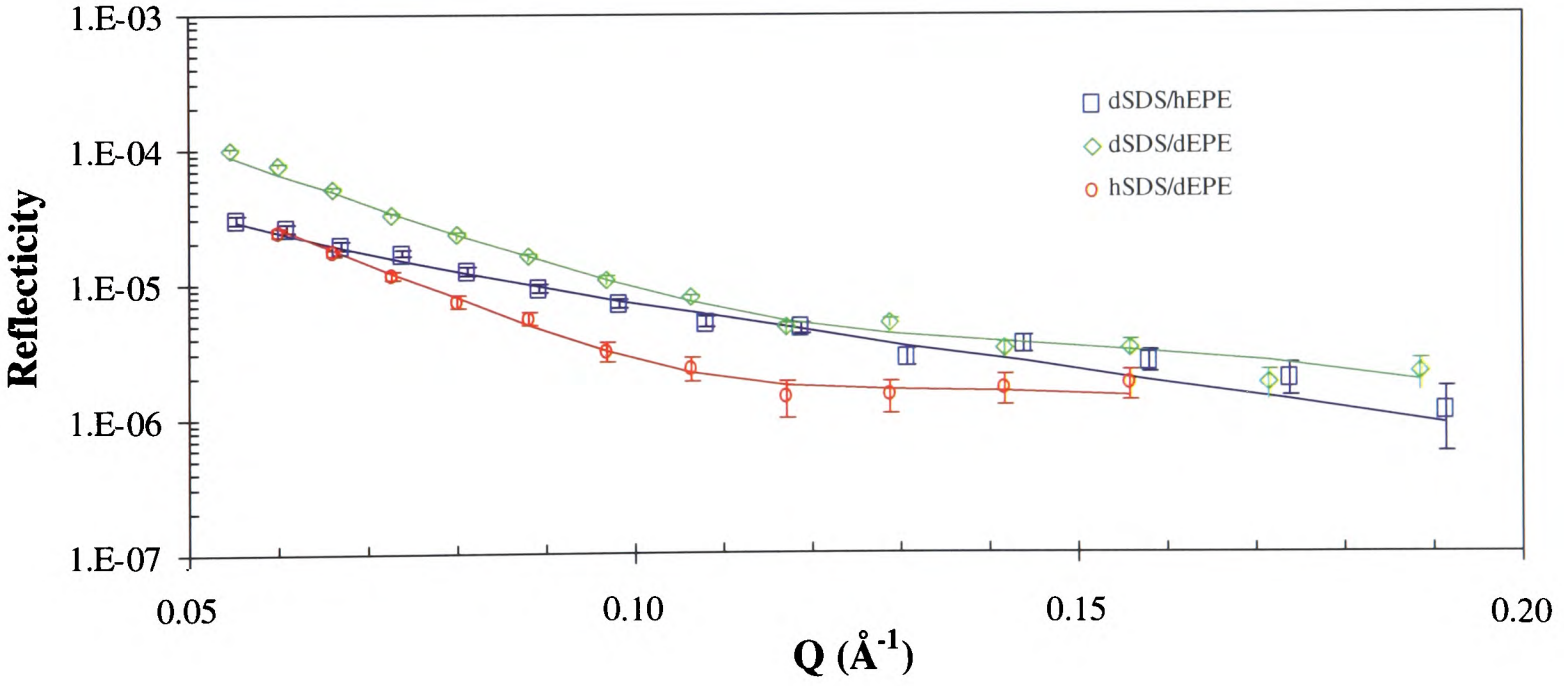


Figure 10. Neutron reflectivity profiles for 90/10 SDS/EPE 3000-14 mixtures at a bulk concentration of $7x10^{-4}$M and in the presence of 0.1M NaCl. The continuous lines are best fits to the data.

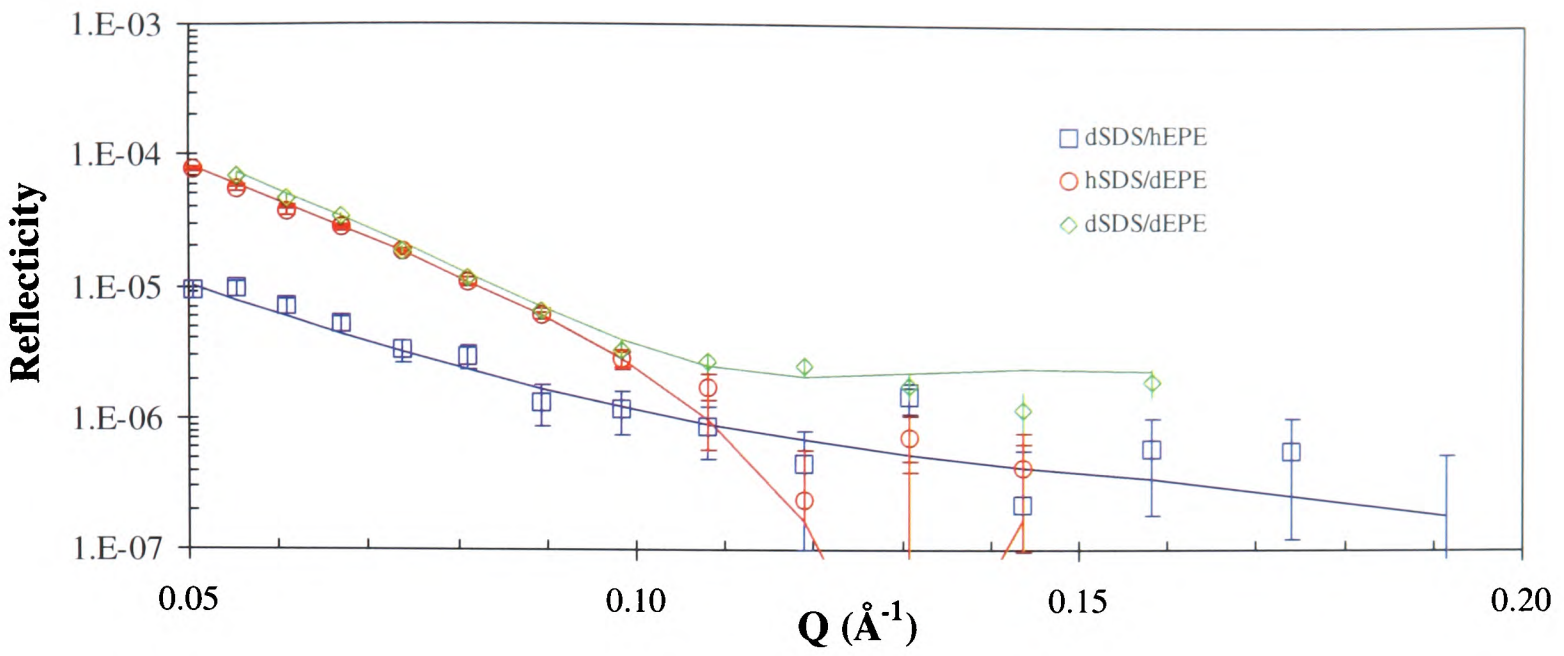


Figure 11. Neutron reflectivity profiles for 90/10 SDS/EPE 3000-14 mixtures at a bulk concentration of $1x10^{-4}$M and in the presence of 0.1M NaCl. The continuous lines are best fits to the data.

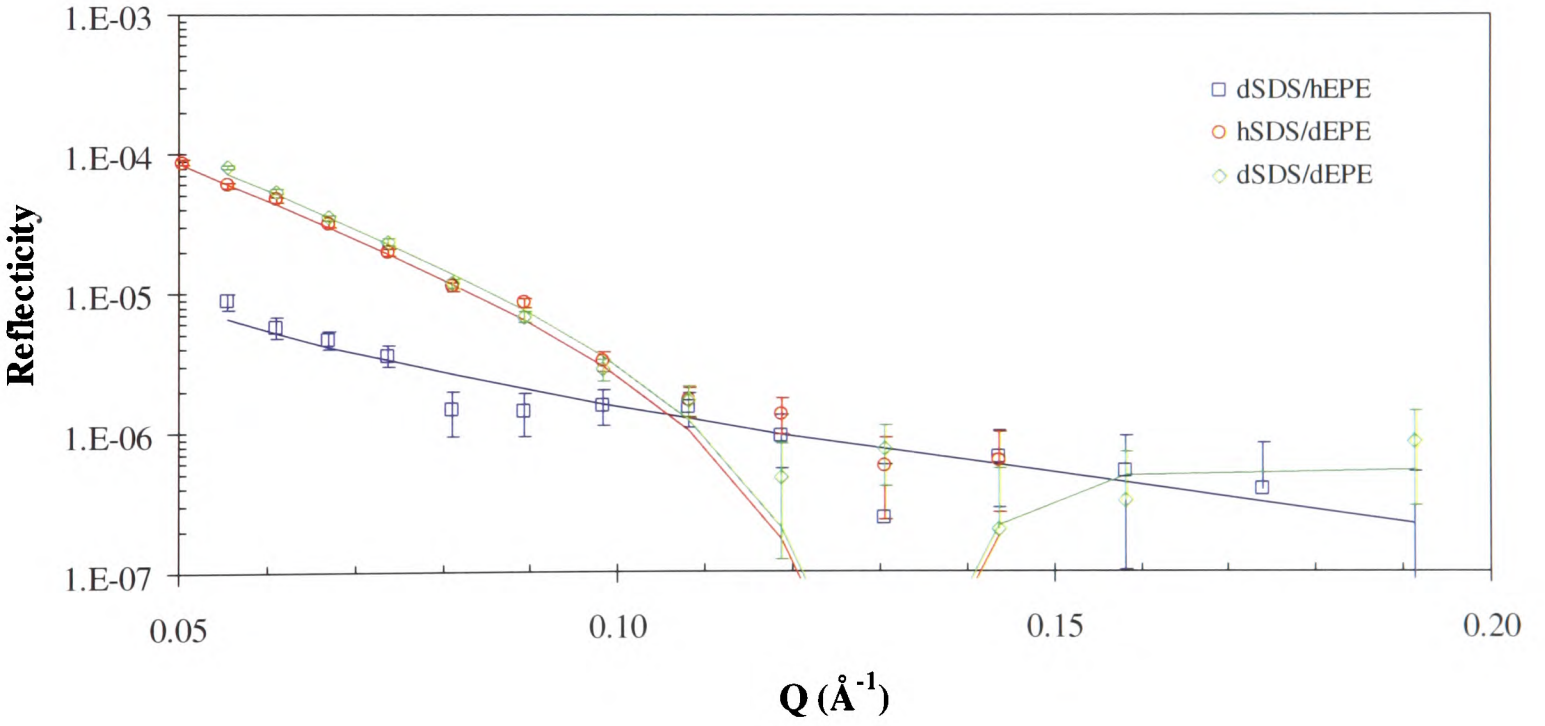


Figure 12. Neutron reflectivity profiles for 90/10 SDS/EPE 3000-14 mixtures at a bulk concentration of $7x10^{-5}$M and in the presence of 0.1M NaCl. The continuous lines are best fits to the data.

Concentration (M)		$3x10^{-3}$			$7x10^{-4}$			$1x10^{-4}$			$7x10^{-5}$			$3x10^{-5}$		
Layer	Parameters	dS/hE	hS/dE	dS/dE	dS/hE	hS/dE	dS/De	dS/hE	hS/dE	dS/dE	dS/hE	hS/dE	dS/dE	dS/hE	hS/dE	dS/dE
1	τ/Å	16±2	16±2	16±2	16±2	16±2	16±2	20±2	48±4	20±2	17±2	49±4	49±4	19±2	47±4	48±4
	$\rho x10^6(Å^{-2})$	1.96	0.09	2.01	1.54	1.33	1.73	0.65	0.93	1.83	0.68	0.97	1.06	0.48	1.02	1.02
2	τ/Å	32±3	32±3	32±3	35±3	35±3	35±3	28±2		28±2	32±3			29±2		
	$\rho x10^6(Å^{-2})$	0.09	0.70	0.64	0.06	0.34	0.73	0.02		0.50	0.02			0.01		
Total	τ/Å	48±4	48±4	48±4	51±4	51±4	51±4	48±4	48±4	48±4	49±4	49±4	49±4	48±4	47±4	48±4
	$\rho x10^6(Å^{-2})$	0.71	0.50	1.10	0.52	0.65	1.04	0.28	0.93	1.05	0.25	0.97	1.06	0.20	1.02	1.02

	A ($Å^2$)	$\Gamma x10^{10}$ (mol/cm^2)	A ($Å^2$)	$\Gamma x10^{10}$ (mol/cm^2)	A ($Å^2$)	$\Gamma x10^{10}$ (mol/cm^2)	A ($Å^2$)	$\Gamma x10^{10}$ (mol/cm^2)	A ($Å^2$)	$\Gamma x10^{10}$ (mol/cm^2)
SDS	91±10	1.82±0.15	130±10	1.28±0.10	450±40	0.37±0.05	600±50	0.28±0.05	-	0.06±0.05
EPE 3000-14	980±80	0.17±0.05	690±60	0.24±0.05	495±40	0.34±0.05	465±40	0.36±0.05	460±40	0.36±0.05
SDS/EPE 3000-14		1.99±0.15		1.52±0.15		0.70±0.05		0.63±0.05		0.42±0.05

Table 8. Parameters and surface excesses obtained neutron reflectivity of three isotopic combinations dSDS/hEPE 3000-14 (dS/hE), hSDS/dEPE 3000-14 (hS/dE), dSDS/dEPE 3000-14 (dS/dE), at different bulk concentrations all in 0.1M NaCl.

The comparison between the interfacial compositions predicted from the Pseudophase Separation Model at a series of surface pressures with experimental values derived from the neutron reflectivity data is given in Table 9.

Surface Pressure (mN/m)	90/10 SDS/EPE 3000-14				
	$C_{SDS:EPE}$ (M)	Ideal Mixing	Nonideal Mixing		Neutron Reflection
		$x_{SDS}^{pred.}$	β^s	$x_{SDS}^{pred.}$	$x_{SDS}^{obs.}$
32.5	3.0×10^{-5}	0.13	-6.1	0.38	0.15
34.7	7.0×10^{-5}	0.41	-7.2	0.48	0.44
35.7	1.0×10^{-4}	0.58	-7.5	0.52	0.56
40.6	7.0×10^{-4}	-	-	-	0.84
44.2	3.0×10^{-3}	-	-	-	0.88

Table 9. Surface composition of SDS/EPE 3000-14 solutions in 0.1M NaCl at 25°C

Because of the high SDS bulk fraction, the surface composition is not sensitive to whether the mixing is ideal or nonideal with a β^s of about –7.0. Note that, although β^s is insensitive to the composition and therefore to the neutron measurements, it is nevertheless well defined by the surface tension measurements. The insensivity of the surface composition to β^s can be seen clearly in Figure 13 where the effect of variation of β^s on the surface composition is plotted as a function of bulk mole fraction of SDS. Near an SDS bulk fraction of 0.9, variation of β^s has almost no effect on the surface composition. At this bulk mole fraction, then, only the ideal model is being tested, not the evaluation of the nonideal activity coefficients. Furthermore at a bulk fraction of 0.85, the surface composition should be entirely independent of nonideality.

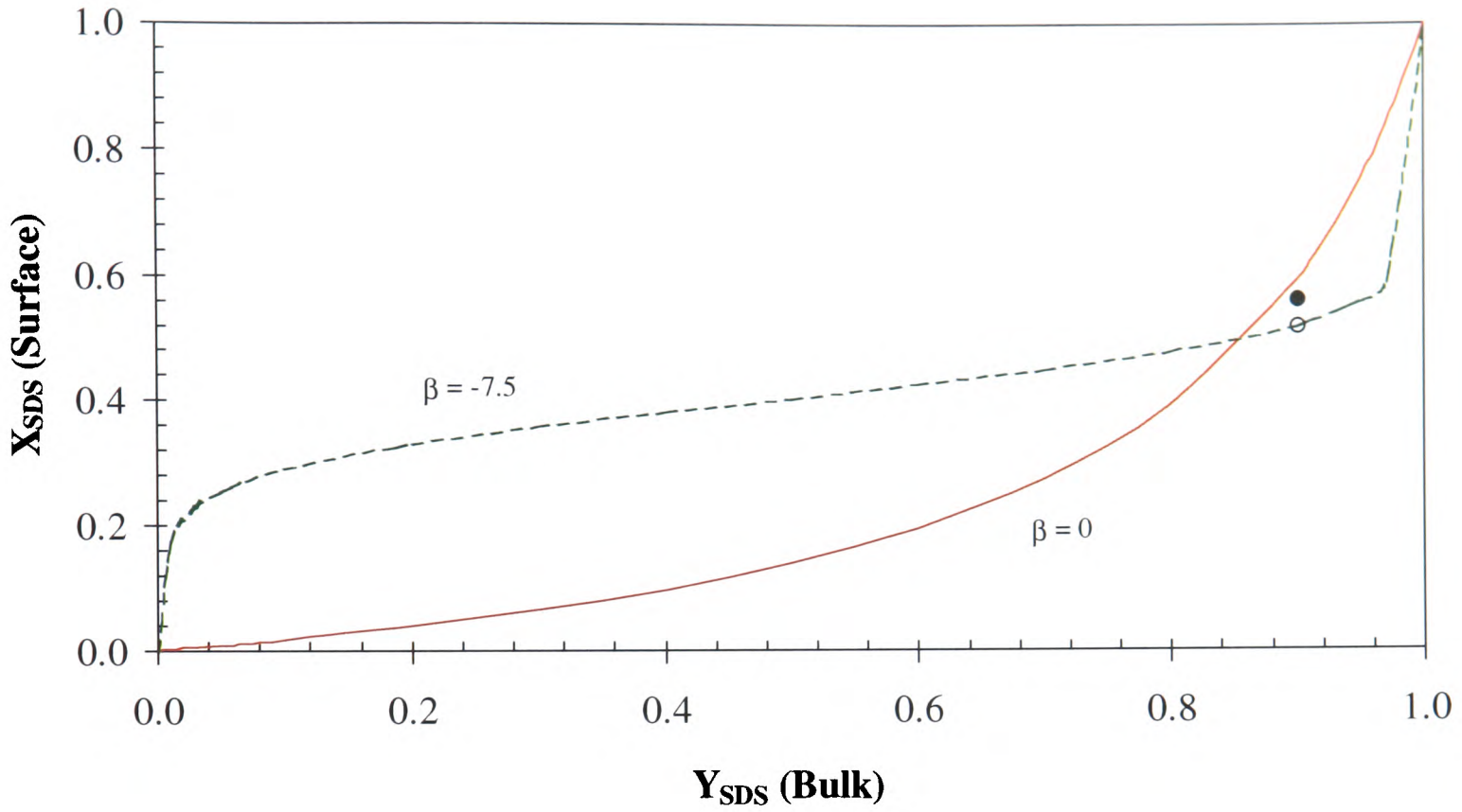


Figure 13. Variation of surface composition with bulk composition for the SDS/EPE 3000-14 system in the presence of 0.1M NaCl for two values of the interaction parameter calculated using the Pseudophase Separation Model. The open circle is calculated from the experimental surface tension data using Regular Solution Model at a surface pressure of 35.7mN/m. The solid circle is the surface composition observed by neutron reflection.

In the presence of 0.1M NaCl, SDS is much more surface active and its presence inside the mixed monolayer can be detected down to the bulk concentration of $7x10^{-5}$M as shown in Table 10. Below the mixed CMC value, the monolayer of the h-SDS/d-EPE 3000-14 mixtures has, within ±2Å, the same thickness as that containing pure EPE 3000-14 at the same surface coverage. This again suggests that the deuterated chains of SDS are, at least, partly mixed into the hydrated layer where the PEO groups of the copolymer are found.

Above the CMC value, as in the system without swamping electrolyte, there is a substantial increase of the molar fraction of SDS in the mixed monolayer. A significant change in the monolayer structure appears to take place. At $7x10^{-4}$M, the monolayer is

mostly composed of SDS, its x_{SDS} is 0.84, and the copolymer appears largely displaced from the surface. The surface excess of the copolymer is reduced to 0.24×10^{-10} mol/cm^2.

C^{bulk} M	C^{bulk}/CMC	x_{SDS}	$\Gamma_{EPE} \times 10^{10}$ mol/cm^2	$\tau_{EPE:SDS}$ Å	τ_{EPE} Å
3×10^{-5}	0.10	0.15	0.36	48	47
7×10^{-5}	0.24	0.44	0.36	49	47
1×10^{-4}	0.34	0.52	0.34	48	47
7×10^{-4}	2.41	0.84	0.24	51	43-44
3×10^{-3}	10.34	0.92	0.17	48	43-44

Table 10. Mixed monolayer mole fraction of SDS, x_{SDS}, EPE 3000-14 surface excess, Γ_{EPE}, and monolayer thickness, $\tau_{EPE:SDS}$, for SDS:EPE 3000-14 90:10 at a range of bulk concentration normalised to the mixed CMC value. τ_{EPE} is the monolayer thickness for pure EPE 3000-14 equivalent to the copolymer surface coverage in the mixture.

EPE 3000-14 is far more surface active than SDS, but it can still be displaced from the monolayer as seen above. In general the displacement of a surfactant from the interface by a second surfactant can take place either by the solubilisation of the adsorbed surfactant into micelles or by a switchover of dominant surface-active component with concentration. In Chapter 5 we showed that the EPE 3000-14 can saturate the interface at concentrations as low as 10^{-5}M. When mixed with SDS, within the concentration range studied here, the surface excess of the copolymer remains constant below the mixed CMC, which indicates that the interface is saturated, as shown in Figure 14. As the bulk concentration of the mixture exceeds the mixed CMC, the concentration of the copolymer at the interface drops rapidly. This suggests that the displacement is probably a result of the incorporation of copolymer molecules into the mixed micelles. The displacement of Pluronic surfactants from the interfacial monolayer of mixture with SDS has been observed previously. The surface tension of solutions of binary mixtures of Pluronic F127 and SDS studied by Hecht *et al.* [1] is depicted in Figure 1. They explained the increase in surface tension of Region II, which goes from about 0.4mM to 2.0mM SDS, in terms of the binding of SDS molecules to the EPE monomers resulting in the formation of less surface-active complexes, which would tend to desorb from the surface. We believe that

the Region II coincides with the formation of mixed micelles and the displacement from the interface is also triggered by the solubilisation of the copolymer by the mixed micelles. This argument is supported by a recent study by Li *et al.*[15] in which they investigated the interaction between SDS and unassociated Pluronic F127 using electromotive force (EMF) and isothermal titration calorimetry (ITC). They found that the concentration of SDS required to form mixed micelles in a solution of 0.1 and 0.01%w/v F127 is 0.13 and 0.15mM, respectively. An abrupt change in the monolayer composition at the mixed CMC has also been suggested by Nikas *et al.*[16] for mixtures of $C_{12}E_6$ and $C_{12}E_8$. The sudden change was rationalised in terms of the changes in the distribution of the two surfactant species between the bulk solution and the monolayer due to the onset of mixed micelle formation. The monolayer composition merely reflects the changes in monomer composition as mixed micelles are formed.

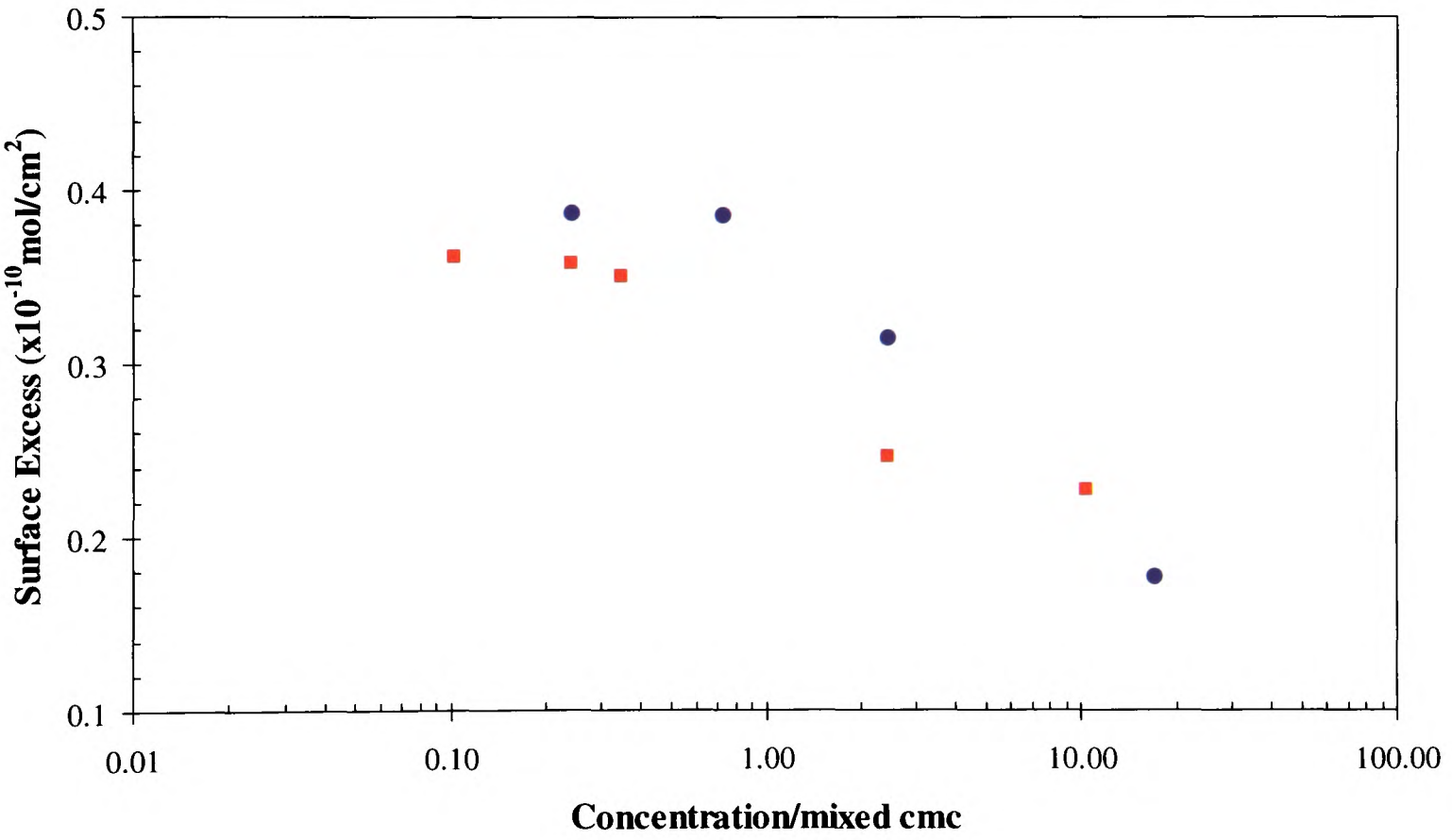


Figure 14. Surface excess of EPE 3000-14 in mixtures with SDS in pure water (●), in the presence of 0.1M NaCl (■). The concentration is normalised to the corresponding CMC.

The displacement of the copolymer from the mixed interface in the presence of 0.1M NaCl appears to be more substantial and abrupt than that without swamping electrolyte. This is likely to be a result of a changeover in the dominant surface active species between SDS and the block copolymer. We have shown in Figure 3 that EPE 3000-14 is

far more surface active than SDS below the mixed CMC and this situation carries over above the mixed CMC when no swamping electrolyte is present. However in a background of 0.1M NaCl, when the bulk concentration of the mixture reaches 10^{-3}M, SDS becomes more surface active than the copolymer and therefore will dominate the surface adsorption. In the same way done in Figure 3, in Figure 15 the surface tension values for the SDS/EPE 3000-14 mixture are compared with those values of surface tension for the pure component taken at the concentration they are present in the mixture.

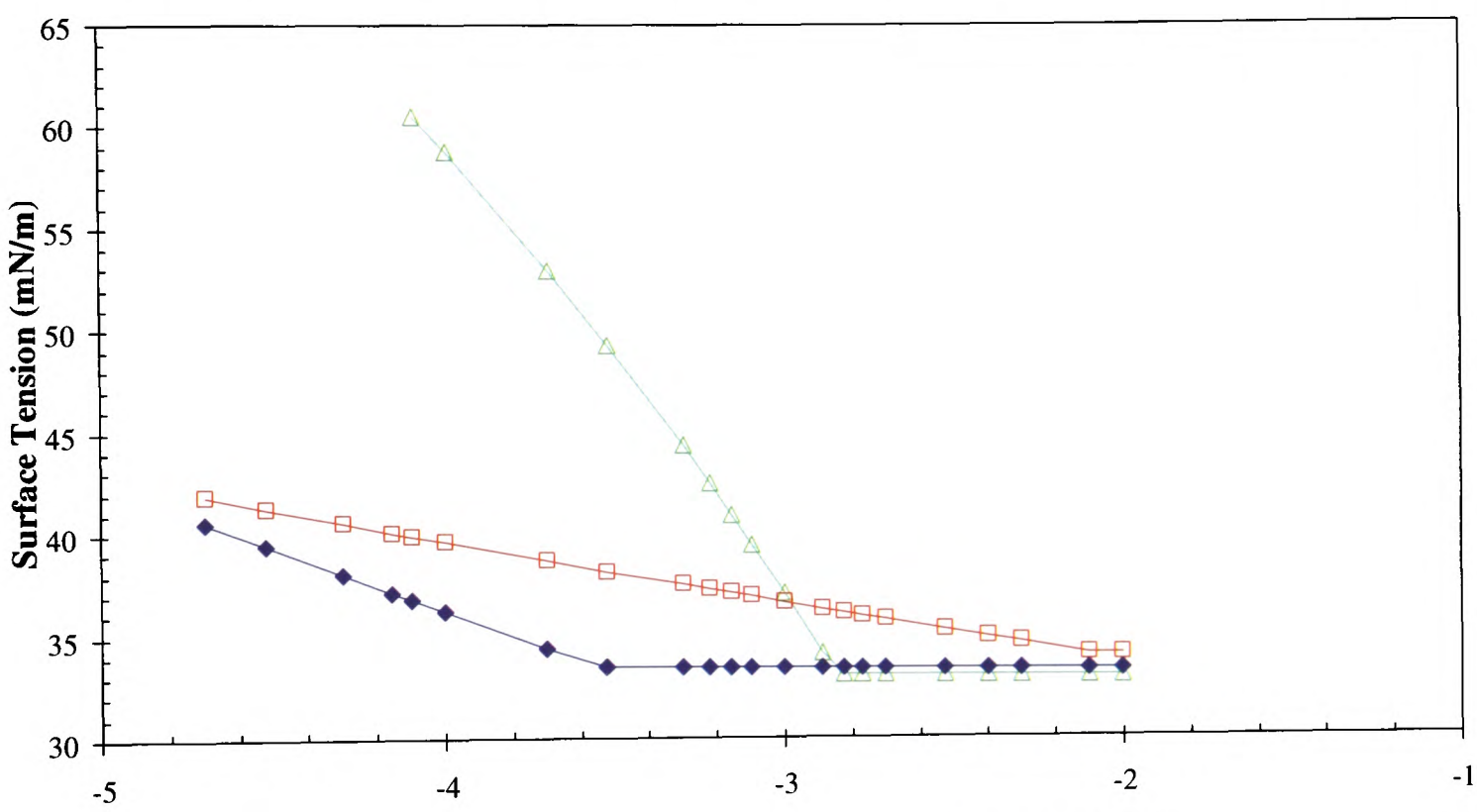


Figure 15. Surface tension against log of the concentration for the SDS/EPE 3000-14 mixture at y_{SDS}=0.9, (♦) in the presence of 0.1M NaCl. Curves with open symbols represent the surface tension of pure SDS, (△), and EPE 3000-14, (□), at each concentration point of the studied mixture

3.2 Mixed Monolayer Formation in the DTAC/EPE 3000-14 system

In comparison with the SDS/EPE 3000-14 system, the interaction between DTAC and EPE 3000-14 in micelles has been found to be much smaller in magnitude. However its β^M value seems somewhat larger than the interaction parameters measured for other cationic/nonionic systems, which was attributed to the same dehydration mechanism as proposed for the mixture with SDS. Hecht *et al*[17] have applied calorimetric measurements

to examine the interaction between Pluronic F127 and dodecyltrimethylammonium bromide (DTAB). They observed that DTAB appears to interact with Pluronic F127 in the same way as SDS, but to a lesser extent. The presence of DTAB reduces the endothermic enthalpy associated with the micellization of Pluronic F127 and its maximum effect is only achieved above the CMC of DTAB, whereas with SDS this occurs just below the CMC of SDS.

In general, the mixing of nonionic and cationic surfactants is expected to deviate from ideality. The negative deviations normally observed for such mixtures being largely a result of the charge-shielding effect of the nonionic co-adsorbed in the layer of the cationic. However, as explained in the previous chapter, the interaction between cationic and nonionic surfactants is much weaker than that between anionics and nonionics. This is mainly attributed to the lack of electrostatic attraction between cationic surfactants and POE groups.

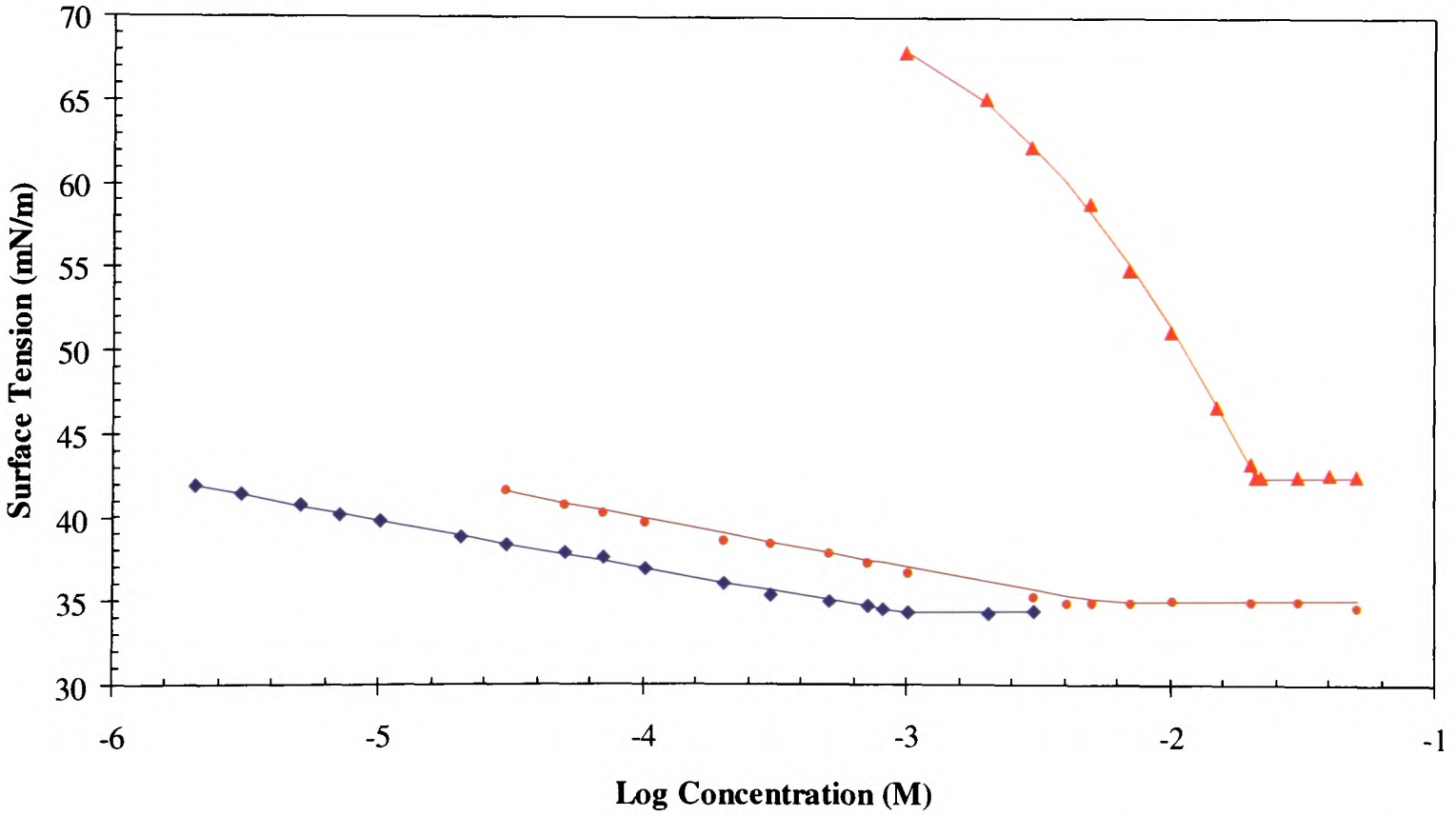


Figure 16. Surface tension against log of concentration for DTAC, (▲), EPE 3000-14, (♦), and the mixture at y_{DTAC}=0.9, (●), measured at 25°C.

To study the effect of cationic surfactants on the adsorption properties of EPE copolymers, the surface tension of DTAC:EPE 3000-14 mixtures was measured as a

function of the total amount of surfactant. The results from Chapter 8 are replotted here in Figure 16 for pure DTAC and EPE 3000-14 together with the 90:10 DTAC:EPE 3000-14 mixture. The values of the limiting surface pressures obtained from the plots depicted are given in Table 11.

Surfactant System	CMC (M)	π^{max} (mN/m)
DTAC	2.1×10^{-2}	30.1
90:10 DTAC/EPE 3000-14	5.8×10^{-3}	37.5

Table 11. Limiting surface pressure values obtained at the CMC and at 25°C.

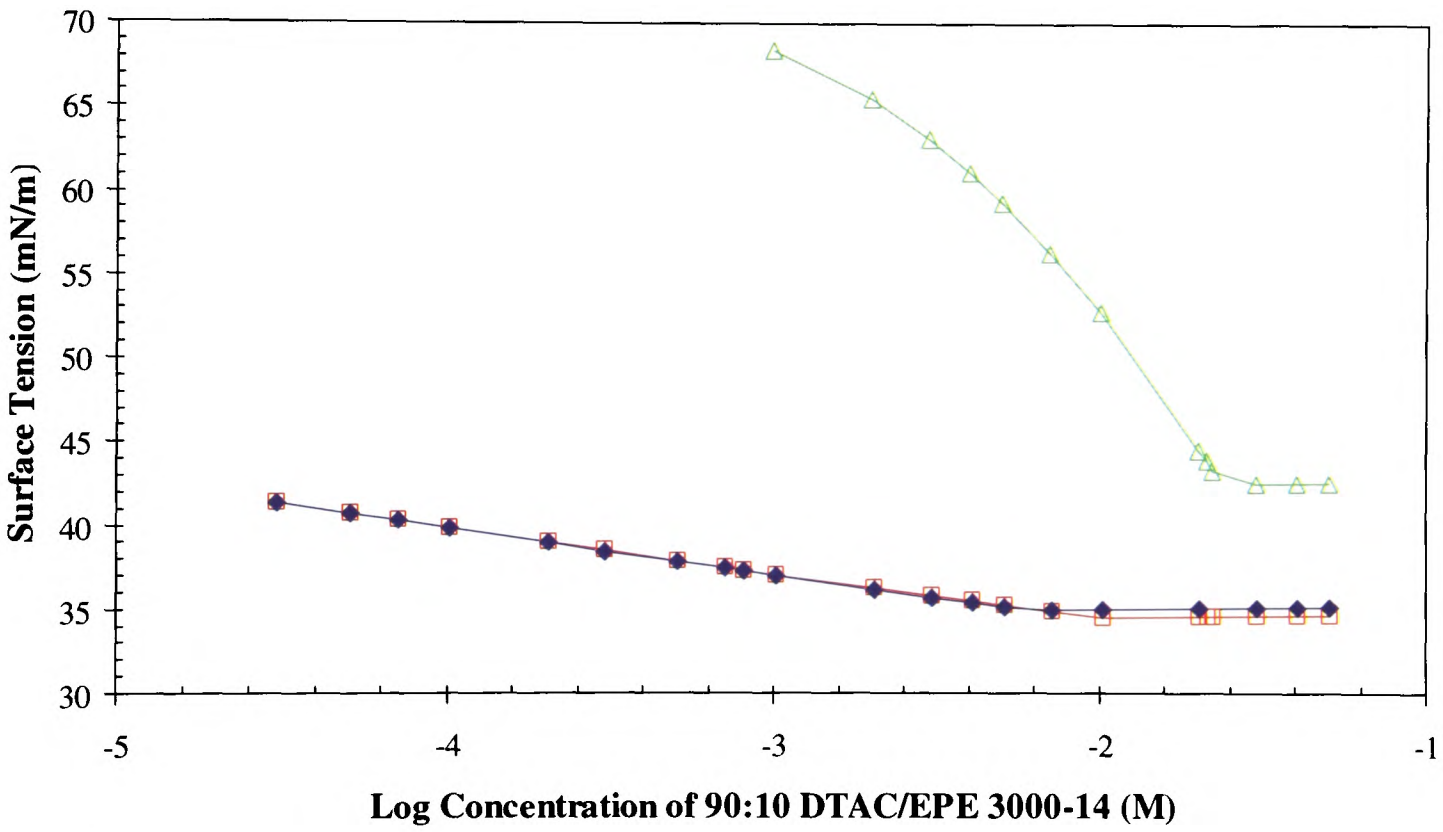


Figure 17. Surface tension against log of the concentration for DTAC/EPE 3000-14 mixtures at y_{DTAC}=0.9, (♦). Curves with open symbols represent the surface tension of pure DTAC, (△), and EPE 3000-14, (□), at each concentration point of the studied mixture

In the SDS/EPE 3000-14 system, the surface activity of the mixture at sub-micellar concentrations is predominantly determined by the copolymer concentration. In the case of DTAC, which is less surface active than SDS, the interaction between DTAC and

EPE 3000-14 is also masked by the large difference in the surface activity of the two components. Figure 17 the surface tension values for the DTAC/EPE 3000-14 mixture are compared with those values of surface tension for the pure component taken at the concentration they are present in the mixture. The resulting surface activity of the mixture is identical to that of pure EPE 3000-14 solution throughout the studied concentration range. Therefore the determination of the β^s parameter is equally impossible.

The compositions at the interface at range of bulk concentration were determined for these mixtures by neutron reflection. Figures 18-21 show the reflectivity plotted against momentum transfer, Q, for the binary mixture, where three different isotopic compositions have been studied: d-DTAC/h-EPE 3000-14, h-DTAC/d-EPE 3000-14, and d-DTAC/d-EPE 3000-14, so that the individual excesses of each adsorbed species, as well as the total surface excess, could be determined. The results obtained by fitting the data are given in Table 12.

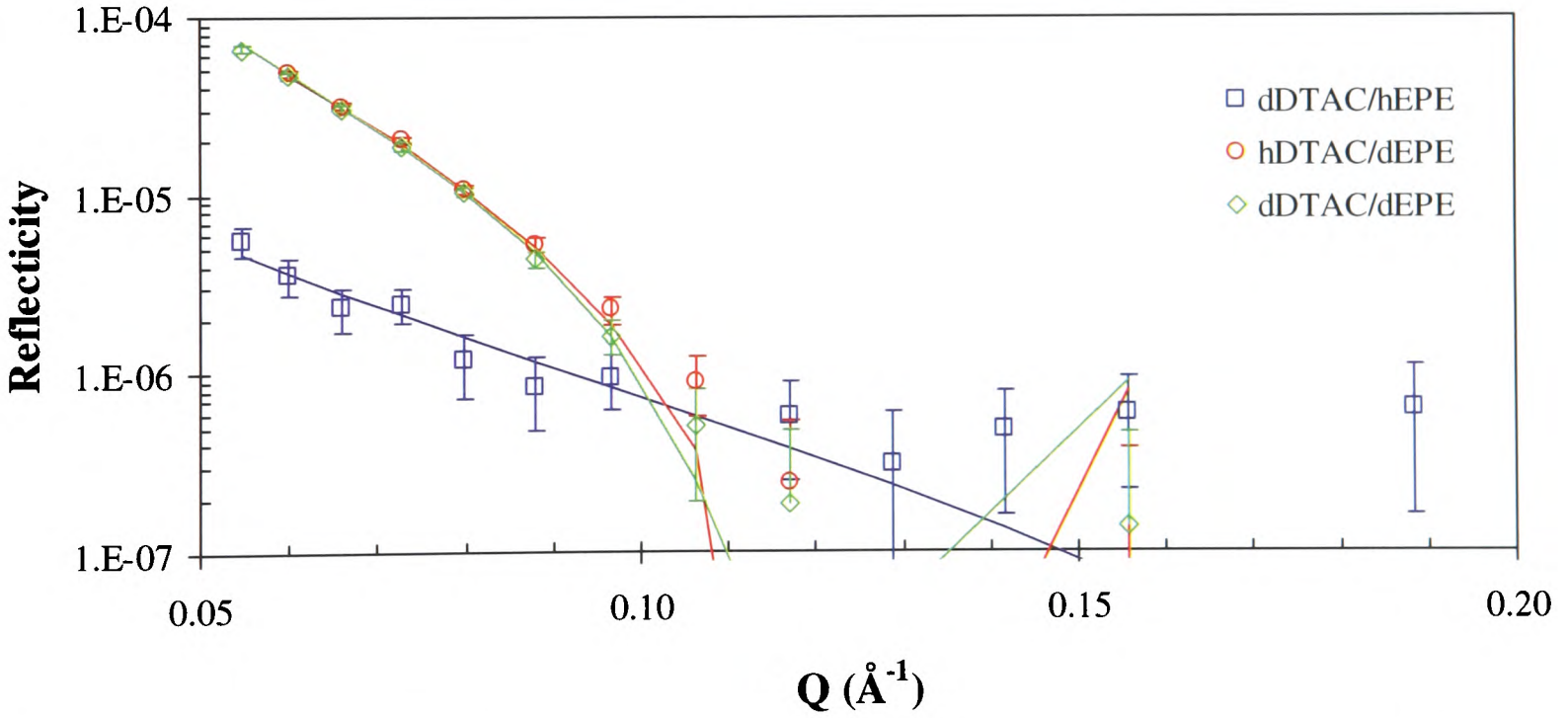


Figure 18. Neutron reflectivity profiles for 90/10 DTAC/EPE 3000-14 mixtures at a bulk concentration of $5x10^{-3}$M. The continuous lines are best fits to the data.

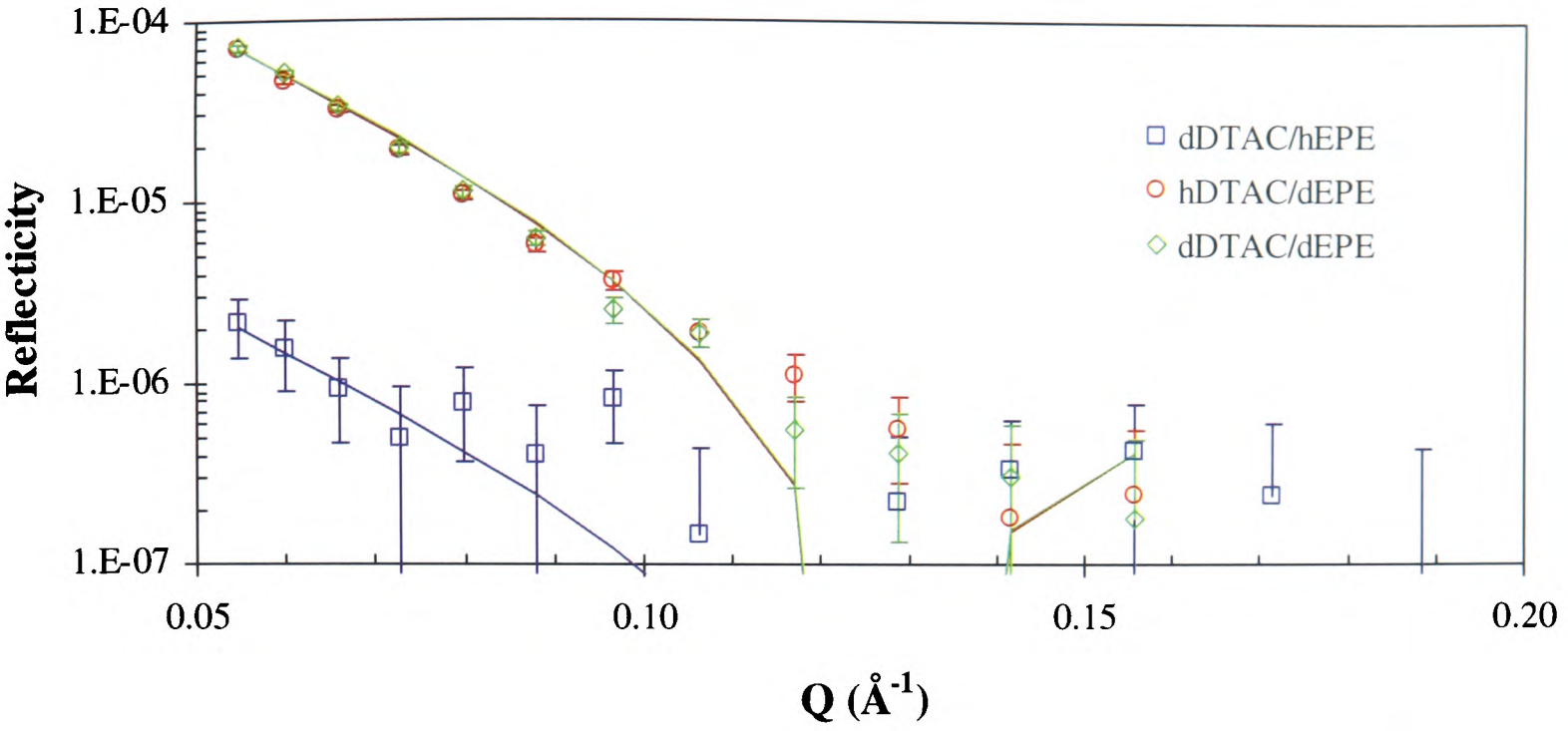


Figure 19. Neutron reflectivity profiles for 90/10 DTAC/EPE 3000-14 mixtures at a bulk concentration of $1x10^{-3}$M. The continuous lines are best fits to the data.

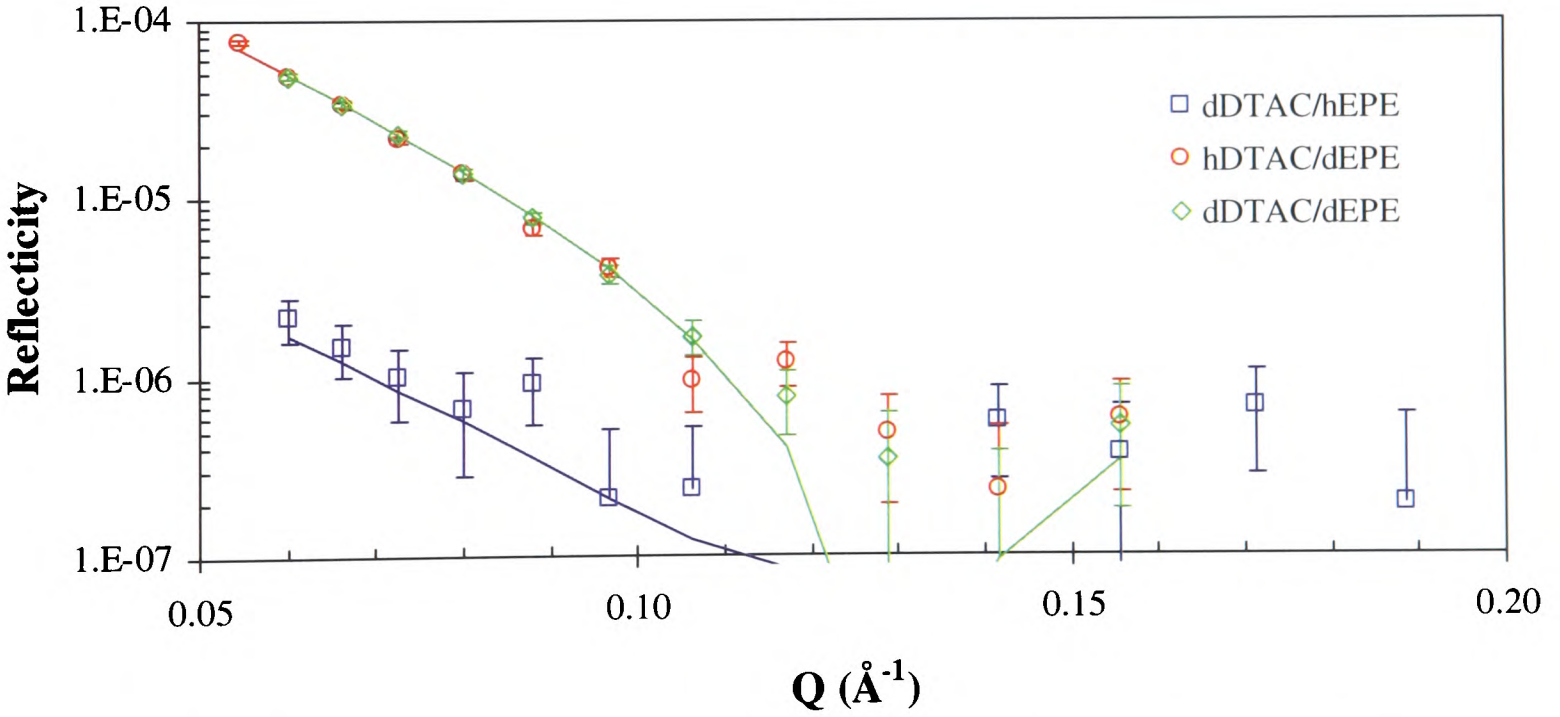


Figure 20. Neutron reflectivity profiles for 90/10 DTAC/EPE 3000-14 mixtures at a bulk concentration of $5x10^{-4}$M. The continuous lines are best fits to the data.

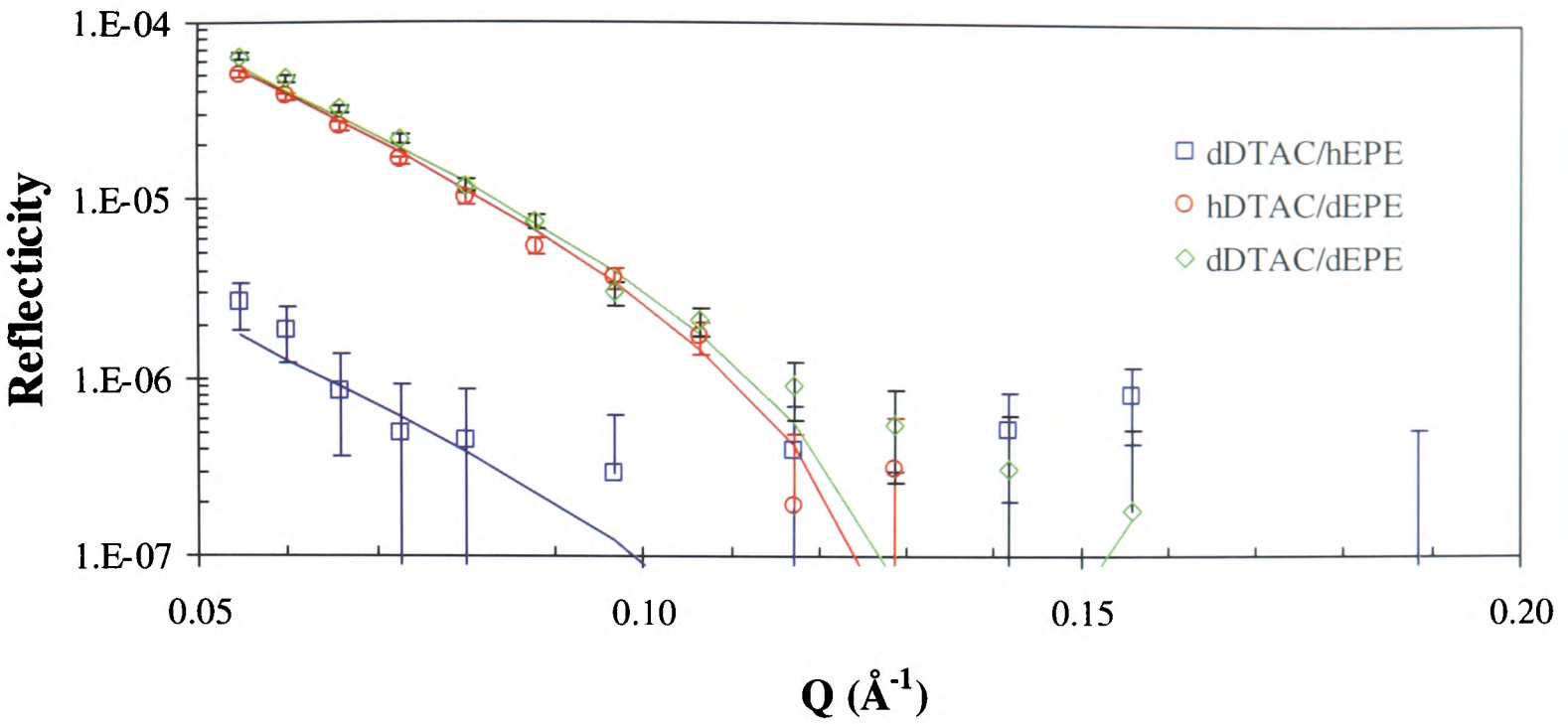


Figure 21. Neutron reflectivity profiles for 90/10 DTAC/EPE 3000-14 mixtures at a bulk concentration of $7x10^{-5}$M. The continuous lines are best fits to the data.

Concentration (M)		$5x10^{-3}$			$1x10^{-3}$			$5x10^{-4}$			$7x10^{-5}$		
Layer	Parameters	dD/hE	hD/dE	dD/dE	dD/hE	hD/dE	dD/dE	dD/hE	hD/dE	dD/dE	dD/hE	hD/dE	dD/dE
1	τ/Å	30±3	54±4	55±4	28±2	49±4	49±4	22±2	48±4	48±4	19±2	47±4	46±4
	$\rho x10^6(Å^{-2})$	0.35	0.99	1.00	0.19	1.01	1.02	0.26	1.02	1.02	0.17	0.90	0.93
2	τ/Å	25±2			21±2			26±2			27±2		
	$\rho x10^6(Å^{-2})$	0.01			0.15			0.12			0.16		
Total	τ/Å	55±4	54±4	55±4	49±4	49±4	49±4	48±4	48±4	48±4	46±4	47±4	46±4
	$\rho x10^6(Å^{-2})$	0.20	0.99	1.00	0.17	1.01	1.02	0.18	1.02	1.02	0.16	0.90	0.93

	A ($Å^2$)	$\Gamma x10^{10}$ (mol/cm^2)	A ($Å^2$)	$\Gamma x10^{10}$ (mol/cm^2)	A ($Å^2$)	$\Gamma x10^{10}$ (mol/cm^2)	A ($Å^2$)	$\Gamma x10^{10}$ (mol/cm^2)
DTAC	-	0	-	0	-	0	-	0
EPE 3000-14	410±30	0.41±0.05	445±40	0.37±0.05	450±40	0.37±0.05	520±40	0.32±0.05
DTAC/EPE 3000-14		0.41±0.05		0.37±0.05		0.37±0.05		0.32±0.05

Table 12. Parameters and surface excesses obtained from the neutron reflectivity of three isotopic combinations dDTAC/hEPE 3000-14 (dD/hE), hDTAC/dEPE 3000-14 (hD/dE), dDTAC/dEPE 3000-14 (dD/dE), at different bulk concentrations.

Table 12 clearly shows that the air-water interface of sub-micellar solutions of DTAC/EPE 3000-14 is indeed dominated by the copolymer. At $5x10^{-3}$M the monolayer is thicker than those of the more dilute solutions, but it coincides with an increase in the concentration of the copolymer at the surface.

The interaction between DTAC and EPE 3000-14 can be enhanced by increasing the surface activity of DTAC with the addition of electrolyte. The surface tension of solutions containing 0.1M NaCl, already shown in Chapter 8, are shown in Figure 22. The values for the limiting surface pressures obtained from the plots are given in Table 13.

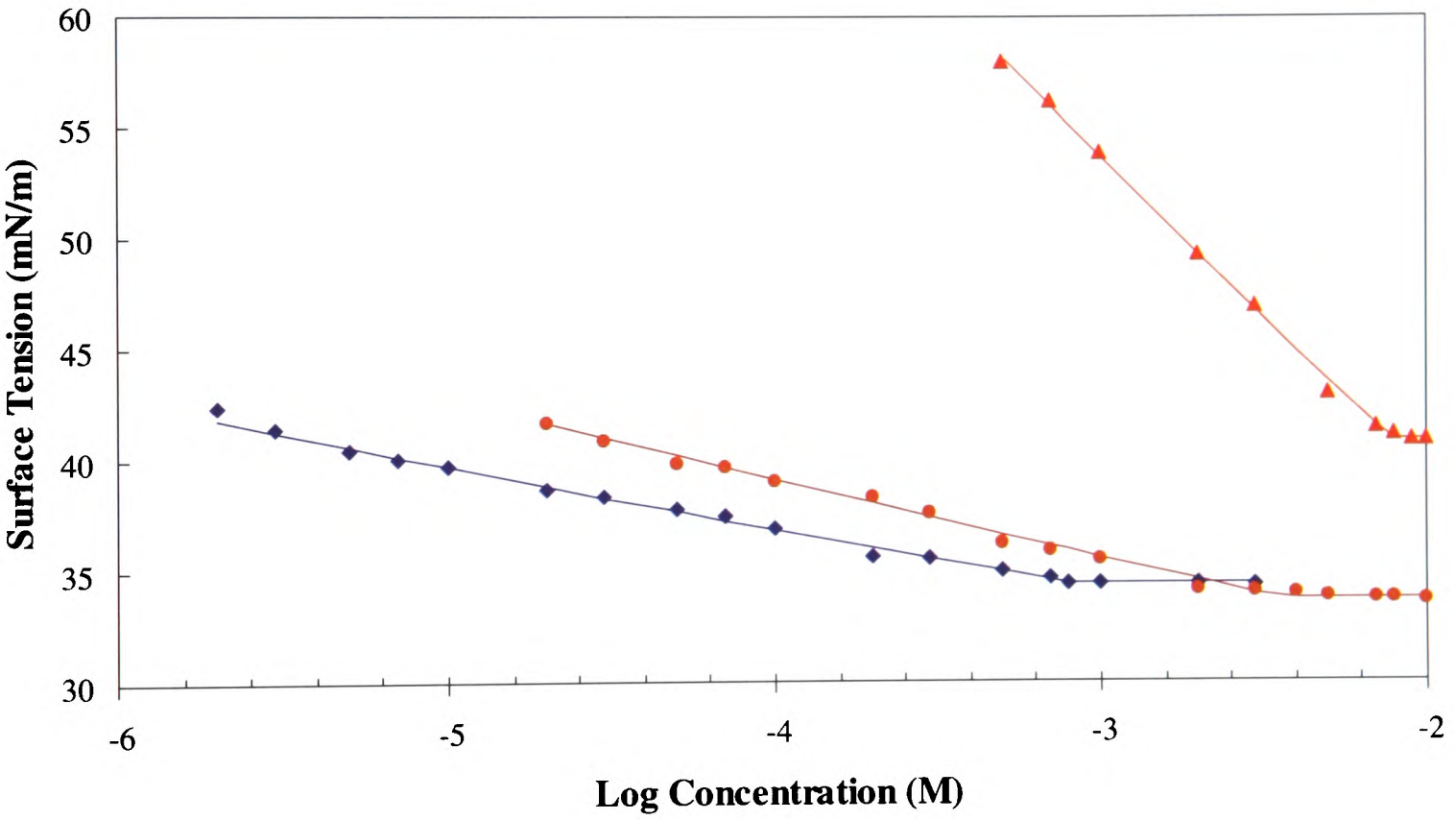


Figure 22. Surface tension against log of the concentration for DTAC, (▲), EPE 3000-14, (♦), and the mixture at y_{DTAC}=0.9, (●), in 0.1M NaCl measured at 25°C.

Surfactant System	CMC (M)	π^{max} (mN/m)
DTAC	$7.8x10^{-3}$	31.1
90:10 DTAC/EPE 3000-14	$2.8x10^{-3}$	38.3

Table 13. Limiting surface pressure values at the CMC obtained at 25°C.

To examine the effect of the salt on the surface activity of DTAC/EPE 3000-14 mixture, the surface tension values for the mixture were compared with those values of surface tension for the pure component taken at the concentration they were present in the mixture. The curves are depicted in Figure 23.

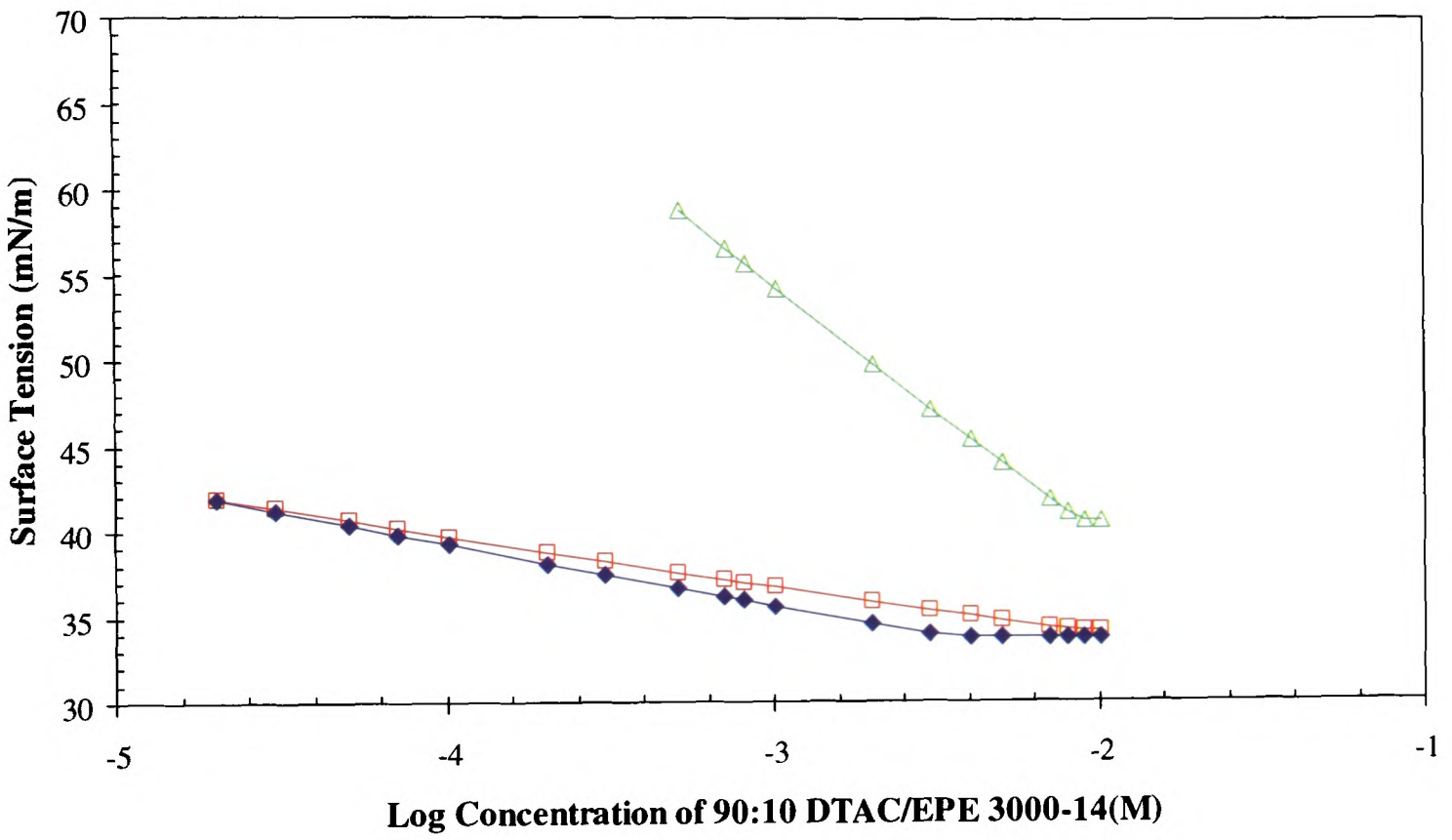


Figure 23. Surface tension against the log of the concentration for DTAC/EPE 3000-14 mixtures at y_{DTAC}=0.9, (♦) in 0.1M NaCl solutions. Curves with open symbols represent the surface tension of DTAC, (△), and EPE 3000-14, (□), at each concentration point of the mixture.

It is apparent from Figure 23 that the presence of the salt produces a much weaker effect on the surface activity of DTAC/EPE 3000-14 mixture than for SDS. The CMC drops slightly from $3.6x10^{-3}$M down to $2.8x10^{-3}$M, and some reduction of the surface tension at the CMC is also observed. Despite the slight enhancement of the surface activity of DTAC in the presence of electrolyte, it is still significantly weaker than that of the block copolymer. Such a difference in surface activity makes the assessment of the ideality of mixing using Equation 9.1 difficult. It is not possible to attain a given surface pressure at which the molar concentrations of both individual components can be obtained, as can be seen in Figure 23. As an alternative we have used the generalized model developed by Holland, which is also based on the Pseudophase Separation Approach but takes the

surface pressure and the molar area into account. The model is described in Chapter 7. The interaction parameter, β^s, was calculated by iterative solution of Equations 9.10 and 9.11 and the results are presented in Table 14.

$$\beta^s = \frac{1}{x_{EPE}^2}\ln\left[\frac{y_{DTAC}C}{x_{DTAC}C_{DTAC}^{\ M}}\right] - \frac{(\pi - \pi_{DTAC}^M)\omega_{DTAC}^M}{RT} \qquad (9.10)$$

$$\beta^s = \frac{1}{x_{DTAC}^2}\ln\left[\frac{y_{EPE}C}{x_{EPE}C_{EPE}^{\ \pi}}\right] \qquad (9.11)$$

The results show that the mixing of DTAC and EPE 3000-14 in the interfacial layer is nonideal. The magnitude of the interaction parameters obtained for DTAC/EPE 3000-14 at the interface is lower than those for SDS/EPE 3000-14 mixtures as expected from the previous discussion. However, it is interesting to observe that the magnitudes of the interaction parameters obtained for DTAC/EPE 3000-14 at the interface are significantly greater than those obtained for the mixed micellization. The suitability of the Pseudophase Separation Model to describe the surface composition for DTAC/EPE 3000-14 mixtures is assessed by comparing the predicted surface compositions with those compositions derived directly by neutron reflection.

Surface Pressure (mN/m)	90/10 DTAC/EPE 3000-14			
	$C_{DTAC:EPE}$ (M)	Nonideal Mixing		Neutron Reflection
		β^s	$x_{DTAC}^{pred.}$	$x_{DTAC}^{obs.}$
32.9	1.0×10^{-4}	-4.8	0.22	0
35.9	7.0×10^{-4}	-3.7	0.36	0.05
38.0	3.0×10^{-3}	-	-	0.48
39.2	7.0×10^{-3}	-	-	0.84

Table 14. Surface composition of DTAC/EPE 3000-14 solutions in the presence of 0.1M NaCl at 25°C.

Figures 24-27 show the reflectivity profiles for the binary mixture of DTAC/EPE 3000-14 in 0.1M NaCl at various surface pressures. Three different isotopic compositions, as described above, were used to determine the individual excesses of each adsorbed species, as well as the total surface excess.

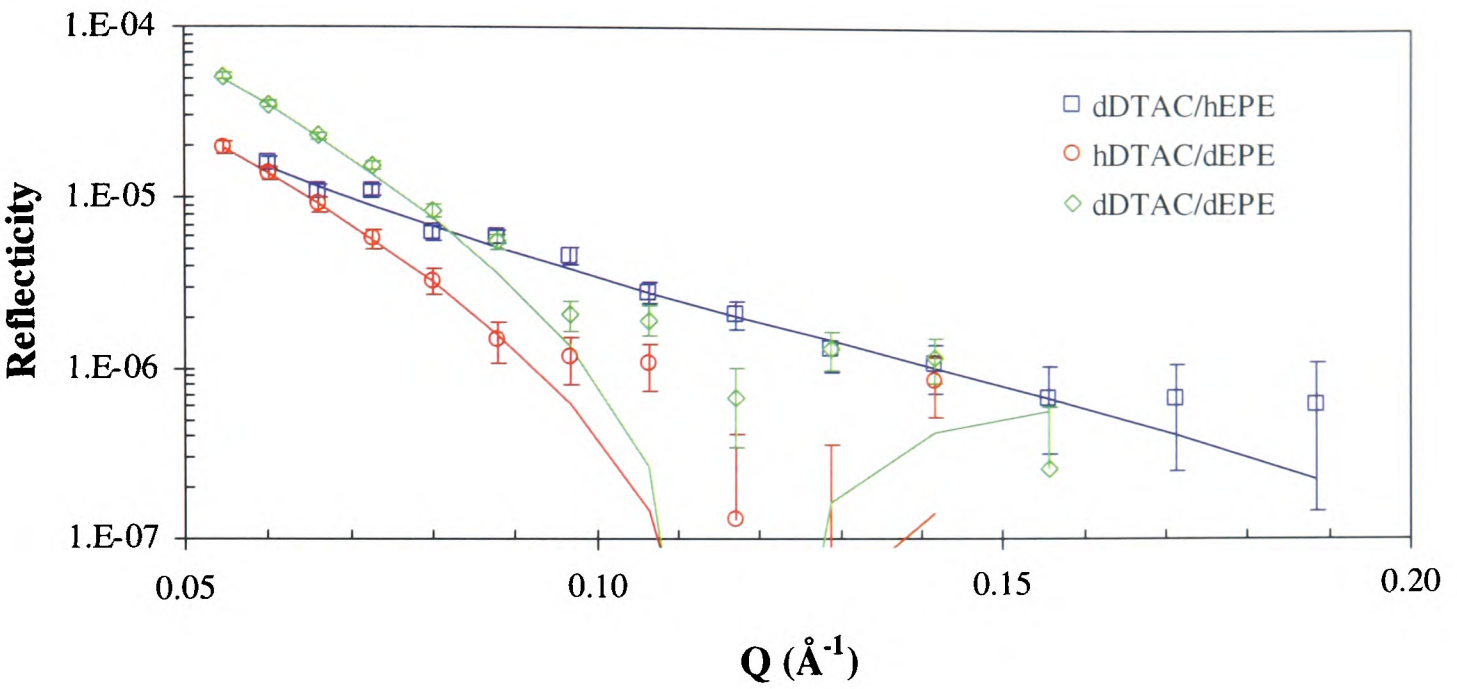


Figure 24. Neutron reflectivity profiles for 90/10 DTAC/EPE 3000-14 mixtures at a bulk concentration of $7x10^{-3}$M and in the presence of 0.1M NaCl. The continuous lines are best fits to the data.

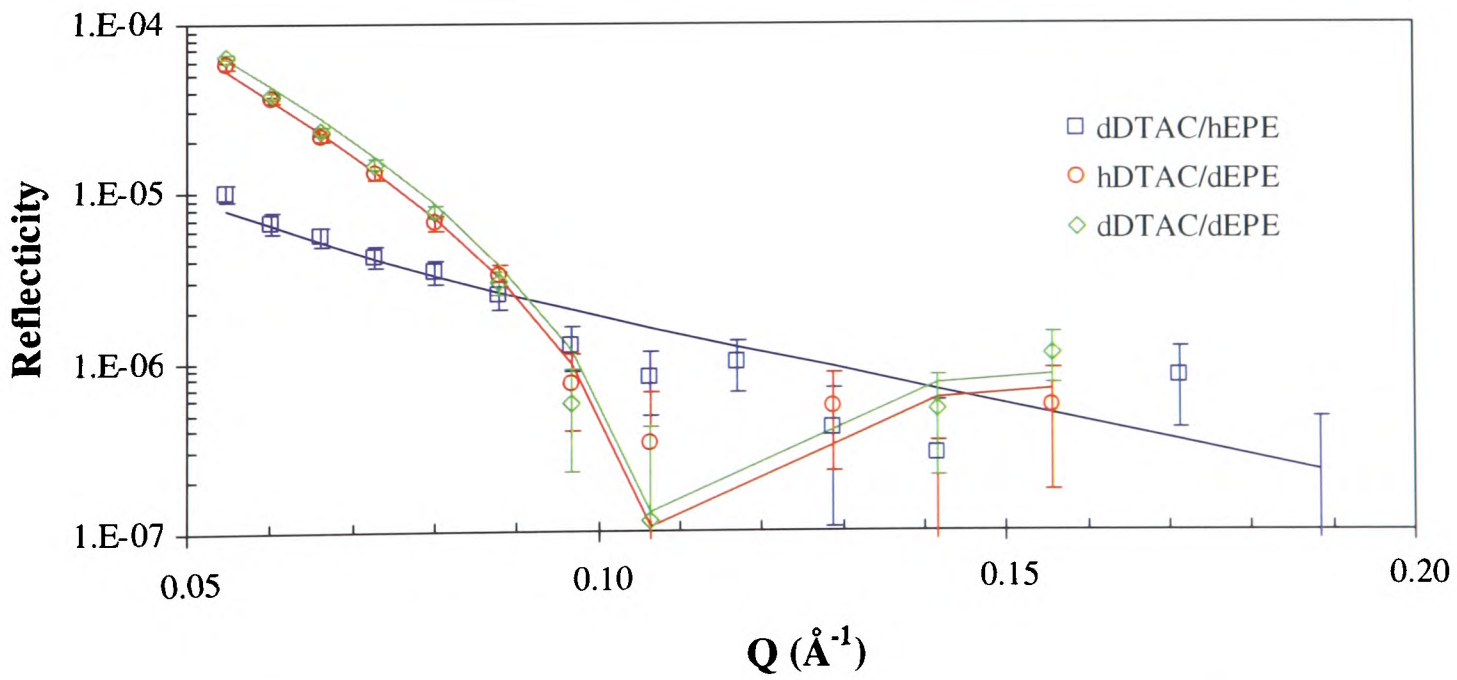


Figure 25. Neutron reflectivity profiles for 90/10 DTAC/EPE 3000-14 mixtures at a bulk concentration of $3x10^{-3}$M and in the presence of 0.1M NaCl. The continuous lines are best fits to the data.

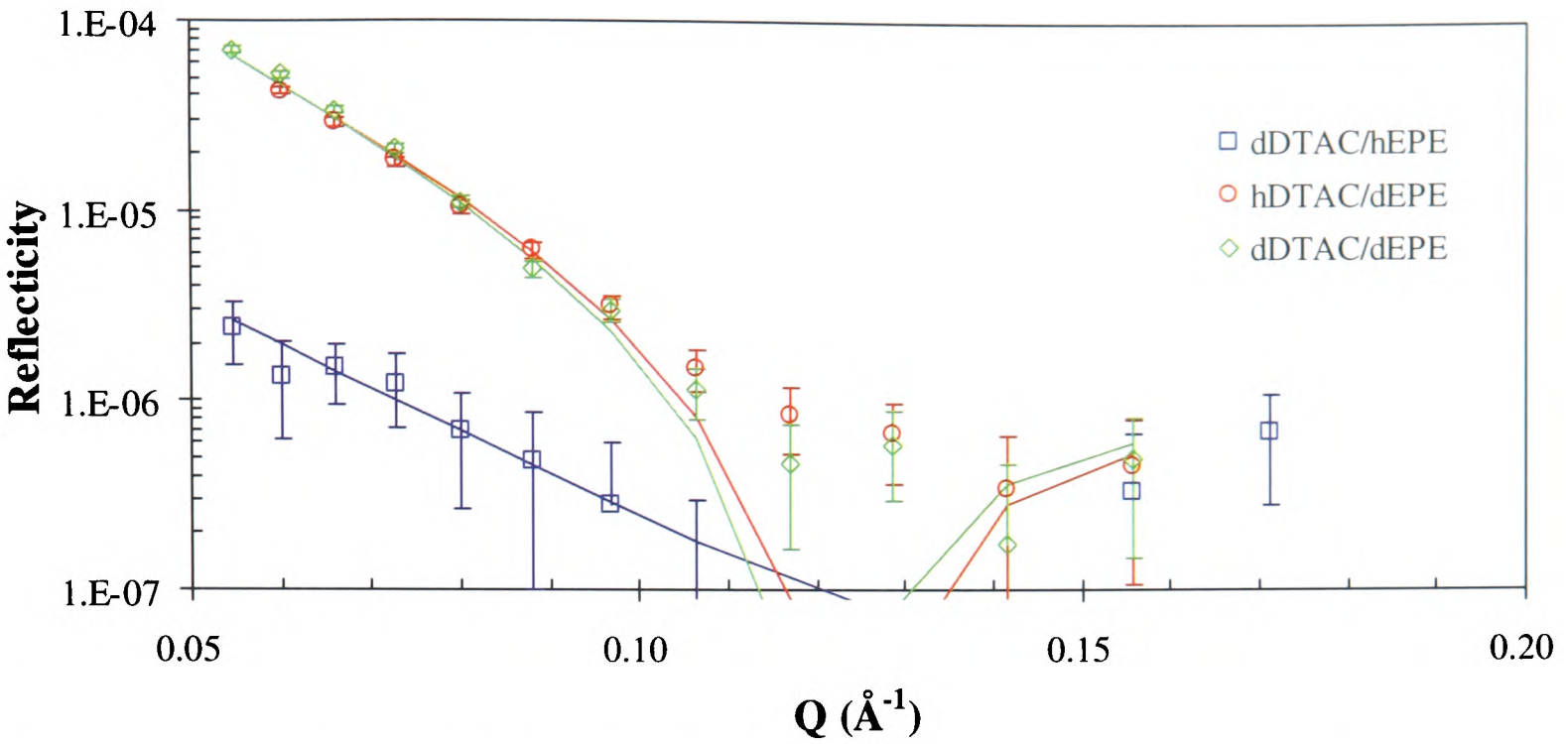


Figure 26. Neutron reflectivity profiles for 90/10 DTAC/EPE 3000-14 mixtures at a bulk concentration of $7x10^{-4}$M and in the presence of 0.1M NaCl. The continuous lines are best fits to the data.

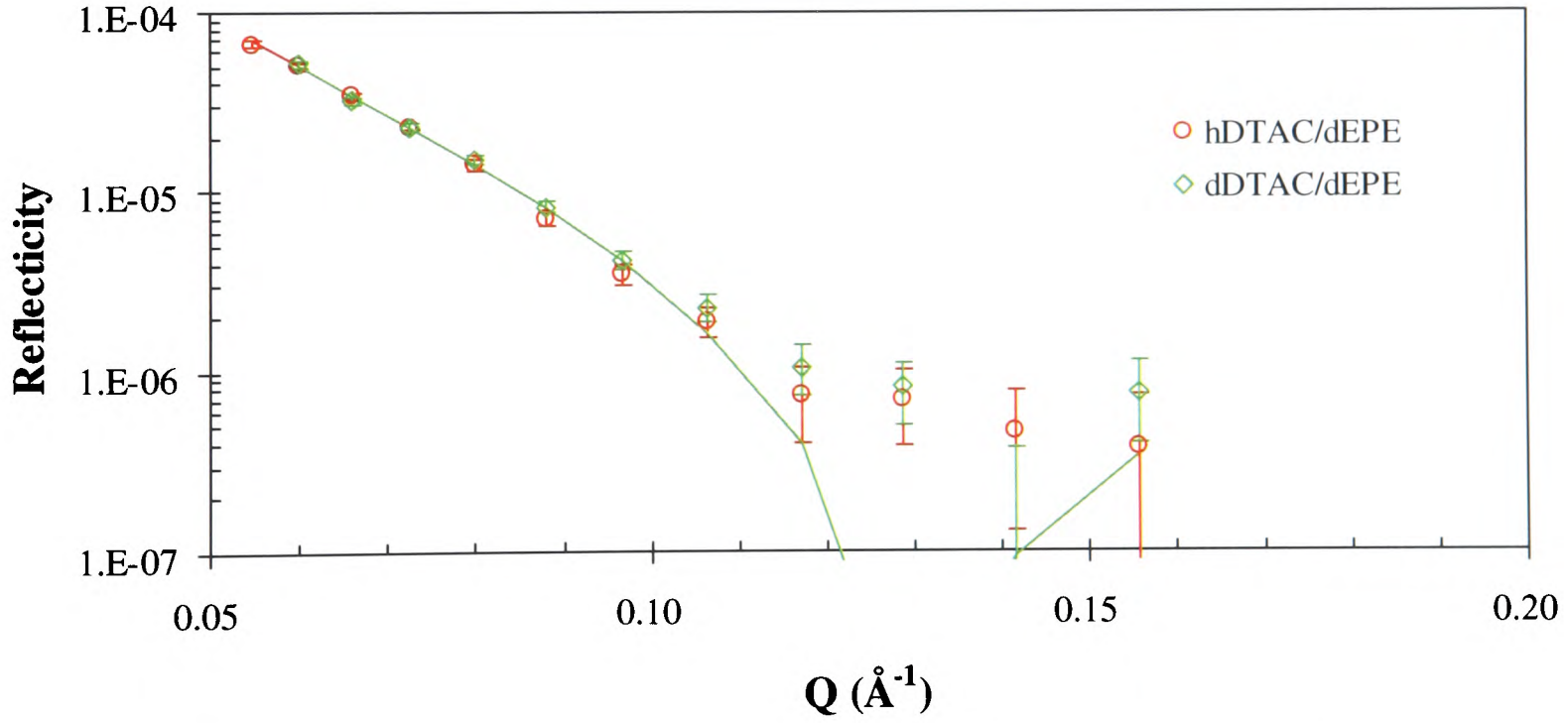


Figure 27. Neutron reflectivity profiles for 90/10 DTAC/EPE 3000-14 mixtures at a bulk concentration of $1x10^{-4}$M and in the presence of 0.1M NaCl. The continuous lines are best fits to the data.

Concentration (M)		$7x10^{-3}$			$3x10^{-3}$			$7x10^{-4}$			$1x10^{-4}$		
Layer	Parameters	dD/hE	hD/dE	dD/dE	dD/hE	hD/dE	dD/dE	dD/hE	hD/dE	dD/dE	dD/hE	hD/dE	dD/dE
1	τ/Å	24±2	53±4	54±4	19±2	56±4	56±4	20±2	49±4	49±4	48±4	48±4	48±4
	$\rho x10^6(Å^{-2})$	0.84	0.53	0.84	0.68	0.85	0.94	0.34	0.96	0.98	0.17	1.02	1.02
2	τ/Å	30±2			37±3			29±2					
	$\rho x10^6(Å^{-2})$	0.05			0.01			0.03					
Total	τ/Å	54±4	53±4	54±4	56±4	56±4	56±4	49±4	49±4	49±4	48±4	48±4	48±4
	$\rho x10^6(Å^{-2})$	0.40	0.53	0.84	0.24	0.85	0.94	0.16	0.96	0.98	0.17	1.02	1.02

	A ($Å^2$)	$\Gamma x10^{10}$ (mol/cm^2)	A ($Å^2$)	$\Gamma x10^{10}$ (mol/cm^2)	A ($Å^2$)	$\Gamma x10^{10}$ (mol/cm^2)	A ($Å^2$)	$\Gamma x10^{10}$ (mol/cm^2)
DTAC	150±10	1.11±0.10	500±40	0.33±0.05	-	0.05±0.05	-	0
EPE 3000-14	770±60	0.22±0.05	460±40	0.36±0.05	465±40	0.36±0.05	448±40	0.37±0.05
DTAC/EPE 3000-14		1.32±0.10		0.69±0.05		0.38±0.05		0.37±0.05

Table 15. Parameters and surface excesses obtained from the neutron reflectivity of three isotopic combinations dDTAC/hEPE 3000-14 (dD/hE), hDTAC/dEPE 3000-14 (hD/dE), dDTAC/dEPE 3000-14 (dD/dE), at different bulk concentrations in the presence of 0.1M NaCl.

The curve for the isotopic combination of dDATC/hEPE 3000-14 at 10^{-4}M is not shown in Figure 27 because its reflectivity signal was at the level of the background reflectivity showing that its coverage was too low to be accurately determined. The results obtained from fitting the reflectivity profiles are given in Table 15. Although a single-layer model would also fit the reflectivity curves for the d-DTAC/h-EPE 3000-14 combinations, a two-layer model was applied in order to yield values of area per surfactant species consistent with the other isotopic combinations.

The comparison between the experimental compositions obtained from neutron reflection and the ones predicted by the Pseudophase Separation Model is made in Table 14. The surface compositions measured by neutron reflection clearly disagree with the predictions of the Pseudophase Separation Model. The study of the interaction between DTAC and EPE 3000-14 is complicated by the large difference in the surface activity of the two components. The dominance of the surface activity of the copolymer particularly below the mixed CMC masks the true situation. A similar effect was also observed with SDS/EPE 3000-14 system in the absence of swamping electrolyte. The addition of electrolyte in this case, does not seem to have the same enhancing effects. As the bulk concentration increases above the CMC, there is however a substantial increase in the DTAC mole fraction at the interface. The evolution of the surface composition indicates an increasing attractive interaction in the interfacial mixing, similar to that observed in the SDS/EPE 3000-14 system.

C^{bulk} M	C^{bulk}/CMC	x_{DTAC}	Γ_{EPE} x10^{10} mol/cm^2	$\tau_{EPE:SDS}$ Å	τ_{EPE} Å
$1x10^{-4}$	0.04	0	0.37	48	47
$7x10^{-4}$	0.25	0.05	0.36	49	47
$3x10^{-3}$	1.07	0.48	0.36	56	47
$7x10^{-3}$	2.50	0.84	0.22	53	43-44

Table 16. Mixed monolayer mole fraction of DTAC, x_{DTAC}, EPE 3000-14 surface excess, Γ_{EPE}, and monolayer thickness, $\tau_{EPE:DTAC}$, for DTAC:EPE 3000-14 90:10 at a range of bulk concentration normalised to the mixed CMC value. τ_{EPE} is the monolayer thickness for pure EPE 3000-14 equivalent to the copolymer surface coverage in the mixture.

The analysis of the variation of layer thickness with the surface coverage of the block copolymer, shown in Table 16, provides further indications of a rearrangement of the copolymer molecules inside the mixed monolayer. Below the CMC, the surface concentration of DTAC is small and therefore the monolayer structure is similar to that of pure copolymer with respect to the distribution of the EO and PO groups within the monolayer. At $3x10^{-3}$M (1.07CMC) the structure of the mixed monolayer appears to change. The monolayer thickness for the isotopic combination of h-DTAC/d-EPE 3000-14 is 56Å and is significantly higher than the 47Å expected for a monolayer containing pure EPE 3000-14 at similar surface coverage. The monolayer thickening coincides with the increase of the concentration of DTAC at the surface, but the copolymer surface excess remains unchanged at $0.36x10^{-10}$mol/cm^2. Given that at this contrast only the EO segments are observed, this must be the result of the rearrangement of the EO groups inside the mixed monolayer, possibly associated with a change near the upper part of the surface as DTAC chains penetrate the PPO region.

As the concentration exceeds the mixed CMC, the structure of the mixed monolayer appears to be more complex. There is a substantial increase in the molar ratio of the DTAC, and the copolymer is largely displaced from the surface. The surface excess of the copolymer at $7x10^{-3}$M (2.50CMC) is reduced to $0.22x10^{-10}$ mol/cm^2. The layer thickness for pure EPE 3000-14 at the same surface excess is 43-44 Å. However the layer thickness for the combination of h-DTAC/d-EPE 3000-14 at $7x10^{-3}$M is 53Å. This increase of the monolayer thickness may be the result of the penetration of a fraction of the deuterated chains of DTAC into the low scattering layer of PPO outside the water.

The results suggest a different mixed layer structure compared with that of SDS/EPE 3000-14. The increase in layer thickness associated with the penetration of deuterated tails of the ionic surfactants is evident at a much lower surface mole fraction for DTAC than for SDS. It appears that DTAC accumulates preferentially in the uppermost part of the interfacial layer, while SDS prefers to be located in the more hydrophilic regions of the layer. This observation agrees with the findings obtained by Baglioni *et al.*[12] on the study of the position of polar headgroups of SDS and DTAC in mixed micelles with $C_{12}E_6$ surfactants. From the analysis of the results of electron spin

echo modulation of doxylstearic acids in mixed micelles, they concluded that both SDS and DTAC are present with their polar headgroups in the ethylene oxide region of the nonionic surfactant. However, the DTAC polar headgroups are located deeper inside the micelle, closer to the core region, while the SDS polar headgroups are located close to the micelle surface in a more hydrophilic region.

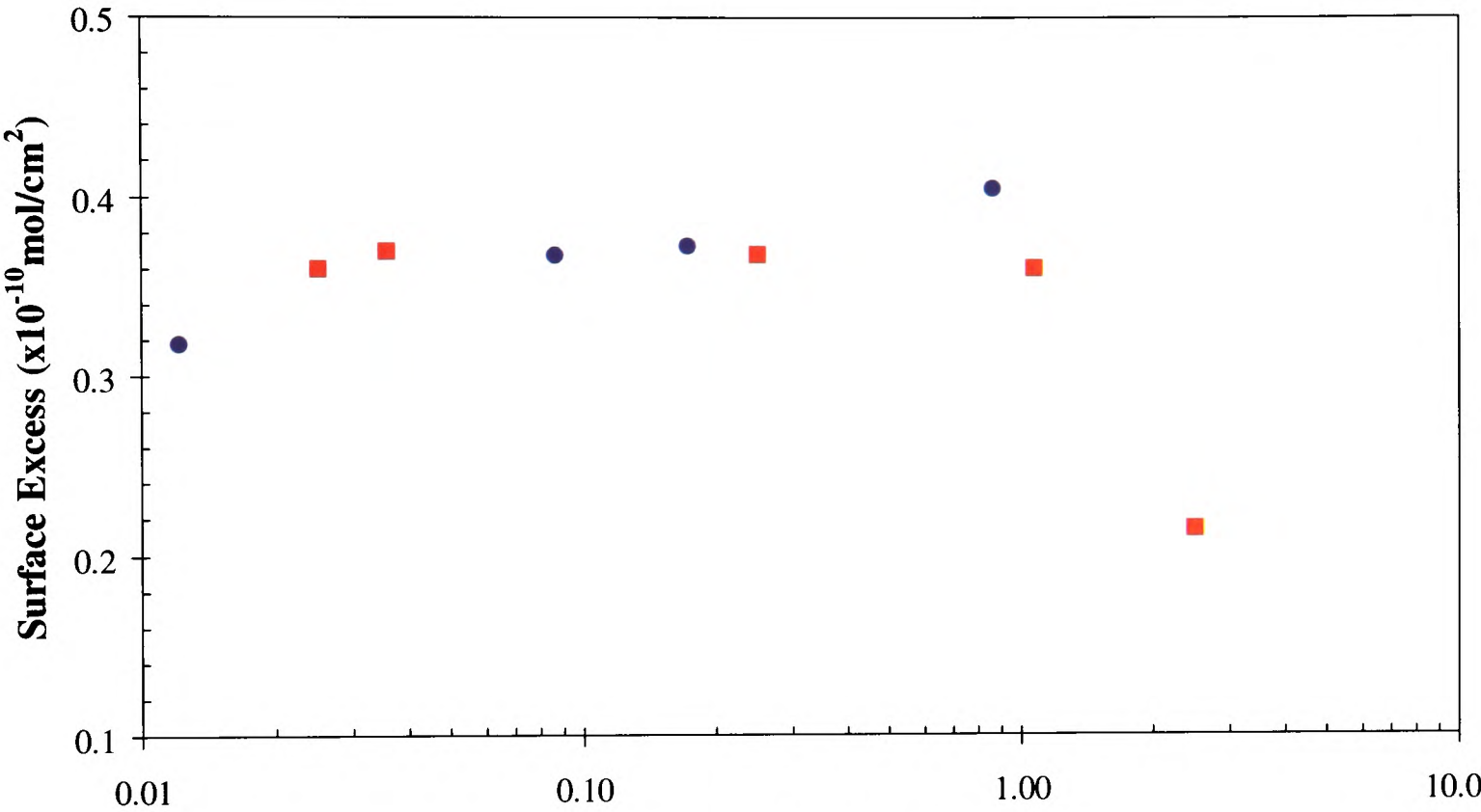


Figure 28. Surface excess of EPE 3000-14 in mixtures with DTAC in pure water (●), and in the presence of 0.1M NaCl (■), as a function of the mixture concentration normalised to the corresponding CMC.

Figure 28 depicts the surface coverage of EPE 3000-14 in its mixtures with DTAC, with and without salt addition, as a function of the bulk concentration normalised to the mixed CMC value. Below the mixed CMC the surface appears to be approximately saturated with copolymer molecules. The addition of salt does not seem to have any effect on the surface activity of EPE 3000-14, as would be expected. However as the bulk concentration exceeds the mixed CMC, the EPE 3000-14 molecules are largely displaced from the interface, similarly to SDS/EPE 3000-14 systems. It appears that the

displacement mechanism is probably a result of the incorporation of copolymer molecules into the mixed micelles.

3.3 Mixed Monolayer Formation in the C_8E_4/EPE 3000-14 system

Due to the lack of strong attractive interaction forces between nonionic surfactants, co-aggregation in such systems would only be favoured by the decrease in free energy associated with random mixing at the interface, which is the basis for ideal mixing. In the case of the mixture C_8E_4/EPE 3000-14, however, a strong repulsive effect was observed in the mixed micellization. We attributed the repulsive interaction to an increase in hydration of the mixed micelle core by the incorporation of the solvated C_8E_4 headgroups. We now consider the mixing behaviour in the interfacial layer. The plots of surface tension as a function of the log of the total surfactant concentration are shown in Figure 29. For this mixture the composition of the mixture is 90/10 C_8E_4/EPE 3000-14.

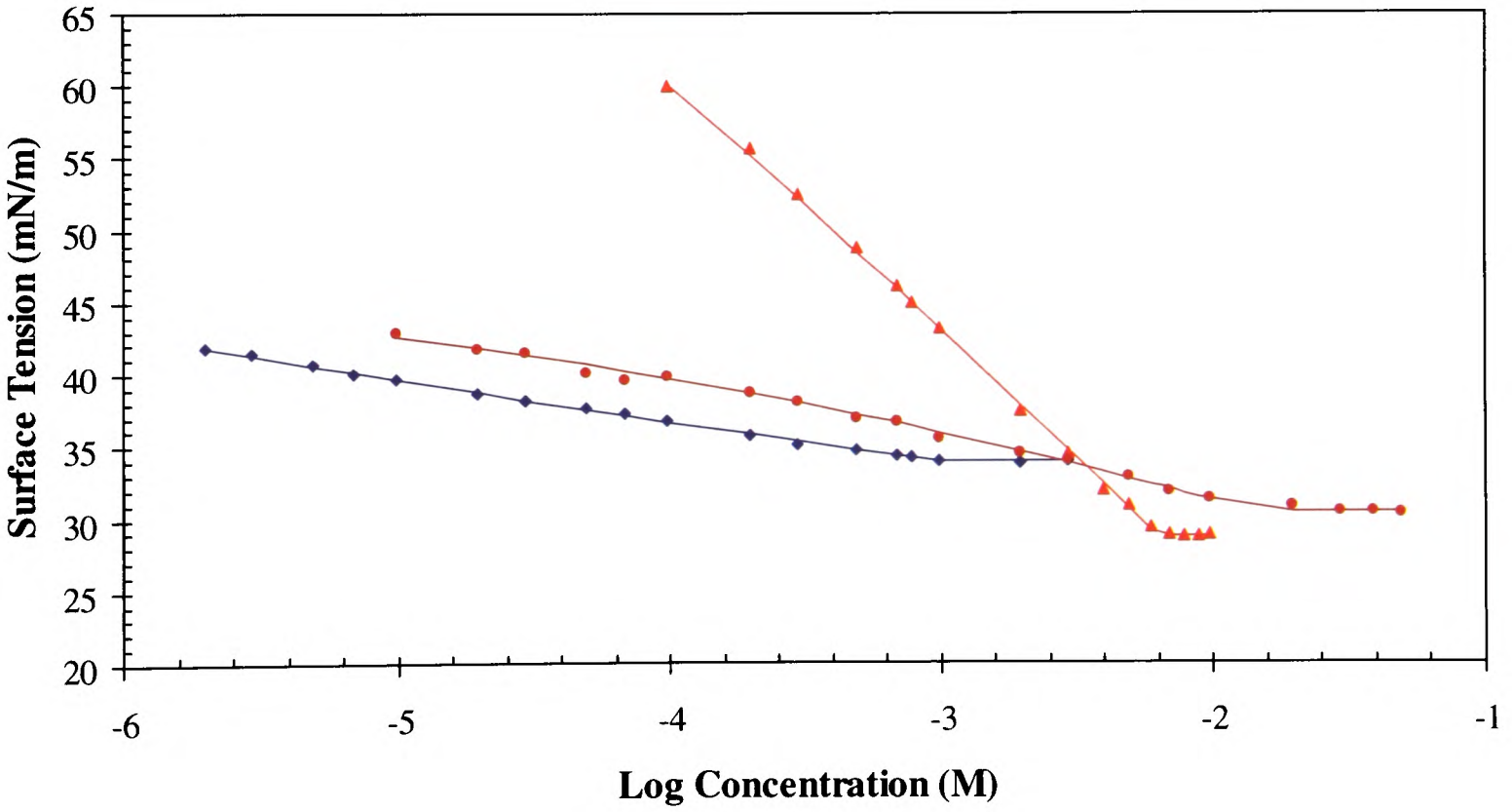


Figure 29. Surface tension against the log of the concentration for C_8E_4, (▲), EPE 3000-14, (♦), and the mixture system at y_{C8E4}=0.9, (●), measured at 25°C.

Figure 29 shows that the surface tension of mixture below the CMC is biased toward that of the copolymer, which is expected from its higher surface activity. The mixed CMC, as

discussed in the previous chapter, is appreciably higher than that of either C_8E_4 or EPE 3000-14, indicating a large departure from ideality. The values for the maximum surface pressures obtained from the plots in Figure 29 are given in Table 17.

Surfactant System	CMC (M)	π^{max} (mN/m)
C_8E_4	$6.3x10^{-3}$	43.2
90:10 C_8E_4/EPE 3000-14	$2.1x10^{-2}$	41.5

Table 17. Limiting surface pressure values at the CMC obtained at 25°C.

The mixing behaviour was analysed according to the Pseudophase Separation Model and the results are given in Table 18.

Surface Pressure	90/10 C_8E_4/EPE 3000-14		
	$C_{C8E4:EPE}$	Ideal Mixing	Neutron Reflection
(mN/m)	(M)	$x_{C_8E_4}^{pred.}$	$x_{C_8E_4}^{obs.}$
31.2	$5.0x10^{-5}$	0.03	0.05
34.8	$5.0x10^{-4}$	0.22	0.19
36.0	$1.0x10^{-3}$	0.39	0.39
39.2	$5.0x10^{-3}$	0.87	0.86
40.7	$1.0x10^{-2}$	0.96	0.93

Table 18. Surface composition of C_8E_4/EPE 3000-14 solutions at 25°C.

The results of Table 18 show that mixing of C_8E_4 and EPE 3000-14 in the interfacial layer, as analysed by the Pseudophase Separation Model, is ideal. This is surprising, as one would expect them to behave in a similar way to the mixed micellization, i.e. antagonistically. The reasons for the quite different behaviour are developed below.

The validity of the Pseudophase Separation Model predictions was tested by direct measurement of the surface composition at each surface pressure by neutron reflectivity,

as described above. The partial coverages were determined for three different isotopic compositions: dC_8E_4/hEPE 3000-14, hC_8E_4/dEPE 3000-14, and dC_8E_4/dEPE 3000-14, all in NRW. Figures 30-34 show the reflectivity profiles for the binary mixture at various surface pressures.

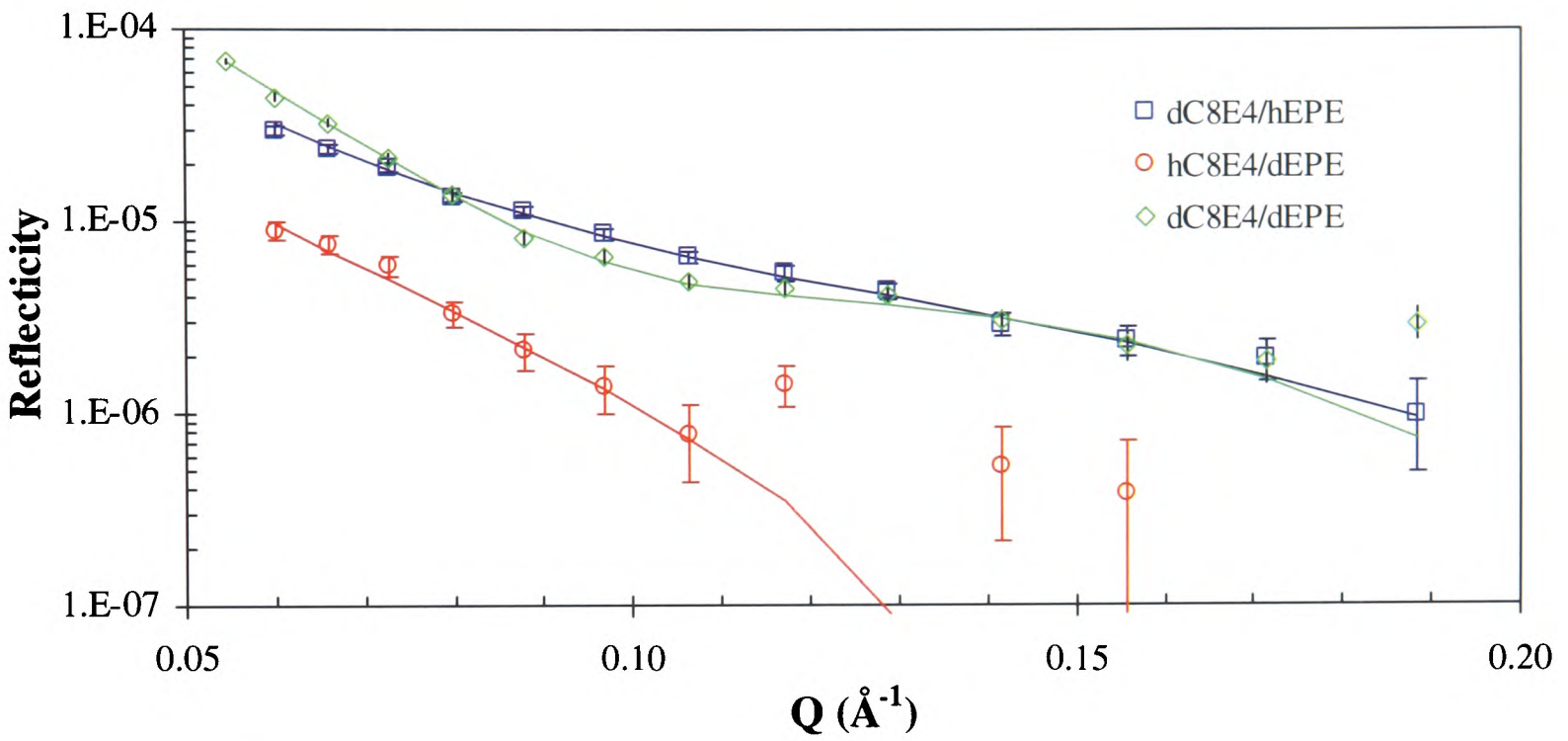


Figure 30. Neutron reflectivity profiles for 90/10 C_8E_4/EPE 3000-14 mixtures at a bulk concentration of $1x10^{-2}$M. The continuous lines are best fits to the data.

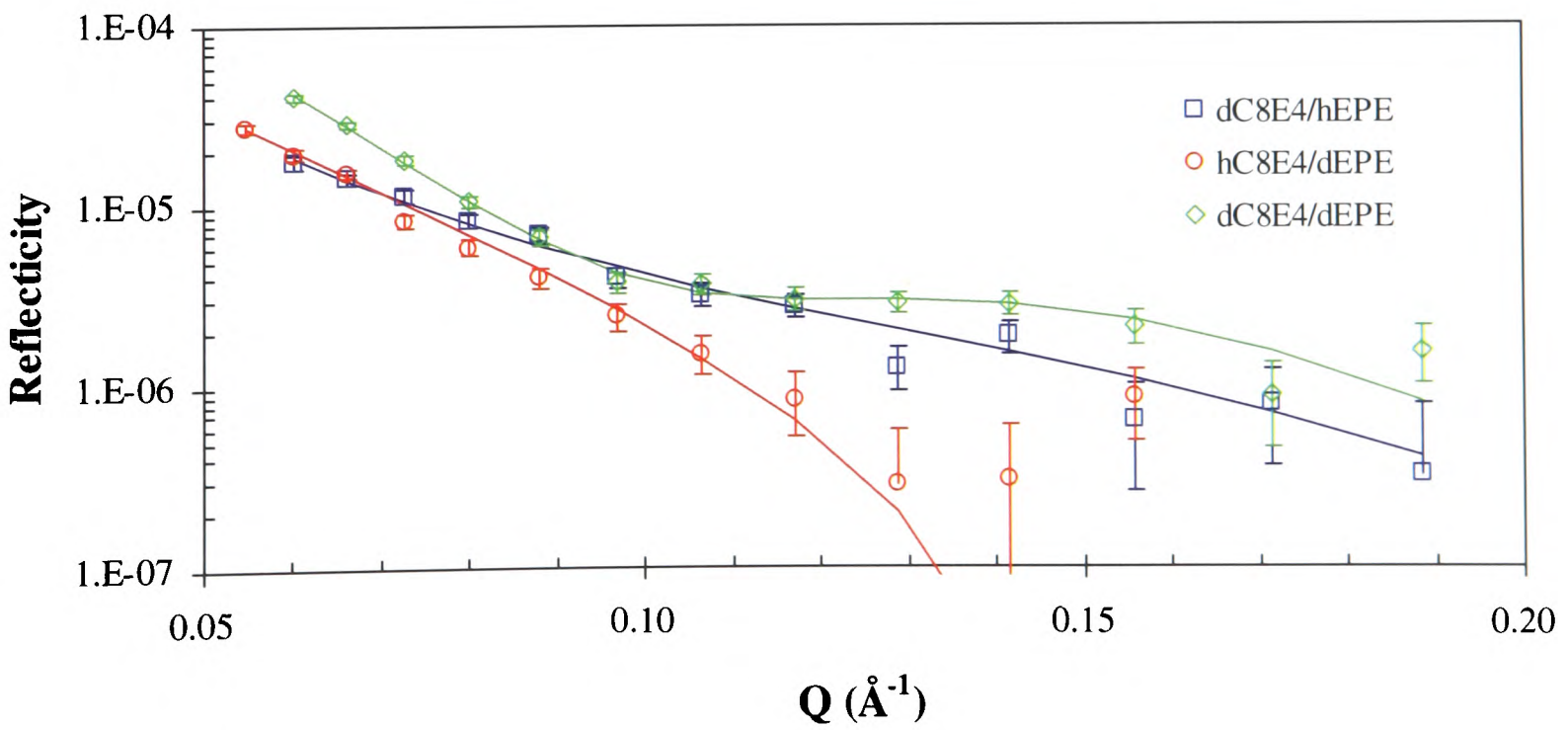


Figure 31. Neutron reflectivity profiles for 90/10 C_8E_4/EPE 3000-14 mixtures at a bulk concentration of $5x10^{-3}$M. The continuous lines are best fits to the data.

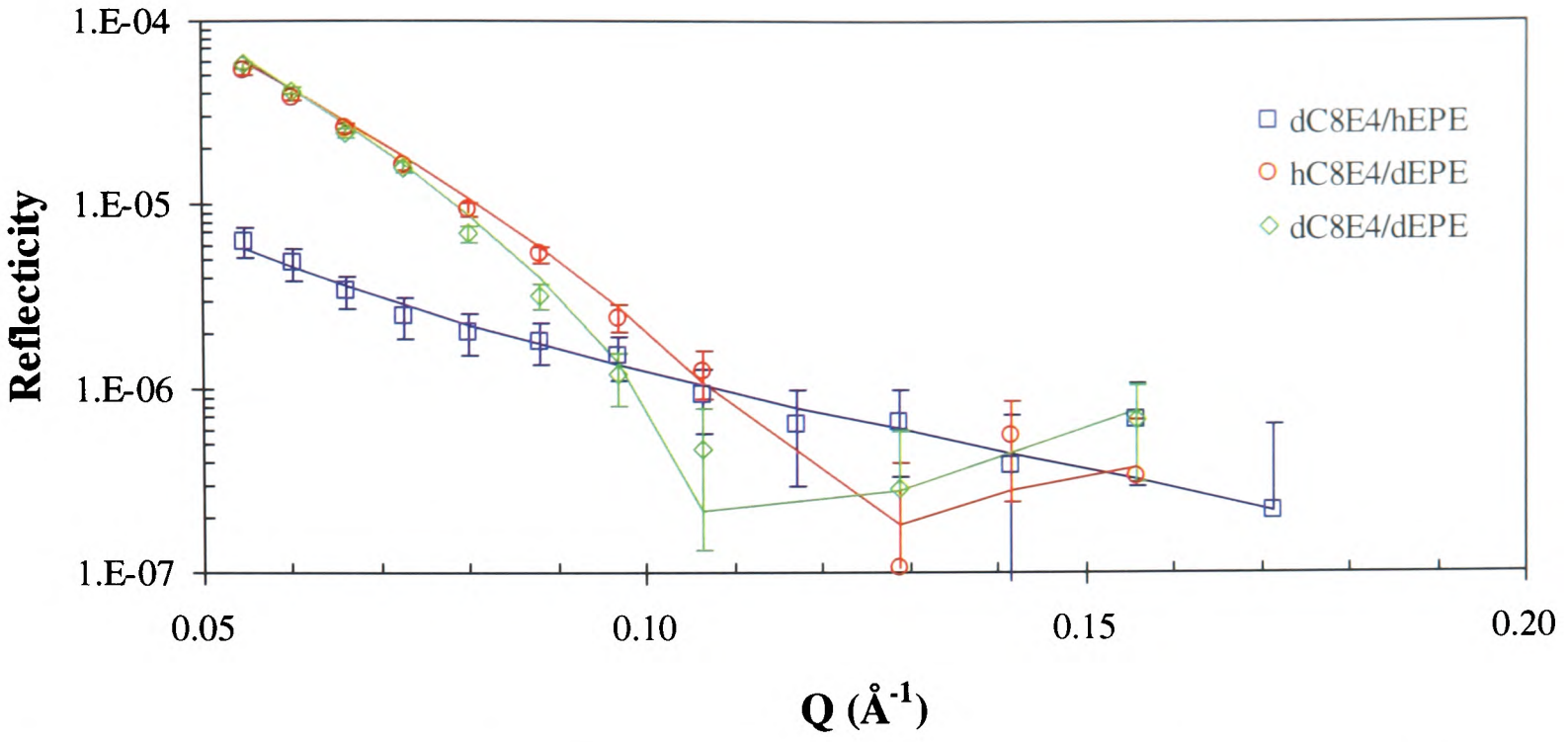


Figure 32. Neutron reflectivity profiles for 90/10 C_8E_4/EPE 3000-14 mixtures at a bulk concentration of $1x10^{-3}$M. The continuous lines are best fits to the data.

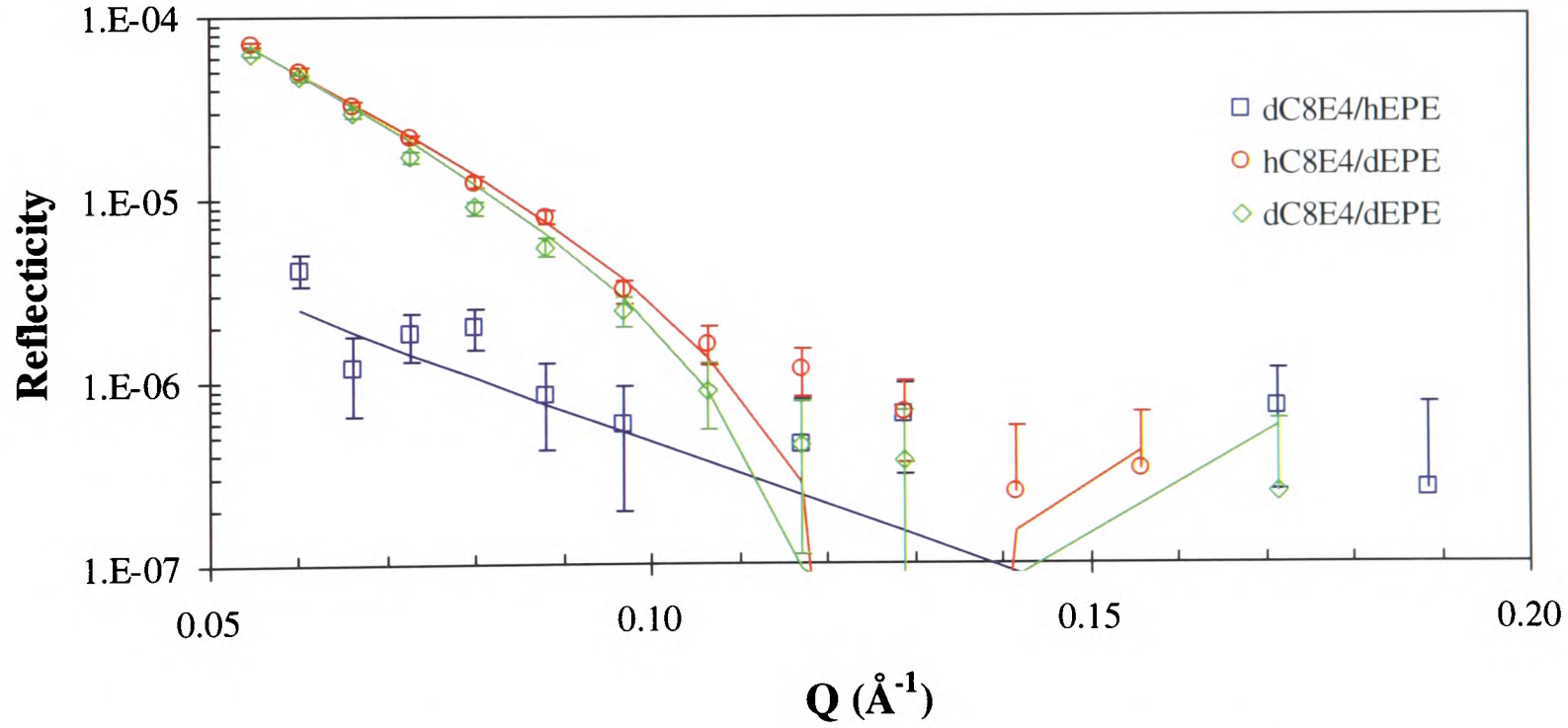


Figure 33. Neutron reflectivity profiles for 90/10 C_8E_4/EPE 3000-14 mixtures at a bulk concentration of $5x10^{-4}$M. The continuous lines are best fits to the data.

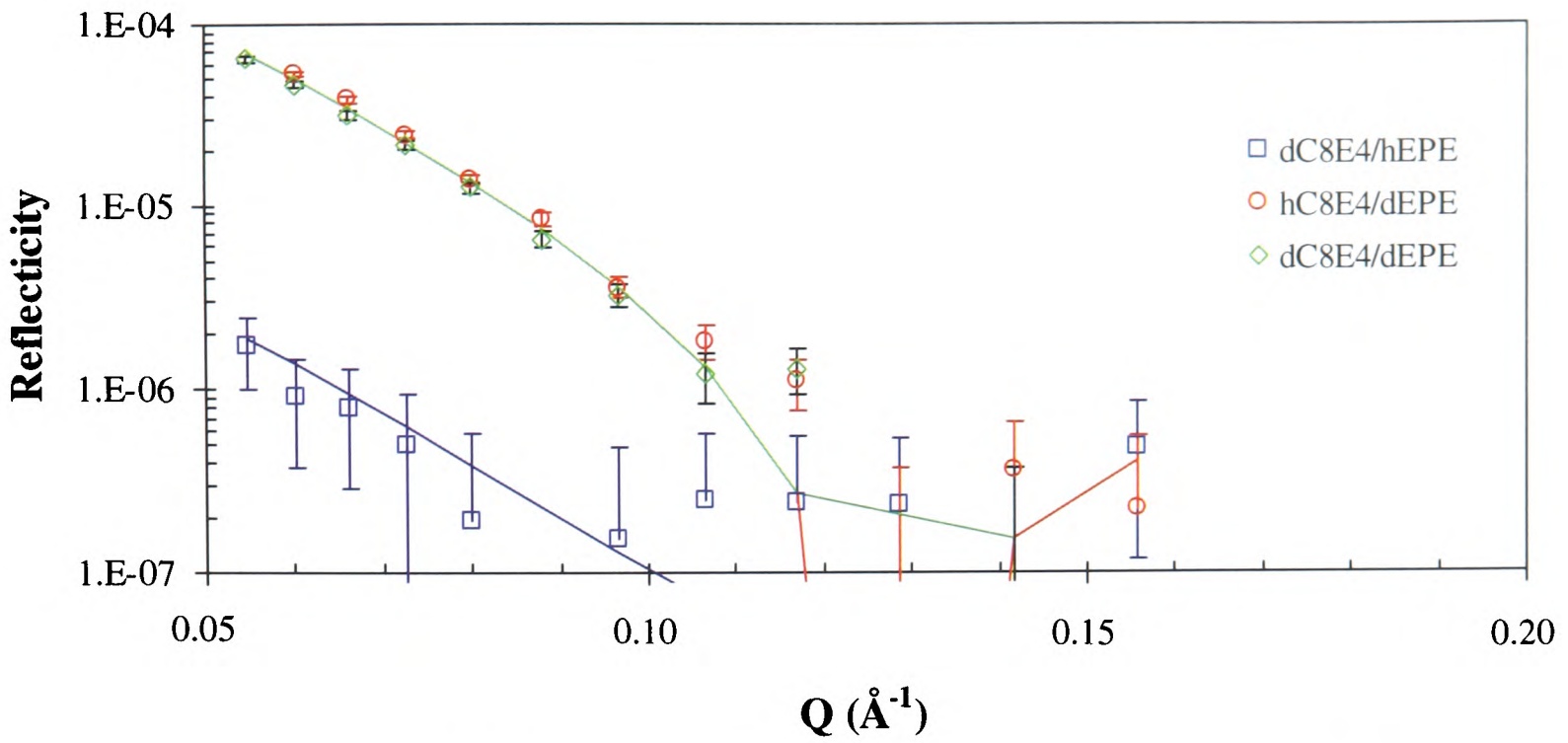


Figure 34. Neutron reflectivity profiles for 90/10 C_8E_4/EPE 3000-14 mixtures at a bulk concentration of $5x10^{-5}$M. The continuous lines are best fits to the data.

The reflectivity data were fitted to a model using just two parameters, the thickness of the interfacial layer and its scattering length density. This model was fitted to the sets of isotopic data in such a way as to give a consistent area per molecule of each surfactant species. The results obtained by this method of fitting together with the individual coverages calculated from areas per molecule using Equation 9.6 are given in Table 19.

Concentration (M)		$1x10^{-2}$			$5x10^{-3}$			$1x10^{-3}$			$5x10^{-4}$			$5x10^{-5}$		
Layer	Parameters	dC/hE	hC/dE	dC/dE	dC/hE	hC/dE	dC/dE	dC/hE	hC/dE	dC/dE	dC/hE	hC/dE	dC/dE	dC/hE	hC/dE	dC/dE
1	τ/Å	20±2	20±2	23±2	22±2	20±2	21±2	20±2	20±2	55±4	28±2	49±4	51±4	16±2	49±4	49±4
	$\rho x10^6(Å^{-2})$	1.46	0.06	1.53	1.02	0.17	1.48	0.55	0.69	0.93	0.30	1.00	0.99	0.27	1.01	1.01
2	τ/Å	38±3	38±3	36±3	35±3	36±3	37±3	35±3	33±3		21±2			33±3		
	$\rho x10^6(Å^{-2})$	0.13	0.47	0.48	0.10	0.70	0.56	0.02	1.01		0.04			0.12		
Total	τ/Å	58±5	58±5	59±5	57±5	56±5	58±5	55±5	53±5	55±5	49±4	49±4	51±5	49±4	49±4	49±4
	$\rho x10^6(Å^{-2})$	0.59	0.33	0.89	0.46	0.51	0.89	0.21	0.89	0.93	0.19	1.00	0.99	0.17	1.01	1.01

	A ($Å^2$)	$\Gamma x10^{10}$ (mol/cm^2)	A ($Å^2$)	$\Gamma x10^{10}$ (mol/cm^2)	A ($Å^2$)	$\Gamma x10^{10}$ (mol/cm^2)	A ($Å^2$)	$\Gamma x10^{10}$ (mol/cm^2)	A ($Å^2$)	$\Gamma x10^{10}$ (mol/cm^2)
C_8E_4	81±10	2.05±0.15	118±10	1.41±0.10	710±60	0.23±0.05	-	0.09±0.05	-	0.02±0.05
EPE 3000-14	1000±80	0.17±0.05	720±60	0.23±0.05	460±40	0.36±0.05	445±40	0.37±0.05	445±40	0.37±0.05
C_8E_4/EPE 3000-14		2.22±0.20		1.64±0.10		0.59±0.05		0.46±0.05		0.39±0.05

Table 19. Parameters and surface excesses obtained neutron reflectivity of three isotopic combinations dC_8E_4/hEPE 3000-14 (dC/hE), hC_8E_4/dEPE 3000-14 (hC/dE), dC_8E_4/dEPE 3000-14 (dC/dE), at different bulk concentrations.

The comparison between the interfacial compositions predicted from the Pseudophase Separation Model at a series of surface pressures with experimental values derived from the neutron reflectivity data is given in Table 18. There is a remarkable agreement between the surface composition predicted by the Pseudophase Separation Model and that measured by neutron reflection. Good consistency between Pseudophase Separation Model and neutron reflection data has been reported for other nonionic binary systems, for example Penfold *et al.*[18] found reasonable agreement between the two techniques for the surface composition of $C_{12}E_3/C_{12}E_8$.

The marked difference in the interaction observed in mixed micelles and monolayer formation with C_8E_4/EPE 3000-14 system may be associated with the structure of the aggregated states. In chapter 6 we found that the monolayer of EPE 3000-14 at the air-solution interface comprises a layer of PO groups, which extends outside the water, and a layer of PO and EO groups that penetrates into the aqueous phase. The orientation is such that the contact of PO groups with water molecules is significantly reduced. In the micellar state, on the contrary, the segregation between PO groups and water is not as strong as one might expect, much less than at the interface, as discussed in Chapter 8. We expect C_8E_4 to be overall more hydrophobic than a PEO block and therefore to mix preferentially with the PPO block. Neutron reflectivity does indeed show that there is preferential adsorption of C_8E_4 molecules in the uppermost part of the interfacial layer rich in PO groups as we discuss below.

The results presented in Table 19 obtained from the reflectivity show a marked increase in layer thickness above a bulk concentration of $5x10^{-4}$M. The layer thickness increase coincides with an increase in the mole fraction of adsorbed C_8E_4 and with displacement of EPE 3000-14 from the interfacial layer. The layer grows surprisingly thick, reaching 58Å at a bulk concentration of $5x10^{-3}$M, at which the surface excess of the copolymer is $0.23x10^{-10}$mol/cm^2. In a solution of pure deuterated PEO/protonated PPO-chain EPE 3000-14 with similar copolymer surface coverage, i.e. $0.23x10^{-10}$mol/cm^2, the equivalent layer thickness would be 43-44Å. As discussed above, the layer thickening appears to be a result of the introduction of the deuterated tails of C_8E_4 into the low-scattering PO layer outside the water. In the case of C_8E_4, the greater thickening observed

in comparison with that in the mixtures with SDS and DTAC, indicates that most of the small C_8E_4 molecules are incorporated into the PO layer.

In Figure 35 we analyse the displacement of EPE 3000-14 as a function of the bulk concentration normalised to the mixed CMC. Up to about one tenth of the mixed CMC the surface appears relatively saturated with the block copolymer. As the bulk concentration goes above this threshold, EPE 3000-14 molecules are increasingly displaced from the interface, and by time the mixed CMC is reached the surface is already considerably depleted of copolymer molecules. The displacement mechanism in this system is not driven by the presence of the micelles, as indicated in the mixtures with SDS and DTAC, but rather by a changeover in surface activity with concentration. The surface tension curves depicted in Figure 35 clearly demonstrate that above one tenth of the CMC, C_8E_4 becomes more surface active than EPE 3000-14 and would therefore dominate the surface composition.

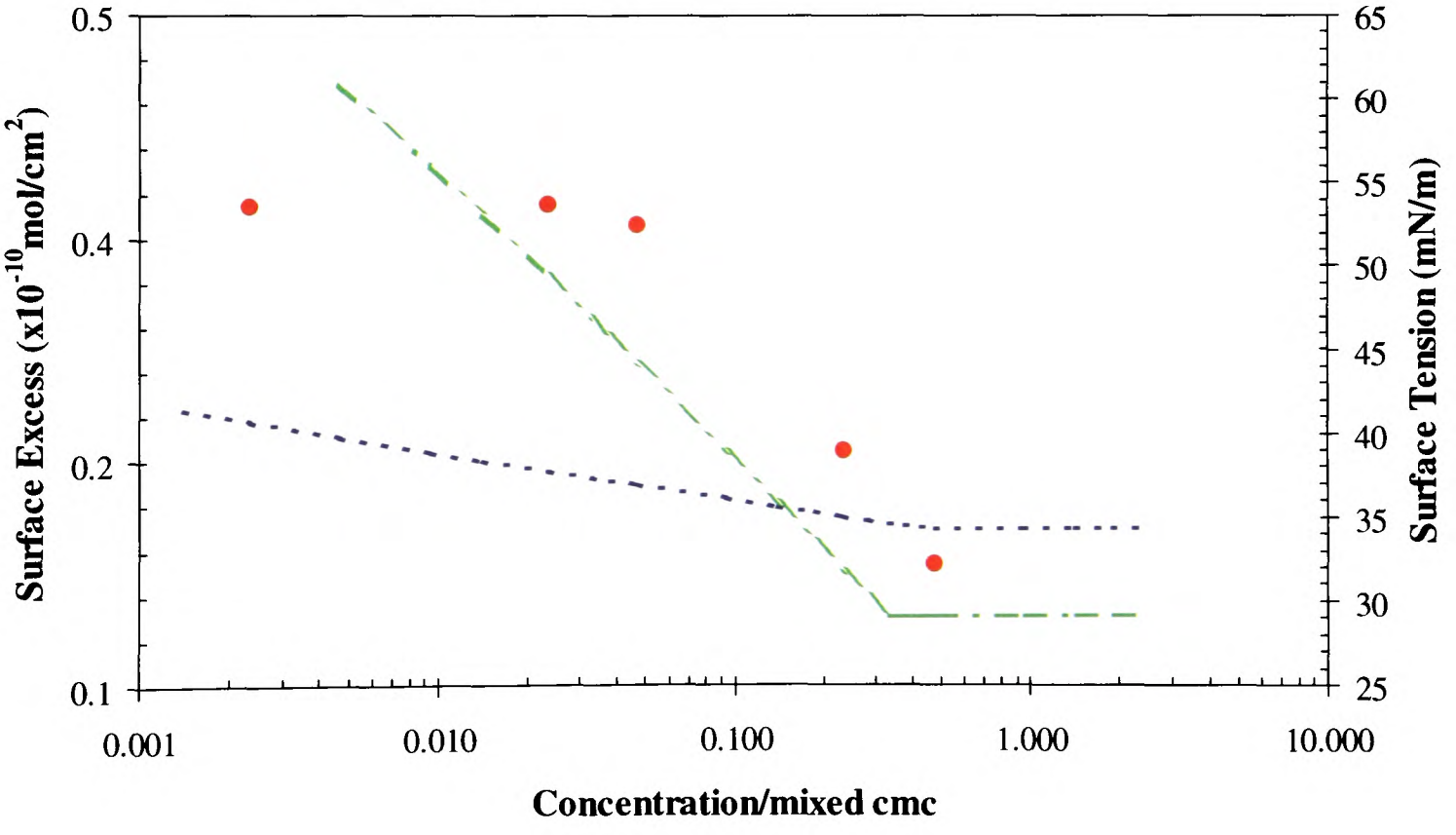


Figure 35. Surface excess of EPE 3000-14 in mixtures with C_8E_4, (●), as a function of the mixture concentration normalised to the mixed CMC. The lines correspond to the surface tension of solutions of pure C_8E_4 (dash lines) and EPE 3000-14 (dash-dot lines).

4 Summary

Surface tension and specular neutron reflection have been used to investigate the adsorption of EPE copolymers in binary mixtures with surfactants such as SDS, DTAC, and C_8E_4 at the air/liquid interface. The effects of swamping electrolyte, 0.1M NaCl, on the monolayer formation of the mixtures with ionic surfactants were also studied.

The surface tension data were analysed in the frame of the Pseudophase Separation Model and surface composition and the interaction parameters were determined. The neutron reflection technique was used to determine the adsorbed amounts at air/liquid interface, and to provide a direct and absolute method of obtaining adsorbed amounts in multi-component mixtures over a wide range of bulk concentrations. To verify the suitability of the Pseudophase Separation Model to describe the surface composition for such mixtures, the predictions were compared with compositions directly measured by neutron reflectivity. For the mixtures of EPE 3000-14 with ionic surfactants, the large difference in surface activity makes the determination of β^s impossible. However in the presence of electrolytes β^s values are large and negative. The surface compositions from neutron reflection generally disagree with the predictions of Pseudophase Separation Model, particularly for the DTAC/EPE 3000-14 systems. We argue that the nonideality observed in the co-micellization of both SDS and DTAC with EPE 3000-14 could be driven by a dehydration mechanism and it would therefore be reasonable to assume that dehydration should also be an important factor in the thermodynamics of monolayer formation. Pseudophase Separation Model does not take into account the hydration changes upon mixing, and we believe that hydration may be responsible for the deviations observed.

Below the mixed CMC, the monolayer appears to be saturated with EPE 3000-14, whose surface excess hardly changes with increasing concentration. As the bulk concentration exceeds the CMC, however, there is a pronounced drop in the copolymer concentration at the interface, which coincides with an abrupt increase in the adsorption of the ionic surfactant. The sudden change is rationalised by Nikas *et al.* in terms of the changes in the distribution of the two surfactant species between the bulk solution and the monolayer due to the onset of mixed micelle formation. The monolayer composition merely reflects the changes in monomer composition as mixed micelles are formed.

The variation of layer thickness with the surface coverage of the block copolymer gives some interesting information about the structure of mixed monolayer. The results show a sudden increase in layer thickness when the bulk concentration approaches or exceeds the mixed CMC. This increase coincides with a steep increase in the molar fraction of ionic surfactant at the interface. The increased thickness observed is believed to be a result of the introduction of the deuterated tails of the ionic surfactant into the low-scattering PO layer outside the water. The results also indicate differences in the mixed layer structure between the surfactants. The layer thickness increase for the ionic surfactants appears at a much lower surface mole fraction for DTAC than for SDS, indicating that DTAC preferably accumulates in the uppermost part of the interfacial layer, while SDS would rather stay in the aqueous phase region, which is more hydrophilic.

For the binary mixtures of C_8E_4/EPE 3000-14, the Pseudophase Separation Model analysis of the surface tension data showed that the two surfactant species mix ideally at the interfacial layer, which is quite different from the repulsive interaction found in the mixed micelle formation. Direct measurement of the surface compositions using neutron reflection were consistent with the Pseudophase Separation Model predictions, confirming that mixing is ideal at the interface. The difference in interaction between mixed micelles and monolayer formation may therefore be associated with the structure of the pseudophases.

The copolymer displacement in the nonionic mixture is distinctly different from the mixtures with ionic surfactants. It appears to be dictated by a changeover in surface activity with concentration rather than by the presence of micelles. At low concentrations EPE 3000-14 is more surface active and the surface coverage results show that the monolayer is saturated with copolymer molecules. As the bulk concentration reaches about one tenth of the mixed CMC, C_8E_4 becomes more surface active and it then dominates EPE 3000-14 in the surface composition.

References:

[1] Hecht, E.; and Hoffmann, H. *Langmuir*, 10, 86 (1994)

[2] Penfold, J.; Staples, E.; Thompson, L.; Tucker, I.; Hines, J.; Thomas, J.K.; and Lu, J.R. *Langmuir*, 11, 2496 (1995)

[3] Staples, E.; Thompson, L.; Tucker, I.; Penfold, J.; Thomas, J.K.; and Lu, J.R. *Langmuir*, 9, 1651 (1993)

[4] Penfold, J.; Staples, E.; Cummins, P.; Tucker, I.; Thomas, J.K.; Simister, E.A.; and Lu, J.R. *J. Chem. Soc. Fraraday Trans.*, 92, 1773 (1996)

[5] Hines, J.; Thomas, J.K.; Garrett, P.R.; Rennie, G.K.; and Penfold, J. *J. Phys. Chem. B*, 101, 9215 (1997)

[6] Rosen, M.J., and Hua, X.Y. *J. Colloid Interface Sci.*, 86, 164 (1982)

[7] Rosen, M.J., and Hua, X.Y. *J. Colloid Interface Sci.*, 125, 730 (1988)

[8] Holland, P.M. *J. Colloid Surf.*, 19, 171 (1986)

[9] Holland, P.M. *Adv. Colloid Interface Sci.*, 26, 111 (1986)

[10] Fried, V.; Blukins, U., and Hameka, H. F. in *Physical Chemistry*, Macmillan Co., New York (1977)

[11] Hines, J.; Thomas, J.K.; Garrett, P.R.; Rennie, G.K.; and Penfold, J. *J. Phys. Chem.*, 101, 7121 (1997)

[12] Baglioni, P.; Dei, L.; Rivara-Minten, E.; and Kevan, L. *J. Am. Chem. Soc.*, 115, 4286 (1993)

[13] Rosen, M.J., and Zhu, B.Y. *J. Colloid Interface Sci.*, 99, 435 (1984)

[14] Hines, J.; Thomas, J.K.; Garrett, P.R.; Rennie, G.K.; and Penfold, J. *J. Phys. Chem. B*, 102, 8834 (1998)

[15] Li, Y.; Xu, R; Bloor, D.M.; Holzwarth, J.F.; and Wyn-Jones, E. *Langmuir*, 16, 10520 (2000)

[16] Nikas, Y.F.; Pruvvada, S.; and Blankschtein, D. *Langmuir*, 8, 2680 (1990)

[17] Hecht, E.; and Hoffmann, H. *Colloids Surfaces A: Physicochem. Eng. A*, 96, 181 (1995)

[18] Penfold, J.; Staples, E.; Thompson, L.; and Tucker, I. *Colloids Surfaces A: Physicochem. Eng. Aspects*, 127 (1995)